THE UNIVERSITY *of* EDINBURGH

Neoproterozoic Low Latitude Glaciations:

An African Perspective

Gijsbert Bastiaan Straathof

Thesis submitted in fulfilment of

the requirements for the degree of

Doctor of Philosophy

to the

University of Edinburgh — 2011

Declaration

I declare that this thesis has been composed solely by myself and that it has not been submitted, either in whole or in part, in any previous application for a degree. Except where otherwise acknowledged, the work presented is entirely my own.

Gijs Straathof

April 2011

Abstract

The Neoproterozoic is one of the most enigmatic periods in Earth history. In the juxtaposition of glacial and tropical deposits the sedimentary record provides evidence for extreme climate change. Various models have tried to explain these apparent contradictions. One of the most popular models is the Snowball Earth Hypothesis which envisages periods of global glaciations. All climatic models are dependent on palaeogeography which as yet remains poorly constrained for the Neoproterozoic. This thesis presents a multidisciplinary study of two Neoproterozoic sedimentary basins on the Congo and West Africa cratons including radiometric dating of glacial deposits themselves.

In the West Congo Belt, western Congo Craton, a new U-Pb baddeleyite age for the Lower Diamictite provides the first high quality direct age for the older of two glacial intervals. This age is significantly different from previously dated glaciogenic deposits on the Congo Craton. This result strongly suggests that the mid-Cryogenian was a period during which several local glaciations occurred, none of which were global. While the palaeomagnetic results from carbonates around the younger glacial interval are probably remagnetised, detrital zircon and chemostratigraphic results allow correlation with numerous late-Cryogenian glaciogenic deposits worldwide and a Snowball Earth scenario is favoured here.

In the Adrar Sub-Basin of the vast Taoudéni Basin, West Africa, the terrigenous Jbeliat glacial horizon has been studied in great detail. Detrital zircon geochronology reveals large changes in provenance through this glacial unit with implications for sedimentological approaches and techniques for provenance characterisations based on one sample alone. Together with recently published U-Pb data these results constrain the age of the Jbeliat

Group to a narrow window providing vital geochronological information for this younger glacial event.

Combining provenance geochemistry, chemostratigraphy and U-Pb dating has greatly improved our understanding of two of the largest Neoproterozoic sedimentary basins. The dominance of Mesoproterozoic detrital material, for which no source has been reported near either of the field areas, has consequences for the proximity of other cratons at the time of deposition, prior to the final amalgamation of Gondwana.

Contents

”Het is een misverstand dat je het aan de werkelijkheid zou kunnen overlaten zichzelf te vertellen.”

”It’s a mistake to leave it up to the facts to tell themselves.”

Tim Krabbé

Chapter 1

Introduction

The Neoproterozoic (1000 – 542 Ma) was arguably one of the most enigmatic and important Eras of Earth history. It was the most active period of crust formation and it spans the break-up of supercontinent Rodinia and formation of supercontinent Gondwana (Moores, 1991; Hoffman, 1991; Dalziel, 1991; Meert and van der Voo, 1997; Rino et al., 2008). It records the appearance of metazoan (multicellular) lifeforms (Knoll, 1991) that led into the Cambrian evolutionary explosion (Knoll and Carroll, 1999). On top of that the late Neoproterozoic rock record contains evidence for the existence of marine glaciers at low to near-equatorial palaeolatitudes (Embleton and Williams, 1986; Evans, 2000). The study of these glaciomarine deposits has gripped the mind and imagination of many researchers over the past century and is the main topic of this thesis.

In the light of the Pleistocene circum-polar glaciations that are so familiar to many of us, low latitude glaciations seem to be an extraordinary phenomenon. Based on evidence for Neoproterozoic glacial rocks at low latitudes a number of different models have been proposed such as the Snowball Earth Hypothesis requiring global glaciation and the High Obliquity Model involving radical changes to the Earth's rotational axis (Harland, 1964; Kirschvink, 1992; Williams, 2008). Despite the high level of interest in this subject during the past two decades there is still controversy over the number of glacial events, the duration, the global extent and the palaeolatitudes involved. These issues boil down to a great lack of precise ages for the glacial deposits which subsequently hampers regional

and global correlations. The synchronicity and global extent are vital aspects of many of the proposed models and form prime objectives for testing them. The aim of this thesis is to investigate the timing, palaeolatitude and palaeogeographic characteristics of two sedimentary sequences recording evidence for Neoproterozoic glaciation which are found on the Congo and West African Precambrian cratons (see Figure 1.1 for a distribution of Precambrian continental crust).

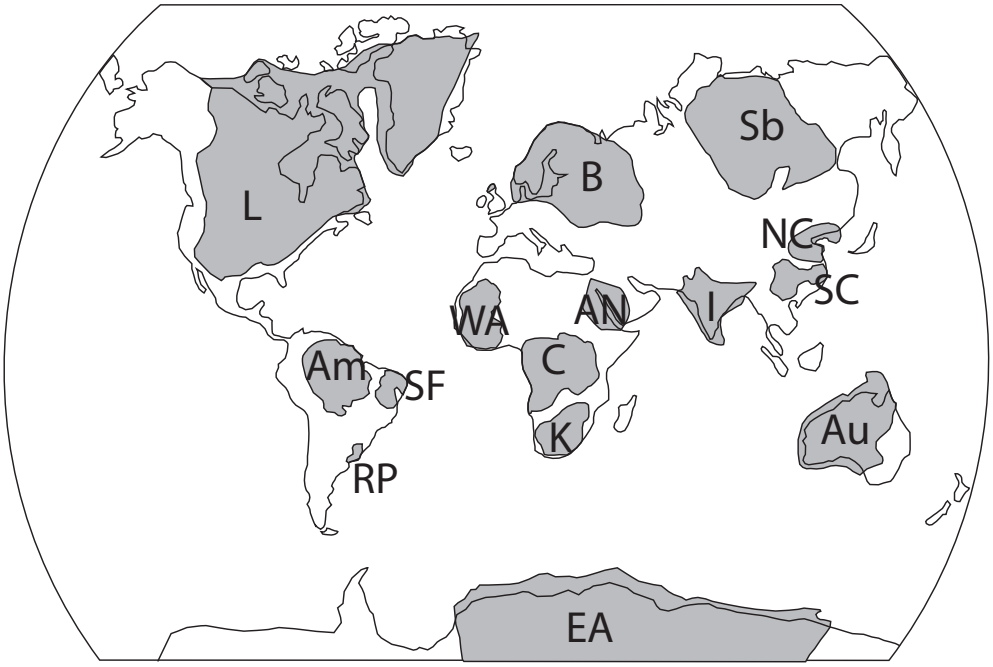

Figure 1.1. Simplified map of Precambrian cratons in their present-day geographical positions. These cratons are discussed in the text below as well as in the following chapters: Am, Amazonia; AN, Arabian-Nubian Shield; Au, Australia; B, Baltica; C, Congo; EA, East Antarctica; I, India; K, Kalahari; L, Laurentia including Greenland; NC, North China; RP, Rio de la Plata; Sb, Siberia; SC, South China; SF, São Francisco; WA, West Africa.

1.1 The Neoproterozoic Sedimentary Record and its Apparent Climatic Paradox

Neoproterozoic glacial deposits are distinctly different from their Pleistocene counterparts because they are closely associated with rocks which indicate warm, tropical climate settings. The end of glacial deposition is typically marked by the presence of thin, laterally persistent carbonates. Abiotic carbonates are formed by chemical precipitation from warm

water saturated in $CaCO_3$ so the juxtaposition of glacial diamictite and carbonate forms an apparent climatic contradiction. Because of their stratigraphic position sharply overlying glacial rocks these carbonates are called “cap carbonates”.

Two main types of glacial rocks are possible: those deposited on land by mountain glaciers (Alpine type) and those formed at sea level where debris is transported and dropped by icebergs (glaciomarine sediments). These last deposits are currently only found at high (>40°) latitudes. A glacial influence in sedimentary rocks is indicated by the presence of striated clasts, striated and/or polished pavements, by the presence of dropstones or can be demonstrated by microscopic observations. When a glacial genesis is clearly recognised the sediment is called a till, and the sedimentary rock a tillite. The non-genetic term diamictite is used when such clear indicators are absent and refers to poorly sorted, conglomeratic rocks with a lack of internal structure and a clay rich matrix. Diamictites are not uniquely glacial and can be formed by various depositional mechanisms. These definitions and descriptions of the palaeoenvironment represented by the deposits are based on studies of modern and Pleistocene glacial deposits (e.g. Boulton, 1972; Eyles and Eyles, 1983; Eyles, 1993).

The fact that Neoproterozoic glaciomarine sedimentary rocks are much more widespread than similar rocks of Phanerozoic age has long ago been noted by researchers (Geikie, 1894; Sayles, 1919; Gevers, 1931; Coleman, 1939). In a pre-plate tectonic context, the presence of glacially derived rocks in equatorial latitudes invoked the suggestion that the Earth once might have experienced a glaciation severe enough for marine ice to reach the tropics. A global glaciation was first postulated by Louis Agassiz who called it ‘die Eiszeit’ (Agassiz, 1866). The beginning of the twentieth century saw a growing support for a ‘worldwide refrigeration’, especially from A.P. Coleman (Coleman, 1926, 1932, 1939). Around this same time, the concept of continental drift was introduced which brought relief to those who struggled with such extreme scenarios: motion of a continental plate could be responsible for transporting glaciomarine sedimentary rocks to low latitudes (Wegener, 1912; Dutoit, 1921; Wegener, 1967). This concept however fell on deaf ears to many prominent geologists who continued favouring models with ice at low latitudes (Coleman, 1932; Willis, 1944; Flint, 1957).

1.1.1 Palaeogeographic Constraints

With the development of palaeomagnetic techniques, evidence from Neoproterozoic sequences in Norway and Greenland suggested a low palaeolatitude for tillite formation (Harland and Bidgood, 1959; Bidgood and Harland, 1961). This was explained by the concept of an 'infracambrian glaciation' which resulted in the near global deposition of coeval tillites (Harland, 1964; Harland and Rudwick, 1964). The fact that these glaciogenic deposits are associated with warm water carbonate rocks was presented as additional evidence for ice extending to tropical environments. The robustness of these early palaeomagnetic results was later scrutinized but the discussion continued and similar sequences have subsequently been recognised on almost every craton (Crawford and Daily, 1971; Schermerhorn, 1974a; Hambrey and Harland, 1981).

The first hard palaeomagnetic evidence for a low latitude glaciation came from Neoproterozoic glacial rocks in the central Flinders Ranges, South Australia (Embleton and Williams, 1986; Schmidt et al., 1991; Schmidt and Williams, 1995; Sohl et al., 1999). The Flinders Ranges contain the glaciomarine Elatina Formation of the Umberatana Group, and the overlying Nuccaleena Formation (Wilpena Group, Preiss and Forbes, 1981). The Elatina Formation comprises a basal diamictite with sandy matrix and tidal rhythmites of alternating siltstones and feldspathic, fine-grained sandstones (Lemon and Gostin, 1990). The overlying carbonate Nuccaleena Formation is a finely laminated, buff-weathered pink dolomite. Palaeomagnetic results from these two formations at three localities, each locality with a contrasting bedding orientation, yielded a stable, high temperature (600 – 675°C) palaeomagnetic direction (Sohl et al., 1999). After bedding reconstruction these results pass a foldtest meaning that magnetisation was acquired before tectonic folding during the Cambrian. The data also reveal the presence of several magnetic polarity reversals. The time it takes for the Earth's magnetic field to change polarity is in the order of several thousand years suggesting a considerable duration of the glaciation (Sohl et al., 1999). The results demonstrate a palaeolatitude of 8.6±3.4° supporting a low latitude for deposition of the Elatina Formation and confirming earlier palaeomagnetic studies (Schmidt et al., 1991; Schmidt and Williams, 1995).

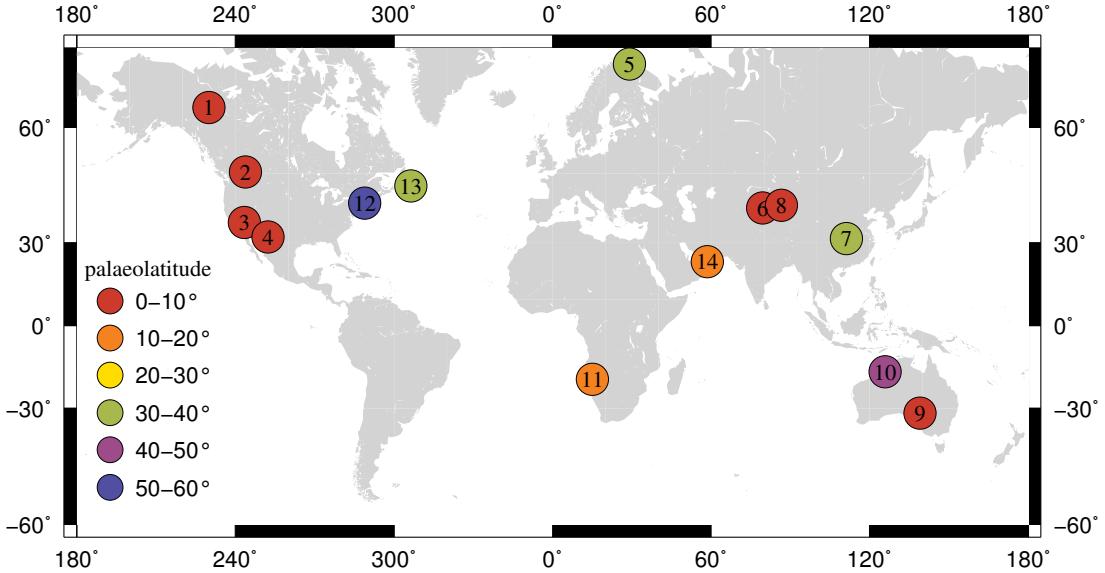

Figure 1.2. Global distribution of palaeomagnetic studies of alleged glaciogenic Neoproterozoic rocks. Numbers correspond with Table 1.1 which lists details and references of each study.

In the past three decades a number of palaeomagnetic studies have been carried out in Neoproterozoic sequences. The most reliable palaeomagnetic data for Neoproterozoic glaciogenic rocks are listed in Table 1.1 and present day locations of the studies are shown in Figure 1.2. The data listed in Table 1.1 are selected according to procedures closely following those of Evans (2000): the quality of the palaeomagnetic results are considered in conjunction with the most recent sedimentary interpretations of the deposits (for a discussion of the quality of palaeomagnetic data see Chapter 5). If the results are not from the glaciogenic deposits themselves a good correlation between the palaeomagnetically studied units and the glaciogenic rocks has to be shown as well. The list clearly indicates that low and moderate palaeolatitudes prevail and high latitudes (>40°) have been reported only in two studies, the Squantum Tilloid in the USA and the Walsh Tillite in Australia (Wu et al., 1986; Li, 2000).

1.1.2 Geochronology of Glacial Events

At least three glacial events are postulated, two of which occurred during the Cryogenian period (850 – 630 Ma, Gradstein et al., 2004) and one during the Ediacaran period (630 – 542 Ma). These are commonly referred to as the 'Sturtian' (age constraints spanning 735

	Formation	Age (Ma) min/max	Site °N	°E	λ (°)	Craton	Reference
1	Rapitan Group	575/773	64	230	6 ± 4	Laurentia	Park (1997)
2	Toby Formation[a]	721/727	50	244	8 ± 4	Laurentia	Buchan et al. (2001)
3	Johnnie Formation	542/1100	37	244	1 ± 4	Laurentia	Gillett and Van Alstine (1982)
4	Florida Mountains	488/509	32	252	3 ± 8	Laurentia	Geissman et al. (1991)
5	Vestertana Group	575/1000	70	29	33 ± 14	Baltica	Torsvik et al. (1995)
6	Tarim Basin	542/1000	41	79	8 ± 6	NW China	Li et al. (1991)
7	Nantuo Formation	542/760	31	111	36 ± 7	S China	Evans et al. (2000)
8	Baiyisi Formation	717/737	42	87	1 ± 3	NW China	Huang et al. (2005)
9	Elatina Formation	575/650	-32	139	9 ± 4	Australia	Sohl et al. (1999)
10	Walsh Tillite	542/1000	-17	126	45 ± 12	Australia	Li (2000)
11	Chuos Formation[b]	550/762	-20	15	10 ± 5	Congo	Meert et al. (1995)
12	Squantum Tilloid	542/598	42	289	55 ± 8	Avalonia	Wu et al. (1986)
13	Gaskiers Formation	579/581[c]	47	306	31 ± 10	Avalonia	McNamara et al. (1997)
14	Huqf Supergroup	544/712	24	59	15 ± 4	Arabia	Kilner et al. (2005)

Table 1.1. Reliable palaeomagnetic studies of alleged glaciogenic rocks. Numbers in the first column correspond to the numbers in Figure 1.2. Ages are for magnetisation and, unless reference is given, are taken from the original publication, from Evans (2000) or by applying ages for geologic periods/eras from Gradstein et al. (2004). λ = palaeolatitude. [a]Palaeomagnetic results from the Franklin Dykes; [b]correlated with Mbozi complex; [c]Bowring et al. (2003).

– 660 Ma, Key et al., 2001; Fanning and Link, 2008), 'Marinoan' (ca. 635 Ma, Hoffmann et al., 2004; Condon et al., 2005) and 'Gaskiers' (ca. 580 Ma, Bowring et al., 2003; Calver et al., 2004) although there is overlap in age ranges (see Fig. 1.3) and severity of the Gaskiers event has been questioned (Hoffman and Li, 2009).

The type locality for the Sturtian is in the Adelaide Rift Complex in South Australia (Preiss and Forbes, 1981) where direct depositional ages are limited to an abstract reporting a 659±6 Ma U-Pb zircon date for an interglacial tuffaceous bed in the lower Wilyerpa Formation, Yudnamutana Subgroup, Umberatana Group (Fanning and Link, 2008). This age is substantially younger than the classical interpreted 750 – 700 Ma age for the Sturtian in southern Australia (Preiss, 2000). Perhaps the most reliable radiometric age is a recently published Th-U-Pb electron microprobe authigenic monazite age of 680±23 Ma obtained from the post-Sturtian Enorama Shale providing an absolute minimum age constraint for the Sturtian glacial deposition (Mahan et al., 2010). Direct depositional ages are available from Sturtian correlatives on other cratons. In the southeastern Democratic Republic of Congo two glacial diamictites are correlated to the two Cryogenian glacial events (Binda and Van Eden, 1972; Cahen and Lepersonne, 1981b). The older of the two, the 'Grand Conglomerate', can be traced into Zambia where a volcanic breccia from within this unit, locally termed the Basal Kundelungu Diamictite (Katanga Supergroup), is dated at 735±5

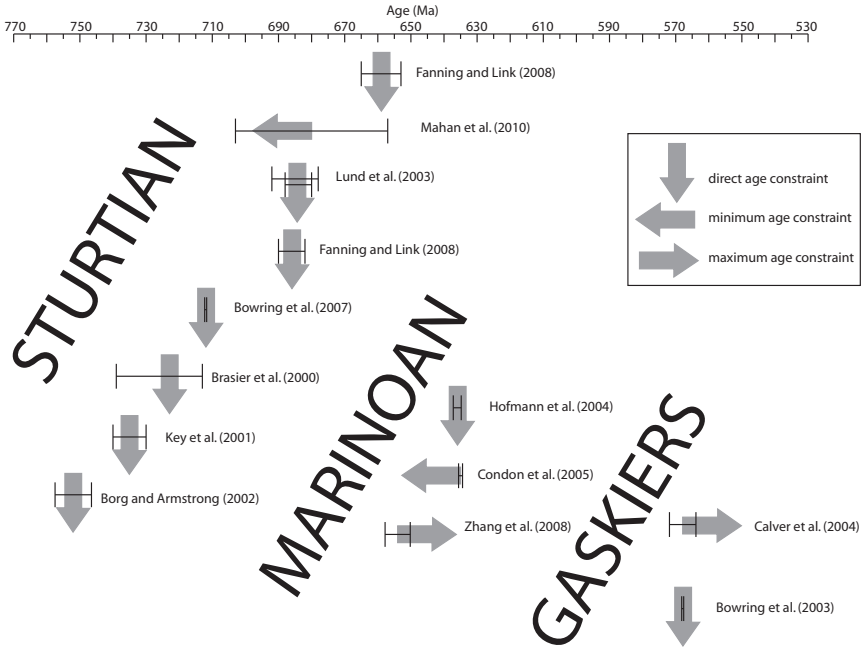

Figure 1.3. Geochronology of the glacial events as described in the text. See text for details on the dating methods and descriptions of the dated (glaciogenic) units.

Ma by 'sensitive high-resolution ion microprobe' (SHRIMP) U-Pb analysis of zircon crystals (Key et al., 2001). Further to the west in Namibia the age of the Kaigas glaciogenic formation is well constrained by a 751.9±5.5 Ma U-Pb SHRIMP zircon age for immediately overlying volcanic rocks of the Rosh Pinah Formation (Borg and Armstrong, 2002). Other direct age of Sturtian glaciogenic deposits include SHRIMP zircon ages of 685±7 and 684±4 Ma for rhyodacites from within the Edwards Formation, central Idaho (Lund et al., 2003), a 686±4 zircon SHRIMP age for a felsic volcanic horizon in the Scout Mountain Member (Pocatello Formation) in southern Idaho (Fanning and Link, 2008) and 723^{+16}_{-10}Ma (SHRIMP) and 711.5±0.3 Ma ('thermal ionization mass spectrometry', TIMS) for a tuffaceous sandstone from within the Gubrah Formation in Oman (Brasier et al., 2000; Bowring et al., 2007). These sequences are all considered to reflect a Sturtian age glaciation, however, the wide range of ages now available question the idea of a single glacial event.

Until recently the late Cryogenian glacial event was called Varanger Glaciation after the Varanger sequences in Finnmark, northern Norway, which are one of the best described Neoproterozoic glacial successions (Edwards, 1984; Rice and Hofmann, 2000). However, age constraints are poor and it has been suggested that they may even be Ediacaran in age

(i.e. equivalent to the Gaskiers glaciation, Nystuen et al., 2008). The term Marinoan is now more generally used for the late Cryogenian event which is named after the Marinoan Glaciation in its type area in the Adelaide Rift Complex. Age constraints from sequences correlated with the Marinoan suggest that it terminated by 635 Ma based on U-Pb zircon ages for an ash bed from within the glaciogenic Ghaub Formation in Namibia of 635.5±1.2 Ma (TIMS, Hoffmann et al., 2004) and for an ash bed in the Lower Dolomite Member overlying the Nantuo Diamictite in South China of 635.2±0.6 Ma (TIMS, Condon et al., 2005). A SHRIMP U-Pb zircon age of 654.5±3.8 Ma (Zhang et al., 2008) from immediately below the Nantuo Formation suggests that the Marinoan could have lasted as long as 23.5 Ma.

A ca. 580 Ma age for the Marinoan Elatina Formation in the Adelaide Rift Complex has been suggested based purely on lithostratigraphic correlation with the Croles Hill Diamictite in Tasmania Calver et al. (2004). The Croles Hill Diamictite is directly underlain by a rhyodacite flow of the Togari Group which is dated 582±4 Ma (SHRIMP, Calver and Walter, 2000; Calver et al., 2004). However, in the most recent publication discussing the Croles Hill deposits this correlation is not considered viable (Hoffman et al., 2009) leaving the possibility for a late Cryogenian age for the Marinoan in its type locality in southern Australia.

The Ediacaran Gaskiers event has been radiometrically dated in its type area in Newfoundland, Canada, although results are only available in an abstract: the Gaskiers Formation contains a subaqueous tuff horizon which yielded a U-Pb TIMS age of 582±0.3 Ma (Bowring et al., 2003). This age corresponds well with the 582±4 Ma minimum age for the Croles Hill Diamictite.

It is clear that for all these events many more reliable ages are needed to establish both regional and global viable correlations.

1.1.3 The Occurrence of Warm Water Cap Carbonates

The Cryogenian glacial deposits are frequently associated with cap carbonates. They tend to sharply overly the glacial rocks without an evident hiatus and are often called 'cap dolostones' reflecting their dolomitic character (Kennedy et al., 1998). Two distinctive varieties of cap carbonates are commonly reported and based on their lithological and geochemical characteristics they are regularly used to correlate glaciations to their Sturtian and Marinoan archetypes in southern Australia. The "Sturtian"-type cap carbonate is organic-rich, rhythmically laminated and occasionally displays rollup structures and slumped microbial mats (Kennedy et al., 1998; Corsetti and Lorentz, 2006). The second type of cap carbonate is generally found overlying Marinoan correlatives and comprises a light-pink coloured dolostone with mechanical (as opposed to chemical) laminae showing sedimentary structures like wave ripples (flaser bedding), dewatering structures (load casts) and cemented sheet cracks (Kennedy, 1996; Hoffman and Schrag, 2002; Shields, 2005). They may also contain aragonite crystal fans, vertical tubular structures and barite deposits (Kennedy et al., 2001; Nogueira et al., 2003; Shields et al., 2007b).

What makes these carbonates really enigmatic is that they record negative δ^{13}C values, a feature that has attracted a lot of attention since the first chemostratigraphic studies of these sequences (Knoll et al., 1986; Kaufman et al., 1991). The ratio between ^{12}C and ^{13}C in carbonate deposits is expressed as δ^{13}C and reflects the composition of ancient sea water (see Fig. 1.4). Excursions during the entire Phanerozoic Eon did not exceed 5‰ (Veizer et al., 1999) and the largest of these excursions are correlated to global events such as mass extinctions, major impacts or orogenic cycles (Prokoph and Veizer, 1999) which can cause major fluctuations in organic carbon reservoirs. The Neoproterozoic record is unusual both for its background values (∼+5‰) and for the sharp, short-lived negative peaks going down to -9‰ (Fig. 1.4). After the initial studies those values have been reported on all major cratons e.g. Australia (Kennedy, 1996), Laurentia (Kaufman et al., 1997; Corsetti and Kaufman, 2003), the Congo Craton (Hoffman et al., 1998; Frimmel et al., 2006), the Amazon Craton (Nogueira et al., 2003), South China (Macouin et al., 2004), Baltica (Halverson et al., 2005), Arabia (Le Guerroué et al., 2006) and West Africa (Shields et al., 2007b). Attempting to explain the occurrence of these warm water cap carbonates with

their remarkable isotopic characteristics and their position immediately overlying glaciogenic sediments has been the focus of many studies (e.g. Hoffman et al., 1998; Shields, 2005; Font et al., 2006; Knauth and Kennedy, 2009) and some of these models will be discussed in more detail in Section 1.2.

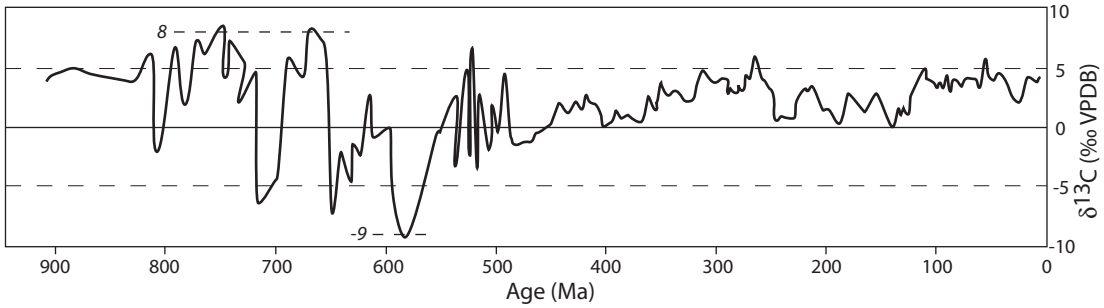

Figure 1.4. Carbon isotope variation from 900 Ma until present. Modified from Halverson et al. (2010) for the data 900-500 Ma and Prokoph et al. (2008) for 500-0 Ma.

1.1.4 Correlations Based on (Chemo)Stratigraphy

Regional and global correlations of Neoproterozoic sedimentary sequences are commonly based on the lithological and isotopic characteristics of these cap carbonates. The widespread occurrence of negative δ^{13}C anomalies has lead to the development of a Neoproterozoic composite carbon-isotope curve (Halverson et al., 2005, 2010) which is frequently used for assigning a Marinoan or Sturtian age to diamictite deposits. However, using this composite record is not without ambiguity as, according to the authors, it *"is incomplete and still poorly calibrated radiometrically*" (Halverson et al., 2005, p.1204).

An increasing number of cap carbonates with radiometric age constraints reveal a complex temporal distribution impeding global correlations of similar type deposits (Corsetti and Lorentz, 2006; Kendall et al., 2009). For example, the "Marinoan"-style cap carbonate of the Pocatello Formation (Idaho, USA) has a minimum age of 667±5 based on a SHRIMP zircon age for an overlying tuffaceous bed (Fanning and Link, 2004) while a similar cap carbonate on top of the Namibian Ghaub Formation has to be younger than an underlying tuff bed of 635±0.5 Ma (TIMS zircon, Hoffmann et al., 2004). U-Pb zircon and Re-Os black shale ages of "Sturtian"-type cap carbonates make their global correlation equally complex (Kendall et al., 2009).

Based on rare earth element (REE) patterns from carbonates Frimmel (2010) demonstrate the ambiguity of using carbon-isotope data for global chemostratigraphic correlation. REE patterns can be used as proxies for the water from which these rocks originated i.e. they can show whether the carbonate was deposited in a marine environment, from river water or by hydrothermal fluids. Only a few of several Neoproterozoic carbonate sections from southern Africa demonstrate an open seawater provenance, the dominantly riverborn REE patterns rather seem to reflect local facies variations (Frimmel, 2009). This casts doubt over the use of elements with similar residence times, such as carbon, for global stratigraphic correlations (Frimmel, 2010). Despite these issues isotopic profiles are still widely applied for stratigraphic correlations because the rather low number of radiometric datings prohibits a more robust correlation scheme for the Neoproterozoic sedimentary sections.

1.2 Models Proposed to Explain Neoproterozoic Low Latitude Glaciation

To explain the apparent low latitude origin of Neoproterozoic glaciomarine sediments and their stratigraphic association with warm water cap carbonates, various different models have been proposed in the literature. The most important models will now be discussed in more detail.

1.2.1 Snowball Earth Hypothesis

On the basis of robust palaeomagnetic data showing glacial rocks were deposited at low latitudes, Kirschvink (1992) argued for a global glaciation and called his model the Global Snowball Model (later renamed as the 'Snowball Earth Hypothesis', Hoffman et al., 1998). The model envisages global sea ice coverage for a considerable length of time (on the order of 10^6 years according to Hoffman and Schrag, 2002). It is primarily based on the fact that the presence of large portions of the continental land mass situated at low latitudes would have had a profound effect on climate. Continents are relatively good reflectors of solar radiation (high albedo) when compared to oceans (low albedo). If energy-reflecting

continents replace energy-absorbing oceans at latitudes where Earth receives most of its solar energy the global climate would gradually cool down. Furthermore, the ice-albedo feedback model of Budyko (1969) has demonstrated that, as soon as polar ice caps reach a critical latitude (∼35°, North et al., 1981) the combination of high albedo and low absorption will cause Earth to plummet into a global freeze.

Although global glaciation had been proposed earlier, the Snowball Earth Hypothesis for the first time provides a mechanism for getting out of such a situation. After polar ice caps reached the critical latitude (35°N) the Earth descended into a state of extreme cold for a long period of time during which geodynamic processes such as plate tectonics and volcanic activity would continue to bring greenhouse gases back into the atmosphere. The ice cover and extremely low temperatures would have severely disrupted the hydrological cycle removing important sinks for CO_2 (e.g. weathering of carbonate rocks) and allowing greenhouse gases to slowly accumulate with time. The greenhouse gas concentrations would eventually reach such high levels (approx. 300 times present day values) that ice would start to melt, resulting in a relatively fast escape from the snowball state. The Snowball Earth Hypothesis has since become the most popular model to explain late Neoproterozoic glacial deposits.

Hoffman et al. (1998) further developed the hypothesis by suggesting that this model could explain the unusual sequence of carbonates overlying glacial diamictites as well as the negative δ^{13}C isotopes. The ice cover would block out sunlight which would result in a shut down of photosynthetic life. Carbonates that precipitated from such an ocean would reflect the isotopic signature of carbon entering the ocean from the mantle which had a value of -5 to -7‰ (Des Marais and Moore, 1984). Using data from the Ghaub Formation in Namibia the large negative isotopic excursions were explained in terms of a Snowball Earth (Hoffman et al., 1998). Hoffman (1999) strengthened the arguments for the initiation of the Snowball Earth suggesting that the break-up of supercontinent Rodinia would increase continental margin area due to rifting, thus creating ideal environments for limestone building organisms (tropical, shallow water platforms). This would draw down atmospheric CO_2 thereby helping to reduce temperature. An ocean covered by sea ice would also become anoxic and rich in dissolved ferrous iron derived from continuous volcanic

activity at the mid-ocean ridges, which in turn would explain the occurrence of banded iron formations associated with Neoproterozoic diamictites in Canada, Brazil, Africa and Australia (Young, 1976; Urban et al., 1992; Martin, 1965; Lottermoser and Ashley, 2000).

While the Snowball Earth Hypothesis might explain the occurrence of glacial deposits and the associated carbonates at low latitudes, it leaves out the challenging question of how Neoproterozoic photosynthetic life survived under such environmental stress. A second problem is that the presence of exceptionally thick diamictites (up to several kilometres e.g. Hambrey and Harland, 1981; Eyles, 1993) can not be explained by an entirely frozen ocean and requires (locally) floating icebergs in an open marine environment (van Loon, 2008). This is consistent with results presented in numerical climate models which have difficulty predicting permanent ice cover at the equator and favour an at least partly open marine environment in the tropics (Hyde et al., 2000; Donnadieu et al., 2003; Pollard and Kasting, 2005). Global climate models have also shown that de-glaciation from a global glaciation requires unrealistic atmospheric carbon dioxide levels, even given the lack of CO_2 sinks in a hypothesised Snowball Earth event (Pierrehumbert, 2005, 2004; Le Hir et al., 2008; Abbot and Pierrehumbert, 2010). Another issue that remains problematic is the presence of terrigenous tillites (such as those preserved in West Africa) as the coupling of global climate models with ice-sheet models has shown that continental ice-sheets are not likely to build up during a snowball event due to effects of sublimation and a limited hydrological cycle (Donnadieu et al., 2003; Pollard and Kasting, 2004). Therefore, whilst the Snowball Earth Hypothesis might be able to explain some aspects of the Neoproterozoic glaciations it leaves a lot of questions unanswered. An important implication of this model is that all tillites must be synchronous.

1.2.2 High Obliquity Model

An alternative explanation for the occurrence of near-equator glacial deposits is that the Earth's rotation axis had acquired a high obliquity during the Proterozoic (Williams, 1993, 2000, 2008), shown schematically in Figure 1.5. When obliquity reaches >54° the annual temperatures at the equator will be lower than at the poles (Ward, 1974), resulting in preferential glaciation at low latitudes and ice-free poles. Modelling has shown that a high

obliquity could indeed result in glacial conditions at low latitudes (Jenkins, 2004; Abbot and Pierrehumbert, 2010).

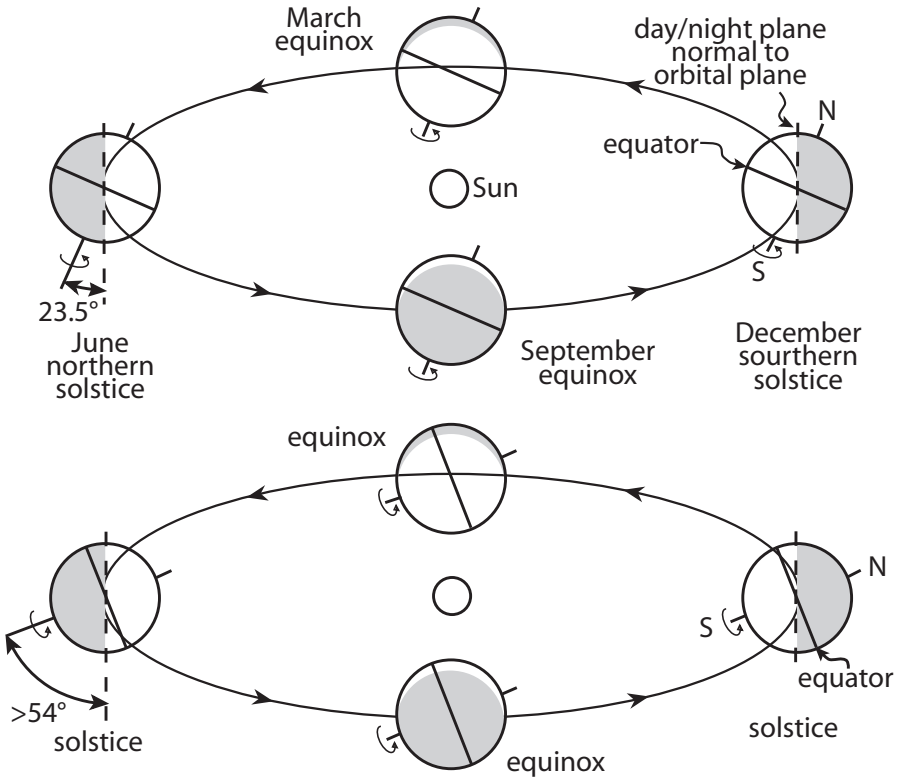

Figure 1.5. The Earth's orbit around the Sun with a present day obliquity (above) and a high obliquity (below), from Williams (2008).

Despite its ability to explain glacial rocks at low latitudes the High Obliquity Model raises some dilemmas. There is no known mechanism to suddenly change Earth's axis of rotation from the Proterozoic to the Cambrian (Néron de Surgy and Laskar, 1997; Pais et al., 1999; Levrard and Laskar, 2003), the model would involve strong seasonality around the equator and it would not be able explain the deposition of massive marine deposits and deposits at high latitudes such as the Squantum Tilloid at 55±8° and the Walsh Tillite at 45±12° (see Table 1.1). These issues were discussed by Williams (2008) who reviews all arguments for and against a so called 'High Obliquity, Low latitude Ice, STrong seasonality' (HOLIST) hypothesis. The model assumes a high obliquity was acquired during the Earth's early history after an impact also responsible for the formation of the Moon (Agnor et al., 1999). If the obliquity remained high for almost the entire Precambrian, it would explain the two Cryogenian ice ages (Sturtian and Marinoan). In this model the Ediacaran (Gaskiers)

ice age represents a transition between different glacial styles going from a Precambrian low latitude style to the Phanerozoic style. Indeed Ediacaran diamictites seem to have occurred predominantly at middle to high (>45°) palaeolatitudes (Hoffman and Li, 2009) suggesting a change with respect to pre-Ediacaran glacial styles.

It is hard to imagine how the wide-spread occurrence of warm water carbonates can be explained when each part of the Earth is turned away from the Sun for a substantial part of the year (Fig. 1.5). Seasonality would be strong in this model since the equator would be relatively warm twice a year around the equinoxes. Williams (2008) argues seasonality is expressed by the strong lamination that is found in many cap carbonates. Between the Marinoan and the first circum-polar glaciation during the Late Ordovician the Earth's obliquity had ca. 200 Ma to return to its modern day value of 23.5° (Williams, 2008). However, the processes that would reduce the obliquity are still not well understood (Néron de Surgy and Laskar, 1997; Williams et al., 1998; Pais et al., 1999). In the HOLIST model a slow, progressive change in obliquity is suggested which could be achieved by global mass distribution on the Earth's surface leading to a change in the rate of spin-axis precession. Williams (2008) suggests that true polar wander (TPW), a concept that assumes rearrangement of the entire Earth's lithosphere with respect to its axis of rotation and which is still heavily debated (Kirschvink et al., 1997; Meert, 1999; Torsvik and Renström, 2001; Maloof et al., 2006; McCausland et al., 2007), may provide a mechanism of reducing the Earth's obliquity.

1.2.3 Sedimentological Model: Zipper-rift

The glacial origin of the Neoproterozoic diamictites has often been challenged (e.g. Schermerhorn, 1974a; Deynoux and Trompette, 1976; Eyles and Januszczak, 2004; van Loon, 2008). In their 'Zipper-rift' model, Eyles and Januszczak (2004) reinterpreted the majority of Neoproterozoic diamictites as gravity induced flow deposits related to rifting of supercontinent Rodinia. They claimed that the hypothesis of global glaciation is largely based on the misinterpretation of sedimentary sequences and that most of the glacial deposits are actually Alpine in origin. The model also discounts all the palaeomagnetic data by contesting either the quality of the data or the age of magnetisation. Even the very reliable

results from the Australian Elatina Formation are questioned (Eyles and Januszczak, 2004, p22).

It is indeed very difficult to distinguish glaciomarine sediments from deposits that have been influenced by e.g. Alpine-style glaciers. Along the western margin of the Congo Craton for example, the West Congolian Group contains two diamictite horizons whose origin has been the subject of much debate: both the Lower and the Upper Diamictite Formations have at various times been interpreted as true glacio-marine diamictites (Kröner and Correia, 1973), as glacially influenced diamictites (incorporating reworked deposits from mountain glaciers, Schermerhorn, 1974b) or as tectonically related gravity flow deposits (Cahen and Lepersonne, 1981a; Trompette, 1994).

Micro-structural and -textural analyses of diamictite rocks can provide important constraints on the mechanism of deposition. The overburden pressure caused by an ice cover can create structures of deformation which can be identified at microscopic level (van der Meer, 1993, 1997; Benn and Evans, 1996; Menzies, 2000; van der Meer et al., 2003; Menzies et al., 2006; Phillips et al., 2007). This is a technique that is not widely applied to Neoproterozoic rocks but can successfully be used to differentiate glacial from glacially influenced sediments as has recently been demonstrated for the Neoproterozoic diamictites of the Democratic Republic of Congo (DRC) (e.g. Delpomdor, 2007; Delpomdor et al., 2008). In the DRC, many of the diamictites lack obvious indicators such as striated clasts and glacial pavements that suggest a sub-glacial environment. On the microscopic level, however, grain edge-to-edge crushing, strain shadows, necking structures, shear zones and water escape structures suggest these diamictites were deposited in water-saturated sediments under high strain rates with moderate to high stress conditions (Delpomdor et al., 2008, 2009; Tait et al., 2011). The cumulative evidence suggests that these diamictites were deposited in proximal sub-glacial and/or subaqueous environments. Distinguishing glacial from gravity induced sediments is essential for testing the Zipper-rift model.

1.2.4 The non-GAD Hypothesis: the Magnetic Field in Precambrian Times

The geocentric axial dipole (GAD) hypothesis is the fundamental principle underlying palaeomagnetic studies. In this model, the averaged geomagnetic field resembles that produced by a magnetic dipole aligned with the rotation axis of the Earth. According to the dipole equation there is a direct relationship between the inclination of the magnetic field (I) and latitude (λ): $tanI = 2tan\lambda$. Inclination varies between +90° and -90° at the geographic north and south pole respectively and is 0° at the equator.

The proposed near-equatorial latitude of Neoproterozoic glacial deposits is primarily based on palaeomagnetic evidence, that leans heavily on the assumption that the geomagnetic field has behaved uniformly during Earth's history. In the non-GAD model, large non-dipole contributions to the ancient geomagnetic field could result in low inclinations at intermediate latitudes invalidating the relationship between inclination and palaeolatitude described above.

Analyses of recent magnetic records have been used to test the GAD hypothesis and based on these results and on geometrical reconstructions it has been validated for most of the Phanerozoic Eon (Kirschvink, 1978; Smith, 1997). For Pre-Pangaean times this model can be tested using the distribution of climatically sensitive sediments. Palaeomagnetic data from evaporites, which are typically restricted to a narrow latitude band between 15 and 35°, show that their palaeolatitudes have not changed significantly from the start of the Proterozoic (Evans, 2006). This demonstrates that the geomagnetic field appears to have been dominated by an axially symmetric dipolar field for times as far back as ∼2.5 Ga. Studies looking at characteristics of the ancient geomagnetic field such as intensity, secular variation and the symmetry of reversals strengthen the GAD assumption and justify the use of palaeomagnetic data for Precambrian times (Biggin et al., 2009; Tauxe and Kodama, 2009; Swanson-Hysell et al., 2009). Of course, assumptions on timing of magnetisation and how reliably the rock magnetisation represents that of the ancient geomagnetic field will need to be evaluated using palaeomagnetic and rock magnetic tests.

1.3 Aims of thesis

As all climate models described above are dependent on palaeogeography it is of vital importance to understand the distribution of the continents during the Neoproterozoic. The Snowball Earth Hypothesis requires most continental land mass to be positioned at low latitudes and glacial deposits to be globally synchronous, the High Obliquity Model would be invalidated by high latitude deposits. Our understanding of the distribution of continental crust for this period is severely hampered by the lack of available data. Palaeomagnetic data indicate a predominantly low latitude for Precambrian glacial deposits (see also Evans, 2003) but unfortunately, as already discussed, the Neoproterozoic data are low in quantity and quality (see Fig. 1.2). For some cratons (e.g. West Africa) there is a complete lack of reliable data during the late Neoproterozoic.

The aim of this project is to resolve long lasting uncertainties concerning the palaeogeography of the Congo Craton and the West African Craton in the Neoproterozoic (Fig. 1.1). This thesis provides a detailed examination of tillite bearing Neoproterozoic sedimentary sequences from these two cratons. The Congo Craton and the West African Craton were covered by two of the largest known Neoproterozoic sedimentary basins and both cratons took part in West Gondwana amalgamation during the late Neoproterozoic and early Palaeozoic (Trompette, 1994; Goodwin, 1996). A review of their Proterozoic tectonic evolution will be given in Chapter 2.

The Congo Craton hosts many Neoproterozoic sedimentary sections that contain one or two diamictite levels (Cahen, 1982). Correlating these diamictites across the craton has proven to be difficult due to large unexposed distances between them and the lack of reliable geochronological constraints. The West Congolian Group, the focus of this study, is exposed along the western margin of the Congo Craton and contains the reported glaciogenic Lower and Upper Diamictite formations (Cahen and Lepersonne, 1981a). The regional geology, largely studied in the 1960's and 1970's, records the development of a passive margin and has strong links with Neoproterozoic belts on the São Francisco Craton in northern Brazil (Pedrosa-Soares et al., 2008). Geochemical, geochronological and chemostratigraphic data for the West Congolian Group are extremely limited or absent

(Tack et al., 2001; Frimmel et al., 2006; Poidevin, 2007). A detailed analysis of the stratigraphy, provenance and geochemistry of the West Congolian Group sediments is presented in Chapter 4 where the sedimentary rocks are characterised by whole rock geochemistry and detrital zircon geochronology. This provides the framework for correlating alleged glacial rocks from across the Congo Craton to the Lower and Upper Diamictite formations. Of particular importance is the presence of Namibian diamictites along the southern margin of the Congo Craton which form the basis on which Hoffman et al. (1998) build their arguments for the Snowball Earth Hypothesis. Chapter 4 also includes a chemostratigraphic profile of stable carbon isotopes and a U-Pb TIMS baddeleyite age for a volcanic unit associated with the Lower Diamictite Formation. All analytical techniques and methods are described in Chapter 3.

The Precambrian palaeomagnetic database for the Congo Craton is extremely poor which is hampering Proterozoic palaeogeographic reconstructions. A palaeomagnetic study of the Neoproterozoic strata of the West Congolian Group is presented in Chapter 5. Along with contributing to the apparent polar wander path of the Congo Craton, results from the Lower and Upper Diamictites and associated rocks will help to constrain the depositional palaeolatitude of these glaciogenic units.

The West African Craton is largely covered by the Mesoproterozoic to Mesozoic Taoudéni Basin (Deynoux et al., 2006). This basin contains a Neoproterozoic tillite which, as part of the three-part 'triad' sequence, has been found and correlated all along its boundaries and is clearly recognised as a terrestrial glacial deposit (Deynoux, 1980). The Adrar sub-basin holds the type locality for the Taoudéni basin (Trompette, 1973) and records almost continuous deposition throughout the Neoproterozoic, a time during which the palaeogeography of West Africa is poorly constrained. A provenance analysis of Adrar sedimentary rocks is carried out to constrain the tectonic evolution of the Taoudéni basin as well as the connections of West Africa with surrounding cratons during the Neoproterozoic. The results are presented in Chapter 6.

Finally a summary is presented in Chapter 7 integrating the results from these two African cratons.

Chapter 2

Proterozoic Palaeogeography and Supercontinents

2.1 Introduction

Defining supercontinent palaeogeographies is important for understanding the mechanisms of continent recycling and more generally the geological evolution of the Earth's surface (Condie, 2002b). A supercontinent forms when most of the continental crust collides to form a single landmass. The most recent supercontinent Pangea was formed during the Palaeozoic by the assembly of Gondwana (which roughly consisted of Africa, South America, East Antarctica, India and Australia) and Laurasia (Laurentia and Eurasia) (Lottes and Rowley, 1990; Rogers, 1996). Reconstruction of these assemblies is to a large extent based on sea floor magnetic data and biostratigraphic comparisons. Clearly these techniques are restricted to the Phanerozoic Eon, making Precambrian (supercontinent) reconstructions more complicated and different techniques have to be used.

The existence of various Proterozoic supercontinents has been proposed on the basis of geological correlations and palaeomagnetic studies (e.g. Condie, 2002a; Rogers and Santosh, 2002; Pesonen et al., 2003). Purely based on palaeomagnetic data Piper (1982) proposed the existence of a Proterozoic supercontinent, possibly from around 2600 Ma (Piper, 1976,

1982, 1987). The palaeomagnetic support for this model has been questioned (e.g. Van der Voo and Meert, 1991) and many of the early palaeomagnetic results do not pass basic reliability criteria (Van der Voo, 1990) making them unsuitable for testing tectonic models. Hoffman (1989) used geological evidence to postulate the existence of a Palaeoproterozoic supercontinent and suggests that it aggregated around 2.0 – 1.8 Ga. Subsequent recognition of coeval collisional belts on several cratons resulted in widespread support for this idea although differences in exact configurations exist (e.g. Windley, 1995; Rogers, 1996; Condie, 2002a; Rogers and Santosh, 2002, 2003; Zhao et al., 2002a, 2004). Reliable palaeomagnetic constraints are low in quantity but are in agreement with formation and existence of this supercontinent (Meert, 2002; Pesonen et al., 2003). A popular model is that of supercontinent Columbia by Rogers and Santosh (2002) who suggest that it formed after amalgamation of three pre-existing continents (see Figure 1.1 for the distribution of Precambrian crust): Arctica (Laurentia and Siberia) incorporated Baltica to form Nena; Kalahari, India and Australia formed a continent named Ur; South America, connected to West Africa and Congo is called Atlantica (Rogers, 1996). These “palaeo-continents" are suggested to have survived more than one supercontinental cycle and remained intact during fragmentation of Columbia around 1.5 Ga (Condie, 2002a). Reorganisation of these palaeo-continents led to the formation of another supercontinent named Rodinia between ca. 1.3 and 1.0 Ga (Moores, 1991; Hoffman, 1991; Dalziel, 1991; Rogers and Santosh, 2002; Li et al., 2008).

Neoproterozoic palaeogeographic reconstructions are dominated by models for the formation and subsequent breakup of this supercontinent Rodinia, reconfiguration of the constituents and the amalgamation of Gondwana (ca. 530 Ma). Over the years a variety of Rodinia models have been presented. The first geological models were based on the recognition and correlation of ca. 1.0 Ga orogenic belts found on Australia, Antarctica and Laurentia (Moores, 1991; Hoffman, 1991; Dalziel, 1991). These belts are called “Grenvillian” after their archetype, the Grenville Belt in eastern Canada (Gower, 1996). Some workers have used palaeomagnetic data to support geologically based reconstructions or have fully integrated palaeomagnetism with stratigraphical, geochronological and tectonic constraints (e.g. Weil et al., 1998; Piper, 2000; Pisarevsky et al., 2003; Li et al., 2008; Evans, 2009). Several of these Rodinia models will be discussed in Section 2.2 below.

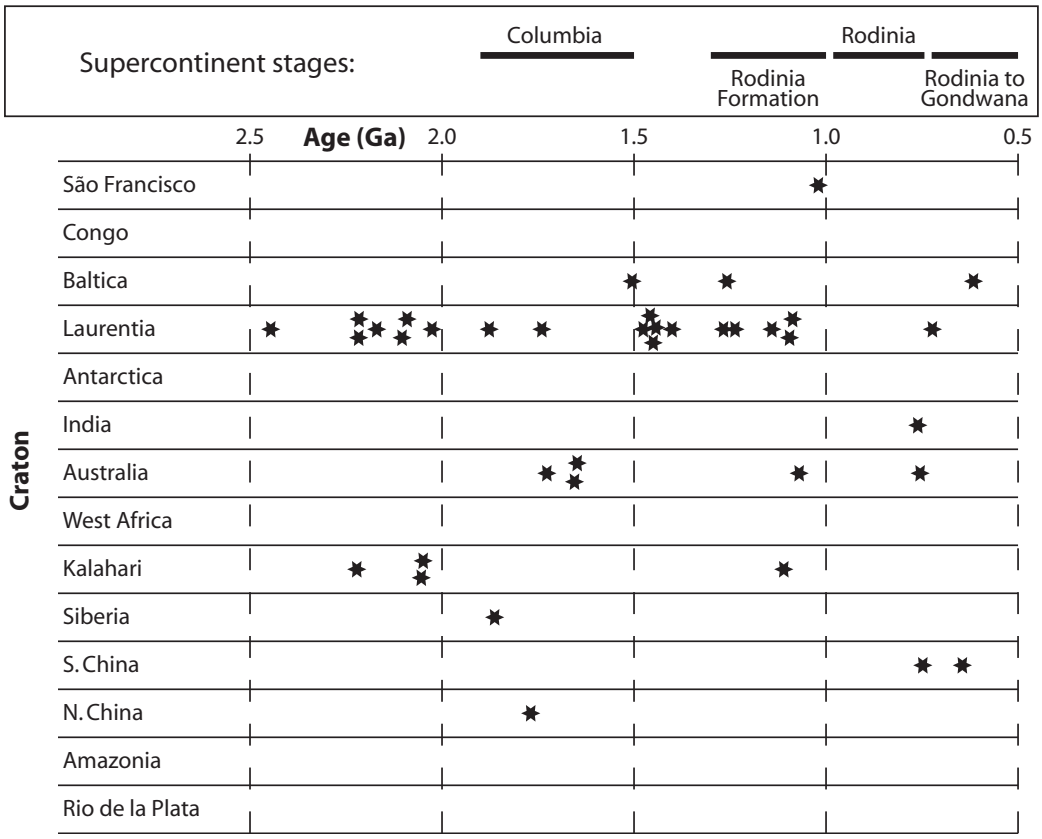

Figure 2.1. Stars indicate the ages of key palaeomagnetic poles for each craton. Key poles were extracted from the Global Palaeomagnetic Database v. 4.6 (Dec. 2004) complemented with recently published data, all compiled in a spreadsheet at the Sixth Nordic Paleomagnetic Workshop, Luleå (Sweden), Sept. 15-22, 2009 (S. Pisarevsky, pers. comm.). The times for the different stages of Columbia and Rodinia are from Rogers and Santosh (2002) and Li et al. (2008) respectively.

With the lack of sea floor spreading data for the Proterozoic, palaeomagnetism in conjunction with high quality radiogenic geochronology is the only method to quantify palaeolatitudes and continental movement. However, the quality and quantity of Proterozoic palaeomagnetic data is often insufficient to test supercontinental configurations. Of invaluable importance for palaeomagnetic reconstructions are so called "key palaeopoles": poles that pass a set of reliability criteria and are also precisely dated. For Precambrian rocks, precise dating can be established by U-Pb or ^{40}Ar-^{39}Ar age determinations and minimum requirements for key poles are discussed by Buchan et al. (2000) who say that age uncertainties should be less than ±20 Ma (at a 95% confidence level). ±20 Ma would equate to a palaeogeographic uncertainty of ±1000km, if a typical Cenozoic plate velocity of 5cm/yr is assumed.

Reliability criteria for the palaeomagnetic data are following Van der Voo (1990). In conjunction with the emplacement/depositional age requirements it must be demonstrated that the palaeomagnetic data are primary by passing a field test such as a baked contact test, a foldtest or a conglomerate test. Further criteria require proper isolation of palaeomagnetic remanence by either thermal or alternating field demagnetisation procedures, a sufficient number of specimen with a satisfactory statistical precision to show that secular variation has been averaged out, structural control should be demonstrated and where appropriate results should be corrected for bedding tilt. When these criteria are applied to all published Proterozoic poles the Laurentia Craton appears to be constrained by 20 key poles while 18 key poles exist for all other cratons together. This is illustrated in Figure 2.1 from which it is clear that many cratons are still unconstrained for long periods of time. Critical times for which more key poles are desperately needed are for example 1.2 – 1.0 Ga (Rodinia formation) and 0.8 – 0.5 Ga (Rodinia breakup and Gondwana amalgamation).

2.2 Rodinia Reconstructions

The Laurentia Craton has played a key role in models for Rodinia following Bond et al. (1984) who interpreted Neoproterozoic tectonic subsidence curves from around the craton margins to suggest simultaneous rifting and formation of passive margins as the result of a supercontinent breaking up. As indicated in Figure 2.1, Laurentia is the only craton with a reasonably well established polar wander path, allowing comparisons of contemporaneous palaeopoles from other cratons. The first Rodinia models placed the southwestern Laurentian margin adjacent to East Antarctica, the so called SWEAT hypothesis (South-West U.S. – Antarctica; Moores, 1991). It is primarily based on geological correlations of the western cordillera of North America with the Pacific margin of the East Antarctica craton and has been the central idea of many subsequent Rodinia reconstructions (Hoffman, 1991; Dalziel, 1991, 1997; Weil et al., 1998, Figs. 2.2a, b and c). An alternative model to SWEAT places Australia adjacent to southwestern Laurentia and was based on the alignment of several rift-transform fault systems on both cratons (Brookfield, 1993). This configuration was later called AUSWUS (Australia – Western U.S.; Karlstrom et al., 1999; Burrett and Berry, 2000, not shown in Fig. 2.2) and it was shown that in this configuration the Aus-

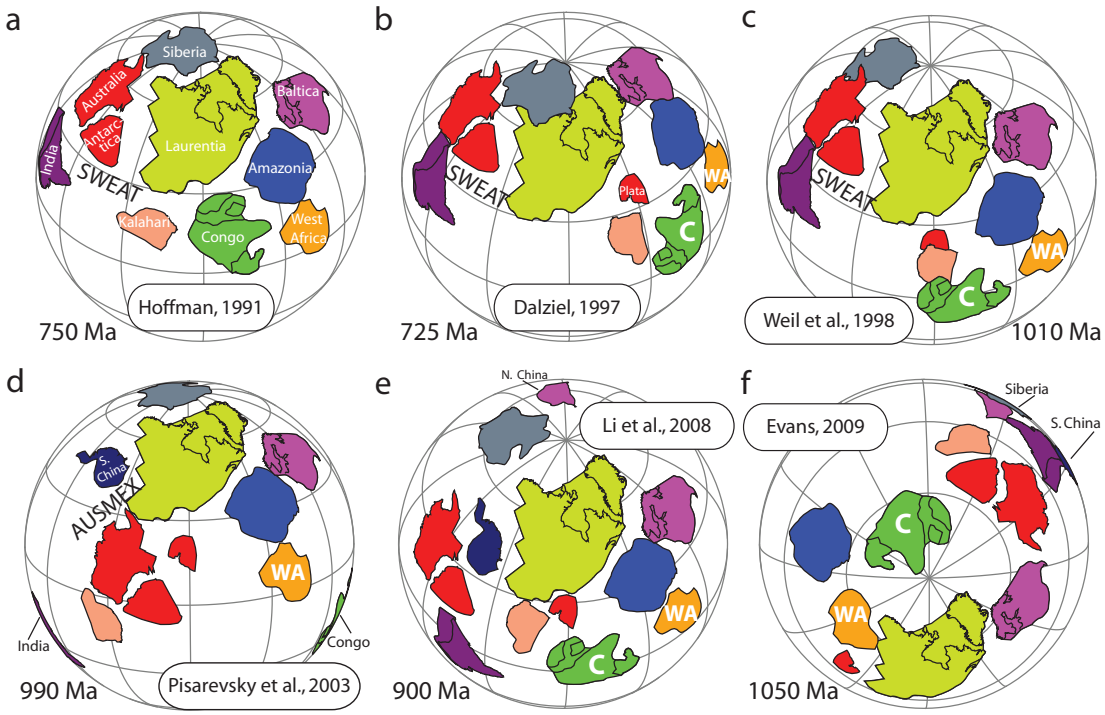

Figure 2.2. Maps for Rodinia according to different models described in the text, all in a North American reference frame. The outlines of the cratons are modified after Li et al. (2008). Reconstructions are made using GPLATES software.

tralia and Laurentia cratons could potentially share a tectonic history from 1.8 Ga until rifting around 0.8 Ga (Karlstrom et al., 2001). Both the SWEAT and the AUSWUS models, however, appeared to disagree with a new, 1070 Ma palaeomagnetic key pole for Western Australia which led to the proposed AUSMEX (Australia – Mexico) connection (Wingate et al., 2002). This fit is palaeomagnetically sound and still allows for most of the geological correlations that were part of the previous models. The AUSMEX fit is adopted by Pisarevsky et al. (2003) in Figure 2.2d.

The role of the Congo Craton and West Africa (i.e. the cratons that form the focus of this study) in Rodinia is still a matter of debate. Evidence from both cratons to support or deny Rodinia participation will be discussed below.

2.2.1 Congo Craton in Rodinia

The Congo Craton consists of several tectonic blocks of Archaean age which amalgamated during the Mesoproterozoic (Fig. 2.3). The Angola-Kasai Block, the NE Congo-Uganda block and the Cameroon-Gabon-São Francisco Block are connected through the Kibaran Belt with the Tanzania Block and the Bangweulu Block (Hanson, 2003). Peak compressional tectonism in the Kibaran Belt suggests the Congo Craton was assembled at ca. 1.38 Ga (Kokonyangi et al., 2004; De Waele et al., 2008; Tack et al., 2010). The basement structure of the Congo Craton to the west of the Kibaran Belt remains poorly understood due to an extensive (up to 9km thick) Phanerozoic cover. Subsurface seismic surveys have identified a failed Proterozoic rift as the main basin forming structure which has been the site of almost continuous sedimentation from the Cambrian until present day (Daly et al., 1992). Prior to opening of the Atlantic ocean in Cretaceous times, the São Francisco Craton in northern Brazil was connected to the Congo Craton, a continental link that has existed since the Palaeoproterozoic Era (Brito Neves et al., 1999; Alkmim et al., 2001; Pedrosa-Soares et al., 2008).

The Congo Craton has at various times been assumed to be part or separated from Rodinia. Based on age comparisons of the Kibaran and Irumide belts (Fig. 2.3) with the Grenvillian type mobile belt system in Amazonia and Laurentia the Congo was considered to be part of Rodinia in the reconstruction of Hoffman (1991, Figure 2.2a). But it is not evident whether or not the Kibaran and Irumide belts represent Rodinia related late Mesoproterozoic tectonics (e.g. De Waele et al., 2008) and their evolution will now be discussed in more detail.

The Kibaran Belt has been subject to several interpretations: it has been suggested to have developed from intracontinental basins that were deformed in response to far-field stresses (e.g. Klerkx et al., 1987; Pohl, 1994; Tack et al., 2010), or due to collisional tectonics (e.g. Kampunzu, 2001; Kokonyangi et al., 2006). The major problem with linking the belt to Rodinia related collision is that Kibaran tectonism (at 1.38 Ga) pre-dates most Rodinia accretionary belts by ca. 200 Ma (Kröner and Cordani, 2003). Late Mesoproterozoic compressional tectonism is, however, recorded along the southern margin of the Congo Craton

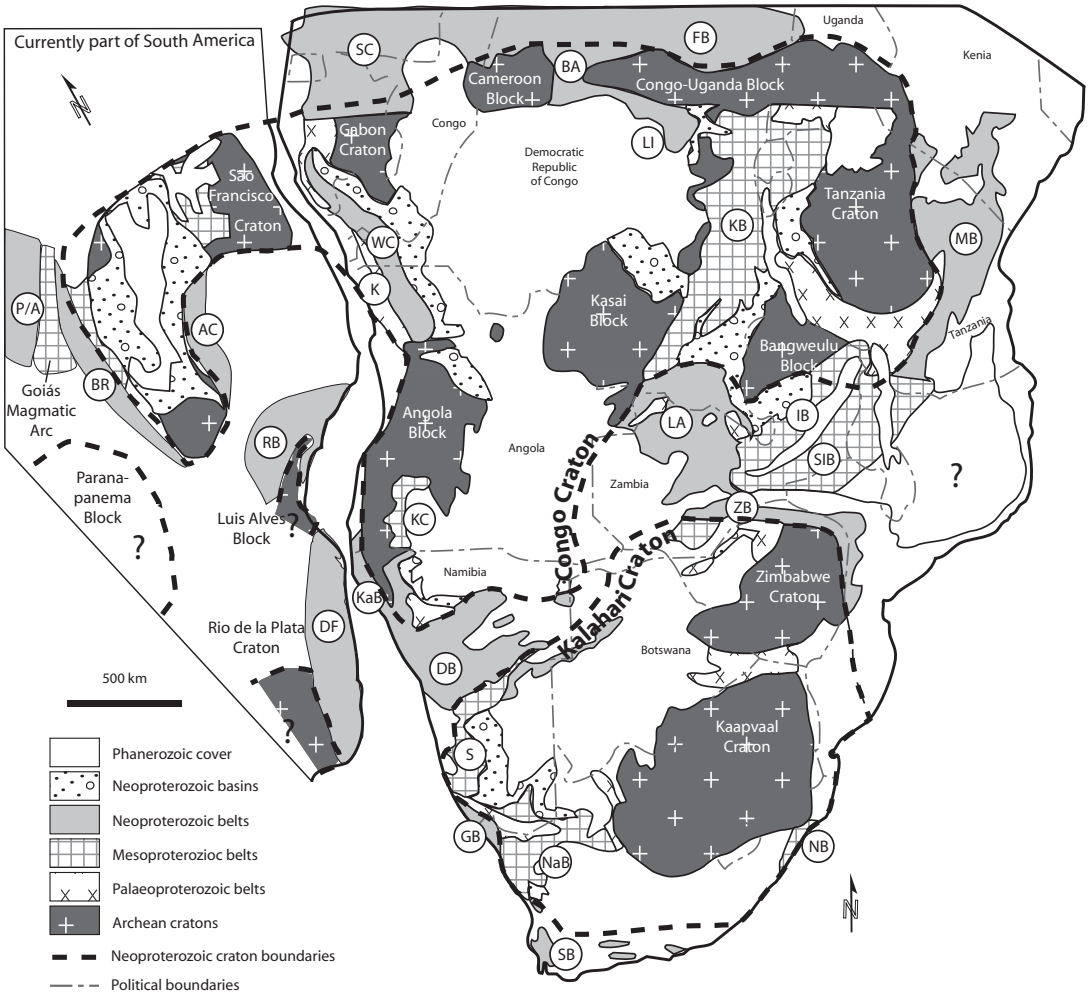

Figure 2.3. Geological sketch map of southern Africa, modified after Hanson (2003); Basei et al. (2008); Tait et al. (2011). AC, Araçuaí Belt; BA, Bangui Belt; BR, Brasília Belt; DB, Damara Belt; DF, Dom Feliciano Belt; FB, Fouroumbala-Bakouma Belt; GB, Gariep Belt; IB, Irumide Belt; K, Kimezian; KaB, Kaoko Belt; KB, Kibaran Belt; KC, Kunene Complex; LA, Lufilian Arc; LI, Lindian Belt; MB, Mozambique Belt; NaB, Namaqua Belt; NB, Natal Belt; P/A, Paraguay-Araguaia Belt; RB, Ribeira Belt; S, Sinclair; SB, Saldania Belt; SC, Sergipe-Central African Belt; SIB, Southern Irumide Belt; WC, West Congo Belt; ZB, Zambezi Belt.

in the Irumide Belt (Fig. 2.3) where peak metamorphism at 1.05 – 1.02 Ga is determined through the dating of zircon rims and high-K granite intrusions (Johnson et al., 2005; De Waele et al., 2008). The southern part of the Irumide Belt, referred to as the 'Southern Irumide Belt', underwent a separate tectonic history and lacks evidence for this late Mesoproterozoic compressional tectonism (De Waele et al., 2008). It comprises calc-alkaline mafic to felsic gneisses and metavolcanic rocks whose trace element geochemistry indicate formation in a continental-arc tectonic setting (Oliver et al., 1998; Johnson and Oliver, 2000, 2004; Johnson et al., 2006, 2007b). Magmatic emplacement ages are constrained between ca. 1095 and 1040 Ma (Johnson and Oliver, 2004; Johnson et al., 2005) which means they pre-date peak metamorphism in the Irumide Belt to the north. De Waele et al. (2008) suggest that the Southern Irumide Belt represents the active margin of a microcontinent that accreted to the Congo Craton resulting in compression in the Irumide Belt. Subduction-related magmatism continued after accretion which is demonstrated by 1040 – 999 Ma calc-alkaline granitoids and gneisses in northern Mozambique where ε_{Nd} isotopes indicate a continental-margin-arc-type setting (Kröner, 2001). These magmatic rocks, in addition to the lack of evidence for Mesoproterozoic compressional tectonism in the Southern Irumide Belt, indicate that this margin was facing an open ocean rather than a large continent at ca. 1.0 Ga (Goscombe et al., 2000; Johnson et al., 2006, 2007a; De Waele et al., 2008). No Grenvillian age rocks have as yet been recorded further along the eastern and northern margins of the Congo Craton (Kröner and Cordani, 2003).

Dalziel (1997) placed the Congo Craton with its western margin towards Laurentia (Fig. 2.2b) with the Kalahari and Congo cratons in their Gondwana-type configuration. This was based on the suggestion that the Zambezi Belt between the Congo and Kalahari is an intracratonic belt (Dalziel, 1997) and the two cratons have been connected since the Mesoproterozoic. This assumption is contradicted by evidence from both the Lufilian Arc and the Zambezi Belt which points to the existence of a Neoproterozoic ocean between these two cratons. First, two phases of extensional tectonism are recognised along this margin which led to the development of an extensive passive margin (Porada and Berhorst, 2000; Johnson et al., 2007a). The first phase is characterised by felsic volcanics with isotopic signatures recording continental extension which occurred between 880 and 820 Ma (U-Pb zircon ages, Johnson et al., 2007a). The start of a second phase is marked

by 765±5 Ma mafic volcanic rocks (zircon U-Pb SHRIMP, Key et al., 2001) overlain by a passive margin type sedimentary sequence (Porada and Berhorst, 2000). Sedimentation continued until subduction of oceanic crust resulted in closure of the basin separating the Congo and Kalahari cratons. This subduction is dated by a Sm-Nd isochron age of 595±10 Ma for eclogite facies metamorphism in the Zambezi Belt (John et al., 2003). A second indication for a Neoproterozoic oceanic basin comes from pressure-temperature estimates of these eclogites: a low geothermal gradient was established in this suture zone implying the existence of a cold subducted lithosphere and a relatively large (>1000km) associated oceanic basin (John et al., 2003). U-Pb monazite dating shows that following 595 Ma subduction the final continental collision occurred at ca. 530 Ma (John et al., 2004).

Following the cratonic margin further westward from the Lufilian Arc, the Damara and Kaoko belts record Neoproterozoic collisional tectonism (Fig. 2.3). They are related to closure of the Adamastor Ocean which separated the Congo-São Francisco, Kalahari and Rio de la Plata cratons. These cratons collided during the amalgamation of West Gondwana and related tectonic belts in South America are the Dom Feliciano and the Ribeira Belt extending along the Atlantic coast of Uruguay and Brazil (Trouw et al., 2000; Goscombe et al., 2005; Gray et al., 2008; Oyhantcabal et al., 2009). None of these belts contain evidence of late Mesoproterozoic high-grade metamorphism (Kröner and Cordani, 2003). The western border of the Congo-São Francisco craton shows evidence of a protracted collision with the Goiás Magmatic Arc (central Brazil, Fig. 2.3). This arc comprises calc-alkaline granitoid orthogneisses and is interpreted as a collage of juvenile, intra-oceanic island arcs that formed between ca. 940 – 620 Ma and collided with the western margin of the São Francisco craton around 650 Ma (Pimentel et al., 2000; Cordani et al., 2003). The existence of the Goiás Arc implies that the western margin of the São Francisco Craton was separated from Amazonia by the Goás Ocean at least since 940 Ma. On the eastern side of the São Francisco Craton, evidence for late Mesoproterozoic and early Neoproterozoic limited rifting is found in the orogenic belts separating it from the Congo Craton. On the São Francisco cratonic margin evidence is limited to the intrusion of 1200 – 1000 Ma mafic dykes in the north of the Mesoproterozoic Espinhaço basin (NE Brazil, Renne et al., 1990; Danderfer et al., 2009). The western margin of the Congo Craton, however, contains early Neoproterozoic bimodal, rift-related volcano-sedimentary sequences (the 1000 – 910

Ma Zadinian and Mayumbian Groups of the West Congo Belt, Tack et al., 2001). These rocks record the development of a relatively restricted oceanic basin (Pedrosa-Soares et al., 1998; Pedrosa-Soares and Wiedemann, 2000; Tack et al., 2001) and are overlain by the West Congolian Group sedimentary sequence which is the focus of Chapter 4. The closure of this aulacogen-type structure during the late Neoproterozoic resulted in the formation of the Araçuía and West Congo orogenic belts (Alkmim et al., 2006).

All these belts surrounding the Congo-São Francisco Craton show little evidence for, or even contradict, late Mesoproterozoic compressional tectonism and it seems unlikely that it formed part of Rodinia. The craton rather appears to be separated by the Goiás, Adamastor and Zambezi oceans from the Amazonian, Rio de la Plata and Kalahari cratons respectively, until these basins closed during amalgamation of West Gondwana in the second half of the Neoproterozoic (Cordani et al., 2003).

Rodinia reconstructions at least partly based on palaeomagnetic data also question whether Congo was part of Rodinia (Weil et al., 1998; Pisarevsky et al., 2003, Figs. 2.2c and d). Combining geological evidence with palaeomagnetic results led Pisarevsky et al. (2003) to suggest a scenario where the Congo Craton was independent from Rodinia (Fig. 2.2d). The authors constrain the Congo Craton using two palaeopoles at 795 and 748 Ma (Meert et al., 1995). Both poles require separation of the Congo from Laurentia and similarly ca. 1080 – 1020 Ma palaeomagnetic data from the São Francisco Craton require separation from Laurentia (D'Agrella-Filho et al., 2004). Despite these results Li et al. (2008) propose that the Congo was part of Rodinia from ca. 1000 Ma. In this model (Fig. 2.2e) the craton is placed with its south-east margin facing Laurentia following Hoffman (1991)'s geologically based reconstruction. According to Li et al. (2008) the 750 Ma passive margin development in the Lufilian Arc is proof of rifting from Rodinia. This is contradictory to the palaeomagnetic poles for the Congo Craton that require separation before ca. 800 Ma, however, reliability of these two poles could be questioned given the lack of field tests constraining the magnetisation age. The reliability of these and all other Neoproterozoic palaeopoles for the Congo Craton is discussed in Chapter 5.

2.2.2 West Africa in Rodinia

The West African Craton has formed a stable cratonic entity since a period of tectonic amalgamation around 2.0 Ga. After that the craton provides no evidence for any major tectonothermal event until formation of Gondwana in the late Neoproterozoic (Deynoux et al., 2006). Most of the margins of the West African Craton are marked by mid Neoproterozoic rifting but these events seem to be back-arc type rifts that briefly opened and closed on themselves rather than record large continental break-up (Rogers, 1996). Palaeomagnetic data from West Africa are absent (for the Mesoproterozoic) or unreliable (Neoproterozoic). A detailed discussion of the geology of the craton is given in Chapter 6.

If West Africa was part of Rodinia it would have had a passive role as part of a larger craton. Following the suggestion of Rogers (1996) for the existence of Mesoproterozoic Atlantic, West Africa could have been part of a stable continent from 2.0 Ga until incorporation in Gondwana (Trompette, 1994; Rogers and Santosh, 2002). This long term stability however remains to be confirmed (Zhao et al., 2006). In the majority of Rodinia reconstructions the West African Craton has been connected to Amazonia, based on the idea of Trompette (1994) and similar to their fit in West Gondwana (as shown in Figs. 2.2a-e, Hoffman, 1991; Dalziel, 1997; Weil et al., 1998; Pisarevsky et al., 2003; Li et al., 2008).

Recently, a completely revised model for Rodinia was proposed by Evans (2009) positioning the Congo Craton to the north and Amazonia west of Laurentia with West Africa filling in a gap between Amazonia and Laurentia (Fig. 2.2f). The Congo-Laurentia connection would have lasted from 1235 to 755 Ma with a loop in their polar wander path between 800 and 750 Ma to account for palaeomagnetic poles from the Congo Craton. The position of West Africa implies a more active role for which evidence remains to be found. The author has subsequently confirmed that the position of the Congo Craton in this model is untenable and more (palaeomagnetic) data are needed to test these models (J. Tait, pers. comm.).

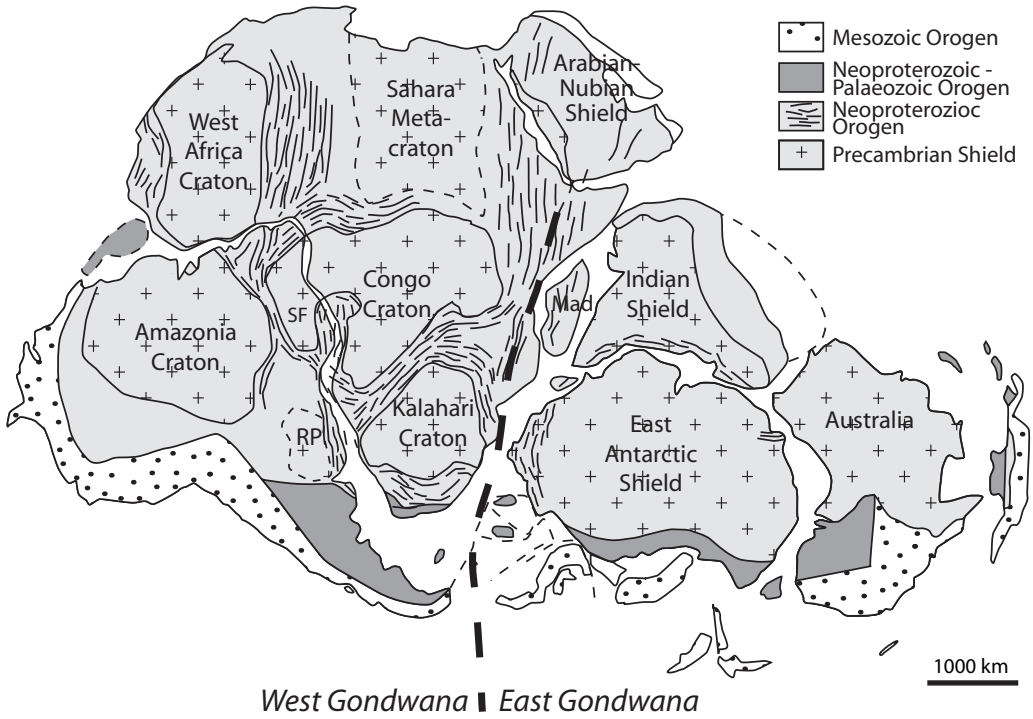

Figure 2.4. Map of Gondwana showing the positions of the cratonic nuclei (modified after Gray et al., 2008). RP, Río de la Plata Craton; SF, São Francisco Craton.

2.3 Gondwana Configuration

Although different models exist for the absolute position of Gondwana (see e.g. Pisarevsky et al., 2008) the relative positioning of cratons can be done with small margins of error (Fig. 2.4; Eagles, 2007; de Wit et al., 2008). The formation of Gondwana is often presented as a merger of East Gondwana (Antarctica, Australia, India) with West Gondwana (those currently in Africa and South America). Evidence especially from the eastern Gondwana cratons, however, indicates that it was not a simple unification of two halves, but rather a poly-phase amalgamation of cratons during the waning stages of the Proterozoic that led to the formation of Gondwana (see discussion by Meert and Lieberman, 2008). Nevertheless, the terms West and East Gondwana remain widely used in the literature in reference to the two groups of cratonic nuclei (Fig. 2.4).

The Congo and West Africa cratons both form part of West Gondwana and are connected through the Borborema Province in northern Brazil (Fig. 2.5). This province is

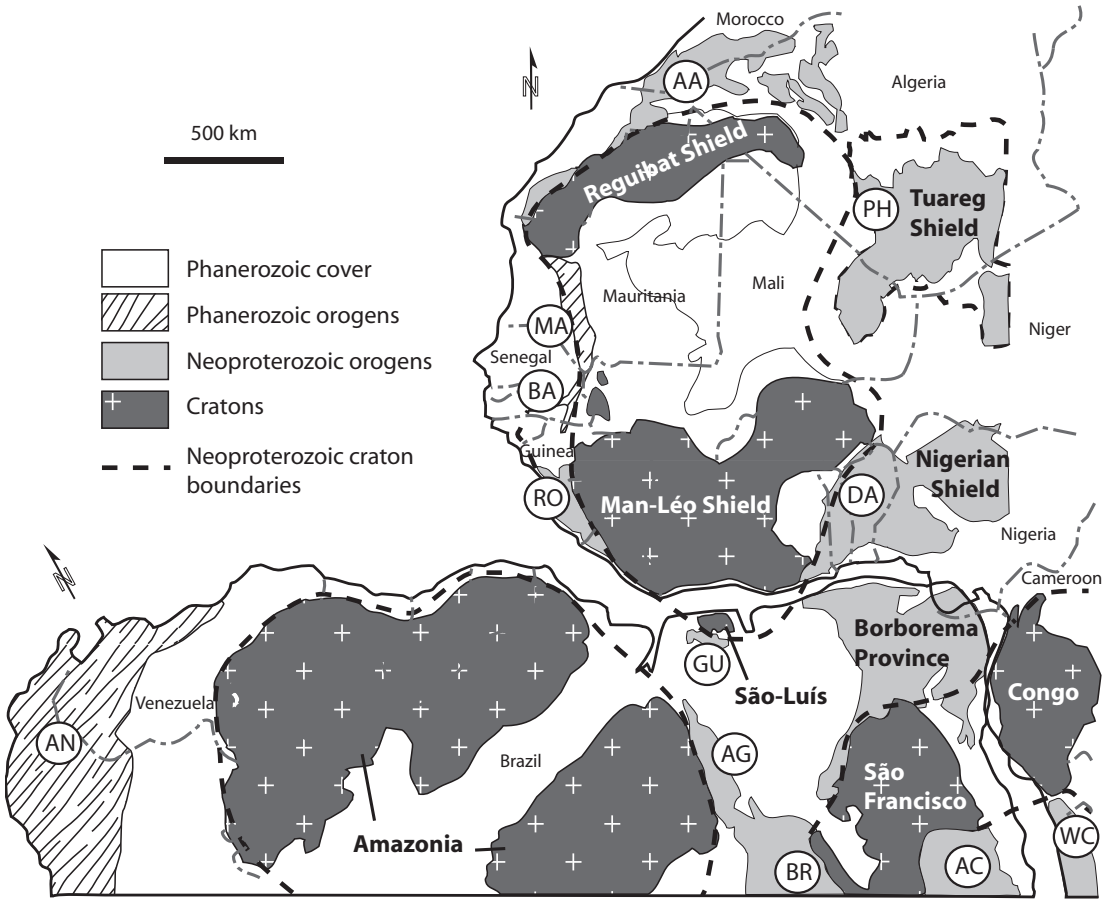

Figure 2.5. Cratonic map of West Africa and surrounding cratons and mobile belts in a pre-Atlantic fit (after Klein and Moura, 2008). AA, Anti-Atlas Belt; AC, Araçuaí Belt; AG, Araguaia Belt; AN, Andean Belt; BA, Bassaride Belt; BR, Brasília Belt; DA, Dahomeyide Belt; GU, Gurupi Belt; MA, Mauritanide Belt; PH, Pharuside Belt; WC, West Congo Belt.

essentially an assemblage of several terrains and comprises reworked Mesoproterozoic-Neoproterozoic metasedimentary rocks and Archean-Palaeoproterozoic crystalline basement (Dada, 2008). Reworking is the result of Neoproterozoic continent-continent collision which caused extensive deformation, migmatization, granitization and intrusion of large volumes of granitoids. Geochronological constraints for the different stages of deformation in the Borborema Province are provided by U-Pb zircon ages of the granitoid plutons (van Schmus et al., 2008). Ages for zircons from syn-tectonic I-type granitoids and zircons from migmatitic gneisses show that deformation started ca. 625 Ma and peaked at about 600 Ma (Guimarães et al., 2004; Neves et al., 2006, 2008). Post-tectonic alkaline granitoids mark the final orogenic stage and U-Pb zircon ages show that deformation

had ceased around 570 Ma (Guimarães et al., 2004; Neves et al., 2008). The Borborema Province is correlated, predominantly on the basis of Sm-Nd model ages and U-Pb zircon ages of Archaean-Palaeoproterozoic basement rocks in conjunction with Neoproterozoic structural tectonic data, with the Central African Fold Belt (Fig. 2.3) and with the Nigerian Shield (Fig. 2.5) in NW Africa (van Schmus et al., 2008; Arthaud et al., 2008; Santos et al., 2008).

The Central African Fold Belt shows a multi-stage geodynamic evolution of nappe emplacement onto the northern edge of the Congo Craton (Toteu et al., 2004). Geochronological constraints reveal a history of individual orogenic stages broadly coeval with those of the Borborema Province: high pressure metamorphism with granulite facies rocks, migmatization and syn-tectonic calc-alkaline and S-type granitoids occurred at 640 – 610 Ma, a post-collisional stage of exhumation and late-tectonic calc-alkaline to sub-alkaline granitoid emplacement is dated at 610 – 570 Ma (Pin and Poidevin, 1987; Toteu et al., 2004, 2006). The exact nature of the continental landmasses involved is still enigmatic. The belt could be entirely the result of collisions between individual blocks and magmatic arcs that are now caught up within the belt in Cameroon and Central African Republic (Toteu et al., 2004) or it could be caused by a collision of the Congo Craton with the ill-defined Saharan Metacraton (Abdelsalam et al., 2002). Monazite ages of 621±26 Ma and 633±27 Ma (U-Pb) in amphibolites from NW Uganda (Appel et al., 2005) suggest this collisional event occurred along the entire northern margin of the Congo Craton.

Neoproterozoic intrusions within the Nigerian Shield reveal a history very similar to that of the Borborema Province (Dada, 2008). Combined structural data and U-Pb ages suggest that an early deformational phase took place at 640 – 620 Ma, peak metamorphism and emplacement of syn-tectonic granitoids is dated between 620 and 600 Ma and a post-tectonic phase from 600 to 580 Ma (geochronological data synthesised by Dada, 2008). In the Tuareg Shield to the north (Fig. 2.5) the amalgamation of several Archaean-Palaeoproterozoic terranes was affected by Neoproterozoic syn- and late-collisional magmatism (Black et al., 1994). Geochronology of these plutons shows that the collisional events occurred diachronously between 620 and 580 Ma (Caby, 2003). The Nigerian Shield and the Tuareg Shield are separated from the West African Craton by the Dahome-

yide and Pharusian belts respectively (Fig. 2.5). Peak metamorphism in the Dahomeyides occurred approximately at 610±2 Ma (Attoh et al., 1991) to 603±5 Ma (Hirdes and Davis, 2002) on the basis of U-Pb dating of zircons obtained from gneisses from granulite facies peak metamorphic zones. Post-collisional exhumation is dated by ^{40}Ar-^{39}Ar muscovite ages of 587±4.3 and 581.9±2.4 Ma (Attoh et al., 1997) which corresponds with rutile ages of 576±2 Ma which represent regional cooling below 400°C (Hirdes and Davis, 2002). The Tilemsi Volcanic Arc of the Pharusian Belt records the closure of the Neoproterozoic Pharusian Ocean between ca. 730 and 620 Ma (Caby, 1994; Dostal et al., 1996). This Island Arc collided with the West African Craton between 620 and 580 Ma, simultaneous with the height of the tectonic events in the Tuareg Shield to the east (Villeneuve and Cornée, 1994; Caby, 2003). This coeval evolution of the Borborema Province, the Central African Fold Belt, the Nigerian Shield (Dahomeyide Belt) and the Tuareg Shield (Pharusian Belt) strongly suggests that this part of West Gondwana had amalgamated by 600 Ma and all tectonic activity had ceased by 570 Ma.

Understanding the geodynamic development of central Brazil, west of the São Francisco Craton, is hindered by the presence of large intracratonic sedimentary basins which developed during the Palaeozoic (Milani and Thomaz Filho, 2000). Underneath the Paraná Basin in south-central Brazil the existence of a palaeo-continent, the Paranapanema Block, is inferred from gravimetric data (Mantovani and de Brito Neves, 2005). The São Francisco Craton collided with this block and simultaneously with the Goiás Magmatic Arc further to the north and both collisions are recorded in the Brasília Orogenic Belt (Fig. 2.3, Valeriano et al., 2008). The Goiás Magmatic Arc is formed by intra-oceanic arc magmatism related to westward subduction of São Francisco oceanic lithosphere. The oldest part of the arc comprises orthogneisses and granitoids whose protoliths show a very primitive, island arc-type geochemical signature and have emplacement ages between ca. 890 and 800 Ma (Laux et al., 2005). Arc magmatism continued until closure of the basin at ca. 650 Ma. Collision of the arc with the São Francisco Craton peaked between 650 and 630 Ma which is documented by U-Pb ages for metamorphic zircons in granulites and syn-tectonic peraluminous granites in the Brasília Belt (Piuzana et al., 2003; Valeriano et al., 2004). Late stage orogenic exhumation of metamorphic nappes occurred ca. 610 – 600 Ma on the basis of U-Pb monazite and K-Ar biotite and muscovite ages (Valeriano et al., 2000, 2008).

Archaean to Mesoproterozoic granite-gneiss-migmatite complexes, greenstone belts and metasedimentary and metavolcanic units belonging to the Goiás Massif are caught up in the Brasília Belt between the Goiás Magmatic Arc and the São Francisco Craton (Valeriano et al., 2008).

Evidence from the Paraguay-Araguaia Belt (Alvarenga et al., 2000) which flanks the western side of the Goiás Arc suggests that the collision of São Francisco/Goiás with Amazonia slightly post-dates the Brasília event at ca. 550 Ma (Moura et al., 2008; Paixao et al., 2008). Biotite and muscovite ages around 530 Ma from Archaean basement gneisses may record late-orogenic cooling in the Araguaia Belt (K-Ar, Macambira, 1983; Moura et al., 2008). This means that Amazonia joined West Gondwana ca. 50 Ma after the peak metamorphic events that record the merging of West Africa with the Congo-São Francisco Craton and possibly the Saharan Metacraton.

During the Neoproterozoic the Adamastor Ocean separated the southern Congo and Kalahari cratons from the Rio de la Plata Craton while the Khomas Sea was in between the Congo and Kalahari cratons (e.g. Stern, 2008). The Adamastor Ocean widened southwards from the Congo-São Francisco cratonic bridge and may have been a continuation of the Macaúbas Basin separating the Congo Craton from the São Francisco Craton (Porada, 1989). Closure of the Adamastor and Khomas basins is recorded in southern Africa by a triple junction of three fold belts: the Kaoko, Gariep and Damara belts (Fig. 2.3). The closure of the Adamastor Ocean resulted in transpression as recognised by S-type granite intrusions and metamorphic mineral assemblages in the Kaoko Belt (Passchier et al., 2002; Goscombe et al., 2003b). Ages for granite orthogneisses range between 580 and 565 Ma and coincide with direct age determinations from peak metamorphic minerals such as garnet and zircon (Seth et al., 1998; Goscombe et al., 2003b, 2005). It is still controversial whether basin closure resulted in westward subduction (Porada, 1989; Gresse and Germs, 1993), eastward subduction (Basei et al., 2000; Alkmim et al., 2006) or did not involve any subduction of oceanic crust (i.e. the Kaoko is an intra-cratonic belt, Dürr and Dingeldey, 1996). The southern Kaoko Belt experienced a younger deformational event at ca. 530 Ma which coincided with a deformation phase in the Damara Belt between the Congo and Kalahari cratons (Goscombe et al., 2003a; Gray et al., 2006). This N-S crustal shortening

is widespread in the Damara Belt (Germs, 1995; Prave, 1996; Goscombe et al., 2003a), affected the Kaoko and Gariep belts (Frimmel and Frank, 1998; Passchier et al., 2002) as well as the Ribeira (Heilbron and Machado, 2003) and Dom Feliciano (Basei et al., 2000) belts flanking the Rio de la Plata Craton in South America (Fig. 2.3). It has been suggested that the Adamastor Ocean closed prior to closure of the Khomas Sea based on the geochronology of deformational events (Germs, 1995; Prave, 1996; Gray et al., 2008) or vice versa based on structural and stratigraphic evidence that the Kaoko and Gariep belts were contiguous during Neoproterozoic transpression (Miller, 1983; Stanistreet and Charlesworth, 2001; Goscombe et al., 2003a).

The geochronology of all belts surrounding the major constituents of West Gondwana suggest a multiphase amalgamation as the cratons merged during the late Neoproterozoic. There are still major problems with the exact evolution of Gondwana amalgamation. For example, eclogite facies metamorphism suggest continent-continent collision at 595±10 Ma in the Zambezi belt, the continuation of the Damara Belt into Zambia, which pre-dates the ca. 530 Ma metamorphic peak in the central Damara Belt (John et al., 2003). Pressure-temperature conditions for these eclogite rocks imply low geothermal gradients from which John et al. (2003) interpret the existence of a large (>1000km) oceanic basin between the Congo and Kalahari cratons. Both U-Pb monazite and U-Pb metamorphic zircon ages from the Lufilian Arc and the Zambezi Belt suggest final crustal thickening took place between 530 and 517 Ma (John et al., 2004; Johnson and Oliver, 2004).

Chapter 3

Methodology and Procedures

Two field campaigns were carried out to collect samples for this project: to the Bas-Congo province of the Democratic Republic of Congo (DRC) in July 2007 and to the Adrar region of the Islamic Republic of Mauritania in January 2009. Fieldwork in the DRC was carried out in collaboration with the "Centre de Recherches Géologique et Minières" (CRGM) in Kinshasa (DRC), the "Université de Kinshasa" and the Royal Museum for Central Africa (RMCA) in Tervuren (Belgium). Support and field assistance of Prof. Dr. Valentin Kanda Nkula, Director General of the CRGM, and Emmanuel Cibambula of the Université de Kinshasa is greatly acknowledged. General support and additional samples were provided by the RMCA, with the help of Dr. Luck Tack and Dr. Max Fernandez Alonso as well as Franck Delpomdor and Dr. Alain Preat of the "Université libre de Bruxelles".

Fieldwork in Mauritania was carried out in collaboration with Prof. Dr. Khalidou B. Lô, Director General of the "Office Mauritanien des Recherches Geologique" (OMRG) in Nouakchott, Mauritania, and with Dr. Roger Key of the British Geological Survey (BGS). Field assistance was provided by the late Mr. N'Diaye Ousmane and by Mr. Med El Moctar O. Dahmada of the OMRG.

Collaborations with many different laboratories have been established for the processing of samples. These will be mentioned and acknowledged in the individual methodology sections below.

3.1 Palaeomagnetism

3.1.1 Palaeomagnetic Procedures

Palaeomagnetic samples were collected using a water-cooled, gasoline powered Echo motor drill. Care was taken not to sample at topographic highs to avoid sampling rocks with a lightning induced magnetism, and samples were collected from the freshest possible exposures. The orientation of all drill cores was measured with a magnetic Brunton compass and also, when possible, with a sun compass reading. For the orientation of hand samples the top surface was oriented and marked after which cores were drilled in the rock cutting facilities at the University of Edinburgh. The marking was subsequently transposed on to the individual samples. In Edinburgh all samples were cut into 24 mm length specimens, where possible two specimens (A and B) were taken from every sample. The rest of the sample material was collected and kept for chemostratigraphic analyses and/or rock magnetic experiments.

The samples for Chapter 5 (samples from the DRC) were measured at Fort Hoofddijk paleomagnetic laboratory in Utrecht (the Netherlands) using a 2G cryogenic magnetometer, housed in a low field space, and were demagnetised using a laboratory-built thermal demagnetiser. All other samples were measured at the University of Edinburgh using a 2G Liquid Helium Free magnetometer, housed in a low field cage (residual field < 100 μT) and were demagnetised with a Magnetic Measurements furnace. The specimens were progressively heated stepwise up to the temperature at which a specimen was totally demagnetised i.e. when the intensity dropped below the magnetometer sensitivity (approx. 10^{-7} mAm^2) or when the signal became erratic. Normally this temperature was determined by carefully demagnetising a few pilot samples of a specific formation or rock type. Display and analysis of the demagnetisation steps was done using software developed at Fort Hoofddijk.

All directions were obtained using principal component analysis (Kirschvink, 1980) from orthogonal and equal area projections. If a magnetic component in equal area projection showed a trend towards the origin it was anchored and was determine to be the char-

acteristic remanent magnetisation (ChRM). If a component was not pointing towards the origin it was drawn using free lines. The maximum angular deviation (mad) was used to discriminate between free or anchored lines in case of doubt. Sometimes the ChRM was obtained with the use of great circles following the procedures described by McFadden and McElhinny (1988): great circles were drawn in an equal area projection and individual directions were taken from great circle intersections. The optimum intersection was obtained by an iterative procedure of determining the maximum vector resultant of all unit vectors. Fisher statistics (Fisher, 1953) were then used to calculate site mean directions from specimens and locality mean directions from site means. In general, acceptable site mean directions would have an α_{95} of ca. 15 and a $\kappa > 30$. Palaeomagnetic poles were obtained by calculating poles from site mean directions which were averaged using the same Fisher statistics. Thermochemical alteration was monitored by measuring susceptibility of a few selected samples after every demagnetisation step. This way, the formation of a new magnetic mineral phase can be detected by the sudden change (increase) in susceptibility.

The time at which a rock acquired its magnetisation was evaluated with fieldtests where possible. These include the test for a common true mean direction in matrix and clasts of a conglomerate/diamictite (conglomerate test), the test for a common direction in rock units with different bedding orientations before and after tilt reconstruction (fold test) and by comparing mean direction for rocks with normal and reversed polarities (reversal test). The tests are documented by Shipunov et al. (1998) (conglomerate test), by McFadden (1990) (fold test) and by McFadden and McElhinny (1990) (reversal test).

3.1.2 Rock Magnetic Tests

A series of rock magnetic tests were conducted to identify the magnetic carriers in the samples. All experiments were carried out on specimen or sample material that had undergone no thermal treatment, where possible sister specimen of palaeomagnetically analysed samples were used.

Isothermal Remanent Magnetisation (IRM) curves were obtained for carefully selected samples which typically represent a particular demagnetisation behaviour. The samples

were exposed to stepwise increasing external fields of up to 0.5 Tesla using a Molspin pulse magnetiser and subsequently up to 4 Tesla using a Redcliff magnetiser. Eighteen steps were selected to be equidistant on a log-scale. Backfield curves were obtained by applying fields in the opposite direction. After each step the IRM was measured using a Molspin 'Minispin' magnetometer. Thermal demagnetisation of multicomponent IRM's (after Lowrie, 1990) was also carried out. Orthogonal fields of 4.7 T, 1 T and 0.15 T were applied using a Redcliff pulse magnetiser and Newport Instruments electromagnet for the highest and lower fields respectively.

High and low temperature susceptibility measurements (from -192 up to 700 °C) were performed on ∼1 gram of powdered sample material using the Agico Spinner Kappa MFK1-FA. Heating was generally performed in air. Corrections for empty sample holder and for instrument drift were applied after acquisition.

3.2 Geochronology

3.2.1 Baddeleyite Dating

Baddeleyite U-Pb dating was carried out on two samples in collaboration with Dr. Richard Ernst (Ernst Geosciences, Canada) and Ulf Söderlund (Lund University, Sweden) as part of the global project "Reconstruction of Supercontinents Back To 2.7 Ga Using The Large Igneous Province (LIP) Record: With Implications For Mineral Deposit Targeting, Hydrocarbon Resource Exploration, and Earth System Evolution" (www.supercontinent.org). Baddeleyites were separated at Lund University using a Wilfley water-shaking table following the technique described by Söderlund and Johansson (2002). Magnetic minerals were removed using a magnet and the best quality baddeleyite grains were hand picked under a binocular microscope. The grains were subsequently transferred into Teflon dissolution bombs, washed in 2-3 N nitric acid and water and was then left overnight in HF:HNO_3 (10:1) to dissolve.

U and Pb were loaded together with silica gel onto an outgassed single Re filament and

three fractions per sample were analysed on a Finnigan Triton thermal ionisation multi-collector mass spectrometer at the Museum of Natural History in Stockholm. Initial common Pb was corrected for using the model composition of Stacey and Kramers (1975). Data reduction and age calculations are from using software developed by Ludwig (2003).

3.2.2 Detrital Zircon Dating

Samples for detrital zircon dating were crushed and separated at GeoTrack International in Melbourne (Australia) using standard heavy liquids and magnetic separation techniques. The separated zircon crystals were mounted in 1 inch diameter epoxy resin discs which were subsequently polished to reveal a section through the crystals. Mounts were then carbon coated for back-scattered electron and cathodoluminescence (CL) imaging under the scanning electron microscope (SEM) using in-house facilities at the School of Geo-Sciences, University of Edinburgh. These images were used to create 'maps' of the zircon mounts, later used to navigate between individual grains during analyses (Fig. 3.1a). The CL images reveal internal structures of the grains including cracks, inclusions and zoning (Fig. 3.1b). Uranium and lead isotopes were measured by HR-SIMS or LA-ICPMS and all analyses are listed in Appendix S1. A selection of CL images to represent each sedimentary unit is provided in Appendix S2.

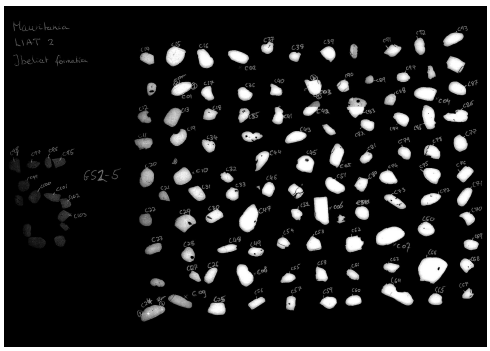

(a) Example of a back-scattered electron image of mounted zircons which was used to navigate between individual grains during analyses (example is for the LIAT 2 sample, Jbeliat Group, Adrar Sub-Basin, Mauritania).

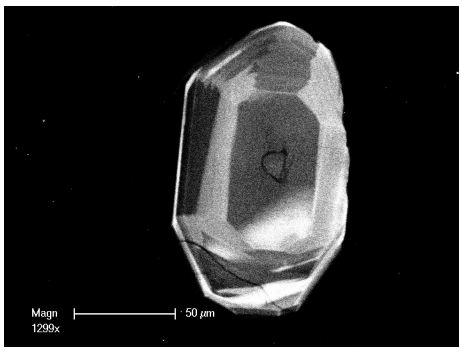

(b) Example CL image of a zircon grain used to place the analysis spot (example is for analysis gs1-3-c2).

Figure 3.1. Images from the scanning electron microscope (SEM). These images are intended to be indicative only.

High-resolution secondary ion mass spectrometry (HR-SIMS) was carried out using a Cameca ims-1270 system at ISEI, Okayama University (Japan), following the protocol of Usui et al. (2002). A total of 79 zircons were analysed. To reduce common Pb contamination on the sample surface, mounts were rinsed with 0.1M HF and placed in a 0.1M HNO_3 ultrasonic bath for 3min. The clean mount was coated with 30nm of gold. A focused O" primary beam of 15nA accelerated to 13kV was used, resulting in a primary beam diameter of $\sim 15\mu m$ sampling diameter. Secondary acceleration power was 10kV and over 5000 mass resolution power ($M/\Delta M$) was applied to remove the mass interferences. Signals from ^{204}Pb, ^{206}Pb, ^{207}Pb and ^{208}Pb were simultaneously collected using electron multipliers of the multi-collection system, and UO was collected by adjusting magnet power.

Raw data were corrected for instrumental mass discrimination and mass fractionation of the U-Pb atomic ratio and Pb isotopic ratios using calibration curves obtained for the PML-Zr zircon standard (Sri Lanka, Usui et al., 2002) and the 91500 standard (Wiedenbeck et al., 1995a, 2004) at the beginning of each analytical session. The Isoplot/EX program (after Ludwig, 1999) was used to regress and calculate an U-Pb concordia age for each analysis.

Laser ablation inductively coupled plasma mass spectrometry (LA-ICPMS) was carried out at the Institut für Mineralogie, Westfälische Wilhelms-Universität Münster (Germany) following the protocol of Kooijman et al. (in preparation). A total of 1196 grains were analysed using a Thermo-Finnigan Element 2 sector field ICP-MS coupled to a New Wave UP193HE ArF Excimer laser system. Operating details are listed in Table 3.1. A tear-drop shaped low volume cell was used which contained both a small resin disk with standard material and the 1" diameter resin disk with the unknowns. During each run, the masses 202, 204, 206, 207 and 238 were measured in peak jumping mode. ^{202}Hg was measured to quantify the interference of ^{204}Hg on ^{204}Pb. Generally a laser spot size of 35μm was used but occasionally a smaller spot size was preferred when the target was smaller than 35μm. All spots were pre-ablated using a larger spot size to remove any surface contamination and to reduce the chance of measuring common Pb from the surface. The total ablation time was 50s with the shutter closed for the first 15s to measure the gas blank (i.e. background). To correct for laser-induced element fractionation and instrumental mass bias the GJ-1 stan-

dard zircon (Jackson et al., 2004) was measured 3 times at the start of each session and after every 10 unknowns.

Laser		ICP-MS	
Model	New Wave Research UP-193HE	Model	Element2, ThermoFinnigan
Type	Excimer	Type	Magnetic Sectorfield
Wavelength	193 nm	Forward power	1300 W
Spot size	35 μm	Scan mode	E-scan
Repetition rate	10 Hz	Scanned masses	202, 204, 206, 207, 238
Laser fluency	~5 J/cm2	Cooling gas (Ar)	16 l/min
Laser warm up	15 s	Auxilliary gas (Ar)	0.9 l/min
Ablation time	35 s	Sample gas (Ar)	1.2 l/min
Washout time	14 s	Carrier gas (He)	0.6 l/min

Table 3.1. Instrument details and operating parameters

Data were processed offline using an in-house developed Excel spreadsheet. The measured isotope signals were corrected for gas blank and time-dependent element fractionation (Sylvester and Ghaderi, 1997). The isotope ratios were carefully monitored to exclude obvious anomalies related to inclusions, common Pb enrichment or different age zones. The reported ^{207}Pb/^{235}U ratios were calculated from the ^{206}Pb/^{238}U and ^{207}Pb/^{206}U ratios assuming a natural abundance of 137.88 for ^{238}U/^{235}U. To monitor reproducibility of the ^{206}Pb/^{238}U-age the 91500 standard zircon (1065±0.4 Ma, Wiedenbeck et al., 1995b, 2004) was analysed as an unknown twice every session of 81 spots. The results of all these 91500 spot analyses are shown in Figure 3.2.

The degree of concordance of the data is calculated using the formula:

$$degree\ of\ concordance = \frac{^{206}Pb/^{238}U - age}{^{206}Pb/^{207}Pb - age} * 100\%$$

The amount of common lead was evaluated using the ^{204}Pb count rates and is expressed as a fraction of the total ^{206}Pb in $\int$206% (see Appendix S1). A common lead correction was applied only if $\int$206 exceeded 1%. The evolution model of terrestrial Pb of Stacey and Kramers (1975) was used to calculate the ratio ^{206}Pb/^{204}Pb at the time (t) of crystallisation:

$$\frac{^{206}Pb}{^{204}Pb}(t) = \frac{^{206}Pb}{^{204}Pb}_{t_0} + \frac{^{238}U}{^{204}Pb}_{t_0} * (e^{\lambda t_0 10^6} - e^{\lambda t 10^6})$$

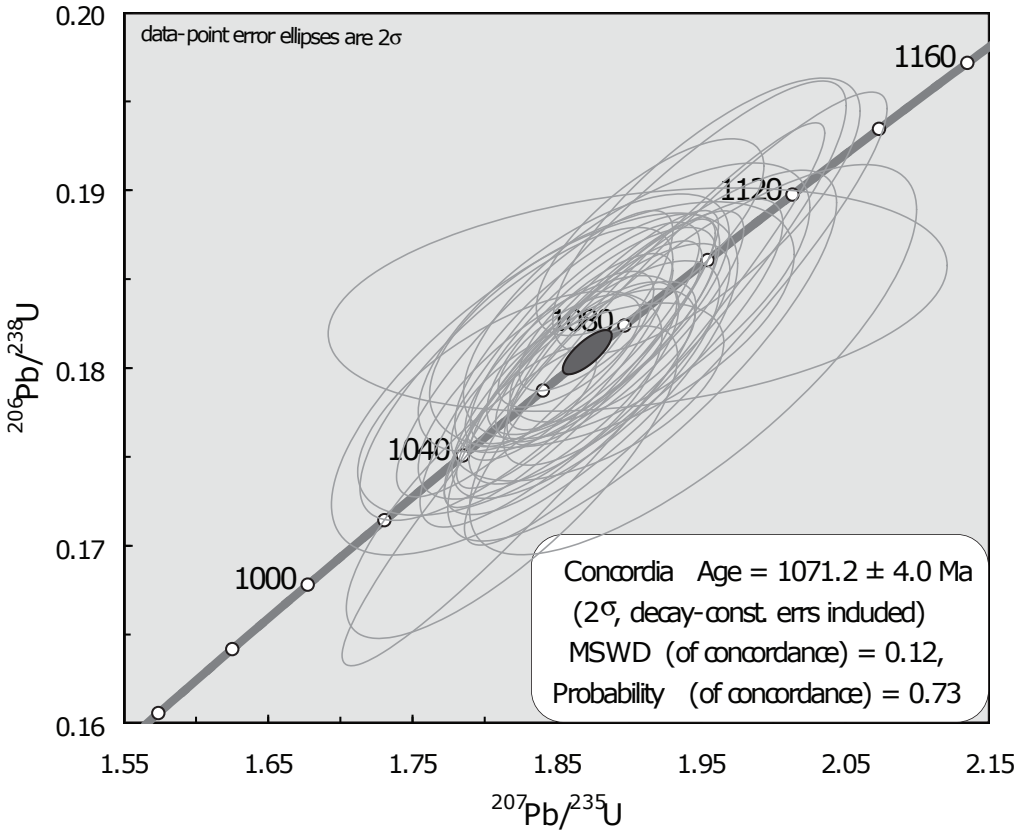

Figure 3.2. Analyses of the 91500 standard zircon. Our concordia age is slightly older than its ID-TIMS age of 1065±0.4 Ma (Wiedenbeck et al., 2004).

where λ is the decay constant of ^{238}U (1.55125E-10) and t_0 is the 'time zero' i.e. the start of a stage of the evolutionary model which has two stages: 4570 – 3700 Ma and 3700 Ma - present. The average values of $^{238}U/^{204}Pb$ during the first and second stage are 7.192 and 9.735 respectively. The ratios $^{206}Pb/^{204}Pb$ at the start of the two stages are 9.307 and 11.152 respectively (Stacey and Kramers, 1975). The ^{206}Pb concentration was subsequently corrected using:

$$^{206}Pb_{corr} = ^{206}Pb - ^{204}Pb * \frac{^{206}Pb}{^{204}Pb}$$

3.2.3 HR-SIMS versus LA-ICPMS

The two techniques used to obtain the detrital zircon geochronological results differ in precision, analysis time and destruction of sample material. HR-SIMS is a very precise analytical technique with an average error on the calculated $^{207}Pb/^{206}Pb$ age of 1.6% (n = 79). The amount of destruction to the grain is minimal: spot sizes are generally $\sim 15\mu m$ in size and not more than a few micron deep (Fig. 3.3). This makes the technique ideal for the analysis of small grains or multiple zones in one crystal. In practice it was not always easy to navigate around the mounts and a uniform area of at least $25\mu m$ was generally needed because of misalignments, all due to the video system that was in place at ISEI. Occasionally the beam appeared to have moved away from the initial target e.g. across a zone boundary leading to discordant results. The analytical time is generally 25 – 30 minutes per analysis. When programming a batch of approx 10 analyses overnight an average of 20 unknowns per day could be reached.

LA-ICPMS is less precise (average error of 3.8%, n=429) but with an analytical time of ca 1.5 minute per spot it is a very time efficient technique (up to 250 analyses could be achieved per day). An average spot size of $35\mu m$ was applied because a smaller spot-size would lead to too much fractionation from the crater pit wall. The amount of destruction to the grain is substantial, pits being 20 - 30 μm deep (Fig. 3.3). Several grains have been analysed using both HR-SIMS and LA-ICPMS and their ages are identical within errors (see Table 3.2).

Analysis	HR-SIMS $^{207}Pb/^{206}Pb$-age (2σ)	LA-ICPMS $^{207}Pb/^{206}Pb$-age (2σ)
DZI2-r1-z012	1272 (14)	1255 (46)
UIA5-r1-z002	694 (7)	726 (35)
UIA1-r1-z004	2628 (3)	2587 (14)
UIA1-r3-z007	745 (10)	762 (59)

Table 3.2. Comparison of 4 grains which are analysed by both techniques.

Provenance analyses require a high number of grains: ca. 120 grains are needed to be 95% sure every population making up 5% or more of the total is sampled (Vermeesch, 2004). The LA-ICPMS technique is ideally suited to detrital zircon studies where the most important consideration is to obtain full age population spectra, not precision analysis of individual grains.

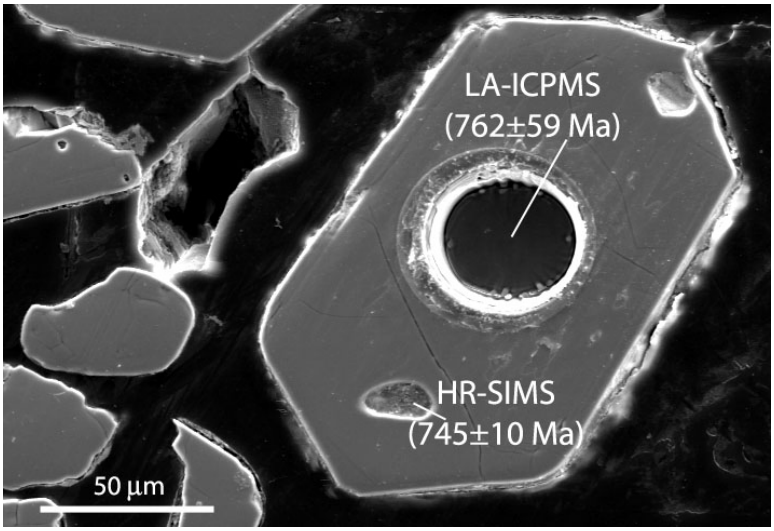

Figure 3.3. Scanning Electron Microscope (SEM) image of two pits, one left by SIMS and one by Laser Ablation analysis (Analysis UIA1-r3-z007).

3.3 Stable Isotopes

Carbon and oxygen isotope data were obtained on bulk rock samples from carbonates above and below the Upper Diamictite Formation (DRC) and above the Jbeliat Group (Mauritania). A Dremel minidrill was used to obtain powders of the samples where care was taken to avoid obvious recrystallised parts of the rock. An attempt was made to check for alteration using cathodoluminescence (CL) but the fine grained carbonate samples did not reveal any clear targets and only showed pervasive dolomitisation in some cases. All stable isotope results are reported as ‰ values relative to VPDB and are listed in Appendix S3.

Isotope analysis for the samples from the Congo (DRC) was undertaken at the Scottish Universities Environmental Research Centre (SUERC) using an automated triple-collector gas source mass spectrometer (Analytical Precision AP2003) linked to an automated gas preparation device. In the latter, c. 1 mg of the powdered sample is reacted with 103% phosphoric acid to produce carbon dioxide which is then purified before analysis. Precision and accuracy are monitored by reference to long-term analysis of laboratory and international standards. Precision is better than 0.2‰ at 1 for carbon and oxygen.

Isotope analysis for the Mauritanian samples was undertaken at the Wolfson Laboratory

at the School of GeoSciences, Grant Institute, University of Edinburgh, where oxygen and carbon stable isotope analyses were performed on 0.02 – 0.1 mg sub-samples. The carbonate samples were reacted with 100% orthophosphoric acid at 75°C in a Kiel Carbonate III preparation device and the resulting CO_2 was then analysed on a Thermo Electron Delta+ Advantage stable isotope ratio mass spectrometer. The standard deviation for 7 analyses of a coral powder (COR1D) run as a sample on the same days as the study samples was $\pm$ 0.04‰ for δ^{13}C and $\pm$ 0.08‰ for $\delta^{18}O$.

3.4 Provenance Geochemistry

Samples for provenance geochemistry have been analysed for major and trace element composition using ICP at Acme Labs in Vancouver (Canada). To avoid contaminating the sample material with Ta from a commonly used Tungsten-Carbide mill crushing and pulverising was done using either ceramic or agate mills. Major oxides were analysed by ICP-emission spectrometry (ICP-ES) and total trace element abundances were determined by ICP-mass spectrometry (ICP-MS). Prepared sample material was mixed with $LiBO_2/Li_2B_4O_7$. Crucibles are fused in a furnace and the cooled bead is dissolved in ACS grade nitric acid. Loss of ignition (LOI) was calculated by heating the sample material at 1000°C. In addition, the total carbon and sulphur was determined by Leco. Inserted in the measuring sequence were duplicates to monitor analytical precision, blanks to provide background measurements and standard reference materials to monitor accuracy.

The behaviour of high field strength elements (like REE, Sc, Zr, Ti etc.) are well understood and useful provenance indicators (e.g. McLennan et al., 1990, 1993, 2003; Taylor and McLennan, 1985; Plank and Langmuir, 1998; Nesbitt and Young, 1982; Fralick, 2003; Bhatia and Crook, 1986; Condie, 1993). They have been used with success to study the provenance of rocks from the Archaean to modern sediments. However, it is important to realise that a mixed provenance is to be expected in sedimentary rocks. Therefore, any line of evidence from the provenance geochemistry will need to be supported by geological and stratigraphic relations and trends throughout the basin deposits to be analysed.

Chapter 4

Provenance of the Neoproterozoic West Congolian Group

4.1 Introduction

The Congo Craton (Fig. 2.3) comprises several Archaean nuclei which welded together during the Palaeoproterozoic and were subsequently effected by Mesoproterozoic tectonism and by Neoproterozoic collisional events leading to the formation of supercontinent Gondwana (De Waele et al., 2008). Before its incorporation in Gondwana, Neoproterozoic rift successions and passive margin sequences developed along the margins of the proto-Congo Craton.

Along the western margin of the Congo Craton, the West Congo Belt exhibits a Palaeoproterozoic basement and early Neoproterozoic volcanic rift sequences followed by passive margin platform deposits of the West Congolian Group (Cahen, 1978). These Neoproterozoic sediments contain two diamictite horizons, first identified by Delhaye and Sluys (1923-4 and 1928-9) and later described in more detail by Lepersonne (1951). The glacial origin of these diamictites has long been a subject of debate (see e.g. Kröner and Correia, 1973; Schermerhorn, 1974b; Cahen and Lepersonne, 1981a). Recent micro-structural analysis of these diamictites has identified grain edge-to-edge crushing, strain shadows, necking

structures, shear zones and water escape structures which suggest these diamictites were deposited in sub-glacial, water-saturated sediments confirming a glacial depositional mechanism for diamictites in the Democratic Republic of the Congo (DRC) (Delpomdor, 2007; Delpomdor et al., 2008, 2009).

Correlations of these diamictites across the craton and beyond are severely hampered by a lack of geochronological and palaeogeographic constraints. This study presents an extensive provenance analysis of the entire Neoproterozoic sedimentary sequence of the West Congo Belt in the DRC. Together with chemostratigraphic analyses it will provide a framework for a basin evolution model and for correlation of Neoproterozoic diamictites elsewhere.

4.2 Geological Setting

In the western part of the West Congo Belt Palaeoproterozoic basement rocks (∼2.1 Ga) of the Kimezian Supergroup have been thrust upon the Zadinian and the Mayumbian groups which in turn are thrust upon the West Congolian Group during the late Neoproterozoic (Tack, 1975; Boudzoumou and Trompette, 1988; Franssen and André, 1988; Maurin, 1993; Tack et al., 2001). The Zadinian, Mayumbian and West Congolian groups are part of the West Congo Supergroup (see Fig. 4.1) which reaches its maximum width in the Bas-Congo province of the DRC.

The oldest, the Zadinian Group, comprises peralkaline granites and rhyolites intruding ca. 1500m of metasediments (metaquartzite, biotite schist, conglomerate and black shale) overlain by a thick (1600 – 2400m) sequence of continental flood basalts. An emplacement age of one of the granites (the Noqui granite, 999±7, Tack et al., 2001) provides an estimate for the onset of rifting in the West Congo Belt. The Zadinian Group is followed by rhyolitic lavas of the Mayumbian Group which are 3000 – 4000m thick in the DRC and are dated at 920±8 to 912±7 Ma from bottom to top. These rhyolites have in turn been intruded by granites with emplacement ages of 924±25 and 917±14 Ma (Tack et al., 2001).

The metasediments of the West Congolian Group unconformably overlie the Mayumbian Group. Sedimentary units show intensive folding in the west but deformation rapidly decreases eastward into gently folded and eventually unfolded tabular sequences resting on Archaean basement rocks. Regional metamorphism in the West Congolian Group is of a low pressure – high temperature type and varies from amphibolite and greenschist facies rocks in the west to unmetamorphosed sequences in the east (Franssen and André, 1988; Tack et al., 2001). Deformation and metamorphism is the result of a 'Pan-African' orogenic event which in this region is called the Araçuaí-West Congo Orogeny and is the result of collision of the São Francisco Craton with the Congo Craton closing the Macaúbas Basin (Pedrosa-Soares et al., 2001). Estimates for the timing of this event vary: based on evidence from the African side it has been suggest to have started between 620 and 600 Ma with a peak metamorphism around 566 Ma (Maurin, 1993; Trompette, 1994; Frimmel et al., 2006). On the São Francisco side pre-, syn- and late-orogenic rocks record events starting 630 Ma and lasting until the Early Cambrian (Pedrosa-Soares et al., 2001, 2008). The West Congolian Group is overlain by post-orogenic, unmetamorphosed, flat lying red bed sediments of the Palaeozoic Inkisi Group (Alvarez et al., 1995).

Opening of the Atlantic in Cretaceous times split the Araçuaí-West Congo Belt into two parts, the South American side of which inherited two thirds of the orogen including all Neoproterozoic ophiolitic slivers, the entire magmatic arc, suture zone and syn- to post-collisional magmatism (Pedrosa-Soares et al., 2008).

4.3 Stratigraphy of the West Congolian Group

The maximum age of the West Congolian Group is constrained by the 912±7 Ma emplacement age of underlying Mayumbian Group granites (Tack et al., 2001). Siliciclastic sedimentary rocks and carbonates of the West Congolian Group (originally described by Cahen, 1978) were deposited on a passive margin platform and have been gently folded by Pan-African deformation. The group has been subdivided into the Sansikwa, Haut-Shiloango, Schisto-Calcaire and the Mpioka Subgroups (Figure 4.2) which have a total stratigraphic thickness of ∼5.5 km although local variations exist. All reported thicknesses

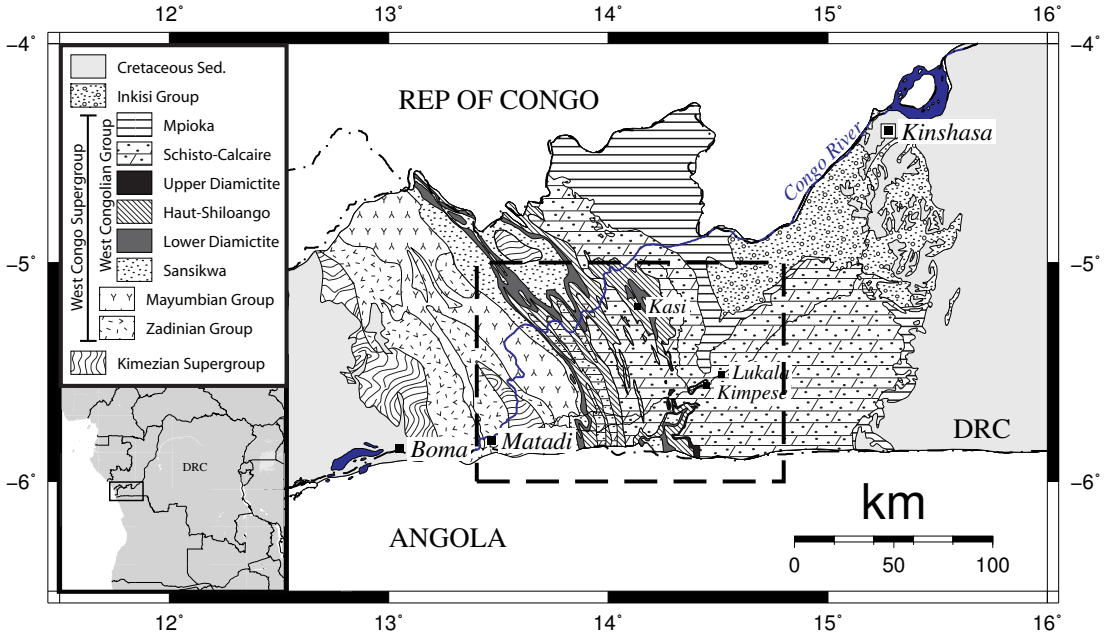

Figure 4.1. Simplified geological map of the Bas-Congo province of the Democratic Republic of Congo (DRC), redrawn from a 1:2,000,000 and a 1:200,000 geological map produced by the Royal Africa Museum Tervuren (Belgium) (Lepersonne, 1973, 1974). The outline of Figure 4.3 is indicated by a dashed line.

in the descriptions below are from Tack et al. (2001).

4.3.1 Sampling

Most samples were collected from outcrops and quarries along the main roads and the localities are described in Table 4.1 and shown in Figure 4.3. Field photographs and photomicrographs to illustrate the rock descriptions are provided in Appendix A.1.

Sansikwa Subgroup

The basal Sansikwa Subgroup is a siliciclastic series of arenites and fine-grained shales and mudstones (ca. 1650m). Most samples from this formation are dominated by silica (up to 96%) and highly depleted in all major elements (notably in MgO, CaO and Na_2O).

Arenites of the Sansikwa Subgroup were sampled in a dry riverbed of a small branch of the Duizi river (DZI locality, no. 1 in Fig. 4.3). Layers of up to 50cm thick, undeformed

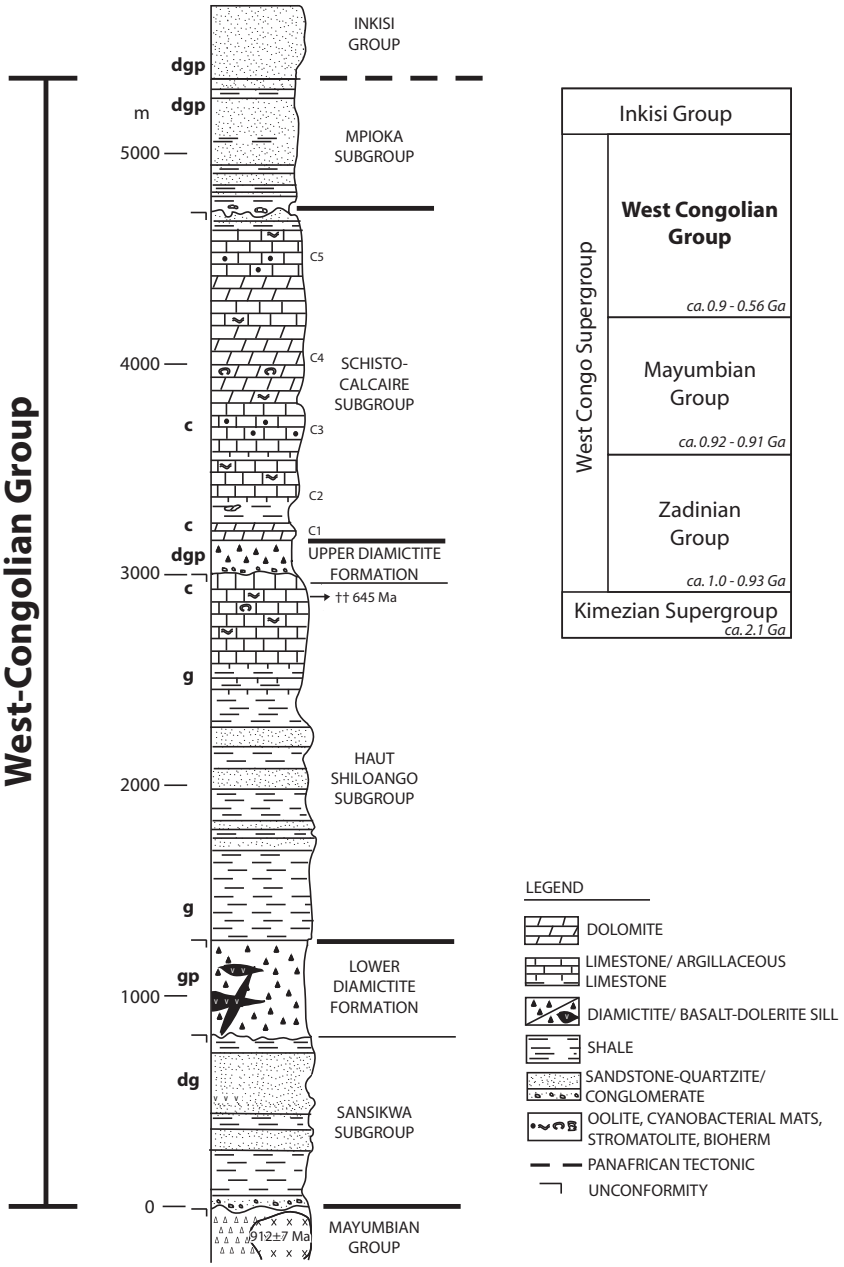

Figure 4.2. Detailed stratigraphic column of the West Congolian Group. Stratigraphic levels from where samples were collected for detrital zircon geochronology (**d**), provenance geochemistry (**g**), chemostratigraphy (**c**) and palaeomagnetism (**p**) are indicated. Modified after Tait et al. (2011).

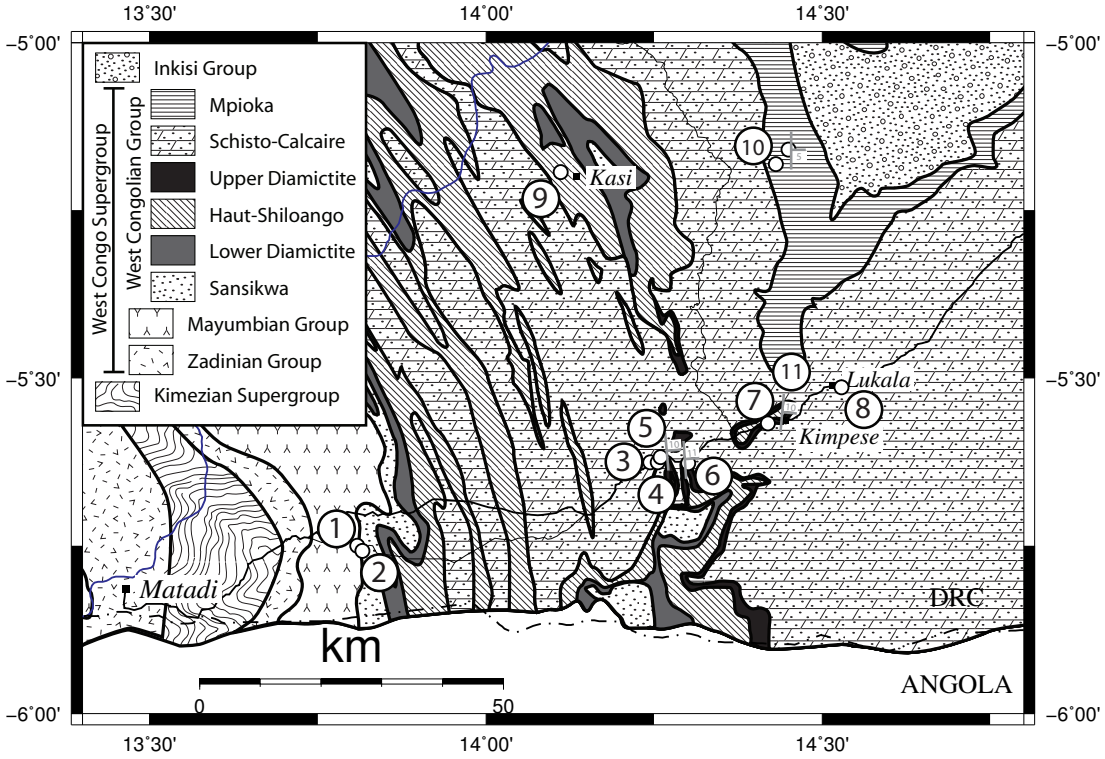

Figure 4.3. Sampling localities in the Bas-Congo province. Numbers correspond with first column in Table 4.1.

arenite are intercalated with fine bedded talcy shale. Ripple marks of 1 – 2cm long indicate N-S-N palaeocurrent directions (Photo A.1). Photomicrographs of thin microscope slides reveal the presence of quartz overgrowths on rounded, twinned quartz grains (Photo A.6a). Secondary quartz grains and white mica crystals fill the pore spaces. Fine grained argillitic material has been sampled 1.2km further west (DZI 1; 3 samples) and at the next locality (BANGU 1; 1 sample). As will be demonstrated below the rare earth element (REE) composition of the DZI 1 samples indicates a weathered tuff/volcanic unit has been sampled.

The top of the Sansikwa Subgroup is marked by the Lower Diamictite Formation which is of variable thickness (up to 400m in some places, decreasing eastward). The Lower Diamictite Formation has been intruded by subaqueous lavas and a feeder system of doleritic dykes and sills can be found intruding underlying sedimentary units (De Paepe et al., 1975). The geochemistry of these magmatic rocks shows they have a tholeiitic composition

	locality	named after	description	analysis	GPS coordinates
1	DZI	Duizi river/village	Quartzite sandstones and a weathered tuff of Sansikwa Subgroup	g,d	S 05.7500 E 013.8089
2	BANGU	Bangu village	Roadcut section of Sansikwa argillite and Lower Diamictite Formation	g	S 05.7579 E 013.8161
3	KUM TANDU	Kumbi village	Abandoned quarry, Upper Diamictite Formation	g,p	S 05.6259 E 014.2444
4	SNEL	SNEL powerstation	Pink dolomitised Schisto-Calcaire Subgroup	c	S 05.6259 E 014.2556
5	KWI	Kwilu river	Pink dolomitised Schisto-Calcaire and fine grained Upper Diamictite	c	S 05.6182 E 014.2596
6	CRO	Crocodile river	Siltstones of the Haut-Shiloango Subgroup	g,p	S 05.6273 E 014.3011
7	SAF	Safricas quarry	Sequence of the Haut-Shiloango, Upper Diamictite and Schisto-Calcaire	g,p,c	S 05.5680 E 014.4193
8	CIL	CiLu quarry	Cement quarry, limestones of the Schisto-Calcaire Subgroup	c	S 05.5141 E 014.5289
9	KAS	Kasi village	Tholeiitic volcanics of Lower Diamictite Formation	g,p	S 05.1931 E 014.1112
10	UIA	Ndembo-Uia village	Sedimentary rocks of Mpioka and Inkisi Subgroups	g,p,c,d	S 05.1811 E 014.4312
11	VAP	Chutes de Vampa	Shales of Mpioka Subgroup near Vampa waterfalls	g	S 05.55 E 014.42

Table 4.1. Description of sampling localities in the Bas-Congo province. g = provenance geochemistry, p = palaeomagnetism, c = chemostratigraphy, d = detrital zircon geochronology.

suggesting an extensional tectonic setting (De Paepe et al., 1975; Kampunzu et al., 1991). Mafic minerals (mainly clinopyroxene) separated from a metadolerite sill which is part of the feeder system are dated 566±42 Ma by the ^{40}Ar-^{39}Ar method by Frimmel et al. (2006) who interpret this age as the time of peak metamorphism during the Araçuaí-West Congo Orogeny.

Three samples of the Lower Diamictite Formation were collected from a road section at the BANGU locality (no. 2 in Fig. 4.3). Tectonically elongated clasts of up to 5 cm length were aligned in a weathered, clay-rich matrix (Photo A.2a). The deformed nature of the BANGU 2 samples is clearly visible in a photomicrograph (Photo A.6b): quartz grains of 0.1 to 1mm long are aligned parallel to a grain of fine clay minerals. The larger grains show shadow zones filled with quartz fragments. Many quartz grains are polycrystalline or show twinning indicating they have undergone deformation.

Samples from subaqueous lavas were collected at the KAS locality (no. 9 in Fig. 4.3). Hyaloclastic brecciated lavas were found in the bed of a small stream and appeared fresh and coarse grained (Photo A.2b). Thin section study showed that the textures are well preserved but the groundmass is completely replaced by chlorite (Fig. A.7a). The chloritised

matrix penetrates clasts indicating that the texture of clasts and matrix is obtained during emplacement. Clasts consist of plagioclase crystals altered to carbonate and the carbonate can be seen mimicking plagioclase twinning. Due to limited exposure no contact with surrounding host rocks could be observed. Two samples of unaltered pillow lavas were provided by the University of Kinshasa (PIL samples).

Haut-Shiloango Subgroup

The Haut-Shiloango Subgroup (ca. 1050 m thick) overlies the Sansikwa Subgroup and consists of a succession of conglomerate, quartzite, sandstone and more fine grained sedimentary rocks including shale and argillite. The upper part of the Haut-Shiloango Subgroup comprises carbonates (with local stromatolites) and the change of conglomerate/sandstone in the lower part to carbonates in the upper part of the sequence represents marine transgression (Tack et al., 2001). The top of the Haut-Shiloango Subgroup is characterised by the Upper Diamictite Formation which is recognised throughout the entire West Congo Belt from Gabon to Angola (Cahen and Lepersonne, 1981a) and varies strongly in thickness (between 2 and 200 m in the field area). The contact with the underlying carbonates has an erosional character and variations in thickness may reflect palaeotopography. The origin of this diamictite has been heavily debated. The occurrence of striated clasts in Angola has led several authors to accept a glacial origin for this diamictite (e.g.Poidevin 2007; Trompette and Boudzoumou 1988, later adopted by Frimmel et al. 2006; Poidevin 2007), but a gravitational flow mechanism with striated clasts derived from Alpine glaciers has been preferred by others (Schermerhorn, 1974a; Vellutini and Vicat, 1983; Schermerhorn, 1981). Recently, micro-structural analyses have provided convincing evidence for a glaciomarine depositional environment for both the Lower Diamictite and Upper Diamictite formations (e.g. Delpomdor, 2007). Clasts in the Upper Diamictite Formation do not contain Zadinian and Mayumbian group lithologies which were exposed to the west of the basin so the clast provenance suggests an east to west transport direction (L. Tack, pers. comm.).

Siltstones of the Haut-Shiloango were sampled near the bridge over the Lukala river (CRO locality, no. 6 in Fig. 4.3). The rocks, along the main road, consisted of very fine grained

Outcrop	Lithology	Sedimentology	Tectonics
Inkisi			
UIA	massive, coarse-grained red sandstone and conglomerate	channel cross-bedding, conglomeratic layers marking bottom of beds fining upward	no deformation, sub-horizontal bedding
Mpioka			
UIA	medium to fine grained sandstone to red/pink mudstones and shales at the top	sandstones, finely bedded	bedding 5° to 090°, recognised three fault planes in shales: NNE-SSW, E-W and NW-SE
VAMPA	red shales and siltstones, intercalated with massive conglomerates	cross-bedding, raindrops, waveripples, mudcracks	shallowly dipping to the east
Schisto-Calcaire			
CILU	grey carbonates (ca. 30 m thick) overlain by red shales	structureless	bedding 9° to 151°
SNEL	pink dolostone, interbedded with fine clay layers	finely bedded, cross-bedding	bedding 23° to 091°
KWI	pink dolostone and alternating shales	wavy bedding, flaser bedding, escape structures	bedding 10° to 085°
SAF	pink dolostone	laminated at bottom, more massive after 2/3 m	bedding 14° to 054° and 10° to 095°
Upper Diamictite			
SAF	1-3 m diamictite	structureless, unsorted clasts predominantly carbonate, others include quartzite, mica schist, granite, gneiss	
KUM	>20m diamictite	massive diamictite, coarse-grained matrix, clasts include carbonate, red granite, mafic volcanic	two fault planes: 29° to 256° and sub-vertical SE-NW
KWI	fine-grained sandstone	structureless	
Haut-Shiloango			
SAF	black/blue carbonates. microbial laminites	clastic content gradually increases towards the top where carbonate forms in situ breccia	
CRO	carbonaceous siltstone beds alternating with argillites	structureless	bedding 11° to 086°
Lower Diamictite			
BANGU	altered clayey siltstone with clasts	clasts < 10 cm	highly deformed, elongated clasts
KAS	hyaloclastic brecciated basalt	coarse grained, no bedding, no structure	
Sansikwa			
BANGU	argillitic claystone	structureless	
DZI	argillites and quartzites	quartzites show well preserved ripplemarks (flow E-W-E), thick (20 – 50cm) bedded at bottom, fine (1 – 5cm) beds of argillite intercalated towards the top	bedding 20° to 116°

Table 4.2. Summary of the geological characteristics of the different outcrops.

carbonaceous siltstone beds of 60 – 70 cm thickness intercalated with finely (1 – 2cm) laminated argillite. The carbonates at the top of the Haut-Shiloango Subgroup, sampled at the SAF locality (no. 7 in Fig. 4.3), looked fresh and unaffected by weathering or diagenesis. They are dark grey in colour and contain microbial laminites (Photo A.3a). The structure is created by an alternation of microbial mats and sediment which seem to have been deformed by syn-sedimentary slumping. Microbial laminites can occur at many depth levels but considering the high amount of clastic sediment among the carbonate a relatively shallow water environment is preferred. Towards the top the amount of clastic material gradually increases and immediately below the Upper Diamictite Formation the carbonate forms an in situ breccia (Photo A.3b). Quartz, often localised along bands, makes up ca. 30% of the rock while the rest is pure $CaCO_3$ with the exception of a few sulphate crystals (as can be seen in photomicrographs, Photos A.8a and A.8b). At both localities samples were collected for palaeomagnetic and geochemical analyses.

The Upper Diamictite Formation was sampled at the KUM/TANDU locality (no. 3 in Fig. 4.3) where it has a minimum thickness of ca. 20m but neither the upper nor the lower contact is exposed. The coarse-grained, quartz rich matrix was generally grey/green but sometimes brown coloured and did not show any sedimentary structures making a direct observation of the bedding orientation impossible. Clasts in the matrix supported diamictite are dominantly 1 – 5cm angular carbonate clasts resembling the underlying carbonates of the Haut-Shiloango Subgroup. Other clasts include igneous and metamorphic rocks which were generally well rounded and not larger than 20 cm. The presence of feldspar needles in the matrix, observed in thin section (Photo A.7b), suggests the presence of a granitic source and a limited amount of transport. The relatively coarse grained matrix contains poorly sorted, rounded and angular clasts with compositions ranging from calcite, polymorph quartzite to chlorite overgrown mafic fragments. Both the matrix and clasts were sampled for provenance and palaeomagnetism.

Beyond the quarry, exposure of the Upper Diamictite Formation is extremely poor due largely to dense vegetation. However, at the KWI locality (no. 5 in Fig. 4.3) the diamictite is exposed in isolated outcrops of fine-grained, homogeneous sandstones which were sampled for provenance analyses. No clasts were observed and the contact with the overlying

Schisto-Calcaire Subgroup was not exposed.

The exposure of the Upper Diamictite Formation at the KUM/TANDU locality is in sharp contrast to its thickness at the Safricas quarry (SAF locality), which is situated ca. 20 km further to the east (Fig. 4.3). Here, the diamictite is exposed as a 2 m thick and poorly exposed unit in between dark grey carbonates from the underlying Haut-Shiloango Subgroup and pink dolomitic carbonates of the overlying Schisto-Calcaire Subgroup. The diamictite covers the brecciated carbonates in what appears to be a continuous sequence, an erosional surface or unconformity could not be recognised. The diamictite was not sampled at the SAF locality.

Schisto-Calcaire Subgroup

Capping the Upper Diamictite Formation is a 10m-thick, finely laminated pink dolomitic carbonate of the Schisto-Calcaire Subgroup (total thickness of 1100 m). This dolomite shares many lithological characteristics with dolostones capping glacial deposits elsewhere (e.g. in southern Namibia, Hoffman and Schrag, 2002). The Schisto-Calcaire Subgroup has been subdivided into five lithofacies on the geological map (Lepersonne, 1973) which can be summarised as follows: c1, 10 – 12m of finely laminated pink or grey dolomitised limestone; c2, argillaceous intercalation of grey to green limestones with carbonaceous schists (400m); c3, grey – blue limestones and carbonaceous schists, overlain by clear, oolitic limestones, massive layers are separated by stylolites and occasionally contain chert nodules (200m); c4, schists, partly dolomitised limestone banks, stromatolitic limestones and abundant chert layers and nodules (300m); c5, crystalline dolomite varying in colour generally black, locally brecciated limestone, overlain by oolitic lenses and silicified grey or black talc schists, overlain by black dolomites passing into grey limestone beds (200m).

The c1 dolomite has been sampled at three different localities (SNEL, KWI and SAF, nos. 4, 5 and 7 in Fig. 4.3) and is generally fresh. SEM images of samples from the KAS locality reveal mainly dolomite with bands of calcite (Photo A.9a) and a small number of clastic fragments (mainly quartz). The contact between the Upper Diamictite Formation and the Schisto-Calcaire Subgroup seems to be continuous at the SAF locality where the lower-

most 5 m of dolomite was sampled for palaeomagnetic and chemostratigraphic purposes. At the SNEL locality finely bedded dolomite, sometimes interbedded with thin beds of clay, are typically 1mm to a few cm's thick revealing cross bedding structures (Photos A.4a and A.4b). This is clearly lithofacies c1 although the contact with the underlying diamictite was not exposed. Similar layered c1-dolomites were sampled at the KWI locality.

Schisto-Calcaire lithofacies c3 samples were obtained at the CiLu cement quarry at Lukala village (CIL locality, no. 8 in Fig. 4.3). A total of ca. 30 m of structureless grey carbonates have been sampled at regular intervals.

Mpioka Subgroup

The Schisto-Calcaire Subgroup is followed by a series of molasse sediments of the Mpioka Subgroup (ca. 1000m thick): shales, siltstones, greywackes and conglomerates make up this youngest unit of the West Congolian Group. Medium to fine grained, bedded red sandstones of this subgroup have been collected at the bottom of the UIA mountain (UIA 4) and further south in a riverbed (UIA 5,6 & 8, no. 10 in Fig. 4.3). Finally one more sample of the Mpioka Subgroup has been taken from near the Vampa waterfalls (VAP, no. 11 in Fig. 4.3) where red shales are intercalated with massive conglomerate beds. Ripple marks, cross bedding, mud cracks and fossilised raindrops were observed in fine grained sandstones and shales (Photos A.5a and A.5b).

Inkisi Group

The West Congolian Group is unconformably overlain by the quartz-arenitic Inkisi Group which is believed to be Phanerozoic in age and has been correlated to post-orogenic cover deposits which are shown to underlie the entire Congo basin (Tack et al., 2001). The Inkisi Group has been sampled at the UIA mountain where it is exposed in a steep wall of massive, medium to coarse grained, cross-bedded red sandstone. Conglomerate levels mark the bottom of fining upward channel fills. The contact with the underlying Mpioka Subgroup was not exposed.

4.3.2 Metamorphism

The West Congo Belt is a fold and thrust belt with rapidly decreasing amount of deformation towards the east (Tack et al., 2001). The West Congo Supergroup has experienced deformation related to the final closure of the Macaúbas Basin during the Araçuaí-West-Congo Orogen (Tack, 1975; Maurin, 1993; Tack et al., 2001). This event caused thrusting of the Palaeoproterozoic Kimezian Supergroup onto the Zadinian Group, itself thrust onto the Mayumbian Group which is overlain by the sediments of the West Congolian Group.

A syn-kinematic metamorphic grade decreases from amphibolite facies in the west to greenschist and eventually to unmetamorphosed sedimentary rocks in the east of the West Congo Belt. Around the city of Boma amphibolite facies metamorphism with maximum temperature of 550-600°C has been observed (Delhal and Ledent, 1976; Franssen and André, 1988) which passes into greenschist facies around Matadi and even lower degrees of metamorphism further eastward (Franssen and André, 1988).

Field observations point to a very low metamorphic grade for sampled outcrops. None of the rocks show cleavage and primary structures are well preserved e.g. sedimentary structures at the DZI and VAP localities (Photos A.1 and A.5b and A.5a) and slumped microbial laminites at the SAF locality (Photos A.3a and A.4b). Microscopic evidence of metamorphic minerals is limited to secondary quartz and white mica formed around pre-existing quartz grains in arenites of the Sansikwa Subgroup at the DZI locality. These minerals are typically found in low-grade metamorphic rocks such as zeolite facies with temperatures up to 150°C. The destruction and chloritisation of the associated KAS volcanics may be a primary or early diagenetic feature and is not necessarily indicative of a metamorphic event. Diagenetic chlorite can form at temperatures as low as 100°C (Gifkins et al., 2005).

4.3.3 Previous Studies

A reconnaissance provenance study of the West Congolian Group in the Bas-Congo Province by Frimmel et al. (2006) has shed some light on the Neoproterozoic evolution of the West Congo Belt. Based on whole rock major and trace element concentrations for

24 siliciclastic rock samples they showed that the passive margin platform sediments had a strong continental arc signature. Detrital zircons were separated from samples from the Sansikwa, Haut-Shiloango and the Inkisi (sub)groups and their U-Pb ages used to obtain maximum depositional ages of the respective stratigraphic units. The analyses however contained many highly discordant results and the 2σ errors are typically around 10% of the U-Pb age. A maximum depositional age of 650 Ma is assigned to the Haut-Shiloango Subgroup but the reasoning remains unclear. The three youngest grains that have concordance of different U-Pb systems <10% are 709±20, 671±20 and 547±45 Ma.

The number of analysed grains per sample (n = 20) is too low for a comprehensive provenance study as a population making up 20% of the actual sample could still be missed at a 95% confidence level (Vermeesch, 2004). Whilst this is a useful pilot study, many more data are required before any reliable age or provenance information can be obtained.

Frimmel et al. (2006) also presented an ^{40}Ar-^{39}Ar age of 566±42 Ma for a doleritic sill which is part of the feeder system of the Lower Diamictite Formation volcanics. The sample is described as a *"coarse grained dolerite, mainly composed of albitised plagioclase and igneous augite, with secondary actinolite, epidote, sericite and minor biotite in microcracks and veinlets*" (Frimmel et al., 2006, p.235). The analysis was performed on a mineral separate containing mainly clinopyroxene and a minor amount of secondary mafic minerals. It is argued by the authors that this is the age of a metamorphic event related to the Pan-African deformation of the West Congolian Group leaving the emplacement age of these volcanics still to be determined. In their conclusion the authors stress the preliminary nature of their work (Frimmel et al., 2006).

4.4 Sample and Analytical Details

Between three and eight siliciclastic samples were collected from the Sansikwa Subgroup, from both diamictite formations, from the Haut-Shiloango and Mpioka subgroups and from the Inkisi Group for provenance geochemistry analysis. In addition seven samples from the subaqueous volcanics of the Lower Diamictite Formation were subjected to geochemical

analysis. Sample DZI 2 of the Sansikwa, KWI 13 of the Upper Diamictite Formation, UIA 5 and UIA 8 of the Mpioka Subgroup and UIA 1 of the Inkisi Group were subject to mineral separation and detrital zircons were analysed. All these results are part of the provenance study in Section 4.7.

A medium-grained doleritic sill associated with the Lower Diamictite Formation was kindly provided by L. Tack of the Royal Museum for Central Africa (Tervuren, Belgium) (registration number "RG 70.838" and accompanying field notes in archive file "G 244") and was sent to Lund University (Sweden) for mineral separation and U-Pb baddeleyite analysis. Mineral separates from the same sample yielded a ^{40}Ar-^{39}Ar age of 566±42 Ma (Frimmel et al., 2006). The baddeleyite analyses results are presented in Section 4.6.

Samples of the Haut-Shiloango and Schisto-Calcaire carbonates were analysed for stable isotopes of carbon and oxygen. The chemostratigraphy is analysed below in Section 4.5.

Finally, palaeomagnetic samples were obtained from carbonates at the SAF and CRO localities, from the Upper Diamictite at the KUM locality, from volcanics at the KAS locality and from oriented hand-samples collected at the UIA locality. Palaeomagnetic analyses are described in Chapter 5. A detailed account of all analytical techniques can be found in Chapter 3.

4.5 Stable Isotope Geochemistry

Comparing secular variations in the carbon isotopic composition of carbonate sediments is a common chemostratigraphic tool for correlating Neoproterozoic sedimentary sequences. Carbon isotopes in carbonates are generally considered a reliable proxy for δ^{13}C of the ocean water they precipitated from, although this assumption has recently been questioned: Knauth and Kennedy (2009) argue that δ^{13}C variations in carbonates rather reflect mixing of meteoric groundwater and seawater. The depositional environment also as to be taken into account when interpreting these isotope ratios (Frimmel, 2009, 2010). Despite this, due to a lack of chronostratigraphic data for Precambrian rocks, comparing C isotopes is often considered one of the most reliable techniques for local, regional or global corre-

lations. Based on the occurrence of some remarkable isotopic excursions, a carbon isotope composite curve has been produced for the Neoproterozoic Era (Halverson et al., 2005, 2010, see Fig. 4.5). This provides a framework for carbon-isotope correlations although it remains poorly time-calibrated and needs more constraints by way of radiometric age determinations (Halverson et al., 2005).

Carbon isotopes are relatively insensitive to diagenesis when compared to oxygen isotopes owing to the extreme differences in the concentrations of these elements in diagenetic fluids. Fluid/rock ratios have to be 3 orders of magnitude higher to replace carbon than for carbonate minerals to equilibrate with the fluid δ^{18}O values (Banner and Hanson, 1990). Carbon and oxygen isotopes from this study and from Frimmel et al. (2006) are plotted together in Figure 4.4 to assess the amount of diagenetic alteration that has taken place in carbonates of the West Congolian Group. According to Knauth and Kennedy (2009), the isotopic system of marine precipitates in coastal areas is highly influenced by meteoric ground waters during lithification. In this process both δ^{13}C and δ^{18}O behave in a co-variant way and decrease along a lithification trend as indicated in Figure 4.4. A rock sample in the lithification domain, e.g. with a strongly negative δ^{13}C, might therefore not reflect the composition of ancient ocean water but might be the result of mixing of seawater with meteoric waters and might represent the initial 'unaltered' value of the rock. The alteration trend in Figure 4.4 reflects the fact that diagenesis results in decreasing δ^{18}O but does not have a significant effect on the carbon isotopic system.

In Figure 4.4 the vast majority of stable isotope results from the West Congolian Group plot left of the lithification trend. This indicates they have undergone isotopic partial resetting. Oxygen isotopes are therefore not considered to be primary but carbon isotopes may still represent the initial unaltered value of the rock because of their insensitivity to diagenesis. The data show groupings around positive (ca. 5‰) and negative (ca. -3‰) δ^{13}C values and these groupings are strongly linked with stratigraphy as will be shown below. The spread is larger for the samples from Frimmel et al. (2006) due to sampling of larger stratigraphic intervals.

Stratigraphic variations of δ^{13}C isotope ratios are presented in Figure 4.5 where data from this study are combined with previously published results (Frimmel et al., 2006). Black

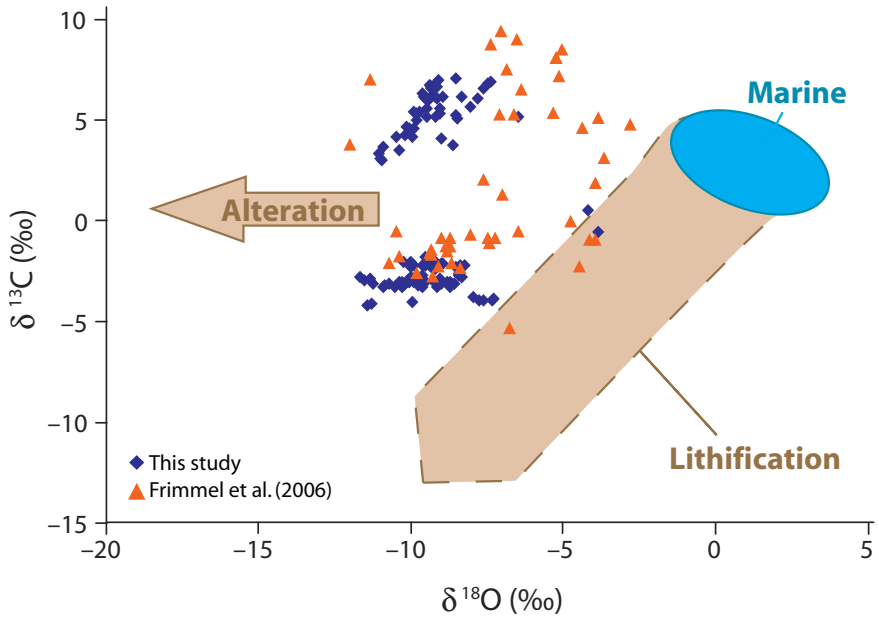

Figure 4.4. Oxygen vs. carbon isotopes after Knauth and Kennedy (2009). Fields indicate the isotopic composition of seawater, the correlation that would result from mixing seawater and meteoric water (lithification) and the effect of diagenetic alteration. All δ^{13}C and δ^{18}O values are listed in Appendix S3.1.

carbonates at the top of the Haut-Shiloango Subgroup show positive δ^{13}C values (7 to 3‰). In contrast the dolomitised carbonates of Schisto-Calcaire Subgroup lithofacies c1, directly above the Upper Diamictite Formation, have δ^{13}C values starting at -2‰ and dropping to -3‰ and eventually -4‰ up sequence. The δ^{13}C profile shows a gradual return to less negative values: results from this study and Frimmel et al. (2006) for lithofacies c3 all plot between -2 and -2.5‰. Results from Frimmel et al. (2006) for c4 and c5 lack a clear trend but are predominantly negative for c4 and positive for c5.

A similar negative swing in δ^{13}C isotopes has been recorded in rocks below and above the Ghaub Diamictite on the Otavi Platform along the southern margin of the Congo Craton in Namibia (Hoffman and Schrag, 2002, Fig. 4.5) and has subsequently been correlated to sections in Canada and Australia and to the global composite curve (Hoffman and Schrag, 2002; Halverson et al., 2005). The Ghaub Glaciation has been dated at 635.5±1.2 Ma (Hoffmann et al., 2004). Limited exposure prohibited constructing a continuous chemostratigraphy for the Schisto-Calcaire Subgroup but the individual and very detailed sections allow a conservative correlation to the Otavi platform deposits and to the

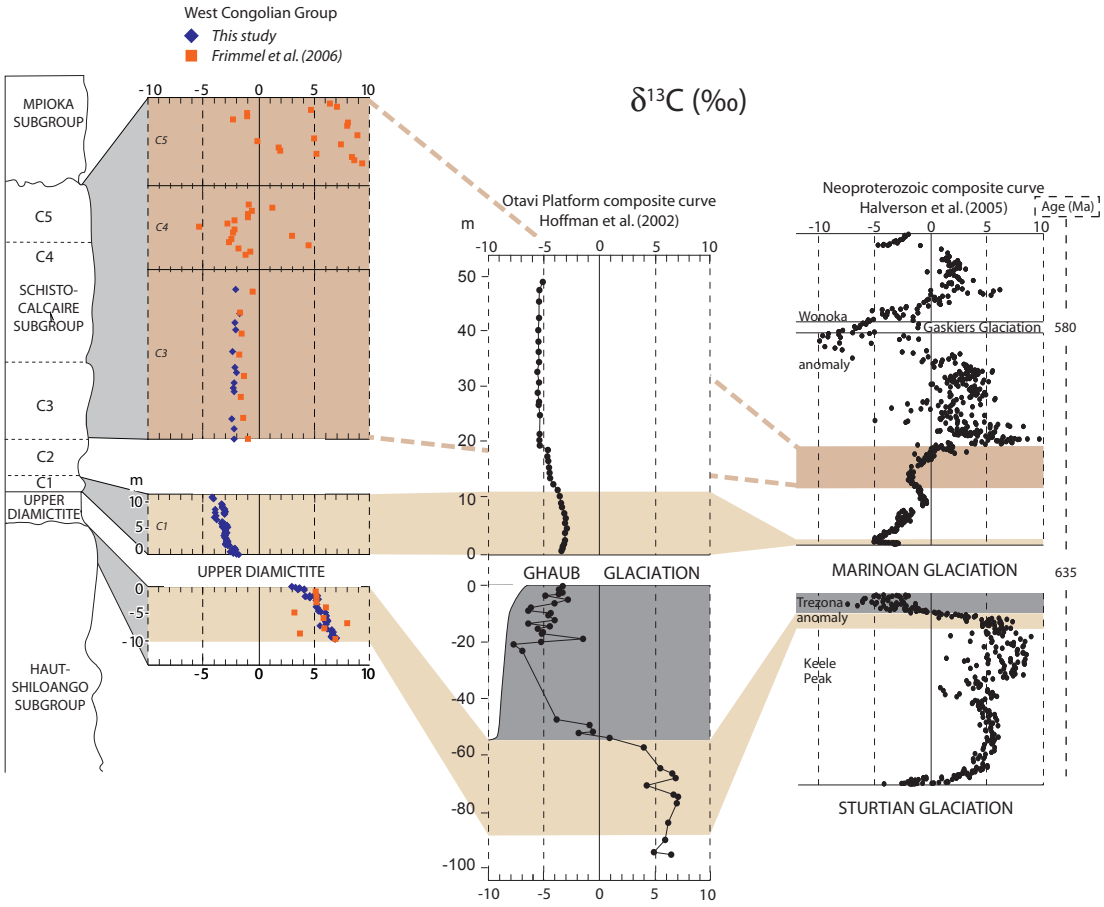

Figure 4.5. Carbon isotopes for the West Congolian Group correlated to a composite profile across the Ghaub Diamictite in Namibia (Hoffman and Schrag, 2002) and to a composite profile for the Neoproterozoic (Halverson et al., 2005).

Neoproterozoic master curve. δ^{13}C values of -2 to -2.5‰ for lithofacies c3 are found at 400 – 600m above the dolomitic cap carbonate (Fig. 4.5). Similar values are reported around 400m at the Otavi platform (Hoffman and Schrag, 2002). When comparing these sections in more detail both cap dolostones start with values around -3‰ for the first 10 – 12 m after which it decreases to below -5‰ in Namibia. In the West Congo Belt only the first 10 m are sampled and the top-most samples are -4.5‰. The Haut-Shiloango carbonates do not show a negative swing (the Trezona Anomaly, see Fig. 4.5) but a basal ^{13}C-depletion below the diamictite is missing in many sections across the world including several sections in Namibia (Hoffman et al., 1998; Halverson et al., 2005). This is illustrated by the incision of the Ghaub Glaciation into the stratigraphic units below and the grey shading in both the Namibian and Neoproterozoic composite curves is the part of the profile that is

often missing. An erosional surface below the Upper Diamictite (Fig. 4.2) could account for this missing part of the δ^{13}C curve in the West Congo Belt. The profile shown in Figure 4.5 is the most complete δ^{13}C curve for the West Congo passive margin ever published and all characteristics are in favour of a correlation to the Neoproterozoic master curve. This makes the Upper Diamictite contemporaneous with Marinoan-type deposits.

4.6 Baddeleyite Age for the Lower Diamictite Formation

		Ratios		Ages (Ma)					
Fraction	U/ Th	$^{207}Pb/^{235}U$ $\pm2\sigma$(%)	$^{206}Pb/^{238}U$ $\pm2\sigma$(%)	$^{207}Pb/$ ^{235}U	$^{206}Pb/$ ^{238}U	$^{207}Pb/$ ^{206}Pb	$\pm2\sigma$ (%)	$\int$206%	concor- dance (%)
1	9.4	0.9722 ± 0.24	0.11268 ± 0.17	689.6	688.3	693.8	3.5	0.058	99.2
2	7.4	0.9624 ± 0.20	0.11149 ± 0.11	684.5	681.4	694.9	3.5	0.056	98.1
3	12.6	0.9790 ± 0.21	0.11342 ± 0.12	693.1	692.6	694.6	3.6	0.079	99.7

Table 4.3. U-Pb baddeleyite TIMS data.

The volcanic rocks intruding the Lower Diamictite Formation are linked to a feeding system of dykes and sills intruding the Sansikwa Subgroup sedimentary rocks (Tack et al., 2001). Whole rock geochemistry for sills and pillow lavas reveal an enriched tholeiitic signature indicating an extensional tectonic setting (see Section 4.7.2, De Paepe et al., 1975; Kampunzu et al., 1991).

A portion of brown euhedral baddeleyite grains was extracted from a doleritic sill. Three fractions were analysed on the Finnigan TRITON thermal ionization mass spectrometer in Stockholm (Table 4.3). They plot along a linear array with one fraction falling close to the Concordia curve (Fig. 4.6). Free regression yields an upper intercept of 694±4 Ma and a lower intercept at -29±390 Ma, indicating recent Pb-loss in some of the grains. The upper intercept is interpreted as the crystallization age of the sample and provides an important new upper age constraint for extensional tectonics in the West Congo Belt. Moreover, it provides an age for the basalts interbedded with the Lower Diamictite Formation and thus a direct age for the diamictite itself.

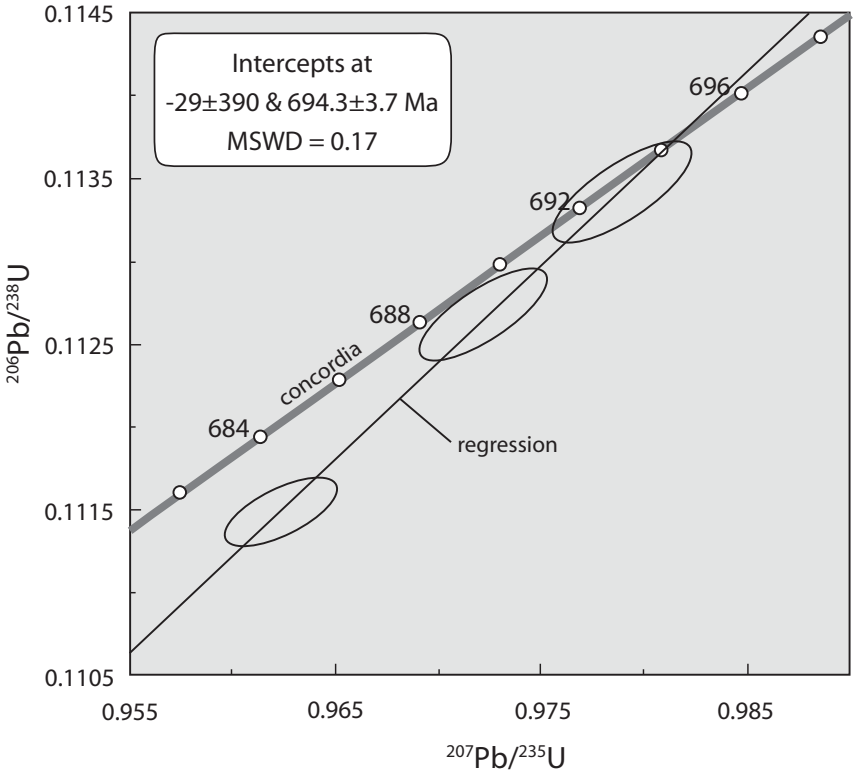

Figure 4.6. U-Pb Concordia diagram for Sumbi sill. All error ellipses are 2σ.

4.7 Provenance Study

4.7.1 Detrital Zircon Geochronology

Samples from the Sansikwa and Mpioka subgroups, from the Upper Diamictite Formation and from the Inkisi Group were selected for mineral separation and detrital zircon analysis. For most samples a minimum of 120 (58 for the Upper Diamictite) zircon grains were analysed for their uranium and lead isotopic composition, the results of which can be found in Appendices S1.1 and S1.2.

Data treatment and construction of probability density plots

Two ages are commonly used in U-Pb studies. They are based on the $^{207}Pb/^{206}Pb$ and $^{206}Pb/^{238}U$ isotope ratios and unless the data are completely concordant there is always

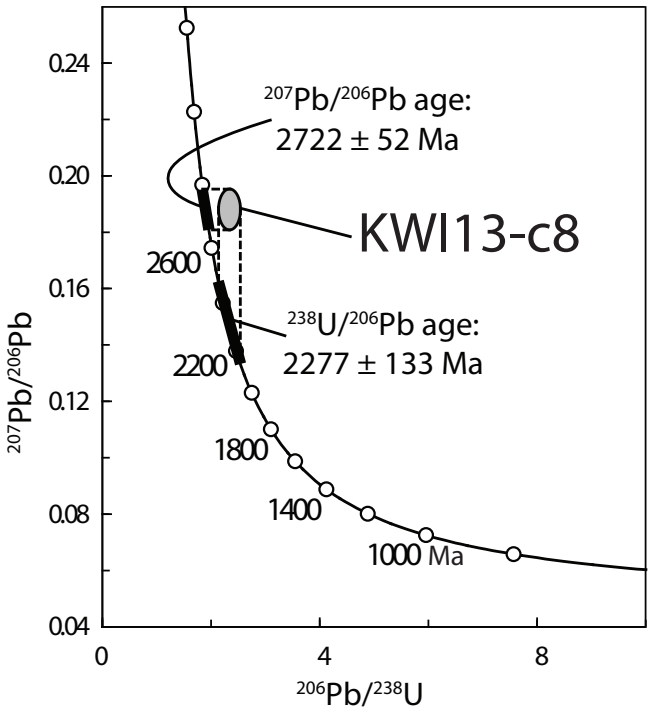

Figure 4.7. Tera-Wasserburg concordia diagram showing the difference between $^{207}Pb/^{206}Pb$ and $^{206}Pb/^{238}U$ ages for discordant grains. Illustration is for one analysis (KWI13-c8) which has a concordance of 84% . The analysis plots closer to the $^{207}Pb/^{206}Pb$ age which in this case is a better approximation to its crystallisation age.

a slight difference between these two. The difference can be visualised using a Tera-Wasserburg concordia plot (Tera and Wasserburg, 1972) which has both isotope ratios on the axes (Fig. 4.7). The $^{206}Pb/^{238}U$ age tends to underestimate the crystallisation age of a zircon grain when it is discordant, especially for old grains (e.g. >1500 Ma). However, for younger grains the $^{206}Pb/^{238}U$ age is more precise because ^{207}Pb cannot be measured with high precision leading to a large analytical error. Nemchin and Cawood (2005) carried out a detailed U-Pb study on a suite of detrital zircon grains and showed that with probability density plots, $^{207}Pb/^{206}Pb$ ages better represent the actual ages of the grains older than ca. 1500 Ma. This age is adopted for this study to switch from using $^{207}Pb/^{206}Pb$ ages to $^{206}Pb/^{238}U$ ages. The age spectra for all samples in this study conveniently contain a break around 1500 Ma making it easy to compare individual datasets.

Probability density plots are constructed to display age groupings but calculating the age of a grain using one isotope ratio only causes difficulties with discordant grains. Groups

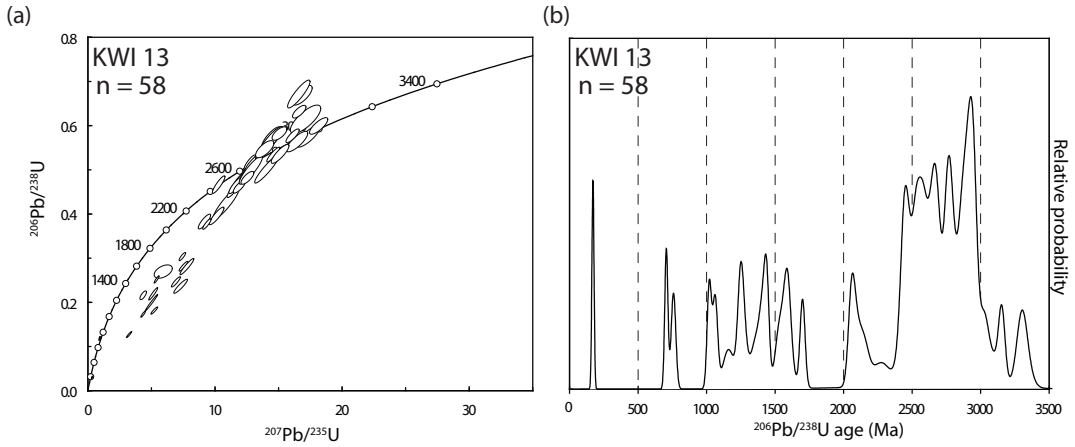

Figure 4.8. The effect discordant grains can have on a probability density plot using $^{206}Pb/^{238}U$ ages only. Many discordant grains in (**a**) result in populations between 2000 and 1000 Ma in (**b**) while these analyses probably lie on a Pb loss trend and belong to the same population (see Figure 4.9).

of discordant grains can create 'additional' age peaks which are artefacts of the data analyses. Figure 4.8 shows how grains which clearly lie on a Pb loss trend (Fig. 4.8a) can lead to many additional age peaks on a probability density plot (Fig. 4.8b). These peaks are meaningless and hamper interpretations. To account for this effect, the analyses are weighted according to their probability of concordance following the methods described by Nemchin and Cawood (2005). Weighting was applied using the formula:

$$f = P\frac{1}{\sqrt{2\pi\sigma}}exp\left[-\frac{1}{2}\left(\frac{T-t}{\sigma}\right)^2\right]$$

where:

t	concordia age for individual analysis
σ	one standard deviation error of this age
P	probability of concordance
T	time at which the contribution is determined

This way the contribution of an individual analysis is proportional to its probability of concordance. The probability of concordance is obtained by calculating the 'concordia age' (Ludwig, 1998) for every analysis using the Isoplot software (Ludwig, 1999).

Nemchin and Cawood (2005) showed the efficiency of this method in removing 'artificial' age peaks which appeared on plots based on $^{206}Pb/^{238}U$ or $^{207}Pb/^{206}Pb$ ages alone (Fig. 4.8). Many studies apply a fixed cut-off to remove the most discordant data, e.g. by rejecting data more than 5% or 10% of concordance. This decision is rather subjective and is avoided using the method described here. However, there are certain drawbacks as well: discordant data which fall on a Pb loss trend can yield valuable information which is lost on a probability density plot. Sometimes their crystallisation ages as well as the age of the Pb loss event can be determined using regression techniques. To detect significant Pb loss trends concordia diagrams are plotted using all data (Fig. 4.9). Another problem is caused by highly discordant data with large errors which has to be taken into account during interpretation of the probability plots.

The probability density plots in Figure 4.9 are created using the method described above. When discussing individual analyses the most reliable age constraints will be those that are close to concordance (between 95 and 105%) and that have a reasonable probability of concordance (above 0.1). HR-SIMS analyses will be used to obtain some very precise ages for probability density peaks. A probability density plot for all HR-SIMS data is presented in Figure 4.10. CL images of a selection of zircon grains to represent each unit is presented in Appendix S2.

Descriptions of probability density plots

A total of 123 analysed grains from a quartz sandstone of the Sansikwa Subgroup are dominated by a Palaeoproterozoic and a late Mesoproterozoic population. The largest peaks center on 1967 Ma (35 grains) and 1002 Ma (24 grains) but several small peaks can be observed close to these ages (Fig. 4.9). Very precisely dated grains at 1918±11, 1937±7 and 1961±6 Ma (dated by HR-SIMS, Table S1.2) suggest that the Palaeoproterozoic populations may reflect several events. A total of 38 Mesoproterozoic and Neoproterozoic grains are identified with a peak at 1002 Ma. Ten grains have Archaean ages and nine of these are centred on 2673 Ma but because of their discordance only the most concordant grain at 2606±38 Ma appears on the weighted density plot. The youngest grain which is reasonably concordant (<5% discordant) and with a probability of concordance >0.1 is

979±31 Ma and provides a maximum age for the Sansikwa Subgroup.

Grains from the Upper Diamictite Formation at the KWI locality were small (generally <40μm), contained many fragments and 25 of the 58 analyses were more than 10% discordant. From the concordia diagram (Fig. 4.9) it appears that many analyses fall on a line towards the origin which could be caused by a recent Pb loss event. Regression on 30 LA-ICPMS analyses results in an upper intercept of 2692±10 Ma (Model 2 solution, Ludwig, 1999) which can be interpreted as the crystallisation age of these 30 grains making it the largest population in this sample. Nine grains are Mesoarchaean in age (i.e. >2800 Ma) and form a peak around 2981 Ma. Only two post-Archaean grains are concordant at 2471±29 and 707±23 Ma with 100% and 103% respectively. All others plot on or close to the regression line. The 707±23 Ma zircon serves as a maximum age for the Upper Diamictite.

Two samples from the Mpioka Subgroup were analysed resulting in a total of 208 zircon ages. The two samples were derived from approximately the same stratigraphic level and the results are therefore combined in Figure 4.9. They contain 11 Archaean grains centred on 2605 Ma although a 100% concordant HR-SIMS age of 2635±4 Ma gives the most precise Archaean age. Palaeoproterozoic ages spread from 2438±23 Ma to 1863±44 Ma but the largest peak is at 1921 Ma. More than half the zircon grains are Mesoproterozoic (56 grains, one peak at 1067 Ma) or Neoproterozoic (71 grains, several peaks) in age. The youngest grain with low (<5%) discordance is 607±16 Ma which gives a maximum age to the Mpioka Subgroup.

The population plot for the Inkisi Group is in many ways similar to that of the Mpioka Subgroup but with a much more pronounces Archaean population (Fig. 4.9). A group of 17 Archaean grains are centred on 2599 Ma but HR-SIMS ages of 2731±3, 2628±3, 2615±4 and 2602±5 Ma point to several zircon growth events. Palaeoproterozoic ages are spread between 2311±21 and 1888±24 Ma. Two mid-Mesoproterozoic grains cause a peak at 1386 Ma but most grains are late Mesoproterozoic in age with the highest peak around 1035 Ma (9 grains). A total of 49 Neoproterozoic grains form several peaks but most are grouped around 719 Ma, similar to the Neoproterozoic peak in the Mpioka Subgroup and the Upper Diamictite Formation. The youngest grain < 5% discordance is 581±18 Ma and

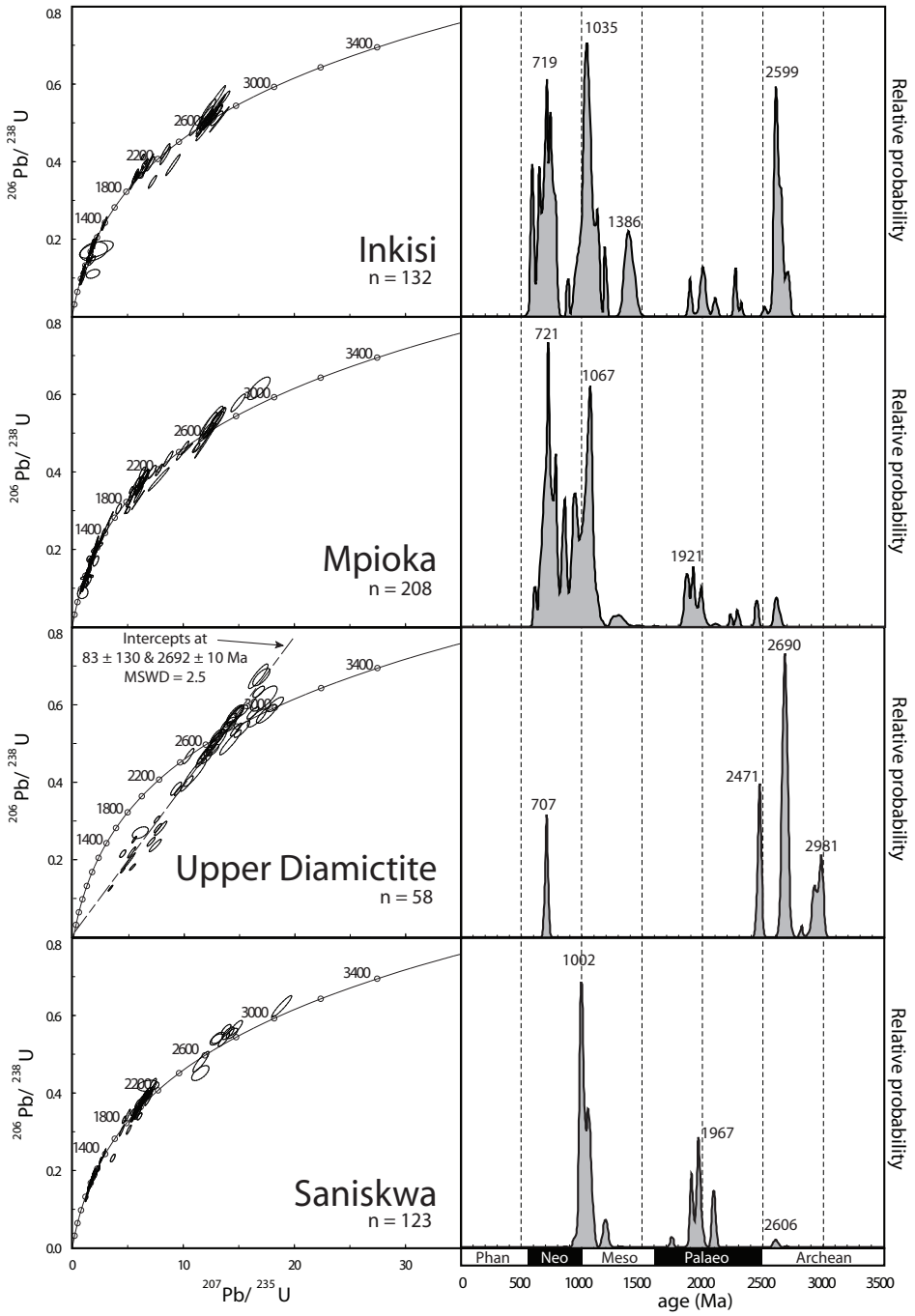

Figure 4.9. U-Pb concordia curves on the left and weighted probability density plots on the right for four formations of the West Congolian Group using the data from Appendix S1.1. All analyses were obtained using LA-ICPMS at the Institut für Mineralogie, Westfälische Wilhelms-Universität Münster (Germany). Average ages of the peaks are in Ma. For the timescale at the bottom: Palaeo, Palaeoproterozoic; Meso, Mesoproterozoic; Neo, Neoproterozoic; Phan, Phanerozoic. n = number of grains.

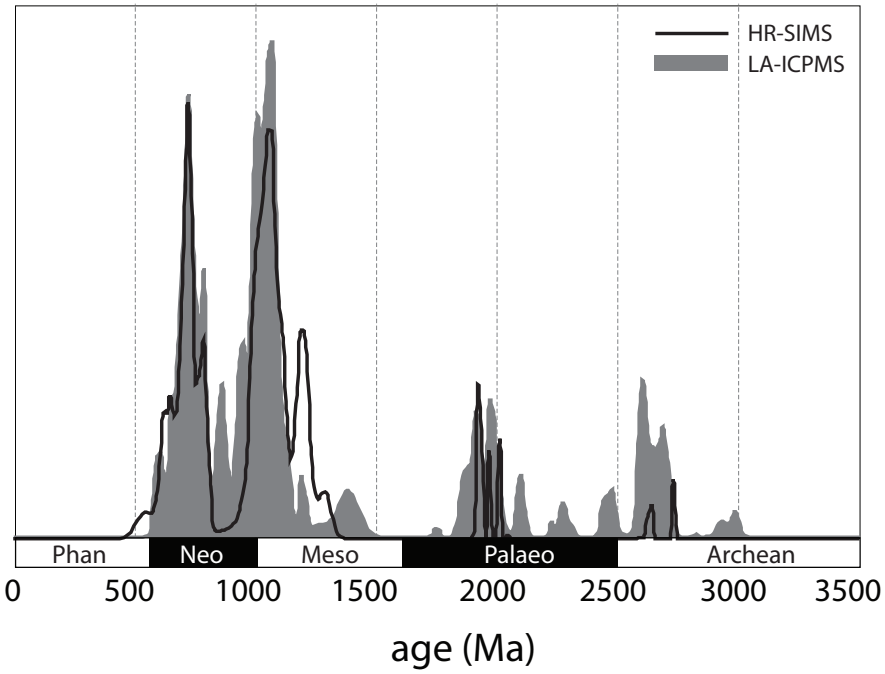

Figure 4.10. Weighted probability density plots for all analyses obtained using LA-ICPMS (n=521) and HR-SIMS (n=90). All peaks of the HR-SIMS data have corresponding peaks in the LA-ICPMS profile.

provides a maximum age for this Group

All grains were categorised according to their shape (rounded / angular), habit (euhedral / subhedral), colour (clear / brown / dark) and level of zoning (magmatic / metamorphic / unzoned). This was done using an optical microscope and using the CL images which are available for some grains (Appendix S2). Unfortunately no correlations between shape, habit or colour and age nor concordance could be established. In the Sansikwa Subgroup 95% of the grains are rounded while for all other units rounded grains make up ca. 50% of the total number. Rounded grains suggest they have undergone a considerable amount of transport.

Age groupings and trends

The probability plots reveal grouping of detrital zircon ages into distinct Archaean, Palaeo-proterozoic and Meso- to Neoproterozoic populations and especially highlight a change in

provenance up sequence (Fig. 4.9). The Sansikwa Subgroup shows predominantly mid-Palaeoproterozoic and Mesoproterozoic-Neoproterozoic boundary age sources while the Upper Diamictite Formation contains predominantly Archaean grains with one Neoproterozoic grain. The Mpioka Subgroup and Inkisi Group show almost identical age spectra, differing only in concentration, ranging from Archaean to the Neoproterozoic with a pronounced gap between 1800 and 1400 Ma (Fig. 4.9).

Source regions

The West Congolian Group comprises Neoproterozoic passive margin platform deposits covering Archaean and Palaeoproterozoic cratonic basement rocks that form a likely source for their oldest zircon populations. Archaean nuclei are exposed at several margins of the Congo craton and are composed of gneissic complexes and greenstone belts with associated magmatic rocks (e.g. Milesi et al., 2006). Several MesoArchaean and NeoArchaean blocks are recognised of which the nearest to the field area are to the north, east and south of the West Congo Belt (all potential source rocks are summarised in Figure 4.11). To the north the Ntem Complex is exposed in Cameroon, Equatorial Guinea, Gabon and the Republic of Congo. It contains, amongst other (older) suites, 2950-2800 Ma intrusives as well as late magmatic rocks including K-rich granitoids and syenogranites (Caen-Vachette et al., 1988; Toteu et al., 1994). Crystallisation ages of 2948±47 Ma and 2678±23 Ma form almost exact matches with some population in our samples (Fig. 4.11). In the Kasai Block to the east of our field area the Malafudi Granites and Migmatites yield a Rb-Sr isochron age of 2593±92 Ma (Delhal and Ledent, 1976) and a zircon U-Pb age of 2680±5 Ma (Cahen et al., 1984). To the south of the West Congo Belt Archaean rocks in western Angola comprise a granite-gneiss-migmatite complex with a Rb-Sr age of 2520±36 Ma (Carvalho et al., 2000). All these Archaean blocks could be sources for the oldest populations in this study.

In the West Congo Belt, the Palaeoproterozoic Kimezian Supergroup comprises metasedimentary rocks with a metamorphic age of ca. 2 Ga (Delhal and Ledent, 1976; Vicat and Pouclet, 2000) and deformed granitoids with a continental arc signature are also dated at 2.0 Ga (Vicat and Pouclet, 2000). In the Republic of Congo the Palaeoproterozoic

Bikossi and the Loukoula Series comprise calc-alkaline granitoids and acidic lavas (Vicat and Pouclet, 2000). The only available radiometric age is a U-Pb zircon age of 2000±80 Ma for a late tectonic granodiorite pluton (the Les Saras Granodiorite Maurin et al., 1990, 1991). These Palaeoproterozoic ages can be found in the Upper Diamictite Formation and younger units (Fig. 4.9).

Mesoproterozoic rocks are found in the Kibaran orogenic belt on the eastern side of the craton (Fig. 2.3) and are abundant on the southern margin but are unknown in the West Congo Belt (Vicat and Pouclet, 2000). The occurrence of Mesoproterozoic detrital zircons led Frimmel et al. (2006) to suggest a close relationship with the São Francisco Craton where Mesoproterozoic rocks are found in the Espinhaço Supergroup. However, reported ages from the felsic rocks of this supergroup are all 1740 – 1700 Ma in age (U-Pb zircon ages Dussin and Dussin, 1995; Martins-Neto, 2000) and, therefore, are too old too be a potential source.

Detrital zircons of this age have also been reported in the Araçuaí Belt (Pedrosa-Soares et al., 2000), the Central Ribiera Belt (Machado and Gauthier, 1996; Söllner and Trouw, 1997; Valladares et al., 2004) and the southern Brasília Belt (e.g. Valeriano et al., 2004). Potential sources for these grains are suggested to be situated in the Borborema Province to the north of the craton where magmatic rocks formed during the Cariris Velhos Event (∼1100-950 Ma, Brito Neves et al., 1995) or the São Francisco Craton where they might still be undetected. The only recognised Mesoproterozoic source rocks in Africa are found in Angola (Basei et al., 2008) where several Mesoproterozoic ages are identified e.g. the 1371±25 Ma Kuene Anorthosite Complex (U-Pb zircon, Mayer et al., 2004) and red granites constrained by several Rb-Sr ages between 1411±24 and 1302±20 Ma (Torquato et al., 1979; Mayer et al., 2004). These African rocks are considered the most likely sources for Mesoproterozoic zircons in this study (Fig. 4.11).

The oldest Neoproterozoic detrital zircon grains could be derived locally from Zadinian granites and Mayumbian rhyolitic lavas which have been dated 999±7 and 912±7 Ma respectively (Tack et al., 2001). An unconformity between the West Congolian Group and the Mayumbian Group indicates that the sediments were deposited after unroofing of the igneous rocks and so they would have been available for weathering (Tack et al., 2001).

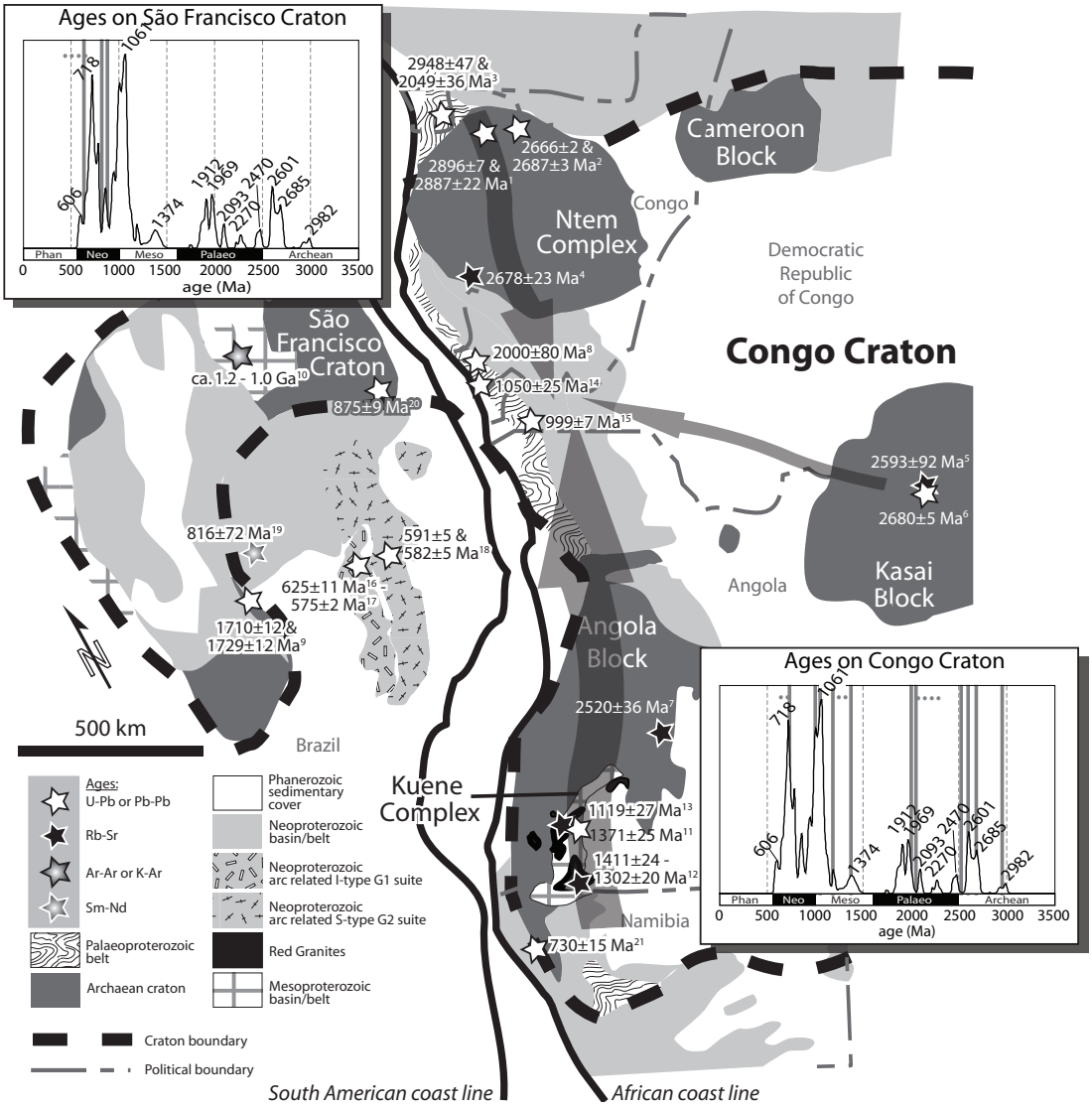

Figure 4.11. Map reconstruction of postulated source rocks surrounding the West Congo Belt. Arrows indicate proposed provenance for the West Congolian Group sediments. Two insets show composite probability density curve for all zircons, grey bars indicate known crystallisation ages, dots are inferred crystallisation ages (see text for details). [1]Charnockites, Toteu et al. (1994); [2]K-rich granitoids, Tchameni et al. (2000); [3]regression concordia intercept ages for zircons from Nyong Series gneisses, Toteu et al. (1994); [4]K-rich granitoids in the Chaillu area, Caen-Vachette et al. (1988); [5]Malafudi granites, Delhal and Ledent (1976); [6]Malfudi migmatites, Cahen et al. (1984); [7]granitoids and gneisses, Andula region (Central Shield), Carvalho et al. (2000); [8]Les Saras Granodiorite, Maurin et al. (1990, 1991); [9]volcanics in lower part of the Espinhaço Group, Dussin and Dussin (1995); Martins-Neto (2000); [10]mafic dykes intruding the Espinhaço Group, Renne et al. (1990); Danderfer et al. (2009); [11]mangerite vein cogenic with the Kuene Anorthosite Complex, Mayer et al. (2004); [12]Red Granite intruding the Kuene Complex, Torquato et al. (1979); [13]noritic dykes cross-cutting the Kuene Complex, Carvalho et al. (1987); [14]Mfoubou and Pk 8 granite, Djama (1988); [15]Noqui Granite, Tack et al. (2001); [16]tonalitic gneiss, Paes (1999); [17]I-type pluton, Noce et al. (2000); [18]S-type plutons, Noce et al. (2000); [19]Amphibolites-ocean floor basalts, Pedrosa-Soares et al. (1998); [20]A-type Salto da Divisa Granite, da Silva et al. (2008); [21]Granodiorite pluton, Kröner et al. (2004).

Other late Mesoproterozoic and early Neoproterozoic intrusions are found along the West Congo Belt to the north such as the Mfoubou and Pk 8 granites, dated by U-Pb zircon age at 1050±25 Ma (Djama, 1988), or the Mount Kanda Granite, the Bibabanka Granite or the Sounda rhyolites (all undated but proposed to be coeval with or slightly post-dating the Mfoubou and Pk8 granites based on stratigraphic relationships, Vicat and Pouclet, 2000). In the northern part of the São Francisco Craton A-type granitic intrusions are date at 875±9 Ma by zircon U-Pb SHRIMP (da Silva et al., 2008, Fig. 4.11).

Neoproterozoic felsic rocks of Brazil range in age from ca. 625 to 570 Ma (see geochronological overview by Pedrosa-Soares et al., 2001). Given that mid Neoproterozoic zircons in this study are restricted to 718 Ma for which no source rock has been identified yet in the Araçuaí Belt makes the São Francisco Craton an unlikely source. A more likely source is the Kaoko Belt along the southwestern margin of the Congo Craton where several mid Neoproterozoic ages are reported and a U-Pb TIMS age of 730±15 Ma for a granodiorite pluton forms an almost exact match with the detrital zircon peak at 718 Ma (Fig. 4.11, Halliday et al., 1998). The most likely sources for the Mesoproterozoic and Neoproterozoic zircons identified here, therefore, is southern Angola and northern Namibia.

4.7.2 Provenance Geochemistry

Provenance geochemistry is used to understand and constrain the relationship between the Congo Craton and its neighbouring cratons as well as to gain insight into the evolution of the West Congo Basin during the Neoproterozoic. Major and trace element concentrations are plotted to construct discrimination diagrams and to characterise the sedimentary rocks of the West Congolian Group. From these plots, trends are identified which may indicate source areas and tectonic settings of the depocentre. All whole rock geochemical data are presented in Appendix S4.1.

In the following diagrams the sediment compositions will be compared to average Proterozoic shale (APS, Condie, 1993) as well as Post Archaean Australian Shale composition (PAAS, Taylor and McLennan, 1985). The Schisto-Calcaire Subgroup is purely composed of carbonates thus no clastic sediments could be collected.

Major element geochemistry

The geochemical analysis of sediments is a valuable tool for provenance studies but only if their chemistry has not been strongly affected by weathering or diagenesis. Therefore the major element geochemistry of all rock units of the West Congolian Group is analysed to monitor weathering rates and element mobility. The chemical index of alteration (CIA) is a good measure of the degree of chemical weathering (Nesbitt and Young, 1982). A high CIA means mobile oxides have been removed from the analysed sample which is indicative of the break down of plagioclase feldspars. The CIA is defined as:

$$CIA = 100 * \frac{Al_2O_3}{Al_2O_3 + CaO^* + Na_2O + K_2O}$$

where CaO^* refers to carbonate that is associated with the silicate minerals, corrected for calcium associated with carbonates and phosphates (following Fedo et al., 1995):

$$CaO^* = CaO - \frac{10}{3}P_2O_5 - CO_2$$

assuming P_2O_5 is entirely associated with apatite and CO_2 with calcite.

Three diagrams in Figure 4.12 are based on the CIA: In Figure 4.12a Al_2O_3, $CaO^* + Na_2O$ and K_2O are plotted in a ternary diagram (A-CN-K diagram after Nesbitt and Young, 1984; Fedo et al., 1995) where the CIA is expressed along the vertical scale bar on the left. An ideal weathering trend for rocks of typical upper crust composition is indicated by a solid arrow. Deviation from this trend can occur if, for example, rocks are enriched in K through metasomatism during diagenesis (Fedo et al., 1995, the dash-dot arrow points towards the K_2O apex in Fig. 4.12a). This K-metasomatism can be caused by conversion of plagioclase to K-feldspar or clay minerals to illite (Condie and Wronkiewicz, 1990). Another potential deviation can be the effect of grain size sorting illustrated by the dashed arrow (Fig. 4.12a). This is because feldspars are more concentrated in coarser (c) grained sediments and clay minerals, relatively rich in Al_2O_3, are more abundant in fine grained (f) fractions (Nesbitt et al., 1996).

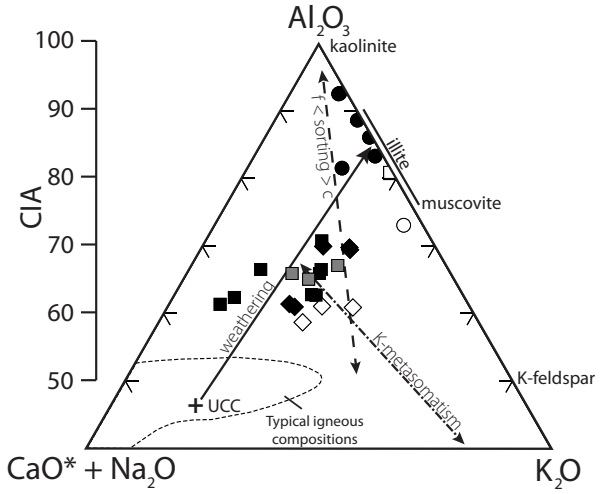

(a) A-CN-K diagram showing major oxides in molecular ratios. Note that only Al_2O_3 >40 is shown. The average composition of typical magmatic source rocks is shown as well as average composition of the upper continental crust (UCC). Arrows are redrawn from Bahlburg and Dobrzinski (2011).

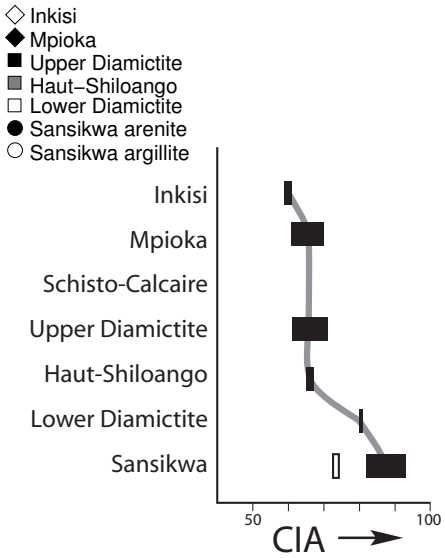

(b) CIA profile of the stratigraphy. The open (closed) boxes for the Sansikwa are for argillite (arenite) samples.

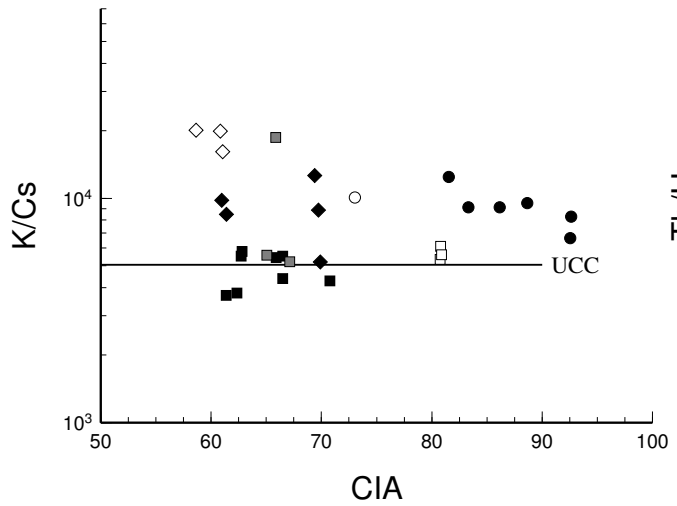

(c) CIA vs. K/Cs (after McLennan et al., 1990). The upper continental crust has a K/Cs ratio of about 5050 (McLennan, 2001).

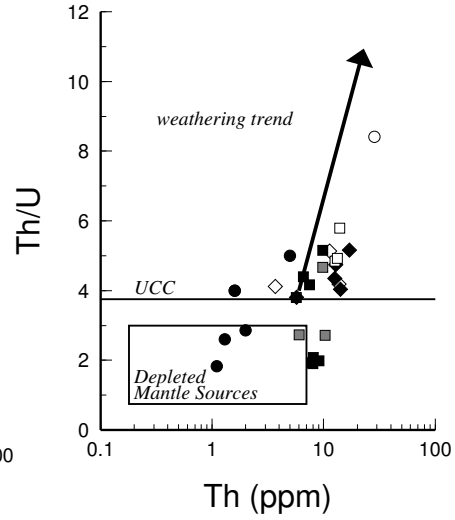

(d) Th concentration (ppm) vs. Th/U (after McLennan et al., 1993).

Figure 4.12. Major element geochemistry plots to indicate the level of chemical weathering and element mobility. All average upper continental crust values are from McLennan (2001). The legend to the symbols used in **(a)**, **(c)** and **(d)** is shown in **(b)**.

Figure 4.12b shows how the CIA changes throughout the stratigraphy. And lastly in Figure 4.12c the CIA has been plotted against K/Cs. Weathering has been shown to fix large cations (such as Cs) but generally leaves the potassium content unchanged (Nesbitt et al., 1980; Nesbitt and Young, 1984; McLennan et al., 1990). The weathering of feldspar to clay minerals will incorporate Cs and is indicated by high K/Cs ratios. Samples with increasing levels of weathering are expected to follow a trend line from the top left to the bottom right hand corner of the diagram (Nesbitt and Young, 1982).

The quartz sandstones of the Sansikwa Subgroup have a high CIA (∼80 – 90, see also Table 4.4) and the argillite shows a slightly lower CIA (∼70) suggesting that variations due to different grain sizes are minor. The Lower Diamictite Formation has a remarkably high CIA (∼80) while its K/Cs value (∼5300 – 6100) is comparable to the average upper continental crust (UCC) value of 5050. The samples for the Lower Diamictite were particularly fine grained. In Figure 4.12a they plot close to the composition of illite suggesting a clay-rich nature for these samples. The CIA decreases significantly from this point in the stratigraphy and the Haut-Shiloango Subgroup (including the Upper Diamictite Formation) plot around the weathering trend in Figure 4.12a. The Mpioka and the Inkisi form two groups in Figure 4.12c with moderate CIA and relatively high K/Cs. They plot slightly below the predicted weathering trend which could be due to their relatively coarse grain size. The majority of samples show moderate CIA values which can be expected for sedimentary rocks and plot close to a weathering trend from UCC composition. The only exception are the Sansikwa Subgroup samples which have lithologically controlled CIA values (due to SiO_2 and clay contents) which means they might not be suitable for provenance geochemical analyses.

Weathering also enhances oxidation of uranium from U^{4+} to U^{6+} making it much more soluble and very mobile (Hurowitz and McLennan, 2005). This causes the ratio Th/U to increase as indicated by the weathering trend in Figure 4.12d. The Sansikwa argillite plots high on the weathering trend while the sandstones are spread, some showing enriched and some depleted Th/U ratios relative to the UCC. All other formations group around and slightly above the UCC value, indicating low to moderate levels of weathering. A few exceptions show high U concentrations (but do not seem to be depleted in Th) which is indicative for the presence of source rocks rich in U such as granites.

Formation/Group	CIA	K/Cs $*10^3$	Th/U
Inkisi	59 - 61	16.1 - 20.1	4.1 - 5.1
Mpioka	61 - 70	5.2 - 12.6	3.8 - 5.2
Upper Diamictite	61 - 71	3.7 - 5.8	1.9 - 4.4
Haut-Shiloango	65 - 67	5.2 - 18.6	2.7 - 5.2
Lower Diamictite	80 - 81	5.3 - 6.1	4.9 - 5.8
Sansikwa-are	82 - 93	6.6 - 12.5	1.8 - 5.0
Sansikwa-arg	73	10.1	8.4
APS	72	-	4.2
PAAS	70	2.0	4.7
UCC	39	5.1	3.8

Table 4.4. CIA and major element ratios for all sedimentary units of the West Congolian Group. Average compositions for sediments and upper crust are from Condie (1993, APS), Taylor and McLennan (1985, PAAS) and McLennan (2001, UCC).

The Lower Diamictite volcanic rocks are plotted in an Alteration Box Plot in Figure 4.13 after Large et al. (2001). This diagram is based on two indices: The alteration index (AI) of Ishikawa:

$$AI = 100 * \frac{MgO + K_2O}{MgO + K_2O + CaO + Na_2O}$$

which is based on the removal of Na and Ca by the breakdown of plagioclase and the Chlorite-Carbonate-Pyrite Index (CCPI):

$$CCPI = 100 * \frac{FeO + MgO}{FeO + MgO + Na_2O + K_2O}$$

reflecting the prominence of chlorite. A high CCPI indicates high levels of alteration to Fe and Mg rich minerals such as chlorite, pyrite, dolomite, magnetite and haematite.

The fields in Figure 4.13 are for modern unaltered volcanic rocks showing the effect of magmatic differentiation. Also shown are several alteration mineral compositions which plot along the margins of the box. The CCPI is naturally high for mafic rocks due to their high FeO and MgO contents. It is clear that our data fall at the very top or above the 'basalt' field, trending towards dolomite/actinolite. This confirms observations of calcite replacing feldspar minerals in thin section and reflects a high degree of alteration and chloritisation.

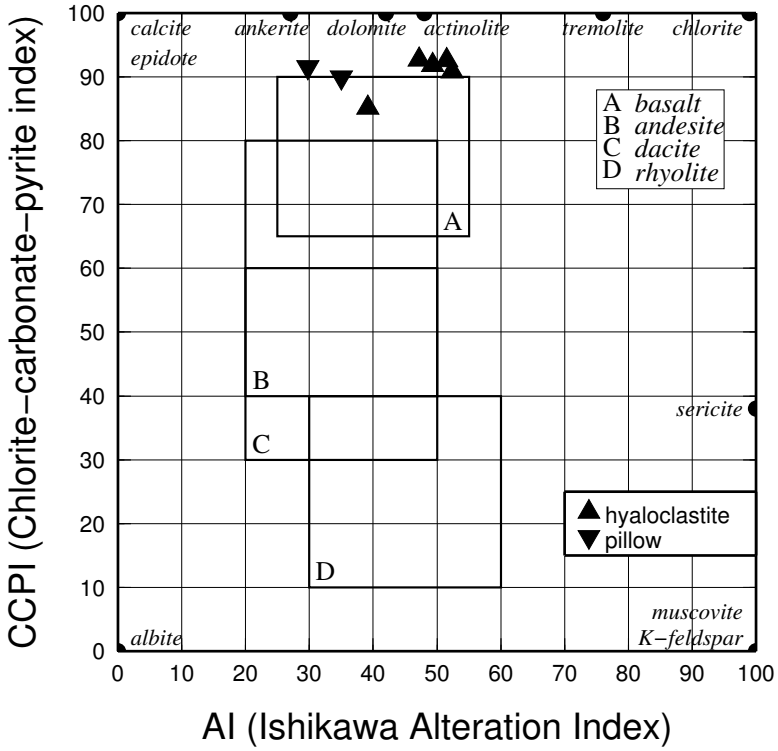

Figure 4.13. Alteration box plot for volcanic rocks after Large et al. (2001).

Compositional trends: minor and trace elements

Originally intended for volcanic rocks, a plot of Nb/Y versus Zr/Ti (Fig. 4.14a) has become popular for its ability to show compositional trends in sedimentary rocks (see e.g. Fralick, 2003; Lacassie et al., 2006; van Staden et al., 2006; Bertolino et al., 2007). Both ratios are relatively resistant to sedimentary processes and should reflect the composition of the sources. The majority of the samples from this study plot along the alkaline trend, close to the composition of post Archaean average shale (PAAS, Taylor and McLennan, 1985). The Sansikwa arenite and Mpioka and Inkisi sandstone samples show influence of more rhyolitic sources. The figure highlights the overall absence of basaltic source rocks.

In Figure 4.14b the same elements are used to classify the volcanic rocks of the Lower Diamictite. Based on their rare earth element content (see below) three samples from the Sansikwa Subgroup (DZI 1A, 1B & 1C) are interpreted to be a volcanic ash and are included in the diagrams for volcanic rocks as 'Sansikwa-tuff'. From the major and trace element geochemical data it is observed that the hyaloclastite samples from the KAS locality have

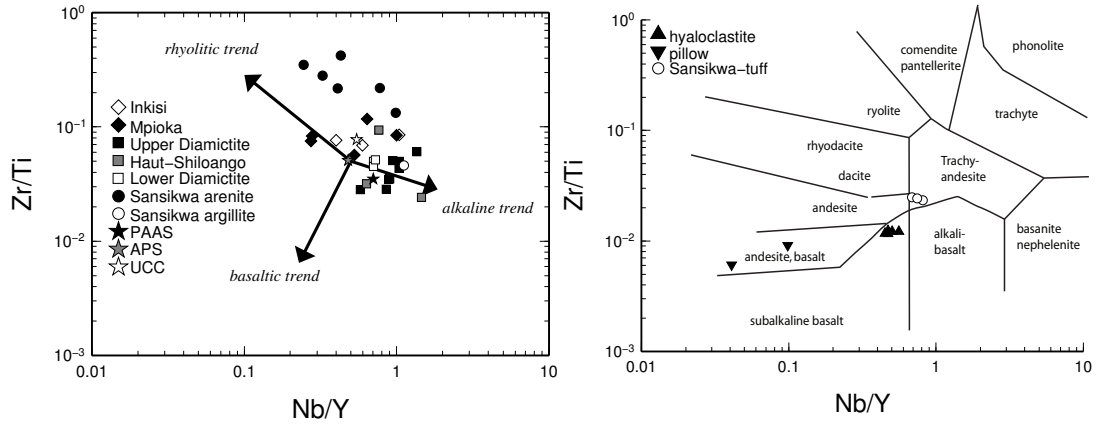

(a) Nb/Y vs. Zr/Ti, first used for sediments by Winchester and Floyd (1977).

(b) Nb/Y vs. Zr/Ti after Floyd and Winchester (1978)

Figure 4.14. Composition of sedimentary and volcanic rocks.

high concentrations of TiO_2 (around 3 %) but are also rich in Zr (> 200 ppm). Both these values are well above the average late Proterozoic basalt composition (1.45% and 128 ppm according to Condie, 1993) but their ratio is almost equivalent. The pillow (PIL) samples have a very high Y content which means they plot away from the hyaloclastites in Figure 4.14b. The Sansikwa-tuffs plot in the trachyandesite field while the hyaloclastite and pillow volcanics plot in the sub-alkaline basalt and andesite, basalt fields respectively.

Formation	Eu/Eu*	La_N/Yb_N	Gd_N/Yb_N	# samples
Inkisi	0.753	13.879	1.787	3
Mpioka	0.617	5.948	1.568	5
Upper Diamictite	0.730	9.573	1.769	8
Haut-Shiloango	0.599	11.038	1.810	3
Lower Diamictite	0.626	7.398	1.463	3
Sansikwa-are	0.636	10.616	1.281	6
Sansikwa-arg	0.647	12.805	1.858	1
APS	0.660	8.978	1.587	
PAAS	0.655	9.511	1.411	
UCC	0.650	9.215	1.400	

Table 4.5. Eu anomalies and REE ratios. La_N means chondrite-normalized (Taylor and McLennan, 1985). The ratio La_N/Yb_N shows LREE vs. HREE and Gd_N/Yb_N is for middle REE vs. HREE. Average Proterozoic shale composition (APS) after Condie (1993), post Archaean average shale (PAAS) after Taylor and McLennan (1985) and upper continental crust (UCC) after McLennan (2001).

.

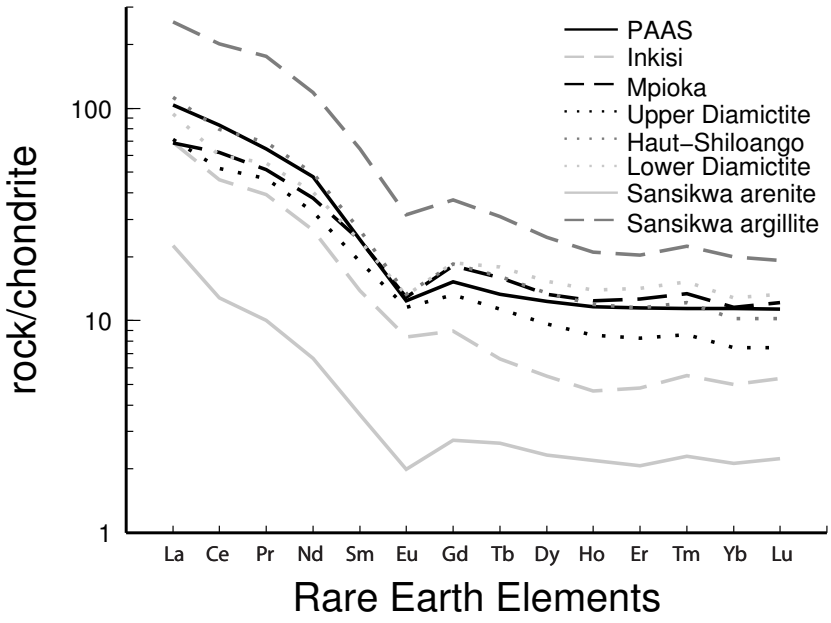

Figure 4.15. REE patterns, chondrite normalised (Taylor and McLennan, 1985), showing averages per rock unit.

The rare earth elements (REE) comprise the series of metals with atomic numbers 57 – 71 (La – Lu) and are insoluble. The effects of weathering and diagenesis are minor which makes REE patterns very suitable for characterising the provenance of clastic sediments. In Figure 4.15 only averages are shown for each formation/group because there appeared to be little variation amongst individual samples of each rock unit. Most rock units show PAAS-like patterns (solid black line): light REE (LREE) enriched, a dip in Eu and a fairly flat heavy REE (HREE) pattern. The Sansikwa arenite, although similar in shape to PAAS, seems heavily depleted in all REE. This is due to its high SiO_2 content which has a strongly diluting effect. Although less pronounced this effect can also be observed in the Inkisi sandstones. The Sansikwa argillite is enriched in all REE which is probably due to its high clay-fraction. The Mpioka is slightly depleted in light REE. All Eu anomalies are < 0.85 and all Gd_N/Yb_N ratios are < 2.0 which is typical for post Archaean sediments (McLennan et al., 1990).

The identification of less fractionated source components is done using compatible and immobile elements Cr and Sc in relation to the incompatible element Th in Figure 4.16.

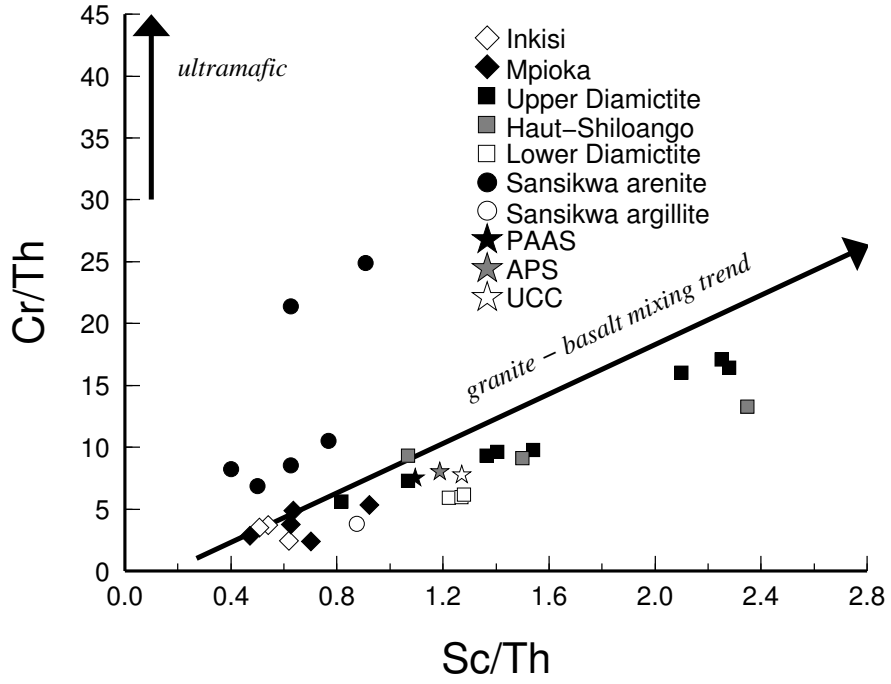

Figure 4.16. Compositional trend diagrams to identify the presence of (ultra)mafic source components. The granite-basalt mixing trend arrow starts at average granite ratios (Condie, 1993).

(Ultra)mafic rocks are enriched in Cr, slightly enriched in Sc and depleted in Th. Ultramafic komatiite has a typical Cr/Th ratio of $>1*10^4$ and basalt ca. 500 (Condie and Wronkiewicz, 1990). The average granite composition plots near the origin in Figure 4.16. The samples from the Sansikwa Subgroup show low Sc/Th but a mixture of low to moderate Cr/Th ratios (Fig. 4.16). The arenites of this subgroup are significantly depleted in all trace elements when compared to upper crustal values. This is probably due to the same dilution effect as observed in the REE data and therefore their ratios are not considered to be reliable provenance indicators. The Lower Diamictite plots very close to UCC composition and the Haut-Shiloango and Upper Diamictite lie close to the granite-basalt mixing trend. The poor spread of the Lower Diamictite samples may reflect the fact that they have been sampled from the same outcrop and therefore they might not be representative for the entire formation. Sc/Th ratios for the Upper Diamictite are different for the KUM/TANDU locality (0.8 – 1.4, average 1.2) and the KWI locality (1.5 – 2.3, average 2.0) pointing to a difference in sources. Both the Mpioka and Inkisi samples group together between UCC and granite values, close to the granite-basalt trend. None of the samples indicates the

presence of ultramafic sources.

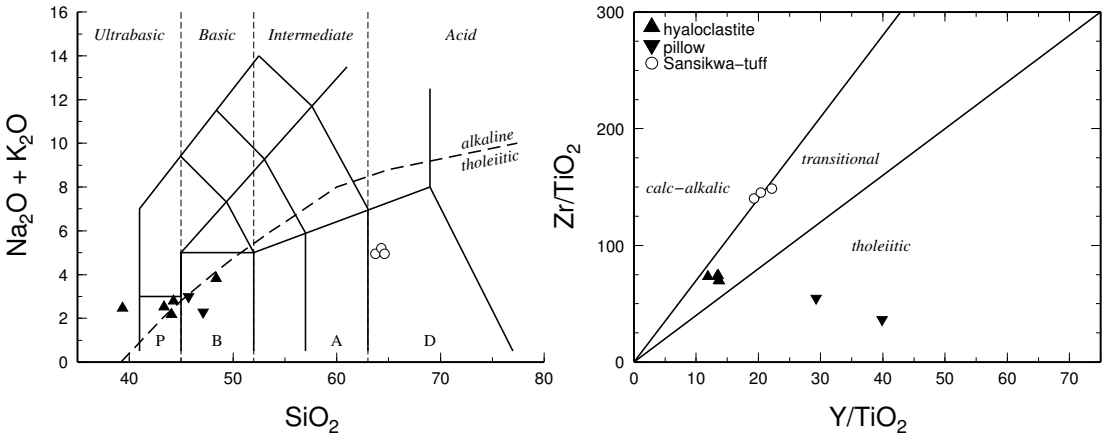

(a) Total alkalies versus Silica (TAS) diagram. The wt % of the oxides are recalculated on a H_2O- and CO_2-free basis. The coordinates for the fields are obtained from Rollinson (1993) and the alkaline-tholeiitic dashed line from Irvine and Baragar (1971). Relevant fields are labelled: P = picrobasalt, B = basalt, A = andesite, D = dacite.

(b) Y/TiO_2 vs Zr/TiO_2 to dicriminate between calc-alkaline and tholeiitic (after Lentz, 1998; Bahlburg et al., 2006).

Figure 4.17. Diagrams to place the basalts in their genetic classification (using the classification scheme originally proposed by Irvine and Baragar, 1971).

The basaltic composition of the volcanic rocks associated with the Lower Diamictite Formation is confirmed in Figure 4.17a. The samples plot in or close to the picro-basalt and basalt fields so according to their silica content the rocks are basic to ultrabasic. They are right on the division of alkaline and tholeiitic differentiation. The Sansikwa tuff samples plot in the dacite field and show a tholeiitic affinity. However, care must be taken with the use of this diagram for weathered or metamorphosed rocks as the alkalis are easily mobilised. For this reason the tholeiitic affinity of the tuffs is doubted and evaluated with the use of discrimination diagrams based on immobile trace elements in Figure 4.17b. This diagram is based on the correlation of Zr/Y being 2 – 4 for tholeiitic and ≥7 for calc-alkaline felsic rocks (Lentz, 1998). Y, representative of heavy REE, is compatible and abundant in tholeiitic samples (>30 ppm) but low in calc-alkaline rocks. Both the hyaloclastites and the tuffs classify as transitional, close to calc-alkaline. The pillow samples show a tholeiitic affinity.

Chondrite-normalised REE patterns show a very weak Eu anomaly for all volcanic rocks (Fig. 4.18). The pillow samples have a very flat pattern which is normal for tholeiitic

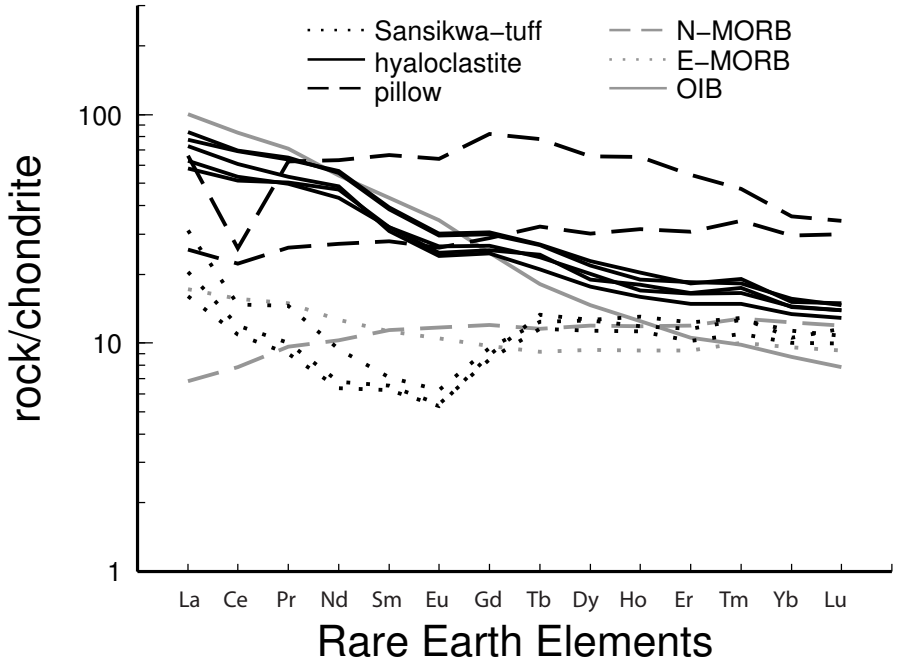

Figure 4.18. REE patterns for the volcanic rocks, chondrite normalised (Taylor and McLennan, 1985). N-MORB, E-MORB and OIB patterns are from Sun and McDonough (1989).

basalts (Rollinson, 1983). The hyaloclastite samples show a light REE enrichment with La_N/Yb_N ratios of 4-5. The shape of their pattern resembles that of enriched mid-ocean-ridge basalts (E-MORB) but their total REE concentrations are close to that of ocean-island basalts (OIB). The Sansikwa tuff samples are extremely depleted in LREE, a feature that is common with volcanic ashes which lose LREE during weathering of volcanic glass (e.g. Utzmann et al., 2002).

Tectonic setting

Th/Sc and Zr/Sc element ratios reveal two trends in Figure 4.19, displaying compositional heterogeneity in the sources and Zr enrichment through sediment recycling (McLennan et al., 1990, 1993). The bulk composition of provenance is shown by Th/Sc and unrecycled samples are expected to plot on a trend from mantle to upper continental crust composition (see also Table 4.6 for ratios of these reservoirs). Sediment recycling will

push the Th/Sc ratio and especially the Zr/Sc ratio up so samples which have undergone considerable recycling are expected to plot on the recycling trend. The Upper Diamictite and the Haut-Shiloango samples at the top of the compositional variation trend clearly show input from less evolved sources. All other units cluster in the upper continental crust compositional field and plot along the sediment recycling trend. This diagram suggests a change in provenance between deposition of the Sansikwa Subgroup, dominated by highly recycled detritus, and the Haut-Shiloango Subgroup which resembles average upper crustal composition.

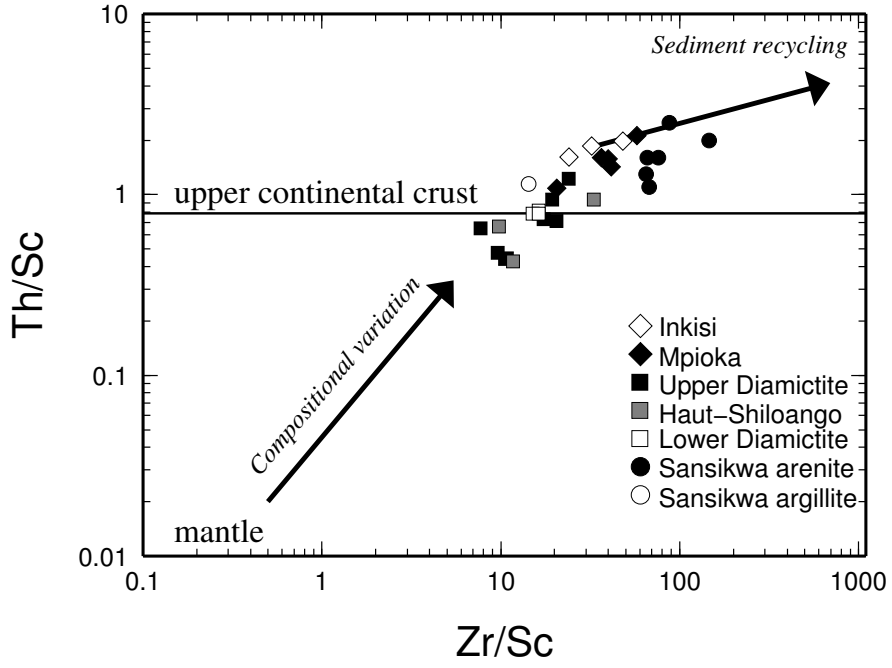

Figure 4.19. Compositional trends and the influence of recycling shown in a Zr/Sc vs. Th/Sc diagram after McLennan et al. (1990).

La and Sc are used together with Th and Zr in two ternary diagrams (Fig. 4.20) to identify the tectonic setting of the deposits (Bhatia and Crook, 1986). The Sansikwa arenites contain very little Sc and plot around the continental margin field in Figure 4.20a, a passive margin according to 4.20b. The diamictites and the Haut-Shiloango samples all fall in the continental arc field while the Mpioka and the Inkisi samples cross from this field into the passive continental margin field. One of the Mpioka samples is depleted in La but plots with the other samples in the continental arc field in Figure 4.20b. These diagrams suggest the presence of arc related sources for the Lower Diamictite Formation, the Haut-Shiloango

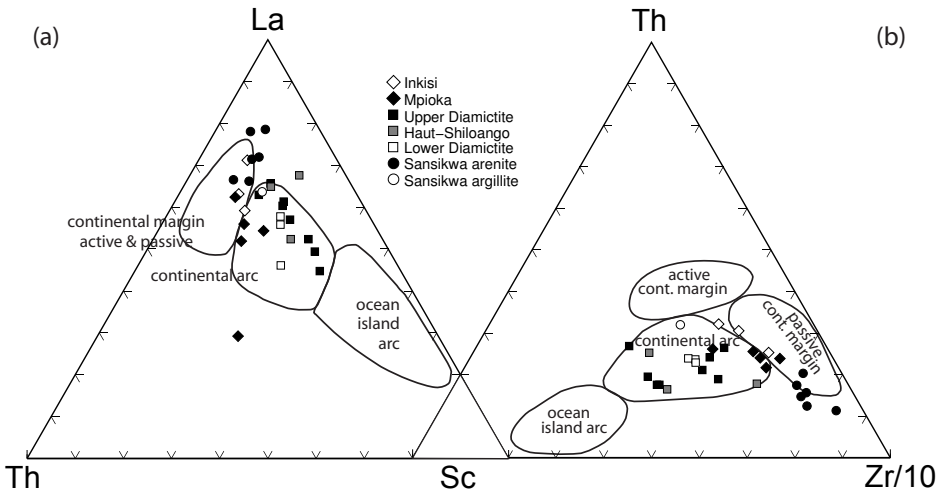

Figure 4.20. Discrimination diagrams to determine the tectonic setting of the depo centre. All diagrams and fields are after Bhatia and Crook (1986).

	SiO_2	La	Th	Sc	La/Sc	Th/Sc	LREE/HREE
Inkisi	77.7 (4.7)	25.4 (10.8)	9.6 (5.3)	5.3 (2.9)	5.3 (1.6)	1.8 (0.2)	11.3 (2.6)
Mpioka	71.4 (4.3)	30.6 (8.3)	14.1 (2.0)	9.3 (2.5)	3.4 (1.2)	1.6 (0.4)	6.8 (2.3)
Upper Diamictite	55 (9.2)	26.2 (3.8)	7.8 (1.3)	12.5 (4.7)	2.4 (1.0)	0.7 (0.3)	8.1 (0.6)
Haut-Shiloango	45.2 (13.6)	41.4 (26.1)	8.7 (2.4)	14.3 (7.6)	2.8 (0.9)	0.7 (0.3)	8.6 (2.7)
Lower Diamictite	71.8 (1.4)	34.7 (7.7)	13.3 (0.7)	16.7 (0.6)	2.1 (0.5)	0.8 (0.0)	6.2 (1.2)
Sansikwa-arenite	94.7 (1.9)	8.3 (3.4)	2.1 (1.5)	1.2 (0.4)	7.1 (2)	1.7 (0.5)	8.6 (1.0)
Primitive mantle	49.9	0.55	0.064	13	0.04	<0.1	1.7
Ocean crust	49.5	3.7	0.22	38	0.1	<0.1	1.4
UCC	66.0	30	10.7	11	2.7	1.0	9.5
APS	31.1	38	14.3	17	2.2	0.8	
PAAS	62.8	38	14.6	16	2.3	0.9	8.1

Table 4.6. Average concentrations (ppm) and REE ratios (including data from Taylor and McLennan, 1985; Condie, 1993). Between brackets is the error (1 σ).

Subgroup and the Mpioka Subgroup.

Two tectonic classification diagrams for volcanic rocks are presented in Figure 4.21 using elements with varying compatibility. Enrichment in incompatible high field strength elements such as Zr, Th and Nb point to the influence of continental crust and evolution in a 'within-plate' environment for the hyaloclastites and Sansikwa-tuffs. The pillow samples however show a much less evolved signature. They are relatively depleted in Th and Nb and have high Y and Yb concentrations which is consistent with their tholeiitic REE profiles (Fig. 4.18).

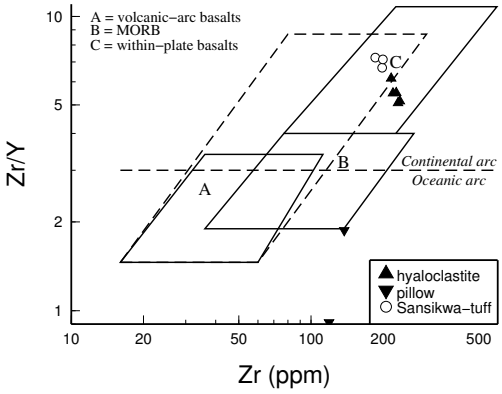

(a) Zr vs Zr/Y after Pearce and Gale (1977); Pearce and Norry (1979); Pearce (1983). The fields are based on modern arc volcanics.

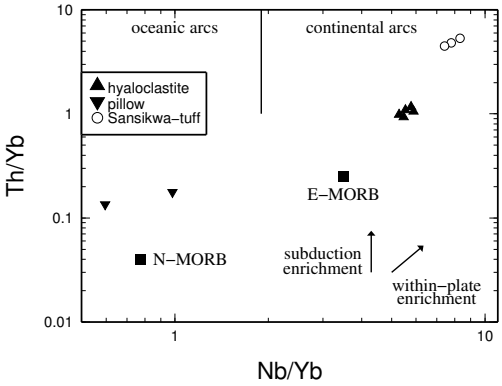

(b) Nb/Yb vs. Th/Yb diagram after Dunphy and Ludden (1998), values for N- and E-MORB from Sun and McDonough (1989).

Figure 4.21. Tectono-magmatic discrimination diagrams.

4.7.3 Provenance Trends and Implications

The Sansikwa Subgroup arenites are characterised by an extremely high SiO_2 content (91 – 97 wt%) suggesting that these sediments are the product of a high level of sediment recycling. This has a diluting effect on all other elements which can be seen in those diagrams that do not use ratios (e.g. in their REE profile, Fig. 4.15). The CIA is high (>80, Table 4.4) but K/Cs is high as well which suggests that re-sedimentation removed feldspars but the rocks have not undergone significant weathering in situ. Another consequence of the diluting effect in the arenites is that concentrations of some elements are below the detection limit (e.g. Sc and V) which makes it hard to use these in discrimination diagrams. From those diagrams that only use ratios it is clear that there is a strong component of old recycled crust (e.g. Fig. 4.19) in a passive margin setting (Fig. 4.20). The detrital zircon profile shows that the detritus is mainly derived from ∼2000 and ∼1000 Ma sources which can be found in the Kimezian Supergroup and the lower part of the West Congo Supergroup exposed along the West Congo Belt. It is interesting, therefore, that despite the likely relatively local source areas, the sediments have been strongly reworked.

Based on their striking REE profile (Fig. 4.15), the DZI 1A, 1B and 1C samples are interpreted to be a volcanic tuff. The enrichment of incompatible elements like Zr, Th and Nb (Fig. 4.21) indicates derivation from continental-arc type crust. It is suggested that this

tuff layer is a far-field expression of a volcanic episode not previously recognised in the Congo Craton.

The Lower Diamictite samples are very distinct from the underlying Sansikwa Subgroup. Thin sections of the soft argillaceous samples reveal a strong lineation fabric and shadow zones around the (dominantly quartz) clasts. They have a relatively high CIA (∼80) which suggests they have undergone strong chemical weathering before deposition of the overlying Haut-Shiloango formation (which has a CIA of <65). Most diagrams show a typical UCC composition (e.g. Figs. 4.16, 4.19) and a continental arc tectonic setting is suggested by ternary diagrams of Figure 4.20. However, care must be taken because all three samples plot closely together indicating that sampling was not very well spread and they might not be an accurate representation of the entire formation.

The Lower Diamictite is interbedded with volcanic rocks which have been reported to show pillow structures and are fed by doleritic dykes and sills (De Paepe et al., 1975; Kampunzu et al., 1991). Hyaloclastic rock samples show a slight calc-alkaline affinity while two fresh-looking pillow basalts are clearly tholeiitic (Fig. 4.17). The pillow samples lack the enrichment in incompatible elements which the hyaloclastite samples do show clearly in Figure 4.21. Judged by their texture and altered mineralogy the hyaloclastites may have been heavily influenced by their subaqueous emplacement which could be responsible for changing their chemistry. The pillow samples thus better represent the Lower Diamictite volcanic phase. Their chemical profile matches earlier studies of doleritic feeder dykes sampled in the same area (De Paepe et al., 1975; Kampunzu et al., 1991).

The Haut-Shiloango Subgroup overlies the Lower Diamictite and consists of a transgressive series of quartz arenites, silt- and mudstones and microbial carbonates. In most diagrams the samples show a good spread with an average composition very similar to UCC values indicating that a wide variety of sources have been sampled, including less evolved material (Figs. 4.16 and 4.19). The distribution of immobile trace elements like Sc, Th, Zr and La in Figure 4.20 indicates they are derived from a continental arc-type source. This gives rise to a contradiction: continental arcs indicate plate convergence and subduction while the transgressive nature of the Haut-Shiloango Subgroup indicates deepening of the basin. The arc-signature is suggested to be caused by the recycling of ancient arc-type rocks.

After the Upper Diamictite Formation the overlying Schisto-Calcaire Subgroup reflects an immediate return to carbonaceous shales and limestones. The Schisto-Calcaire Subgroup is overlain by a sequence of shales, siltstones, greywackes and conglomerates of the Mpioka Subgroup. Quartz sandstones of this subgroup and of the post-tectonic Inkisi Group behave very similarly and are close to UCC composition (e.g. fig 4.14a). They are depleted in compatible elements (e.g. Sc in fig 4.16) and enriched in Zr (Fig. 4.19) which suggests they are the product of high levels of recycling. Their association with both passive margin and arc fields in Figure 4.20 suggests that the West Congo Belt is changing to a predominantly passive margin setting.

4.8 Discussion and Conclusions

4.8.1 Age of Diamictites and Global Correlations

Lower Diamictite Formation

A new radiometric age of 694±4 Ma has been obtained for volcanic rocks in the Lower Diamictite Formation at the base of the West Congolian Group in the West Congo Belt. Until now, direct age constraints for this Lower Diamictite were absent, approximate ages of ca. 750 – 720 Ma were inferred on the basis of lithostratigraphic and chemostratigraphic correlations with the ∼750 Ma Kaigas and Chuos diamictites of Namibia (Frimmel et al., 2006; Poidevin, 2007) and with the “Grand Conglomérat” diamictite of Katanga-Zambia (Kanda Nkula et al. 2004), dated by Key et al. (2001) at 735±5 Ma. Our new age constraint (694±4 Ma) obtained from the West Congo Belt sill, therefore, is of direct significance to our understanding of Neoproterozoic glacial events.

The Chuos diamictite is not directly dated but has been correlated to numerous Sturtian type glacial rocks on other cratons. Geochronological constraints for the Sturtian range widely including syn-glacial U-Pb ages from 735±5 to 659.7±5.3 Ma and a minimum age of 751.9±5.5 Ma for the Kaigas Formation in Namibia (Key et al., 2001; Borg and Armstrong, 2002; Fanning and Link, 2008, see Chapter 1 for more details). Based on this

large timespan it has been suggested that the Sturtian represents several discrete glacial events rather than a single glaciation. Correlations of the Lower Diamictite with the Chuos Diamictite in southern Namibia are based on Sr isotopic data (Poidevin, 2007). The Sr isotopic evolutionary trend, however, is low in resolution and accordingly there is no unique solution. This correlation needs further work to be justified. Recently, the Lower Diamictite has been correlated to the Lower Tillite Formation of the Lindi Supergroup in the Fouroumbala-Bakouma Basin (northern Congo Craton, Fig. 2.3) based on Sr isotopes, SHRIMP data and revised lithological comparison (Tack et al., 2001; Frimmel et al., 2006; Poidevin, 2007; Tait et al., 2011). Although more geochronological constraints are needed to confirm this correlation, our results may provide an age for the Lower Tillite Formation.

This means that on the Congo Craton alone at least three pulses of glaciation occurred between 755 Ma (Kaigas, Namibia) and 694±4 Ma (West Congo Belt). The new 694 Ma age has not been reported before for Cryogenian glacial rocks and is younger than the traditional view on the age of the Sturtian glacial event (750 – 700 Ma, e.g. Hoffman and Schrag, 2002). Our age is however compatible with the most reliable age constraints for the Sturtian archetype in southern Australia which is a minimum age of 680±23 Ma for authigenic monazite in post-Sturtian shales (Mahan et al., 2010). Results from the glaciogenic Edwardsburg Formation, Windermere Supergroup (central Idaho) have an error margin which overlaps with the age identified here: rhyolite flows interfingered with glaciogenic diamictites are dated at 685±7 and 684±4 Ma by U-Pb SHRIMP analyses on zircons (Lund et al., 2003).

Upper Diamictite Formation

Direct ages for the Upper Diamictite Formation in the West Congo Belt are absent and correlations are predominantly based on litho- and chemostratigraphy. The sudden occurrence of the diamictite in a transgressive sequence of carbonate deposits, capped by a striking layer of pink, laminated dolostone makes a correlation with the Namibian Ghaub Formation, dated at 635.5±1.2 Ma (Hoffmann et al., 2004), hard to deny. The newly obtained chemostratigraphic profile of stable carbon isotopes for the West Congolian Group supports this correlation and allows correlation to a global Neoproterozoic carbon isotope

record (Halverson et al., 2005). The Upper Diamictite therefore seems to be coeval with the Marinoan glacial event.

An age of ca. 635 Ma is consistent with a maximum age of 707±23 Ma which is determined by the youngest detrital zircon grain in a rock sample from the Upper Diamictite at the KWI locality.

If an age of 635 Ma for the Upper Diamictite Formation is to be accepted then the underlying Haut-Shiloango strata separating the two diamictite horizons represent ca. 60 Ma of geological history (694 – 635 Ma). These lithologies make up ca. 1km of stratigraphic thickness, approx. two third of which consists of shales, fine grained sandstones and siltstones and approx. one third of it are limestone deposits (see stratigraphic column in Figure 4.2). With a lack of major unconformities ca. 1km of rocks deposited in 60 Ma equates to $\sim$1 – 2mm ky^{-1}. Compaction levels are unknown and sedimentation rates are notoriously difficult to establish but 1 – 2mm ky^{-1} is in the same order of magnitude as interglacial highstand sediment accumulation rates as recorded in various depositional systems on modern day Atlantic passive margins (Schlager, 1991).

4.8.2 Palaeotectonic Evolution

The Neoproterozoic kinematics of basement rocks to the Pan-African West Congo Belt are closely linked to those of the Araçuaí Belt on the São Francisco Craton. Both regions formed two arms around an epeiric sea which existed during most of the Proterozoic. The sea widened in the Neoproterozoic to form the Macaúbas Basin around 1000 - 900 Ma and ultimately closed during the Araçuaí-West-Congo Orogeny which formed part of the Pan-African assembly of Gondwana. The Neoproterozoic evolution of the West Congo Belt is schematically represented by the five cross-sections in Figure 4.22. The Macaúbas Basin, which terminated against the cratonic bridge linking the São Francisco Craton and the Congo Craton (Pedrosa-Soares et al., 2001; Alkmim et al., 2006), is the northerly expression of the Adamastor Ocean. Two phases of rifting are recognised in the Macaúbas Basin, the 999±7 – 912±7 Ma Zadinian and Mayumbian events, related to opening of the basin, and the newly dated 694±4 Ma tholeiitic magmatism, which was probably a local

event.

After unroofing of the Zadinian and Mayumbian bimodal volcanic rocks (Tack et al., 2001) deposition of the Sansikwa Subgroup commenced with a conglomeratic level, continued with sandstones and argillaceous siltstones and ended with deposition of the Lower Diamictite Formation and coeval emplacement of tholeiitic sills and pillow lavas (Figs. 4.22b and c). The detrital zircon results show that the Sansikwa Subgroup is dominated by local detritus, derived from the ca. 2 Ga Kimezian basement rocks and ca. 1 Ga underlying volcanics of the West Congo Supergroup. Both the rounded zircon grains and the sedimentary geochemistry indicate deposition of highly recycled detritus, probably in a high energy and shallow water environment.

The Lower Diamictite Formation is overlain by a series of shelf deposits of the Haut-Shiloango Subgroup which start with clastics (stilstones, fine grained sandstoness) and gradually become carbonate dominated. The microbial laminites found near the top of the Haut-Shiloango contain ca. 30% quartz suggesting a moderate to shallow depositional environment. The very top of the Haut-Shiloango Subgroup is marked by the glaciogenic Upper Diamictite Formation which unconformably overlies the underlying strata (Fig. 4.22d). In the SAF sampling locality the carbonates become brecciated towards the top and space is filled with clastic content (Photo A.3b). The change from carbonate to clastic sedimentation is interpreted as a shallowing-upward sequence and may enclose a period of non-deposition. Provenance of the Upper Diamictite indicates derivation from the east: clasts lack Zadinian and Mayumbian lithologies which are found to the west and the detrital zircon profile shows almost exclusive sampling of Archaean cratonic basement which can be found to the (north-)east of the field area. Immediately after this glacial interval the Schisto-Calcaire Subgroup shows a return to carbonate sedimentation starting with a pink, laminated dolostone and continuing with ∼1km of alternating argillites and partly dolomitised limestones.

The molasse sediments of the Mpioka Subgroup have been subject to moderate-high levels of recycling and contain a relatively large amount of ca. 720 Ma zircon grains. The most likely sources for these grains are found in the Kaoko and Damara Belts in southern Angola and northern Namibia (Fig. 4.11). Several Neoproterozoic crystallisation ages for rocks

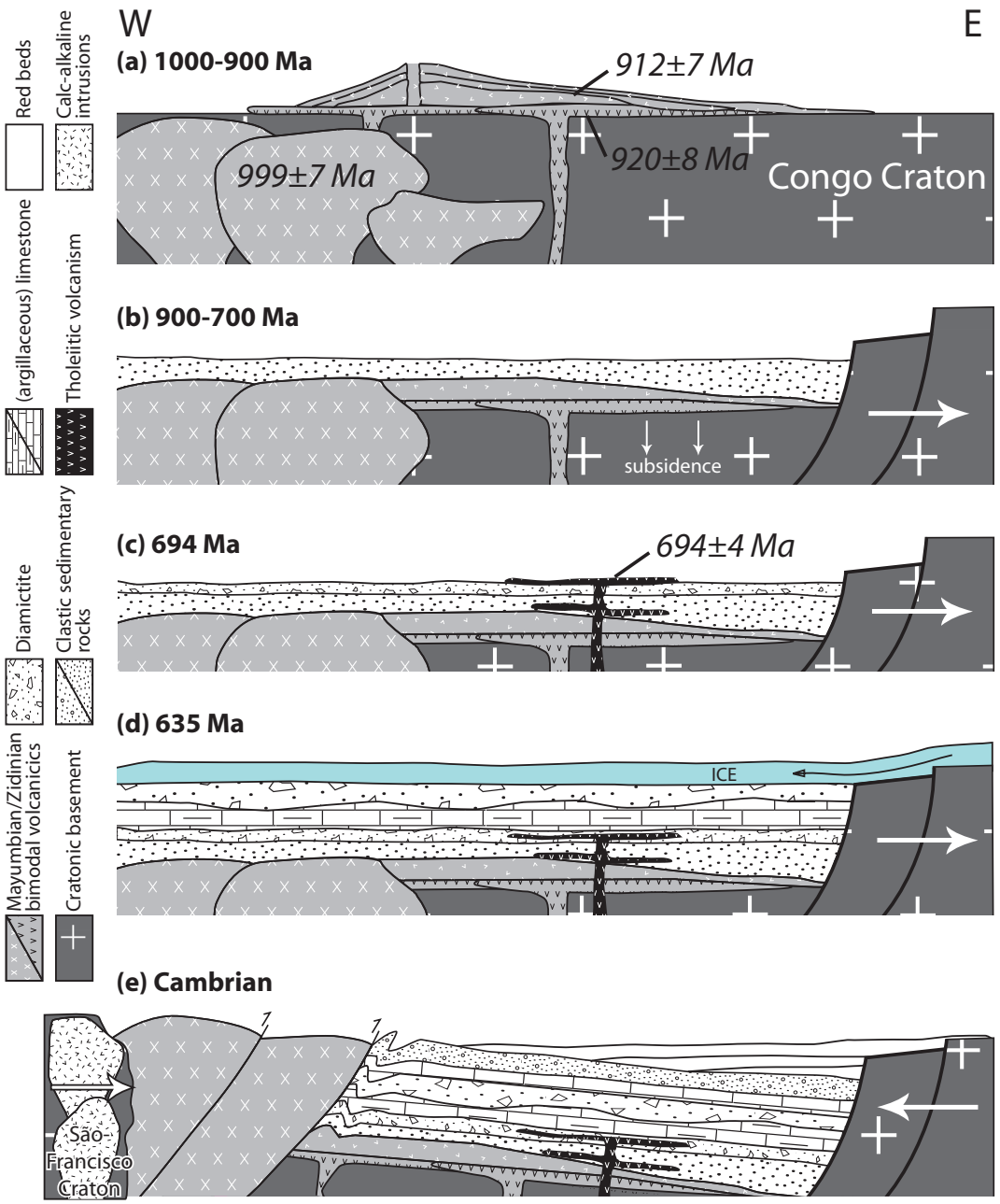

Figure 4.22. Schematic representation of the Neoproterozoic evolution of the West Congo Belt. Aspect ratios have not been maintained. Subsidence is a result of opening of the Macaúbas Basin between the Congo Craton to the east and the São Francisco Craton to the west (not shown). Ages in (**a**) are from Tack et al. (2001).

found in the São Francisco Craton are absent or at least not prominent in detrital zircon profile for the Mpioka Subgroup. This suggest that detrital material was not derived from the Araçuaí Belt with developed to the west and now flanks the São Francisco Craton. The initial closure of the Macaúbas Basin started around 630 Ma and is recorded by I-type granitoids in the Araçuaí Belt (Pedrosa-Soares et al., 2001). Closure and granite emplacement continued at least until 585 Ma (Pedrosa-Soares et al., 2008). East-ward subduction only occurred in the south of the basin, related magmatic arc rocks are now found in east Brazil (Pedrosa-Soares and Wiedemann, 2000; Alkmim et al., 2006). The Mpioka Subgroup is interpreted to have been deposited during the first phase of collision, the northern Macaúbas Basin would have remained unaffected by subduction to the south and derived little detrital material from the approaching São Francisco Craton.

The next and final phase, starting ca. 585 Ma, involved a continuation of the closure of the Macaúbas basin. During this phase the West Congo Belt underwent inversion where Zadinian and Mayumbian groups overthrust the West Congolian Group (Fig. 4.22f) and are in turn overthrusted by Kimezian basement (Tack et al., 2001). As a result of these collisional events the West Congolian sedimentary rocks in the field area for this study are mildly folded and tilted ca. 10° eastwards. Crustal thickening is believed to have led to orogenic collapse documented by granitic suites in the Araçuaí belt (Alkmim et al., 2006). Deposition of the foreland-basin red beds of the Inkisi Subgroup would not have started until after the complete closure of the epeiric sea at about 535 Ma. The re-occurrence of a prominent Archaean zircon population in the Inkisi Group demonstrates a tectonic change after deposition of the Mpioka Subgroup during which Archaean basement rocks became available for weathering.

Chapter 5

Palaeomagnetic Constraints for the Congo Craton

5.1 Introduction

The Precambrian palaeogeography of the Congo Craton is poorly constrained until its incorporation in Gondwana near the end of the Neoproterozoic. The global palaeomagnetic database (GPDMB v. 4.6, Dec. 2004) contains 27 Neoproterozoic records for this craton (summarised in Table 5.1) but most of these results do not pass modern day reliability criteria e.g. adequate demagnetisation procedures or acceptable statistics. The lack of a sound Precambrian apparent polar wander path (APWP) for the Congo Craton hampers understanding of its role in Proterozoic reconstructions, especially its position within Rodinia reconstructions (see Chapter 2).

Palaeomagnetic sampling of Neoproterozoic strata in the West Congo Belt has been carried out to improve the Precambrian palaeomagnetic record for the Congo Craton. A detailed account of sampling localities is given in Chapter 4. Analyses of samples from diamictites and associated carbonate formations is aimed at constraining the palaeolatitude of glaciomarine diamictite deposition on the Congo Craton.

#	Rock name	Place	Age (Ma) min	Age (Ma) max	Dir D(°)	Dir I(°)	Pole lat(°N)	Pole lon(°E)	N	n	A_{95}(°)	Quality	Reference
Congo Craton													
1	Manyovu Redbeds	Tanzania	650	795	246	-02	22	117	5	44	40	0**0**0**0**111 **3**	Piper (1972)
2	Plateau Series 700	Zambia	700	1000	159	-72	22	019	2	15	40	0**0**0**0**100 **1**	Piper (1975)
3	Lower Buanji Seriesd	Tanzania	700	1000	358	-20	87	263	6	25	9	0**1**0**0**100 **2**	Piper (1975)
4	Lower Plateau Series	Zambia	700	1000	013	-41	71	173	6	31	15	0**1**0**0**100 **2**	Piper (1975)
5	Mpulungu Plateau Series	Zambia	700	1000	085	-69	10	172	2	8	10	0**0**0**0**100 **1**	Piper (1975)
6	Upper Plateau Series	Zambia	700	1000	177	-37	60	025	3	13	13	0**0**0**0**110 **2**	Piper (1975)
7	Bukoban Intrusives	Tanzania	788	802	077	32	11	101	16	76	19	1**0**0**0**111 **4**	Piper (1972)
8	Gagwe/Kabuye Lavas	Tanzania	788[a]	802	241	-39	-25	273	12	80	10	1**1**1**0**101 **5**	Meert et al. (1995); Piper (1972)
9	Mbozi Mafic Complex	Tanzania	742[b]	754	320	16	46	325	10	64	9	1**1**1**0**111 **6**	Meert et al. (1995); Piper (1975)
10	Hook Intrusives	Zambia	560[c]	570	300	50	14	337	3	10	32	1**0**0**0**101 **3**	Brock (1967)
11	Nosib Group nq3	Namibia	742[d]	746	102	-13	09	295		13	13	0**0**1**0**0**0**1 **2**	McWilliams and Kröner (1981)
12	Nosib Group nq2	Namibia	742[d]	746	012	36	51	033	7	28	12	0**1**1**0**0**0**0 **2**	McWilliams and Kröner (1981)
13	Nosib Group nq1	Namibia	742[d]	746	312	40	28	323	6	25	15	0**1**1**0**0**0**0 **2**	McWilliams and Kröner (1981)
14	Otavi Gp. dc2+3	Namibia	634[e]	637	336	-65	55	224	10	26	15	0**1**1**0**0**1**0 **3**	McWilliams and Kröner (1981)
15	Otavi Gp. dc1	Namibia	634[e]	637	354	34	52	006	4	15	35	0**0**1**0**0**1**0 **2**	McWilliams and Kröner (1981)
16	Mulden Group dc3	Namibia	550[f]	560	278	-34	12	270	6	24	16	0**0**1**0**0**1**0 **2**	McWilliams and Kröner (1981)
17	Chela Gp.	Angola	742	746	311	49	23	329	3	16	34	0**0**1**0**100 **2**	Jones et al. (1992)
18	Mangbai-Balché CM1	Cameroon	560[g]	600	359	06	84	204	12	75	8	0**1**1**0**0**1**0 **3**	Ponte-Neto (2001)
19	Mangbai-Balché CM2	Cameroon	560[g]	600	217	-46	51	068	5	16	24	0**0**1**0**0**0**0 **1**	Ponte-Neto (2001)
20	Mangbai-Balché CM3	Cameroon	560[g]	600	199	48	-47	349	6	24	19	1**0**1**0**0**1**1 **4**	Ponte-Neto (2001)
São Francisco Craton[1]													
21	Itabuna Dykes IT1	Brazil	646	674	350	-26	40	263	13	57	6	0**1**1**0**0**1**0 **3**	Ponte-Neto (2001)
22	Itabuna Dykes IT2	Brazil	762	800	265	-16	-42	266	10	55	8	0**1**1**0**0**0**0 **2**	Ponte-Neto (2001)
23	Itabuna Dykes IT3	Brazil	762	800	245	54	-49	337	10	41	11	0**1**1**0**0**1**0 **3**	Ponte-Neto (2001)
24	Bambuí Carbonates B	Brazil	500	550	026	68	27	359	33	369	3	0**1**1**0**100 **3**	D'Agrella-Filho et al. (2000)
25	Bambuí Carbonates C	Brazil	500	550	007	58	32	339	17	116	4	0**1**1**0**100 **3**	D'Agrella-Filho et al. (2000)
26	Salitre Carbonates B	Brazil	500	550	034	61	44	003	13	71	10	0**1**1**0**100 **3**	Trindade et al. (2004)
27	Salitre Carbonates C	Brazil	500	550	006	63	34	339	24	233	4	0**1**1**0**100 **3**	Trindade et al. (2004)
Gondwana													
28	Ntonya Ring Structure	Malawi	509	535	311	43	28	345	1	27	2	1**1**1**0**101 **5**	Briden (1968); Briden et al. (1993)
29	Sinyai Dolerite	Kenya	543	551	541	20	-29	319	1	42	5	1**1**1**0**111 **6**	Meert and Van der Voo (1996)

Table 5.1. Neoproterozoic palaeomagnetic poles for the Congo Craton between 800 and 550 Ma. N/n = number of sites/samples; Quality factor (bold) indicates the number of criteria that are met following Van der Voo (1990), see text for explanation. Pole numbers in boldface are those that are considered reliable (again see text for explanation). Ages reported by: [a]Deblond et al. (2001); [b]Mbede et al. (2004); [c]Hanson et al. (1993); [d]Hoffman et al. (1996); [e]Hoffmann et al. (2004); [f]Clauer and Kröner (1979) recalculated by Evans (2000); [g]Montes-Lauar et al. (1997). [1]Position of palaeomagnetic poles are presented in African coordinates to account for Atlantic rifting, using an Euler pole at 45.5°N, -32.2°E, +58.2° (Lawver and Scotese, 1987).

5.2 Previous Studies

All previously published palaeomagnetic results for the Congo and São Francisco cratons between 800 and 550 Ma are summarised in Table 5.1. Each result has been assigned a quality factor according to the criteria of Van der Voo (1990). The numbers of this index stand for: (1) A well-determined age for the magnetisation of the rock unit, (2) a sufficient number of samples (> 24) and precision (k > 10 and A_{95} < 16), (3) adequate demagnetisation procedures, (4) the presence of field tests to constrain the age of magnetisation, (5) structural control of the studied area, (6) the presence of reversals, (7) no suspicion of remagnetisation and no resemblance to younger palaeopoles (see Van der Voo, 1990, for detailed descriptions of these criteria).

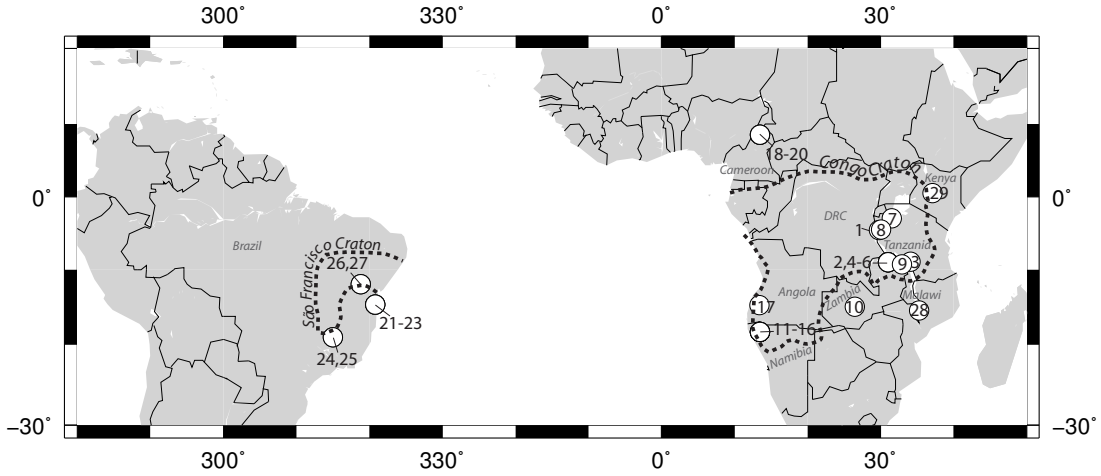

Figure 5.1. Geographical distribution of sampling sites for Neoproterozoic palaeomagnetic poles for the Congo Craton. Numbers correspond with pole numbers in Table 5.1.

In general, passing criteria 2, 3 and 5 is considered essential for a reliable result: adequate statistical parameters ensure that secular variation of the geomagnetic field has been averaged out (criteria 2) and demagnetisation should encompass stepwise demagnetisation and principal component analysis to identify all palaeomagnetic components (criteria 3). Also, the structural relationship of the sampled formation with its surrounding units needs to be understood (criteria 5). If a pole fails any of these criteria it is not considered reliable. Poles that pass these plus at least one additional criteria (so a quality factor ≥ 4) are considered reliable enough to use for palaeogeographic reconstructions. The palaeomagnetic poles of Table 5.1 will now be discussed in more detail.

5.2.1 Congo Craton

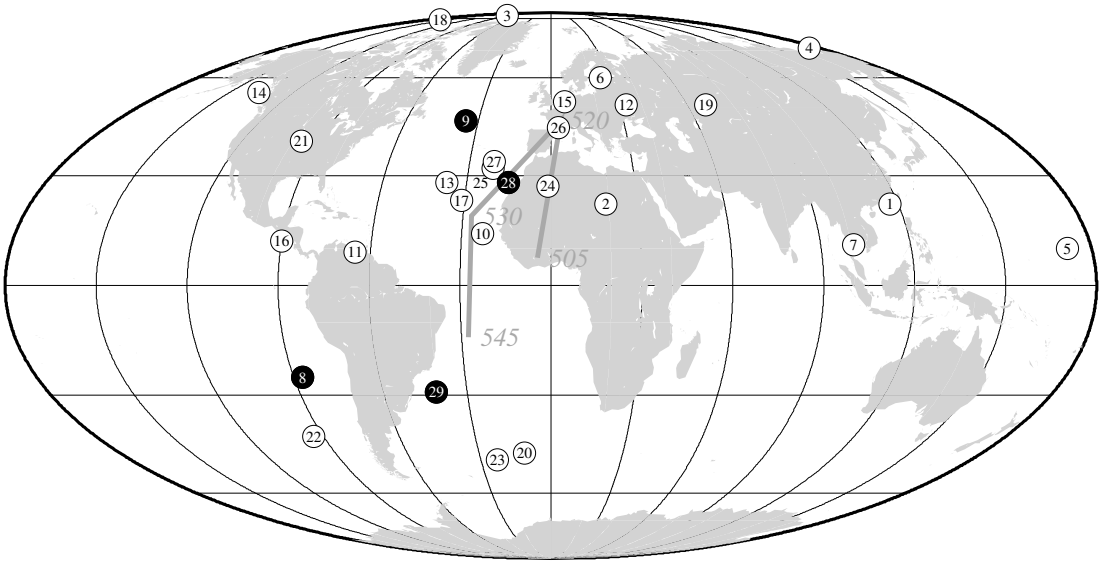

Figure 5.2. Neoproterozoic palaeomagnetic poles for the Congo Craton in a Mollweide projection with 30° grid spacing. Poles are rotated into an African reference frame. Only pole positions and not their circles of confidence are shown for clarity. Numbers correspond with pole numbers in Table 5.1, black circles are poles that are considered reliable (see text for explanation). In dark grey is the Cambrian APWP for Gondwana after McElhinny et al. (2003), calculated back to south African coordinates using Euler pole 9.3°N, 5.7°E, angle: 7.8° (Lottes and Rowley, 1990).

A total of 10 palaeomagnetic poles for the Congo Craton are available from rocks in Zambia and Tanzania (poles 1-10). Some of these localities have been studied twice (i.e. pole 8 and 9): after initial publication in the 1970s (Piper, 1972, 1975) the studies are repeated by Meert et al. (1995) and the combined results are now some of the best constrained poles (see below). Many of the original studies however were obtained by employing single step magnetic cleaning (poles 1 – 7) which is not according to modern day requirements as it can fail to detect important palaeomagnetic directional results (shown e.g. by Meert et al., 1995). Many of these studies also have an insufficient quantity of samples. Poles 1 – 7, therefore, are not considered to provide reliable palaeogeographic constraints for the Congo Craton.

Palaeomagnetic studies of the Gagwe/Kabuye lavas (dated at 795±7 Ma by ^{40}Ar-^{39}Ar, Deblond et al., 2001) and the Mbozi Mafic Complex (U-Pb zircon age of 748±6 Mbede et al., 2004), originally studied by Piper (1972) and Piper (1975), were redone by Meert et al. (1995) which led to two well constrained poles. The original results for Gagwe/Kabuye

lavas (pole 8) were included in the more recent results while the new Mbozi Mafic Complex results (pole 9) supersede the original data. Both the Gagwe and Mbozi poles are well dated, indicate a subtropical (∼25°) position for the Congo Craton but require a 90° rotation between 795 and 748 Ma. De Waele et al. (2008) reported that unpublished results from 765 Ma volcanics in Zambia show a Mbozi-like primary magnetisation but a Gagwe-like secondary magnetisation casting some doubt over the primary origin of the Gagwe pole (8). However, these results remain unpublished so both the Mbozi and Gagwe poles are considered reliable for this study.

The main body of the Hook Intrusives (pole 10) in the Lufillian Arc of Zambia is a syntectonic composite granite batholith which has been dated at ca. 570 – 560 Ma (Hanson et al., 1993). Palaeomagnetic results have been published from post-tectonic satellite bodies of gabbro, diorite and syenite and the resultant pole at 14°N and 337°E plots on the Gondwana APWP (Brock, 1967) close to the 530 Ma reference pole (Fig. 5.2). Unfortunately these results suffer from their low number of samples (n = 10) which gives them a high degree of directional uncertainty ($A_{95} = 32°$) so this pole is not considered reliable.

Several palaeomagnetic poles have been reported for sedimentary units of the Nosib, Otavi and Mulden Groups of northern Namibia (Table 5.1, poles 11 – 16). From the Nosib Group, three components are recognised but only the medium and high temperature (nq2 + nq1) are considered to be stable by the original authors. U-Pb zircon ages from a volcanic rock at the top of the Nosib Group give a depositional age of 744±2 Ma (Hoffman et al., 1996) but constraining the magnetisation age for both components is problematic: reported foldtests are inconclusive and the nq2 *in situ* pole is very similar to the 520 Ma reference pole for Gondwana (McElhinny et al., 2003). The nq1 pole is slightly further from the reference path but has overlapping A_{95} confidence cones with the 530 Ma Gondwana pole. All Nosib Group results have a low quality factor (2) and are not considered reliable, especially given their similarity to younger poles. Results from the Otavi Group (with a depositional age ∼635 Ma, Hoffmann et al., 2004) produced two components: a poorly defined high temperature component dc1 which is partly or completely overprinted by a post-folding dc2+3 component (according to McWilliams and Kröner, 1981). Unpublished palaeomagnetic results from the Ghaub Formation identified a consistent, dc1-like direction in clasts of the

diamictite, suggesting that dc1 is also an overprint direction (Evans, 2000). Sediments from the overlying Mulden Group have a Rb-Sr depositional age of 560 – 550 Ma (Clauer and Kröner, 1979). Two metamorphic events left their imprint, indicated by greenschist facies mineralogy and dated at 537±6 and 457±12 Ma (Rb-Sr, Clauer and Kröner, 1979), which could have been responsible for re-magnetising the rocks. The resultant pole (16) however is unlike any other pole and both the *in situ* and tilt corrected poles plot far away from the APWP for Gondwana. Because it differs significantly from the coeval, very reliable 551 – 543 Ma Sinyai Dolerite pole (pole 30, Meert and Van der Voo, 1996) and because of the low quality factor (2) and the low number of samples (n = 24) pole 16 is rejected for palaeogeographic reconstructions.

Flat lying sedimentary units of the Chela Group in Angola are correlated to the ∼744 Ma Nosib Group in Namibia and have been palaeomagnetically studied by Jones et al. (1992, pole 17). The results however are low in quality ($A_{95} = 34^{\circ}$, n = 16). The palaeopole plots within 5° of the 530 Ma reference Gondwana pole, and, given a lack of reliable fieldtests, a Cambrian remagnetisation direction can not be ruled out. This pole is not considered reliable.

Three components are reported for the Mangbai-Balché Dykes in Cameroon (poles 18 – 20, Ponte-Neto, 2001), dated at 580±20 Ma by the Rb-Sr isochron method (Montes-Lauar et al., 1997). Components CM1 and CM2 are dismissed respectively as a present day overprint and an unknown, poorly constrained magnetisation. The high temperature/high coercivity component CM3 results in a pole ca. 30° south of the 545 Ma Gondwana reference pole (Fig. 5.2). Unfortunately the results are published in a PhD thesis from which only the abstract is available. Because of the low number of samples (n = 24) and a lack of bedding control pole 20 is not considered reliable.

5.2.2 São Francisco Craton

Ponte-Neto (2001) reports results from the Itabuna Dykes in Brazil (poles 21 – 23) which have Rb-Sr isochron ages of 660±14 (pole 21) and 781±19 Ma (poles 22 and 23). Components IT1 and IT2 are questioned for their reliability and meaning: there is no proof for

structural control on the samples outcrops and the resultant poles plot far away from the Gondwana APWP (Fig. 5.2). The high temperature component of these dykes (pole 23) is very similar to that of the Mangbai-Balché Dykes of Cameroon (pole 20) even though the cooling ages of the Itabuna Dykes are 150 Ma older than those of Cameroon. The emplacement age of the IT3 dykes is coeval with the Gagwe Lavas in Tanzania but their palaeomagnetic poles (23 and 8 respectively) do not coincide. The lack of structural control for the Itabuna Dykes IT3 pole and the suspicion of remagnetisation which follows from its similarity to the 150 Ma younger pole from dykes in Cameroon, pole 23 is not considered reliable.

Palaeomagnetic results from carbonates in the south (Bambuí Carbonates, poles 24 and 25) and the north (Salitre Carbonates, poles 26 and 27) of the São Francisco Craton were shown to be remagnetised during a Cambrian remagnetisation event (D'Agrella-Filho et al., 2000; Trindade et al., 2004). Pb-Pb isochrons indicate isotope resetting between 550 and 500 Ma (Babinski et al., 1999). At both localities two magnetic components were isolated and their respective palaeomagnetic poles were compared with reference Cambrian poles for Gondwana. The high temperature components C from both localities overlap and plot halfway the 530 – 520 Ma segment of the Gondwana APWP (poles 25 and 27 in Fig. 5.2) suggesting remagnetisation around 525 Ma. Both components B (poles 24 and 26) plot close to each other and suggest remagnetisation shortly after 520 Ma.

5.2.3 Palaeogeographic Implications

Only the 795 Ma Gagwe and 748 Mbozi poles are available to constrain the 800 – 550 Ma segment of the APWP for the Congo-São Francisco Craton. Both palaeopoles indicate low to moderate palaeolatitudes for the Congo Craton but require a 90° rotation between acquisition, i.e. between 795 and 748 Ma. The craton is subsequently palaeomagnetically unconstrained for ca. 200 Ma until incorporation in Gondwana during the Cambrian. Two reliable Cambrian poles at 522 and 547 Ma (28 and 29) from central Africa are compared with coeval data from other Gondwana cratons (like Australia and Antarctica) and demonstrate that this part of Gondwana amalgamated around 550 Ma. These poles have been used in constructing the Gondwana APWP of McElhinny et al. (2003) which is used as a

reference for Cambrian apparent polar wander of the Congo.

5.3 Palaeomagnetic Sampling Strategy and Results

5.3.1 Sampling

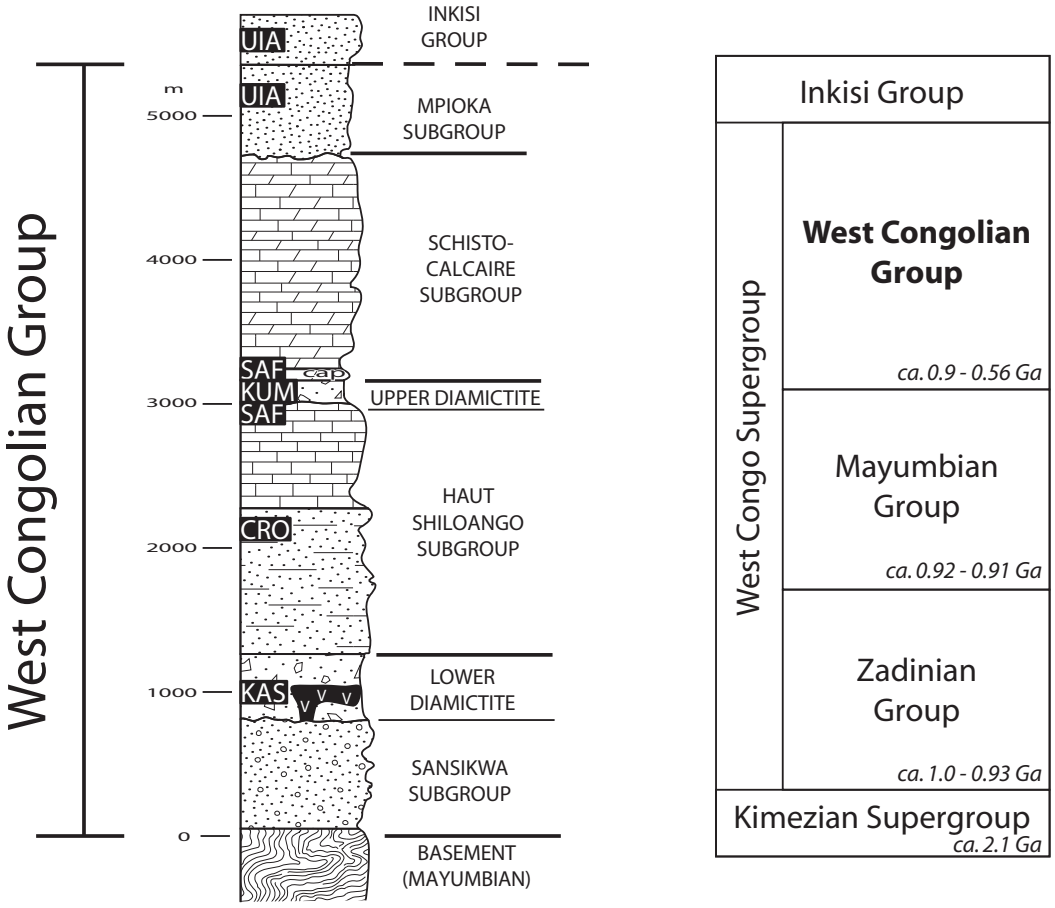

Figure 5.3. Schematic representation of the stratigraphic column for the West Congolian Group (detailed column in Figure 4.2). Sampling localities are indicated in black boxes.

Volcanic and sedimentary rocks of the West Congolian Group have been sampled for palaeomagnetic analyses (Fig. 5.3, see Chapter 4 for a map of the sampling localities in Fig. 4.3). Four sites were collected from a coarse crystalline, hyaloclastic, basaltic breccia associated with the Lower Diamictite Formation. These were sampled in a small stream at the KAS locality: two sites at the riverbed and two sites on a dry riverbank. Palaeomagnetic samples were also collected from carbonate rocks of the Haut-Shiloango and the Schisto-

Calcaire subgroups at the SAF locality (Fig. 5.3). The top 10m of the Haut-Shiloango Subgroup, which separates the two diamictite units, was sampled at 20 cm intervals and and samples were grouped to form 10 sites of 5 samples each. Sampling continued at the base of the Schisto-Calcaire Subgroup, which includes the cap carbonate immediately overlying the Upper Diamictite Formation, with the same spacing resulting in a further 35 samples divided over 6 sites representing 5.5 m of stratigraphy. Another 10 samples (2 sites) were collected from carbonaceous siltstones of the Haut-Shiloango Subgroup at the CRO locality. Samples from the Upper Diamictite Formation were collected at the KUM locality where both clasts and matrix were targeted resulting in a total of 28 samples. Taking oriented drill cores from sandstones of the Mpioka Subgroup and the Inkisi Group proved impossible due to limited accessibility. Instead, oriented hand samples were collected at the UIA locality, two samples from the Mpioka Subgroup in a riverbed and two samples from a cliff section which exposed massive red sandstones of the Inkisi Group.

5.3.2 Results of Palaeomagnetic Experiments

All oriented hand samples have been drilled using in house rock drilling facilities and palaeomagnetic samples were cut into 2.4 cm length specimens. Details of the demagnetisation and measuring procedures as well as component analyses and statistical techniques are described in Chapter 3. The obtained site mean directions are presented in Table 5.2 and will be discussed below. Stereographic projections of the distribution of sample magnetisation directions of each palaeomagnetic site are shown in Appendix S5.

Lower Diamictite Formation volcanic rocks, Kasi village (KAS)

Palaeomagnetic results from the volcanic rocks associated with the Lower Diamictite Formation were demagnetised up to 400°C. Samples from site KAS 2 and KAS 3 displayed very similar behaviour: in orthogonal projections demagnetisation steps plot on a line towards the origin identifying the presence of a single magnetisation direction (Fig. 5.4). Intensities were typically around 20 – 40 mA/m. All samples have a south-easterly directed palaeomagnetic direction but inclinations are highly varying (Fig. 5.4b). Both sites

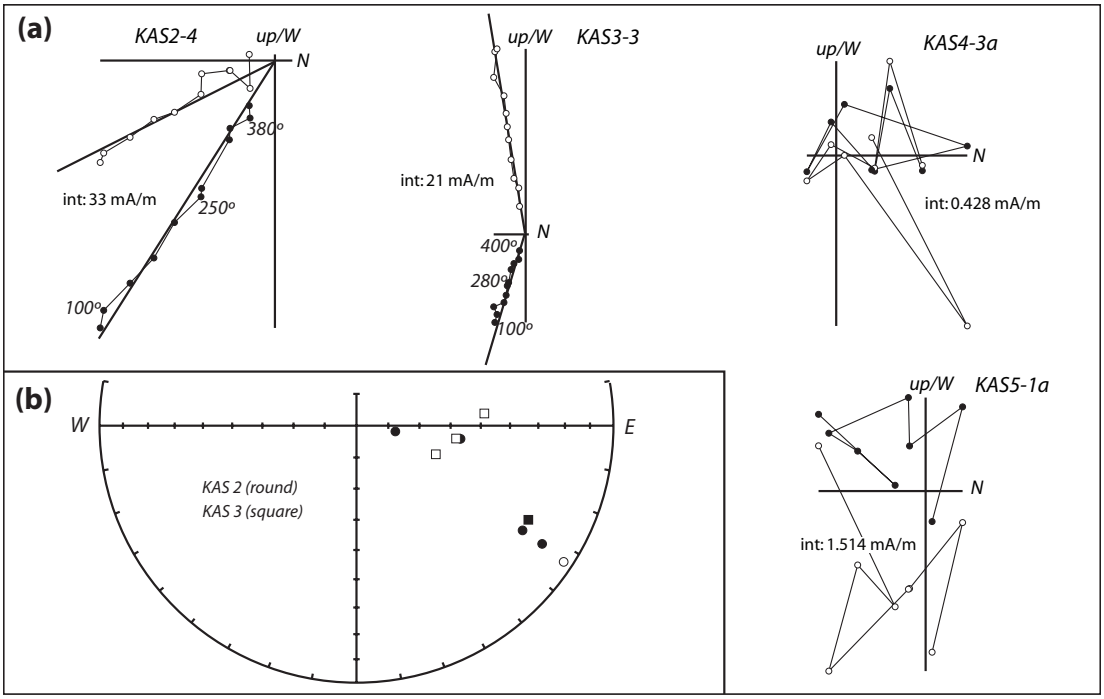

Figure 5.4. Demagnetisation characteristics for the KAS locality. (**a**) orthogonal 'Zijderveld' (Zijderveld, 1967) projections of individual samples illustrating well defined directions of sites KAS 2 and 3 and unstable magnetic directions for sites KAS 4 and 5. Demagnetisation steps are in °C. (**b**) equal area projection of samples from sites KAS 2 and 3.

revealed a poor within site consistency which is demonstrated by the high α_{95} confidence cones in Table 5.2. Samples from sites KAS 4 and KAS 5 displayed an erratic signal (Fig. 5.4). Intensities were typically around 0.5 – 1.5 mA/m, at least one order of magnitude less than for sites KAS 2 and KAS 3, and none of the samples displayed a stable magnetic direction. Looking at these volcanics in thin section, chloritisation of the glassy matrix reveals that they have been subjected to a high degree of alteration (Photo A.7a). This could have affected the crystallography and possibly destroyed the primary magnetisation. No average direction could be calculated from this locality.

Haut-Shiloango Subgroup, Kwilu bridge locality (CRO)

Two sites were collected from carbonaceous siltstones of the Haut-Shiloango Subgroup at the CRO locality. Demagnetisation first revealed a low temperature component with unblocking temperatures between 20 and 200°C in all 10 samples (component A in Table

Locality										
lat(°) / lon(°)				tilt	*in situ*		tilt corrected			
site	T(°C)	Na	Nc	dip/dipdir(°)	D(°)	I(°)	D(°)	I(°)	κ	α_{95}(°)
Present Day Field					**0.0**	**-10.9**				
Kasi Village (KAS)		**4**	**0**							
S 05.1931 / E 014.1112										
KAS 2	100-400	5	5	00/000	117.5	34.1			5.9	34.4
KAS 3	100-400	5	4	00/000	103.9	-39.9			3.9	53.8
Crocodile river (CRO)										
S 05.6182 / E 014.2596										
Component A		**2**	**2**		**47.6**	**10.6**	**48.3**	**1.5**	**-**	**-**
CRO 1	20-200	5	5	11/078	36.7	10.3	37.8	2.6	22.7	16.4
CRO 2	20-200	5	5	11/078	58.5	10.5	59.0	0.4	43.0	11.8
Component B		**2**	**2**		**315.8**	**65.7**	**341.1**	**70.4**	**-**	**-**
CRO 1	200-360	5	5	11/078	328.1	65.5	353.4	67.8	649.7	3.0
CRO 2	200-360	5	5	11/078	303.7	65.0	326.0	71.9	113.8	7.2
Safricas Quarry (SAF)										
S 05.5678 / E 014.4193										
Haut-Shiloango - A		**10**	**10**		**0.6**	**-23.0**	**356.4**	**-22.6**	**77.1**	**5.5**
SAF 1	20-200	5	5	10/091	7.3	-25.0	2.6	-25.7	102.5	7.6
SAF 2	20-200	5	5	10/091	358.9	-28.2	353.6	-27.4	11.4	23.7
SAF 3	20-200	5	3	10/091	7.0	-33.1	0.4	-33.6	10.7	24.5
SAF 4	20-200	5	4	10/091	350.2	-18.2	347.2	-16.1	8.0	34.6
SAF 5	20-200	5	4	10/091	353.7	-16.7	350.9	-15.2	7.6	35.7
SAF 6	20-200	5	5	10/091	6.8	-18.6	3.4	-19.3	61.2	9.9
SAF 7	20-200	5	5	10/091	355.8	-32.6	349.6	-31.2	18.0	18.6
SAF 9	20-200	5	4	10/091	0.2	-13.6	357.8	-13.3	49.8	11.0
SAF 10	20-200	5	5	10/091	10.5	-23.7	6.0	-25.0	22.2	20.0
SAF 11	20-200	5	4	10/091	356.6	-19.0	353.3	-17.9	50.2	10.9
Haut-Shiloango - B		**10**	**10**		**320.7**	**58.9**	**336.3**	**64.3**	**156.8**	**3.9**
SAF 1	200-420	5	5	10/091	324.0	57.0	338.8	62.0	377.5	3.9
SAF 2	200-420	5	5	10/091	321.5	54.2	334.4	59.7	143.7	6.4
SAF 3	200-420	5	3	10/091	326.8	48.5	337.6	53.3	104.5	12.1
SAF 4	200-420	5	4	10/091	331.9	61.9	351.0	65.3	51.0	13.0
SAF 5	200-420	5	4	10/091	322.6	53.4	335.3	58.8	28.4	17.5
SAF 6	200-420	5	5	10/091	311.6	61.7	327.8	68.4	81.1	8.5
SAF 7	200-420	5	5	10/091	308.6	59.3	322.4	66.5	69.4	9.2
SAF 9	200-420	5	4	10/091	315.8	64.3	335.4	70.2	121.9	8.4
SAF 10	200-420	5	5	10/091	323.2	60.8	340.7	65.7	111.4	7.3
SAF 11	200-420	5	4	10/091	317.1	65.8	338.6	71.4	99.3	9.3
Schisto-Calcaire		**6**	**6**		**331.9**	**63.9**	**351.0**	**65.6**	**173.7**	**5.1**
SAF 14	200-420	5	4	14/050	341.1	67.8	5.5	60.1	26.4	18.2
SAF 15	200-420	5	4	10/091	331.6	57.9	347.6	61.6	110.1	8.8
SAF 16	200-420	5	3	10/091	335.9	61.3	341.1	62.7	111.7	11.7
SAF 17	200-420	5	5	10/091	336.5	68.1	2.5	70.2	44.0	11.7
SAF 18	200-420	7	7	10/091	323.9	64.1	344.4	68.7	62.0	7.7
SAF 19	200-420	7	6	10/091	323.9	63.6	344.0	68.3	64.8	8.4
SAF + CRO combined		**3**	**3**		**322.8**	**63.0**	**342.8**	**66.9**	**335.5**	**6.7**
SAF + CRO combined		**18**	**18**		**323.6**	**61.4**	**341.6**	**65.5**	**336.3**	**3.0**
Kumbi village (KUM)										
S 05.6259 / E 014.2444										
matrix	200-420	21	21	10/085	347.2	26.2	352.2	27.2	6.8	13.2
UIA mountain (UIA)		**4**	**4**		**316.6**	**-2.4**	**294.3**	**1.3**	**8.1**	**34.5**
S 05.1811 / E 014.4312										
UIA 1	20-710	7	6	05/090	303.4	-11.0	303.0	-6.8	15.0	17.9
UIA 2	20-710	8	5	05/090	259.3	4.5	259.2	9.4	9.8	25.7
UIA 5	20-710	7	7	05/090	301.6	-21.8	300.7	-17.3	43.0	9.3
UIA 6	20-710	4	4	05/090	312.4	16.0	313.5	19.7	21.1	20.5

Table 5.2. Summary of all palaeomagnetic directions. Na and Nc respectively give the number of analysed and the number used in calculating the mean direction, κ is Fisher's precision parameter (Fisher, 1953), α_{95} is the 95% cone of confidence.

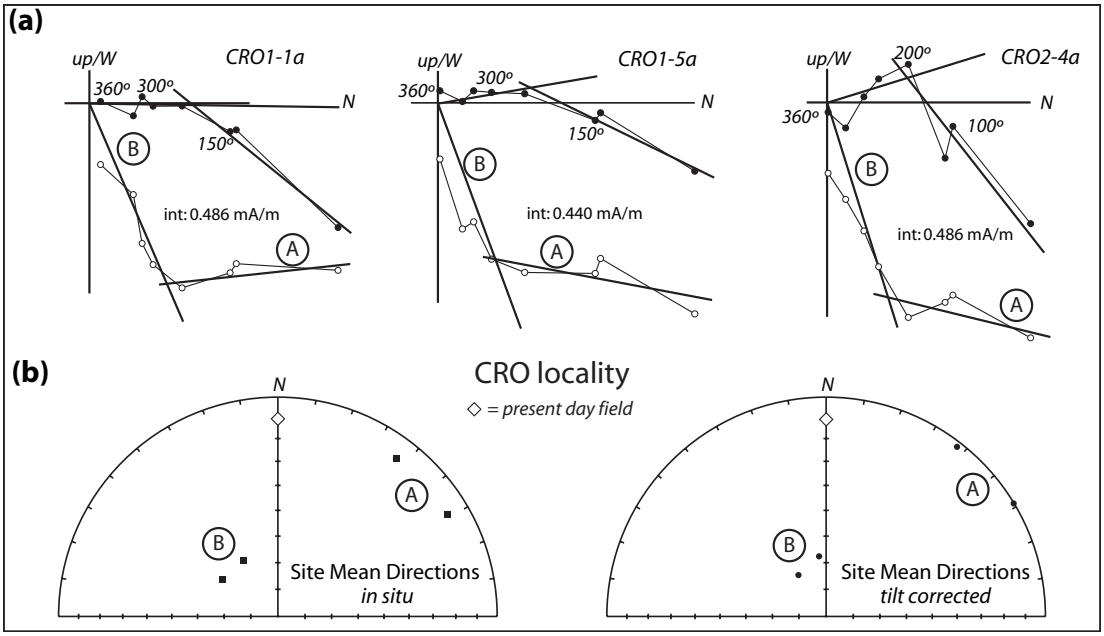

Figure 5.5. Demagnetisation characteristics for the CRO locality: (**a**) orthogonal projections of three samples showing typical behaviour for this locality, demagnetisation steps are in °C. (**b**) equal area projections of site-mean directions. Two components are labelled A and B.

5.2). This component has a shallow inclination and is directed towards the north-east. Further demagnetisation revealed a stable component between 200 and 360°C. Intensities were typically below 0.5 mA/m and dropped below 0.01 mA/m after heating at ca. 300 – 360°C. These low intensities prevented demagnetisation to higher temperatures as they drop below the detection limit of the magnetometer (ca. 10^{-7} mAm^2). This second component (component B) was stable, directed towards the origin in orthogonal projections (Fig. 5.5) and is determined to be the characteristic remanent magnetisation (ChRM). Two site mean directions resulted in an overall site mean direction for component A of D = 47.6°, I = 10.6° *in situ* and D = 48.3°, I = 1.5° (n = 10) after tilt correction. Component B has a mean *in situ* direction of D = 315.8°, I = 65.7° and a tilt corrected direction of D = 341.1°, I = 70.4° (n = 10).

Haut-Shiloango and Schisto-Calcaire Subgroups, Safricas quarry (SAF)

A total of 10 sites were collected from carbonates of the Haut-Shiloango Subgroup at the Safricas quarry (SAF locality). The demagnetisation diagrams reveal similar behaviour in

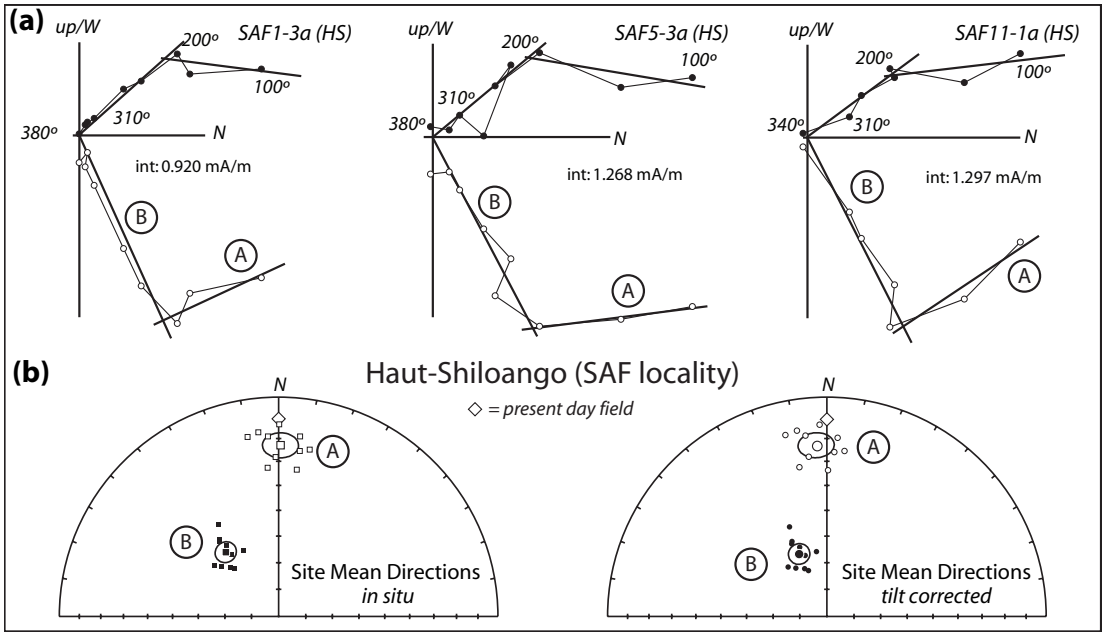

Figure 5.6. Demagnetisation characteristics for the HS locality: (**a**) orthogonal projections of three samples showing typical behaviour for this locality, demagnetisation steps are in °C. (**b**) equal area projections of site-mean directions. Two components are labelled A and B.

all samples: weak magnetisation (typically 0.1 – 5 mA/m) but consistent directions (Fig. 5.6). Principal component analyses resulted in the identification of two stable magnetic directions: a component with low unblocking temperatures (<200°C, component A) and a medium/high temperature component B with unblocking temperatures between 200 and 420°C (Table 5.2). In orthogonal projections component B is directed towards the origin (Fig. 5.6), is identified with single polarity in 44 samples and is determined to be the characteristic remanent magnetisation (ChRM). Component A has an overall site mean direction of D = 0.6°, I = -23.0° before tectonic correction and D = 356.4°, I = -22.6° after correction ($\alpha_{95} = 5.5$). Component B has a mean direction of D = 320.7°, I = 58.9° before and D = 336.3°, I = 64.3° ($\alpha_{95} = 3.9$) after tectonic correction.

After removal of a poorly defined low unblocking temperature overprint below heating to 200°C, samples of the Schisto-Calcaire Subgroup yielded a well defined magnetisation, directed towards the origin in orthogonal projections (Fig. 5.7), with unblocking temperature 200 – 420°C. It is identified in 29 samples (6 sites) with a single polarity. This component of the Schisto-Calcaire samples is interpreted as the ChRM and yields an overall site mean direction of D = 331.9°, I = 63.9° before and D = 351.0°, I = 65.6° ($\alpha_{95} =$

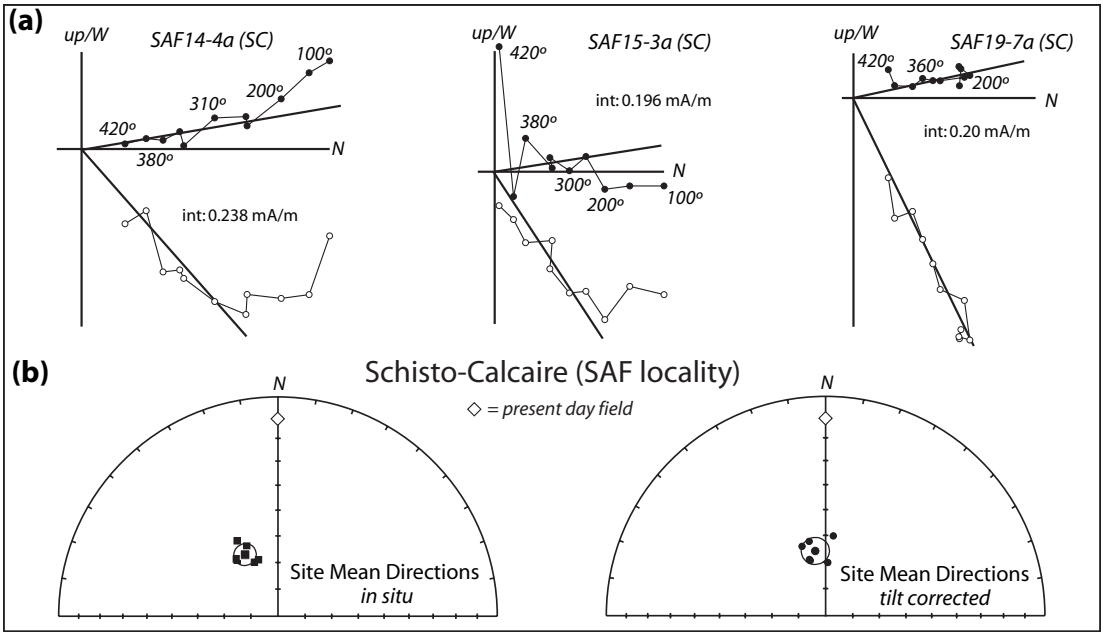

Figure 5.7. Demagnetisation characteristics for the SC locality: (**a**) orthogonal projections of three samples showing typical behaviour for this locality, demagnetisation steps are in °C. (**b**) equal area projections of site-mean directions.

5.1) after tectonic correction.

Upper Diamictite Formation, quarry near Kumbi village (KUM)

The Upper Diamictite was sampled at the KUM locality to conduct a conglomerate test. Approx. 20 m of exposed diamictite stratigraphy yielded only a limited number of adequately sized clasts for palaeomagnetic sampling. Seven samples were collected from clasts, 2 carbonate and 5 granite clasts, and 21 samples were taken from the relatively coarse grained, green coloured sandy matrix. The structureless diamictite did not allow identification of the bedding plane so the bedding of overlying carbonate formations was taken instead.

Demagnetisation of the matrix samples revealed the presence of a poorly defined low temperature component with unblocking temperatures <200°C and a stable component with unblocking temperatures between 200 and 420°C in all 21 samples. Intensities varied between 0.2 and 3 mA/m and the stable component is directed towards the origin in orthogonal projections (Fig. 5.8c). The magnetic direction of all samples is not very consistent as

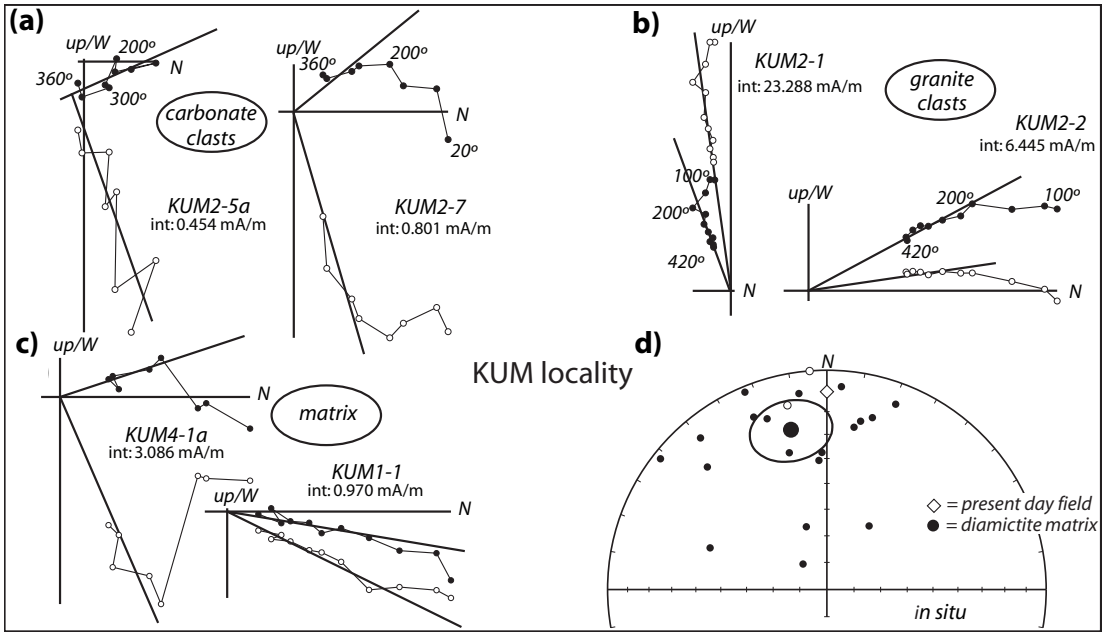

Figure 5.8. Demagnetisation characteristics for the KUM locality: (**a**) and (**b**) orthogonal projections of two carbonate and two granite clasts (**c**) orthogonal projection of two matrix samples (**d**) equal area projection of all matrix samples and their overall mean directions.

can be seen in an equal area projection of all directions (Fig. 5.8d). The matrix samples resulted in a overall mean direction of D = 347.2°, I = 26.2° before and D = 352.2°, I = 27.2° (α_{95} = 13.2) after tilt correction. A κ of 6.8 indicates high dispersion for the large number (n = 21) of samples (Table 5.2).

The demagnetisation behaviour of both carbonate clasts is shown in Figure 5.8a which reveals the presence a stable component with unblocking temperatures between ca. 250 and 360°C. The palaeomagnetic directions for this component are almost identical in both samples. In the granite clasts, after removal of a poorly defined low temperature magnetic component below 200°C, a stable component was revealed in four samples. In orthogonal projection of results this component is directed towards the origin (Fig. 5.8b) and, even thought the samples are not fully demagnetised at 420°C this component is identified as the ChRM. The granite clasts have an essentially random distribution of remanence directions.

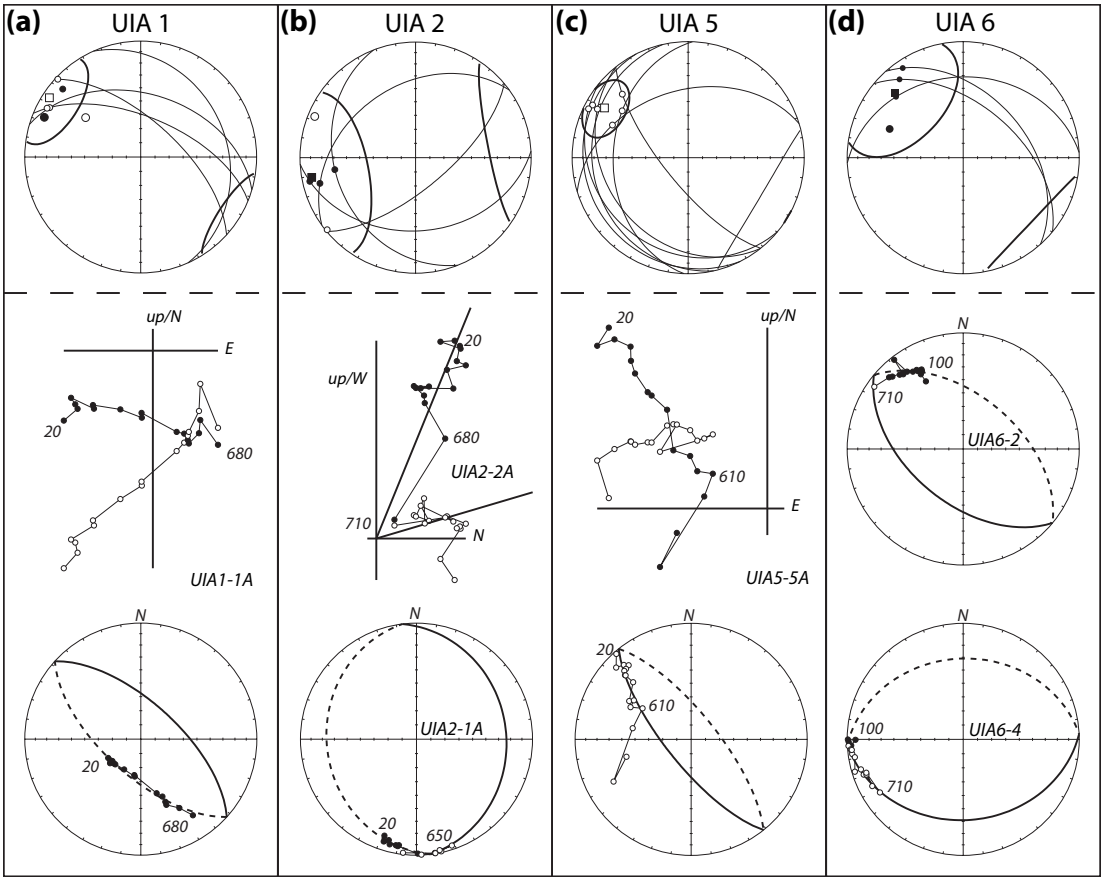

Figure 5.9. Aspects of demagnetisation for the UIA locality. Site mean plots with great circles are shown at the top of each column, great circles are only shown for the hemisphere in which the site mean direction plots. Underneath the dashed line are samples to illustrate typical behaviour observed in that site: (**a**) sample UIA1-1A does not trend toward the origin in orthogonal projection, demagnetisation steps plot along a great circle in equal area projection. (**b**) a trend towards the origin in UIA 2-2A showing a big loss in intensity between 680 and 710°C, another great circle in UIA2-1A. (**c**) UIA5-5A steps plot along a great circle up to 610°C. (**d**) two great circles, both samples trend away from the site mean direction.

Mpioka Subgroup and Inkisi Group, Ndembo-Uia village (UIA)

Palaeomagnetic samples were drilled from oriented hand-samples from the Mpioka Subgroup (UIA 5 & 6) and the Inkisi Group (UIA 1 & 2) collected in a riverbed and on UIA mountain close to the village of Ndembo-Uia. This resulted in a total of 11 samples (2 sites) for the Mpioka Subgroup and 15 samples (2 sites) for the Inkisi Group which have been thermally thermal demagnetisation up to 710°C. All samples show little decrease in intensity after stepwise heating up to 680°C, some samples show a sudden drop in intensity after heating to 710°C. In orthogonal projections only four samples display a trend towards the origin indicating shallow, north-westerly directions with mixed polarity (2 x normal, 2 x reversed polarity). Orthogonal projection indicate the presence of two magnetisations with overlapping blocking temperature spectra for 18 samples and these samples were interpreted with the use of intersecting great circles. Equal area projections revealed that, upon demagnetisation, most of these samples moved along a great circle away from, but occasionally towards, a shallow westerly direction (Fig. 5.9). For each site, great circles were combined with stable end point directions (i.e. the samples that trended towards the origin) in an equal area projection (top row of Fig. 5.9). For each great circle, the point closest to a mutual intersection was taken as a palaeomagnetic direction for that sample. These directions were combined with the stable end point directions to calculate site mean directions and an overall site mean direction of D = 316.6°, I = -2.4° before and D = 294.4°, I = 1.3° (A_{95} = 34.5°) after tectonic correction (Table 5.2).

As the NW shallow direction is associated with the lower part of the unblocking temperature spectra of a large number of samples it is interpreted to be a remagnetisation direction. This direction is similar to the late Palaeozoic direction for Gondwana. Because a possible remagnetisation can not be ruled out and because of the poor statistics (high α_{95}) this locality is excluded from further analysis.

Interpretation of palaeomagnetic results

Stable palaeomagnetic directions were obtained for the Haut-Shiloango and the Schisto-Calcaire subgroups at the CRO and at the SAF localities. The low temperature components

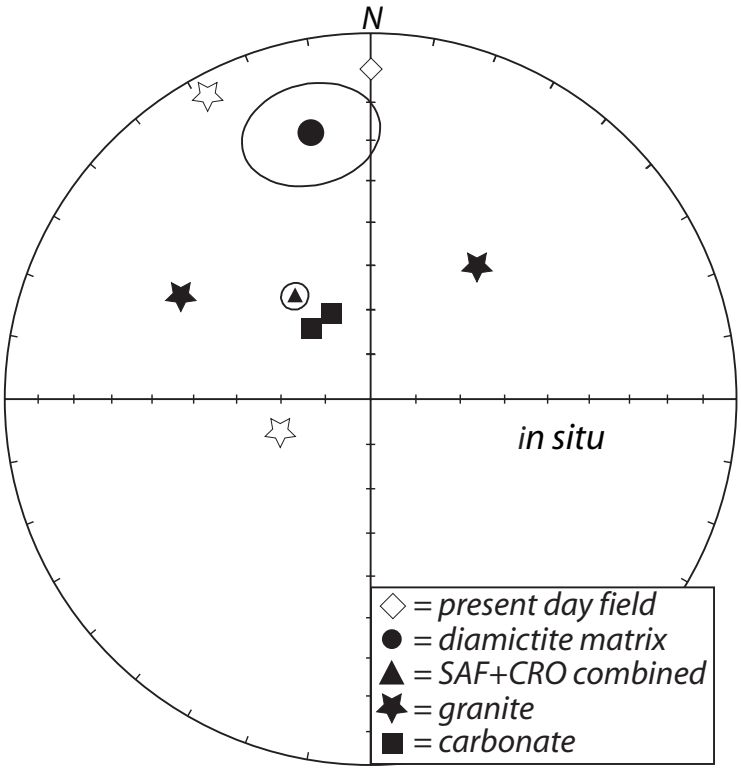

Figure 5.10. Conglomerate test. Stable palaeomagnetic directions for 6 clasts (4 granite, 2 carbonate) are compared to the average direction of the matrix and the SAF+CRO combined overall mean direction.

for the Haut-Shiloango at the SAF and CRO localities do not overlap. The *in situ* SAF component A is close to the present day field direction and is therefore regarded as a recently acquired magnetisation. CRO component A is unlike any other stable direction obtained in this study and is unlike any Phanerozoic palaeomagnetic direction for Africa. Because the time of magnetisation is unknown and because it is only recognised in 10 samples this component is not part of any further analysis.

Component B for the Haut-Shiloango Subgroup at the CRO locality is very similar to component B at the SAF locality which is why they are combined and compared to the high temperature component of the Schisto-Calcaire Subgroup. The overall site mean directions of both subgroups have overlapping α_{95} confidence cones and therefore all directions are combined resulting in an overall mean directions for the Haut-Shiloango and the Schisto-Calcaire subgroups. The overall mean is calculated in two ways, first using the three locality means resulting in D = 322.8°, I = 63.0° before and D = 342.8°, I = 66.9° ($\alpha_{95} = 6.7$, N

= 3) after tectonic correction. Because the CRO locality only consists of 2 sites and is over-represented using the locality mean an alternative way of determining the overall mean direction is employed by averaging all sites resulting in D = 323.6°, I = 61.4° before and D = 341.6°, I = 65.5° (α_{95} = 3.0, N = 18) after tectonic correction (Table 5.2). Although there is little difference between these two means the later is considered more appropriate. Due to the uniform bedding orientation a foldtest could not be used to determine whether the magnetisation was acquired before or after tectonic tilting.

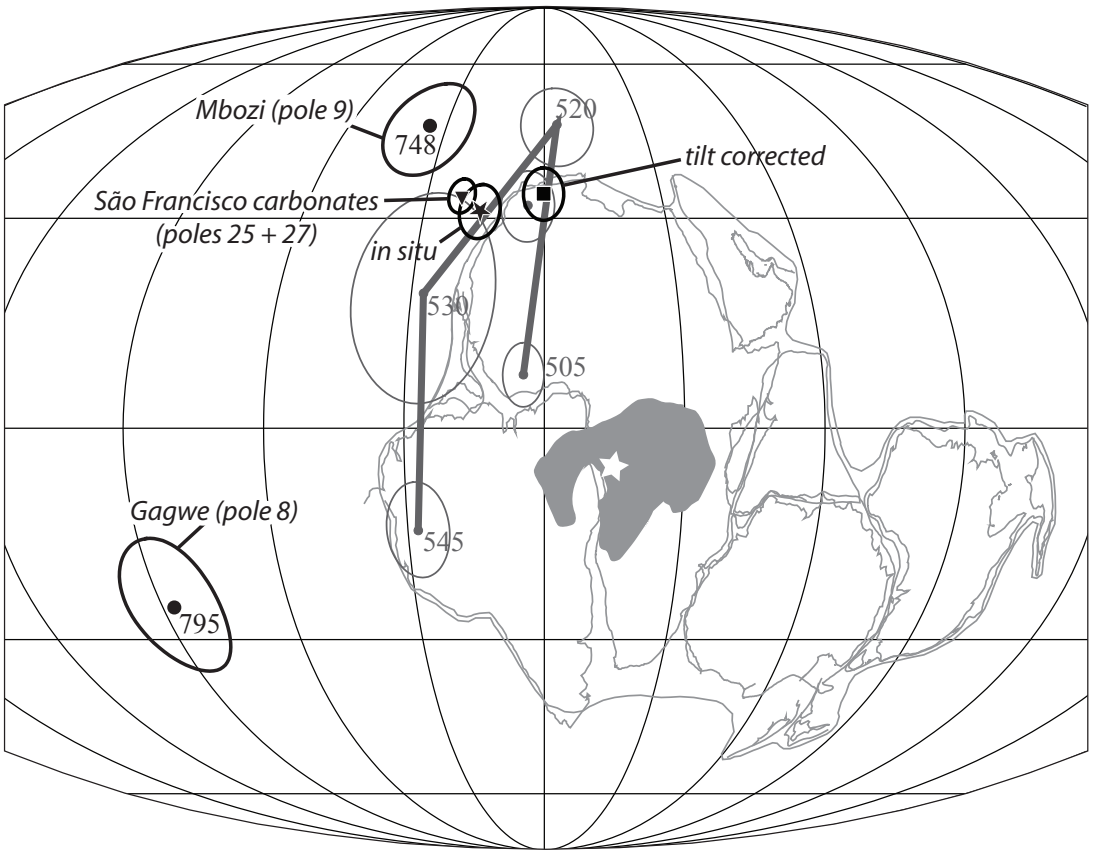

Figure 5.11. Palaeomagnetic poles for the Congo craton in a Mollweide projection. An *in situ* and a tilt corrected pole from this study, obtained from combining the Haut-Shiloango and Schisto-Calcaire subgroups, are shown together with three published poles in African co-ordinates: Gagwe (795 Ma, pole 8), Mbozi (748 Ma, pole 9) and a mean pole position for remagnetised carbonates on the São Francisco Craton (Bambuí C, pole 25, and Salitre C, pole 27). The Cambrian APWP for Gondwana in dark grey is after McElhinny et al. (2003). Also shown is the Congo-São Francisco Craton and an outline of Gondwana constituents with Africa in its current geographic position. The white star indicates the sampling area at 5°S and 14°E.

Sampling for a conglomerate test resulted in 21 analyses giving a highly dispersed (κ = 6.8) average direction for the matrix and 6 stable magnetic directions for clasts. The

stable clast directions are compared to the mean matrix direction and to the SAF+CRO combined mean direction in Figure 5.10. The granite clast directions are significantly different from all mean directions but the carbonates plot very close to the SAF+CRO combined overall mean direction. This indicates that both the carbonate clasts and the Haut-Shiloango and Schisto-Calcaire subgroups carry a similar magnetisation. The test is not statistically reliable because of the low number of clasts but it provides a strong indication that the carbonate clasts acquired their magnetisation at the same time as the samples of the Haut-Shiloango and the Schisto-Calcaire subgroups.

The SAF+CRO combined mean direction corresponds to an *in situ* palaeomagnetic pole of lat = 31.3°N, long = 343.9°E, A_{95} = 4.0° and a tilt corrected pole of lat = 33.9°, long = 359.7°, A_{95} = 4.3° (Table 5.3). From Figure 5.11 it can be seen that both poles plot onto the Cambrian reference APWP path for Gondwana.

	N	Plat(°N)	Plon(°E)	A_{95}(°)	λ(°)	Reference
SAF+CRO (*in situ*)	18	31.3	343.9	4.0	43	this study
SAF+CRO (tilt corrected)	18	33.9	359.7	4.3	48	this study
Gagwe (795 Ma)	12	-25	273	10	8	Meert et al. (1995)
Mbozi (748 Ma)	10	46	325	9	23	Meert et al. (1995)
Gondwana (530 Ma)	39	18.8	332.9	15.3	42	McElhinny et al. (2003)
Gondwana (520 Ma)	30	46.4	004.2	6.9	37	McElhinny et al. (2003)
São Francisco carbonates	41	33.6	338.7	2.8	39	Trindade et al. (2004)

Table 5.3. Palaeomagnetic poles for the Congo Craton in African coordinates. N = number of sites; λ = palaeolatitude for a locality at 5°S and 14°E.

5.3.3 Rock Magnetic Tests

Magnetic susceptibility

High temperature susceptibility measurements were carried out on selected samples from the Haut-Shiloango and the Schisto-Calcaire subgroups at the CRO and the SAF localities (results shown in Figure 5.12). Samples were selected to represent different lithologies: one sample from the Haut-Shiloango siltstones at the CRO locality, two samples from the Haut-Shiloango carbonate rocks at the SAF locality (one from the bottom and one from the top of the section, both show identical behaviour and only the bottom sample is shown

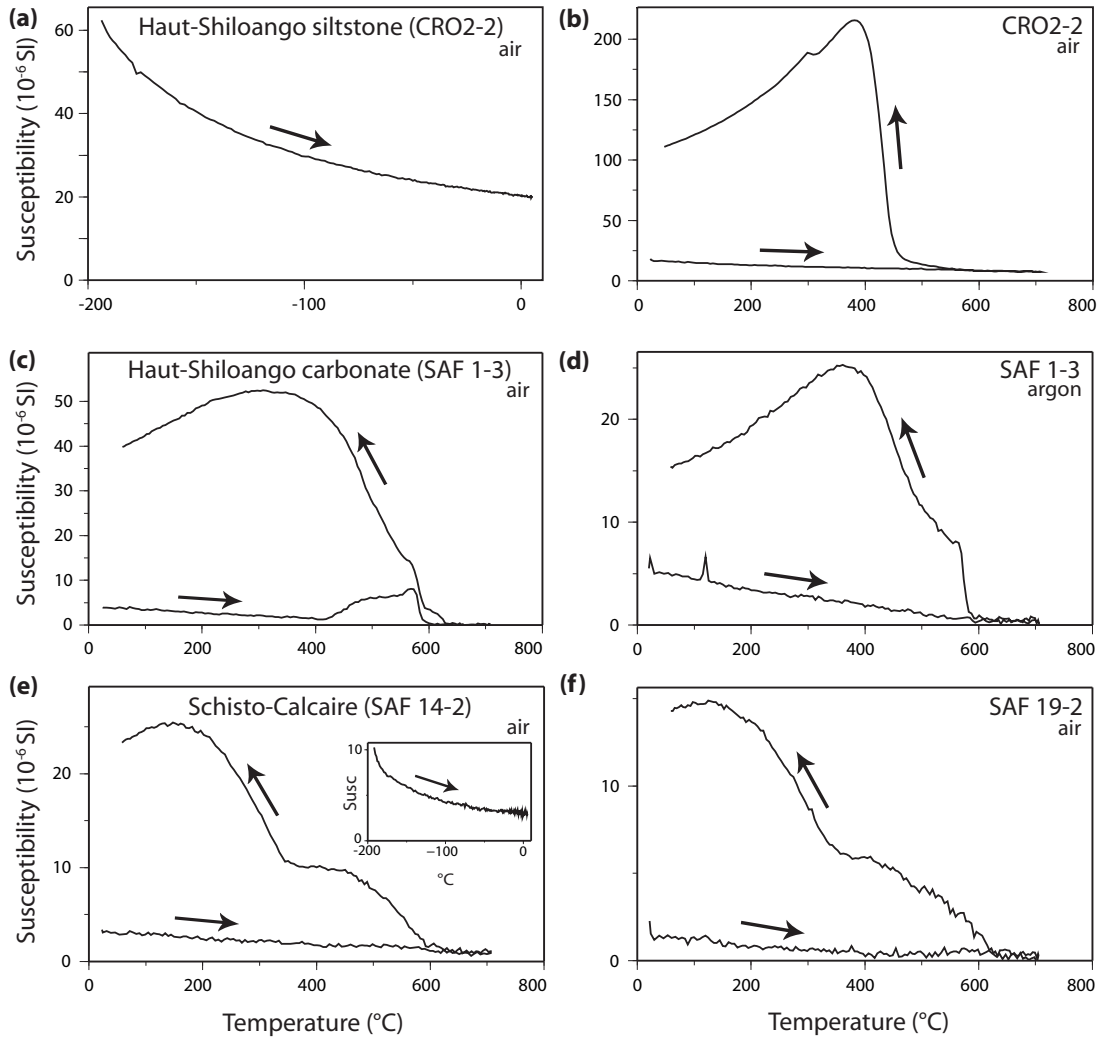

Figure 5.12. Susceptibility plots for selected samples, arrows indicate heating and cooling.

in Figure 5.12) and two from the Schisto-Calcaire dolomitised carbonate rocks (again one from the bottom and the top). All samples were analysed in air except one sample (SAF 1-3) which was measured in both air and argon to see the difference between oxic and anoxic conditions. Low temperature susceptibility analysis was performed on two samples, one from each subgroup.

Figure 5.12 shows that for all samples the cooling curves are distinctly different from the heating curves when experiments were carried out in air as well as in argon. The heating curve for the Haut-Shiloango siltstone is parabolic in both the low temperature and the high temperature analysis (Figs. 5.12a and b). The cooling curve in Figure 5.12b

starts to deviate from the heating curve at ca. 550°C and shows a pronounced increase in susceptibility at between ca. 435 and 400°C. Further cooling results in slowly decreasing susceptibility to half the value of the peak (Fig. 5.12b). The heating curve for the Haut-Shiloango carbonate (Fig. 5.12c) starts parabolic, increases at ca. 410°C and shows a sharp drop at ca. 580°C. The cooling curve shows a stepwise increase in susceptibility, a small step at 620°C and a large step at 580°C. Susceptibility continues increasing until 350°C after which it slowly starts to drop (Fig. 5.12c). Repeating the analysis under anoxic conditions does not show an increased susceptibility upon heating and the cooling curve shows a single, pronounced susceptibility increase around 580°C (Fig. 5.12d). The maximum susceptibility in argon is almost half that in air. Both samples from the Schisto-Calcaire show a similar pattern: slowly decreasing susceptibility upon heating and a two step increase upon cooling (Figs. 5.12e and f). The first step occurs at ca. 580°C for SAF 14-2 and 620°C for SAF 19-2, the second step occurs around 350°C for both samples. The peak susceptibility is after cooling to ca. 150°C. The low temperature susceptibility curve for SAF 14-2 shows an inverse, parabolic relationship with temperature (Fig. 5.12e).

The change in susceptibility between the heating and the cooling curves is probably due to mineralogical changes in the sample during the heating process. For each sample the heating curve has a parabolic shape which becomes particularly apparent in the two low temperature experiments (Figs. 5.12a and e). This inverse relationship between susceptibility and temperature is typical for paramagnetic minerals, whereas the high susceptible mineral phase which has developed upon cooling has a curve typical for ferromagnetic minerals (Svoboda, 2004). These minerals appear to have a range of unblocking temperatures between the maximum unblocking temperature and the peak susceptibility. Maximum unblocking temperatures are approximated by applying the two-tangent method of Grommé et al. (1969) on the inflection in the curves. This results in unblocking spectra for CRO 2-2 (400 – 435°C), SAF 1-3 (air: 350 – 630°C, argon: 400 – 580°C), SAF 14-2 (150 – 580°C) and SAF 19-2 (150 – 630°C).

Isothermal remanent magnetisation

Representative samples were selected from the different lithologies and localities to carry out isothermal remanent magnetisation (IRM) analyses using the techniques described in Chapter 3. The same selection criteria and number of selected samples applied here as with the susceptibility experiments. The acquired remanent magnetisation is plotted versus the log of the applied field in linear acquisition plots (LAPs) along the top row of Figures 5.13 and 5.14. The middle rows show a plot of the gradient vs. the log of the applied field in gradient acquisition plots (GAPs). The bottom rows show the result of multicomponent IRM experiments which will be described below. The LAPs and GAPs were analysed using modelling software developed by Kruiver et al. (2001) to identify individual coercivity components that construct the total IRM. Each coercivity component is characterised by its saturation remanent magnetisation (SIRM), the field at which half of the SIRM is reached ($B_{1/2}$) and the standard deviation of the logarithmic field. The LAPs show that after applying the maximum field of 4T only the Haut-Shiloango siltstone sample has become totally saturated.

Based on the LAP and GAP plots either two or three components were needed to fit the IRM curves. For samples from the Haut-Shiloango Subgroup two types of behaviour were identified: one in the siltstone sample from the CRO locality and one in the carbonate rocks from the SAF locality. The siltstone contains two coercivity components: component 1 constitutes 95% of the saturation IRM (SIRM) and has a $B_{1/2}$ of 50mT. Component 2 ($B_{1/2} = 603$mT) contributes only 5% to the SIRM (see Figs. 5.13a and c). In the carbonate rocks three components are modelled to fit the IRM curve (Fig. 5.13). The dominant two components have a $B_{1/2}$ of 59mT and 263mT and contribute 57% and 41% to the SIRM respectively. The third, high coercivity component ($B_{1/2} = 1.6$ T) is not fully saturated but contributes 2% to the SIRM after applying a max. field of 4 T (Figs. 5.13b and d).

Two types of behaviour were identified in samples from the Schisto-Calcaire Subgroup at the SAF locality. To investigate the stratigraphic relationship of this change in magnetic behaviour two more samples were analysed. This showed that the changes occurs approx. 2m above the contact with the Upper Diamictite Formation. In the lower part of the

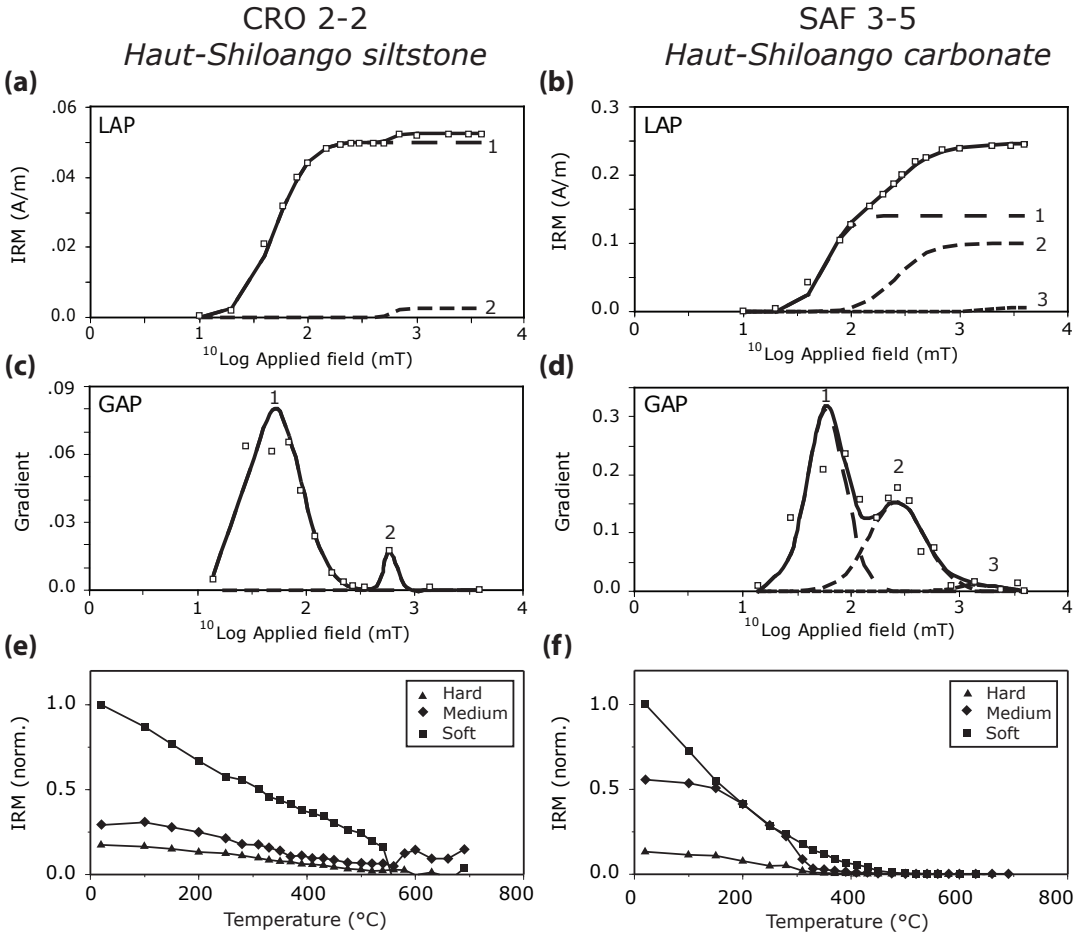

Figure 5.13. IRM acquisition curves for two representative samples from the Haut-Shiloango Subgroup. (**a-d**) the dashed lines are individual coercivity components which are numbered, the solid line is the cumulative of these components that fits the observed IRMs (square symbols). (**e**) and (**f**) results of the multicomponent SIRM demagnetisation (Lowrie test).

sequence (<2m) component 1 constitutes 75% of the total IRM and has a $B_{1/2}$ of 63mT, component 2 ($B_{1/2} = 447$mT) contributes 24% and a third component ($B_{1/2} = 3.2$ T) 1.5% to the total IRM. The later component is not completely saturated at 4T. The second type of behaviour is found in samples higher up the sequence (i.e. from 2 to 5.5m above the contact with the diamictite). Here only two components are found: component 1 contributes 12% ($B_{1/2} = 63$mT) and component 2 ca. 88% ($B_{1/2} = 525$mT) to the total IRM although the sample has clearly not reached saturation after applying the max. field (Figs. 5.14b and d).

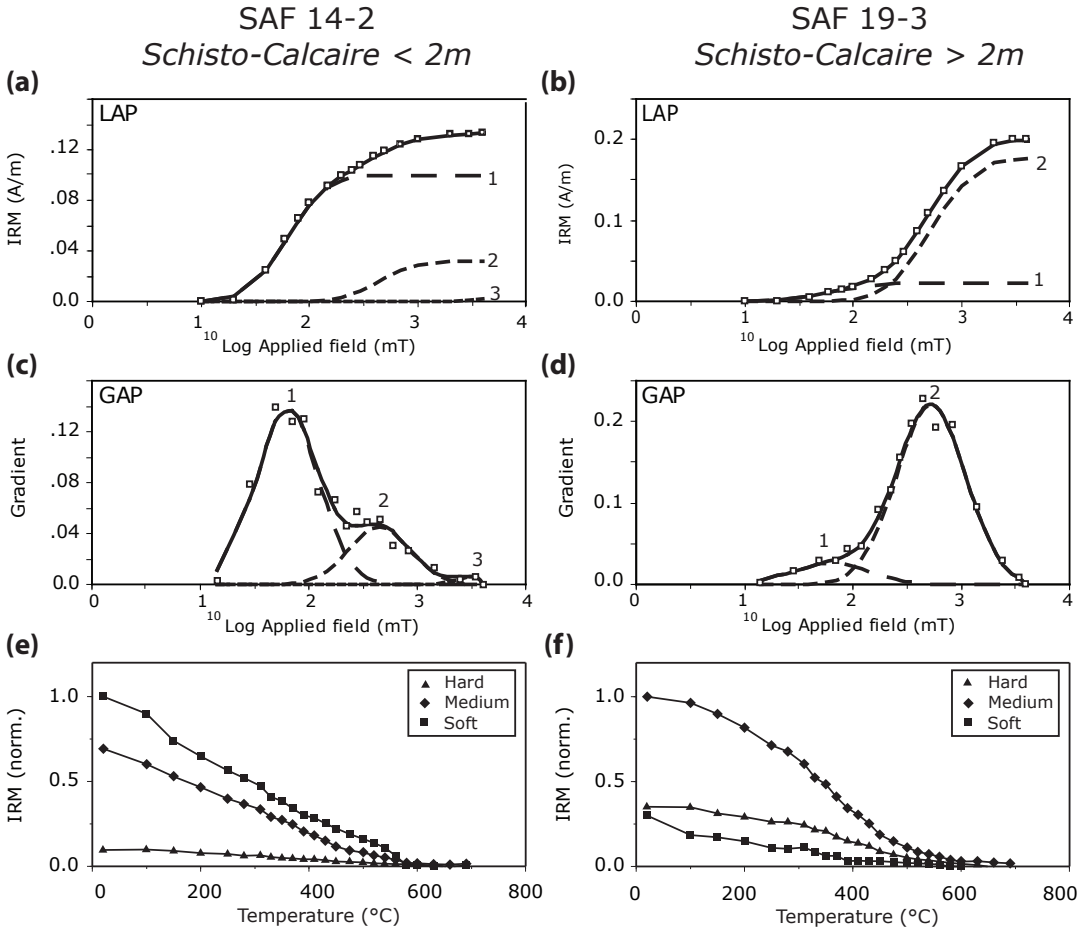

Figure 5.14. IRM acquisition curves for two representative samples from the Schisto-Calcaire Subgroup.

Multicomponent IRM (Lowrie test)

Multi component IRM experiments (Lowrie test, Lowrie, 1990) were carried out on the same samples that were used for the IRM acquisition experiments. Fields of 4.7T, 1T and 0.15T were applied in orthogonal directions and samples were thermally demagnetised. Demagnetisation of the SIRM shows that for the Haut-Shiloango Subgroup a low coercivity (<0.15T), 'soft' component is the largest contributor to the total IRM (Figs. 5.13e and f). For the siltstone sample the soft component is completely demagnetised by 580°C (Fig. 5.13e), the 'medium' component (<1T) shows a gradual demagnetisation until 580°C when its magnetisation suddenly increases and the 'hard' component (<4.7T) is completely demagnetised at 600°C. The carbonate sample has lost ca. 80% of its total IRM after

heating to 350°C (Fig. 5.13f): the soft component is completely demagnetised by 420°C, the medium component around 320°C and the hard component around 310°C.

For the Schisto-Calcaire Subgroup the SIRM demagnetisation reveals a change in behaviour between the lower and the upper part of the sequence and the change occurs ca. 2m above the contact with the Upper Diamictite Formation. In the lower part, the largest contributor to the SIRM is a low coercivity (<0.15T) component (Fig. 5.14e) which is completely demagnetised after heating to 580°C. A medium component (<1T) is also demagnetised at 580°C and a hard component (<4.7T) has a very small contribution to the total IRM and is demagnetised around 550°C. In the upper part of the sequence the IRM dominated by a medium coercivity component (Fig. 5.14f) which is largely demagnetised after heating at ca. 600°C but still present at 680°C. A hard and a soft component are demagnetised at 630 and 580°C respectively.

Magnetic mineralogy

The magnetic susceptibility measurements identified the presence of a paramagnetic mineral and the formation of ferromagnetic minerals upon heating. The iron carbonate mineral siderite ($FeCO_3$) is known for its paramagnetic behaviour and its ability to decompose to ferromagnetic minerals such as maghemite, magnetite and haematite (Svoboda, 2004). These transitions typically occur upon heating of siderite bearing rocks (Ellwood et al., 1986; Hirt and Gehring, 1991).

The ferromagnetic minerals that have developed upon heating during the susceptibility experiments can be recognised by their unblocking temperatures displayed in the cooling curve. Magnetite is characterised by a Curie temperature of 580°C while titanomagnetite, depending on the amount of Ti substitution, has lower Curie temperatures down to e.g. 150°C for TM60 (i.e. 60% substitution of Ti^{4+} for Fe^{3+}, Dunlop and Özdemir, 1997). Maghemite and haematite have Curie temperatures between 590 and 675°C. Titanium substitution in haematite also lowers the Curie temperature for titanohaematite. Maghemite is metastable and can convert to haematite or magnetite upon heating above 250°C. The susceptibility plots (Fig. 5.12) indicate the formation of titanomagnetite in the

Haut-Shiloango siltstone (unblocking temperatures 400 – 435°C), a mixture of magnetite and titanomagnetite in the Haut-Shiloango carbonate (350 – 580°C) and the lower part of the Schisto-Calcaire dolomite (150 – 580°C) and possibly a mixture of (titano)magnetite and titanohaematite in the upper part of the Schisto-Calcaire sequence (150 – 630°C).

Isothermal remanent magnetisation experiments showed that the magnetic phase carrying most of the total IRM in the entire Haut-Shiloango Subgroup and in the lower part of the Schisto-Calcaire Subgroup is characterised by low coercivity ($B_{1/2}$ of 50 - 65mT). Demagnetisation of the SIRM shows unblocking temperatures of 350 – 580°C for the low-coercivity (soft) component in these samples (Figs. 5.13e and f and 5.14e). These unblocking temperatures and coercivities are interpreted as indicating the presence of titanomagnetite. In the Haut-Shiloango carbonate sample a considerable portion (ca. 40%) of the IRM is carried by a medium-coercivity ($B_{1/2}$ = 263mT) magnetic phase which has an unblocking temperature of ca. 320°C. This temperature is indicative for the presence of monoclinic pyrrhotite (Curie temperature = 325°C, Dekkers, 1989). In the lower Schisto-Calcaire carbonate ca. 25% of the IRM is carried by a medium-coercivity magnetic phase which has unblocking temperatures between ca. 150 and 580°C and is also determined to be titanomagnetite. In all these samples (CRO 2-2, SAF 3-5 and SAF 14-2) a third, high coercivity (hard) component is demagnetised between 310 and 600 °C and may be haematite.

The IRM in sample SAF 19-3, representing the upper part of the Schisto-Calcaire sequence (i.e. 2 – 5.5 m above the Upper Diamictite Formation), is dominated by a medium coercivity component ($B_{1/2}$ = 525mT). The IRM demagnetisation experiments showed unblocking temperatures for the medium and hard components range from ca. 200 to >600°C and this component is therefore interpreted to be titanohaematite. A low-coercivity component ($B_{1/2}$ of 63mT), demagnetised between 400 and 580°C, contributes ca. 10% to the total IRM and is determined to be titanomagnetite.

The range of unblocking temperatures in the IRM demagnetisation experiments (Lowrie tests) show that all samples have lost 50% of their magnetisation after heating to 350°C. This is in agreement with the NRM demagnetisation experiments which show that the demagnetisation carried by these samples is usually stable up to 360 – 420°C. Considering

the formation of titanomagnetite and -haematite during the susceptibility experiments the magnetic minerals carrying the NRM may be authigenic, formed during thermal alteration of siderite.

5.4 Discussion and Conclusions

5.4.1 Age of Magnetisation

Constraints for the depositional age of formations of the West Congolian Group have been presented in Chapter 4. Maximum ages for the Sansikwa and Mpioka Subgroups of 979±31 and 607±16 Ma respectively are determined by detrital zircon geochronology. The age of the Lower Diamictite Formation is now well determined by a U-Pb baddeleyite age of 694±4 Ma for volcanic rocks associated with the diamictite. This provides a minimum age for the Sansikwa Subgroup and a maximum age for the overlying Haut-Shiloango Subgroup. A minimum late Neoproterozoic age (ca. 560 Ma) for the entire West Congolian Group is provided by the age of the Araçuaí-West Congo Orogen which affected all sedimentary rocks near the end of the Neoproterozoic. Estimates for the timing of this event are mainly based on the dating of pre-, syn- and late-orogenic granites in the São Francisco Craton which give a time-frame of 630 – 585 – 560 Ma for these three stages (Pedrosa-Soares et al., 2001, 2008). On the African side, an ^{40}Ar-^{39}Ar age of 566±42 Ma from a doleritic sill most likely reflects metamorphic resetting (Frimmel et al., 2006) and records the peak of the Pan African orogenic event in the West Congo Belt. The emplacement age for this doleritic sill is now dated by the 694 Ma baddeleyite age which is obtained for the same sample as the ^{40}Ar-^{39}Ar age. The Mpioka Subgroup is suggested to be a molasse sequence which formed during the late orogenic stages giving it an approximate depositional age of 560 - 530 Ma (Alvarez and Maurin, 1991; Tack et al., 2001). All other Subgroups are expected to be at least older than peak metamorphism around 566 Ma. The overlying tabular Inkisi Group is post-orogenic and from deposits overlying Inkisi-correlates in Angola it is determined to be older than Permian (Alvarez et al., 1995).

The palaeomagnetic results are thus obtained from rocks with a depositional age between

ca. 694 and 566 Ma. However, proximity of the *in situ* palaeomagnetic pole to the Cambrian APWP of Gondwana (Fig. 5.11) together with the lack of reliable fieldtests strongly suggest a remagnetisation of the weakly magnetised carbonate rocks. From the rock magnetic experiments it is concluded that the remnance is mainly carried by (titano)magnetite and that this may be authigenic magnetite formed by thermal alteration of siderite. This could have happened during the Araçuaí-West Congo Orogen and from the position of our pole between the 530 and 520 Ma Gondwana reference poles the remagnetisation has an approximate age of 525 Ma.

5.4.2 Geodynamic Implications

Neoproterozoic-Cambrian collisional events are recorded along all margins of the Congo-São Francisco Craton and are related to the amalgamation of West Gondwana (see Chapter 2). To the west of the craton, in South America, several collisions are referred to as the Brasiliano Orogeny, the main structure of which runs from north to south across the entire continent and effected the Amazonian, the Rio de la Plata and the São Francisco Cratons as well as other smaller cratonic entities (Brito Neves and Cordani, 1991; Cordani et al., 2000). Several discrete metamorphic pulses are recognised in the Brasiliano Orogenic belts (Brito Neves et al., 1999), e.g. the Paraguay-Araguaia Belt to the west of the São Francisco Craton records collision between São Francisco and Amazonia around 550 Ma (Moura et al., 2008; Paixao et al., 2008). This is coeval with peak metamorphism in the Araçuaí Belt which flanks the eastern margin of the São Francisco Craton (Pedrosa-Soares et al., 2001). Following peak metamorphism, the period 550 - 500 Ma is marked by the emplacement of several post-orogenic suites (Pedrosa-Soares et al., 2001): peraluminous, post-orogenic granitic plutons of ca. 535 Ma are followed by inversely-zoned diapirs plus calc-alkaline, metaluminous granites from 520 to 500 Ma (Noce et al., 2000). The Araçuaí Belt in South America and the West Congo Belt in Africa represent the closure of a restricted oceanic basin separating the São Francisco and Congo cratons (Alkmim et al., 2006).

This Araçuaí-West-Congo Orogen has left no igneous traces on the African side: the West Congo Belt is void of any alkaline intrusions, ophiolitic remnants or high-grade metamorphic rocks (Trompette, 1994; Tack et al., 2001). The sediments of the West Congolian

Group suffered only moderate deformation owing to the protection of the Archaean Craton to the east. Peak metamorphism may be recorded by ^{40}Ar-^{39}Ar resetting at ca. 566 Ma (Frimmel et al., 2006), remagnetisation of the West Congolian Group carbonates around 525 Ma may be an expression of post-collisional hydrothermal activity in the West Congo Belt (see discussion below on the origin of the remagnetisation).

Dating the remagnetisation at 525 Ma assumes overlapping Cambrian APWPs for the Congo Craton and Gondwana. Justification of this assumption is established by comparing the high quality 547 Ma Sinyai Dolerite pole (pole 30 in Table 5.1) and the 525 Ma Ntonya Ring pole (pole 29) with palaeomagnetic poles for Australia, Arabia and Antarctica (McElhinny et al., 2003). Agreement of these poles confirms an early Cambrian amalgamation of this part of Gondwana and that the Cambrian APWP for Gondwana can be used for the Congo Craton. The youngest Precambrian palaeomagnetic pole for the Congo Craton is the 748±6 Ma Mbozi pole at 46°N, 325°E (pole 9). This and our 525 Ma pole give a palaeolatitude for the West Congo Belt (5°S, 14°E) of 23° and 43° respectively. It thus seems that the sedimentary rocks of the West Congolian Group, including two glaciomarine diamictites, are deposited at subtropical latitudes.

5.4.3 Continental Scale Carbonate Remagnetisation

Two palaeomagnetic studies of Neoproterozoic carbonates on the São Francisco Craton resulted in four palaeomagnetic poles (pole 24 – 27 in Table 5.1), two of which are indistinguishable from each other (poles 25 and 27). Both these poles are obtained from weakly deformed carbonate sequences in Brazil (Fig. 5.15) and are associated with unblocking temperatures between 350 and 530°C. In the southern part of the São Francisco Basin 17 sites from sub-horizontal Bambuí carbonates yielded a magnetisation that corresponds to pole 25 (D'Agrella-Filho et al., 2000). Rocks to the west and to the east of the study area are affected by the Neoproterozoic (∼600 – 550 Ma) Brasília and Araçuaí fold belts respectively. U-Pb and Pb-Pb isotopic data obtained from both deformed and undeformed strata identified a widespread fluid percolation event which strongly affected the isotopic system of these rocks between 550 and 500 Ma (Babinski et al., 1999). Rock- and palaeomagnetic experiments suggest the magnetisation which corresponds to pole 25

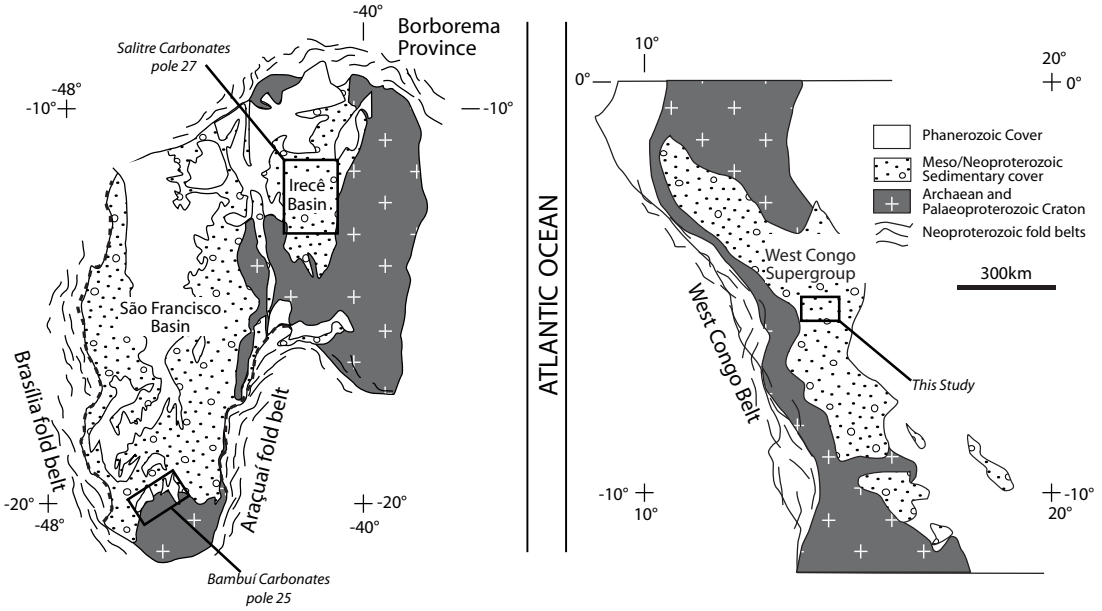

Figure 5.15. Simplified geological maps of the São Francisco Craton and the West Congo Belt (modified after Trindade et al. (2004) and Tack et al. (2001)). Study areas for poles obtained from carbonates on both sides of the Araçuaí-West Congo Belt are indicated.

is carried by remagnetised authigenic magnetite (D'Agrella-Filho et al., 2000). Approximately 900 km to the north of this locality, the weakly deformed Salitre Formation carbonate rocks in the Irecê Basin were studied palaeomagnetically (Trindade et al., 2004). Deformation is a far-field expression of intense folding in the Araçuaí fold belt to the south and the Borborema Province to the north. A magnetic component very similar in direction and thermomagnetic characteristics to the Bambuí stable component was recognised in 24 sites (and resulted in pole 27, Trindade et al., 2004). Pb isotopes from the Salitre carbonates yielded isochron ages of 522±25, 514±33 and 480±28 Ma i.e. very similar to the 550 – 500 Ma Pb-Pb ages obtained from the southern part of the São Francisco Basin (Babinski et al., 1999). Comparison of the palaeomagnetic results with the Gondwana APWP led Trindade et al. (2004) to assign a 525 – 520 Ma age for a simultaneous remagnetisation event in both localities. An overall mean pole for these remagnetised carbonate rocks on the São Francisco Craton (in African coordinates: 33.6°N, 338.7°E, $A_{95} = 2.8°$) has been added to Table 5.3 and Figure 5.11.

The simultaneous remagnetisation and resetting of the U-Pb isotope system on the São Francisco Craton may be the result of buoyancy driven fluid flow derived from the moun-

tain chains that were formed prior to 550 Ma (Trindade et al., 2004). The orogenies which shaped the surrounding fold belts (the Brasília Belt to the west and the Araçuaí Belt to the east) left the sedimentary basins almost intact, probably owing to the protection of underlying cratonic basement. Orogen-derived fluids interacting with sediments are a common mechanism for widespread remagnetisation (Oliver, 1986; Garven, 1995). It is for example the dominant process behind widespread remagnetisation of Palaeozoic sedimentary rocks in Europe and North America following the Hercynian Orogeny (McCabe and Elmore, 1989). On the São Francisco Craton, post-tectonic fluid flow is also linked to Pb-Zn mineralisations and sulphides in various parts of the São Francisco Basin (Iyer et al., 1992) which show a 520 Ma intercept on Pb evolution curve.

In the West Congo Belt a very similar situation arises: weakly deformed carbonates and siltstones carry a magnetisation which was acquired during thermal alteration of siderite around 525 Ma. The resultant palaeomagnetic pole coincides with the poles 25 and 27 obtained from the São Francisco Craton (after rotation to a pre-Atlantic fit, Fig. 5.11). The West Congo Belt formed the foreland basin to the Araçuaí Belt and it thus seems likely that the remagnetisation in the West Congolian carbonate subgroups was associated with buoyancy driven fluid flow which could have transported the necessary heat to trigger the mineralogical changes. In the West Congo Belt, fluid flow might be demonstrated by the horizontal banding of calcite and dolomite in the carbonates of the Schisto-Calcaire Subgroup immediately above the Upper Diamictite Formation, as shown in photomicrographs (Photo A.9). Elsewhere in the West Congo Belt, undated Cu-Pb-Zn mineralisations (including sphalerite and galena) cross-cut the Palaeozoic red beds of the Inkisi Group in Congo-Brazzaville (L. Tack, pers. comm.). These minerals may be related to the fluid migration which caused simultaneous mineralisation and remagnetisation in the São Francisco Craton. They form a potential target for providing an age for the migration event as well as a minimum age for the Inkisi Group.

Chapter 6

The West African Craton: Provenance and Palaeogeography

6.1 Introduction

On the West African platform the Taoudéni Basin records an almost continuous history of sedimentation from the Mesoproterozoic to the Mesozoic (Trompette, 1973; Bronner et al., 1980; Benan and Deynoux, 1998; Deynoux et al., 2006). Of particular interest are the late Neoproterozoic sediments that are characterised by the so called Triad sequence: a three-part stratigraphic marker of tillite, dolomitised carbonate and bedded chert. This glaciogenic deposit is one of the best-preserved records of a purely continental glaciation (Deynoux and Trompette, 1976; Deynoux, 1985; Deynoux et al., 2006) and has featured prominently in discussions of the Snowball Earth Hypothesis (e.g. Kennedy, 1996; Hoffman and Schrag, 2002; Eyles and Januszczak, 2004). Synchronicity of the Triad sequence across the West African Craton and correlation with similar deposits on other cratons remain disputed issues (Deynoux et al., 1978; Porter et al., 2004; Álvaro et al., 2007).

Another problem related to these Neoproterozoic glaciogenic deposits is the palaeogeographic position of West Africa at the time of deposition. Reconstructions lack robust constraints and are often based on the absence rather than presence of data (e.g. Hoffman,

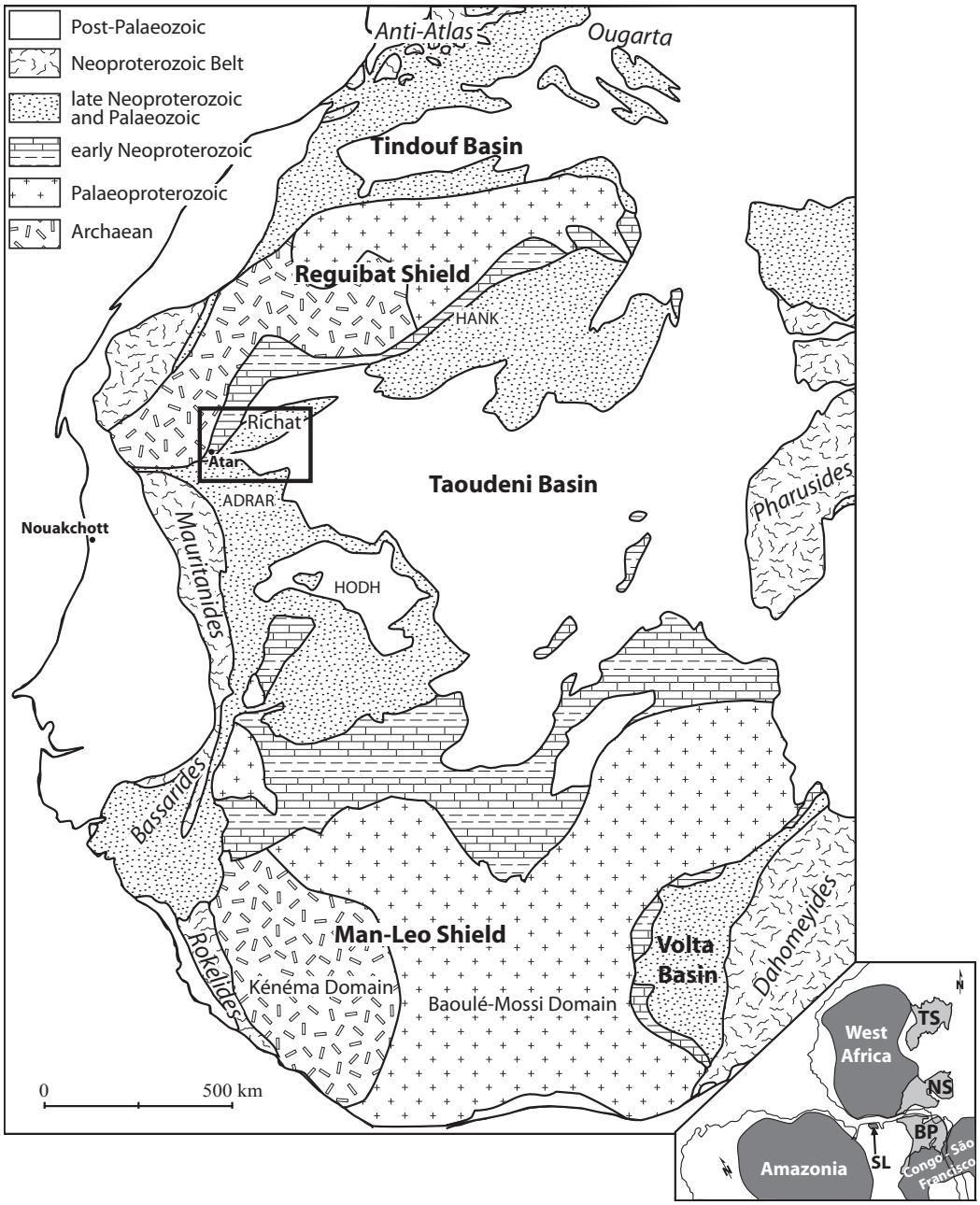

Figure 6.1. Geologic sketch map of West Africa after Deynoux et al. (2006). Field area is indicated by the black box which is an outline of Figure 6.6. Inset in bottom right corner shows the coastlines of South America and Africa before opening of the Atlantic Ocean and the possible extent of the West African Craton into South America which is represented by the São Luś Block (SL); BP = Borborema Province, NS = Nigeria Shield, TS = Tuareg Shield.

1991; Li et al., 2008). Here a full provenance analysis of Neoproterozoic sediments collected in the Adrar region (Fig. 6.1) is presented including geochemical analyses, stable isotope stratigraphy and detrital zircon dating. Also presented are palaeomagnetic results for late Neoproterozoic sandstones and a large (>100km) dyke cross-cutting basement. This dyke is dated by U-Pb baddeleyite and zircon ages.

6.2 Geological Setting

The West African Craton was one of the main constituents of West Gondwana (Unrug, 1992; Trompette, 1994, 1997; Rogers et al., 1995). The Borborema Province marks the southern margin of the craton and connexion with the Congo-São Francisco Craton to the south-east and the Amazonian Craton to the south-west (see inset in Fig. 6.1). The eastern margin is formed by a mosaic of terranes and continental blocks which form the Tuareg Shield and the Saharan Metacraton (Black et al., 1994; Abdelsalam et al., 2002). Archaean to Palaeoproterozoic basement rocks, now exposed in the Reguibat and the Man-Léo shields, amalgamated by mid-Palaeoproterozoic times and have formed a stable tectonic craton since ∼1.7 Ga. Much of the craton is covered by sediments of the Taoudéni Basin which stretches between the two basement shields (Fig. 6.1). Sedimentation started in the late Mesoproterozoic and continued until the Carboniferous (Cahen et al., 1984). The youngest sediments covering the craton are Mesozoic and Cenozoic sediments of the Sahara Desert.

The craton is surrounded by Neoproterozoic mobile belts (Fig. 6.1) which record early Neoproterozoic rifting and subsequent suturing from 685 to 550 Ma during the Pan-African orogenies leading to the formation of Gondwana. The term 'Pan-African' is used here to indicate the combination of Neoproterozoic tectonic events that ultimately led to the formation of West Gondwana, approx. from 725 to 500 Ma. Effects of the Palaeozoic Variscan orogeny can also be observed in the west (Mauritanides Belt) and the north (the Anti-Atlas mountains, Villeneuve, 2008; Soulaimani and Burkhard, 2008). Mesozoic opening of the Atlantic Ocean separated the West African Craton from North and South America which resulted in separation of the São Luís Block from the West African Craton. The São Luís

and the Borborema Province now form northeastern Brazil (Fig. 6.2; Santos et al., 2008; Klein and Moura, 2008).

6.2.1 Basement Rocks

In west Africa the cratonic basement is exposed on the Reguibat Shield in the north, on the Man-Léo Shield in the south and as some smaller inliers in the Bassaride and Mauritanides fold belts in the west (Fig. 6.1). The São Luís Block in north-west Brazil is probably an extension of the Man-Léo Shield. The main basement blocks are discussed below.

Reguibat Shield

The Reguibat Shield consists of two units: an Archaean province in the south-west and a Palaeoproterozoic 'Birimian' province in the north-east (Dillon and Sougy, 1974; Bessoles, 1977; Rocci et al., 1991). The term Birimian is unique to West African geology and refers to rocks of early Palaeoproterozoic age (2.5 - 2.0 Ga) which were effected by the ∼2.0 Ga Eburnian orogeny. Collisional belts of this age are recognised in almost all cratons and are one of the main criteria used for reconstructing the supercontinent Columbia (Rogers and Santosh, 2002; Zhao et al., 2002b). In West Africa and South America these orogenic belts are termed the Eburnian and Trans-Amazonian orogens respectively (Hurley et al., 1967; Lemoine et al., 1990; Boher et al., 1992; Trompette, 1994; Cordani and Teixeira, 2007). Hereafter the term Eburnian will be used to indicate tectono-metamorphic activity recognised in the West African Craton, occurring 2.1 - 1.8 Ga.

The Archaean province of the Reguibat shield is subdivided into the western Tasiast-Jijirit Terrane and the eastern Choum-Rag el Abiod Terrane (Pitfield et al., 2004; Key et al., 2008). The Tasiast-Tijirit Terrane consists of typical Archaean granites, greenstone belts and granitoid gneisses. Most of the plutonism appears to have taken place at about 2.9 Ga (Pitfield et al., 2004). The Choum-Rag el Abiod Terrane exposes a polyphase history of metamorphism, tectonism and magmatism: greenstone remnants in migmatitic gneisses record crustal growth from about 3.5 Ga and the terrane experienced granulite-phase

metamorphism at 3.0 Ga (Potrel et al., 1996; Key et al., 2008). Shortly after this (at 2.95 Ga, Pitfield et al., 2004) the two terranes merged and underwent bimodal, post-tectonic magmatism dated at ∼2.7 Ga (Potrel et al., 1998).

The Palaeoproterozoic Birimian province in the north-east of the Reguibat Shield contains remnants of Archaean basement but consists mostly of Palaeoproterozoic (Birimian) metasediments and late-Eburnian granites (Trompette, 1994; Schofield et al., 2006). Early Palaeoproterozoic supracrustal rocks representing continental margin sedimentation rest unconformably upon Mesoarchaean basement (Hurley et al., 1967; Rochette et al., 1990). The sediments, now metamorphosed, consist of graywackes, arkoses, schists; there are also mafic and acidic lavas (Trompette, 1994). Migmatitic gneisses and granodiorite intrusions record a phase of crustal thickening, metamorphism and granite emplacement at ∼2.1 Ga, in response to the emplacement of outboard arc terranes on the Archaean basement (Lahondère et al., 2003; Schofield et al., 2006).

A remarkable feature of the Reguibat Shield are the presence of numerous widespread dyke swarms including the prominent, 1.5 km wide and >100 km long Ahmeyim Great Dyke of Mauritania (Pitfield et al., 2004). Pre-metamorphic (Eburnian) metamafic dykes and anorthositic dykes are found within the Choum-Rag el Abiod Terrane. They are considered to be Neoarchaean in age but not older than ∼2700 Ma (Pitfield et al., 2004). Several post-metamorphic dyke swarms are recognised in the Reguibat Shield: 1) E-W oriented gabbroic dykes are only found in the southern part of the shield. Their emplacement age is unknown but they must be one of the oldest dyke sets since they are cross-cut by N-S trending microgabbro dykes and NE-SW trending fissile mafic dykes. 2) NE-SW oriented fissile mafic dykes are the most abundant of all. They generally form 1 – 2 km long, ∼10 m wide unaltered basaltic or microgabbroic structures and one of them is dated at 1949±9 Ma (Pitfield et al., 2004, report pers. comm. by J.-P. Lefort). They are covered by sediments of the Mesoproterozoic Char Group (Pitfield et al., 2004). 3) Less common are N-S and E-W to ENE-WSW trending gabbro dykes which follow pre-existing faults and structures. Some are very long and they have a brown weathering surface. They cut and displace the dominant NE-SW trending dykes. Based on their orientation and the way they fill pre-existing structures a Jurassic age has been assigned to these dykes, related to the opening

of the Atlantic Ocean. 4) The 030° layered gabbroic Ahmeyim Great Dyke of Mauritania is a prominent feature both in the field and on satellite images (see e.g. Fig. 6.7). It is up to 4 km thick and its main lithology is coarse-grained orthopyroxene-gabbro. It contains metabasalt xenoliths, chlorite veining and less common felsic veins. The main crystals found are plagioclase, pyroxene and augite with minor hornblende and biotite. Strong vertical layering is shown by grain-size variations and subtle differences in mineralogy. The southern part of the dyke is cross cut by members of the NE-SW trending dyke swarm which is described above.

A reconnaissance geochronological study of the Great Dyke resulted in a few concordant U-Pb zircon ages around 550 Ma (Pitfield et al., 2004). Other ages identified are interpreted as inherited 600, 750, 2000 Ma and Archaean (∼2.5 Ga) grains. These results are inconsistent with its relationship with the NE-SW trending dyke swarm which is dated Palaeoproterozoic based on mineral ages and observations of Mesoproterozoic sediments covering parts of these dykes.

Man-Léo Shield

The Man-Léo Shield in the southern part of the West African Craton consists of the Kénéma-Man Domain (mainly Archaean in age) to the west and the Baoulé-Mossi Domain (Palaeoproterozoic in age) covering most of the center and the eastern portion (Fig. 6.1, Feybesse and Milési, 1994). In the Kénéma-Man Domain, Archaean granito-gneisses, granulites and metasediments (marbles, schists, mafic volcanic rocks) were intruded by granite magmatism and altered by granulite facies metamorphism between 2910 and 2800 (Thiéblemont et al., 2004). Overlying these are volcano-sedimentary units including metabasite, banded iron formations (BIFs) and pelitic sediments with zircon ages of 2871 – 2615 Ma (Billa et al., 1999; Thiéblemont et al., 2004). All these units are intensely deformed and intruded by biotite-granites during the Eburnian orogeny which has been dated in syenites 2080 - 2020 Ma (Thiéblemont et al., 2004).

The Baoulé-Mossi Domain consists of early Palaeproterozoic metavolcanic rocks (tholeiitic to subordinate komatiitic basalts, along with calc-alkaline rhyolites) and metasedimentary

rocks (clastic sediments intercalated with felsic to intermediate metavolcanic and pyroclastic rocks, Sylvester and Attoh, 1992; Feybesse and Milési, 1994; Caby et al., 2000; Hein et al., 2004). The effect of the Eburnian orogeny is widepread and expressed through metamorphism (greenschist to lower amphibolite facies, Vidal and Alric, 1994) and granitic magmatism (two phases at 2155±15 Ma and 2100±10 Ma, Doumbia et al., 1998).

Connection with the São Luís Block

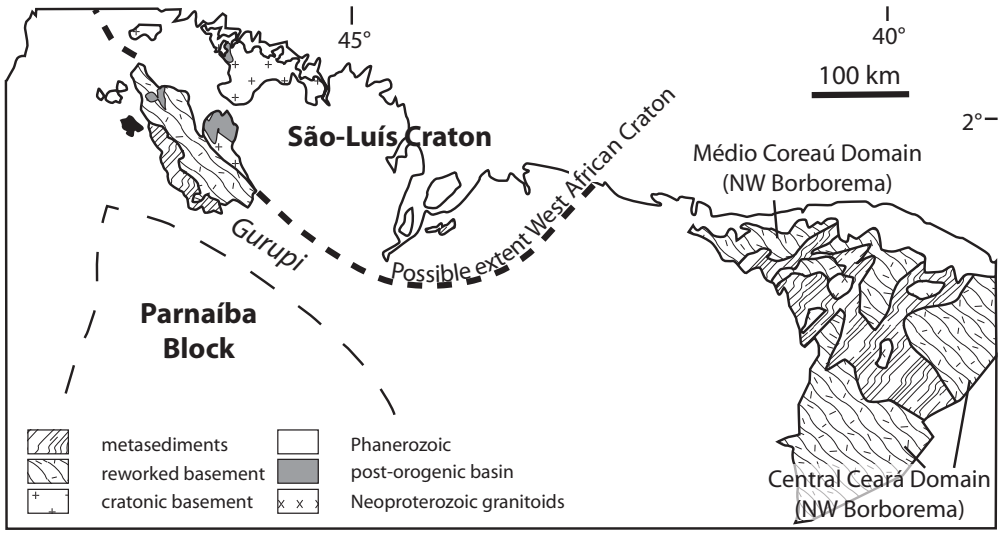

Figure 6.2. Simplified geolocial map of the São Luís Craton in Northern Brazil after Klein and Moura (2008).

The extension of the Man-Léo Shield into Brazil has been demonstrated by geochronological evidence (Hurley et al., 1967; Klein et al., 2005b). The São Luís Block and the basement inliers of the Gurupi Belt (Fig. 6.2) show three phases of magmatism (at 2240±5, 2160±10, 2080±20, Klein et al., 2005b). These are also found on the West African Craton suggesting that these terranes were contiguous in Palaeoproterozoic times. Palaeogeographic reconstructions based on sea-floor topography of the equatorial Atlantic place the São Luís Craton opposite the Baoulé-Mossi Domain of the Man-Léo Shield (Bullard et al., 1965; Nürnberg and Müller, 1991; Sandwell and Smith, 1995), suggesting the connection lasted until the opening of the Atlantic Ocean in Mesozoic times. Other evidence for a long lasting connection comes from the Neoproterozoic Gurupi Belt which to the east has been correlated with the Médio Coreaú Domain in the Borborema Province based on its in-

ternal structure and geophysical evidence (Lesquer et al., 1984; Klein and Moura, 2008). The Médio Coreaú Domain has been correlated to the Daohomeyide belt in West Africa (Fig. 6.1) based on the interpretation of positive gravity anomalies reflecting a concealed suture zone between the West Africa-São Luís Craton and the Borborema Province (Lesquer et al., 1984). This inferred suture zone, representing the closure of an oceanic basin, is supported by a continental arc batholith, developed between 665 and 620 Ma in the Borborema province (Fetter et al., 2003; Santos et al., 2008). Based on these papers, the Gurupi belt is likely part of a wide system of Brasiliano/Pan-African Neoproterozoic mobile belts, although an incomplete lithological record, due to a widespread Phanerozoic cover, prevents more comprehensive correlation.

6.2.2 Mesoproterozoic Evolution of the West African Craton

No major tectono-metamorphic events have been recognised in the West African Craton during late Palaeoproterozoic and Mesoproterozoic times. The absence of “Grenvillian" age (around 1.0 Ga) orogenies in West Africa excludes an active role in the formation of supercontinent Rodinia which amalgamated between 1300 and 900 Ma (Li et al., 2008).

In Proterozoic palaeogeographic reconstructions, the West African Craton is often positioned adjacent to the Amazonian Craton, similar to their relative positions in Gondwana (eg, Hoffman, 1991; Dalziel, 1997; Weil et al., 1998; Li et al., 2008). However, Zhao et al. (2006) stressed that this cratonic link is one of the key issues of Proterozoic supercontinents not yet resolved. West Africa and Amazonia, together with Congo-São Francisco are suggested to have formed a Proterozoic supercontinent called Atlantica (Rogers, 1996; Trompette, 1994; Rogers and Santosh, 2002). According to Condie (2002a), Atlantica was integrated into Columbia during the Palaeoproterozoic and subsequently Rodinia in Mesoproterozoic times without any major reconfiguration. The participation of West Africa in Atlantica is based on the correlation of rock types, timing of events and structures of Palaeoproterozoic ($\sim$2 Ga) orogenic belts on the Amazonia and West African cratons (Ledru et al., 1994; Caby et al., 2000; Hartmann, 2002).

Palaeomagnetic studies

Establishing Proterozoic palaeogeographic relationships between the West Africa and Amazonia cratons based on palaeomagnetic data are hampered by a lack of quantity and quality of available data. After analysing all available studies at that time Onstott and Hargraves (1981) suggested that Amazonia and West Africa had a joint apparent polar wander path from 2.1 Ga until 1.5 Ga. Based, however, on relatively low quality data, their model requires large scale (∼1000 km) Proterozoic shearing along Brasiliano mobile belts for which no further support has been published. Recent studies of Palaeoproterozoic granites and metasediments from the Guiana Shield on the Amazonian Craton and the Man-Léo Shield in West Africa resulted in virtual palaeomagnetic poles for both Cratons around 2 Ga (Nomade et al., 2003; Théveniaut et al., 2006) which are indistinguishable from each other after rotation of South America with respect to Africa into their Gondwana fit (using rotational parameters of Lawver and Scotese, 1987). It thus seems probable that the West African Craton and the Amazonian Craton belonged to the same land mass at ∼2 Ga, in agreement with a sequence of tectonic events suggesting convergence of the land masses at 2.1 - 2.0 Ga (Ledru et al., 1994). For the time interval 2.0 - 1.0 Ga there are no West African palaeomagnetic poles but the position of Amazonia is constrained in reconstructions of Columbia (Bispo-Santos et al., 2008) and Rodinia (Tohver et al., 2002; D'Agrella-Filho et al., 2008; Elming et al., 2009).

Palaeomagnetic studies of Neoproterozoic redbeds from the Taoudéni Basin reveal multicomponent magnetisations (Perrin et al., 1988). In subsequent analyses, however, all components were reinterpreted and shown to record Palaeozoic remagnetisation events (Perrin and Prévot, 1988; Evans, 2000). A palaeomagnetic study of the Adma intrusion (∼620 Ma) in the Hoggar Shield was conducted by Morel (1981). The magnetisation lacks field tests to prove a primary origin and is suspiciously similar to Cambrian Gondwana poles (Meert and van der Voo, 1997; Evans, 2000; Tohver et al., 2006).

This means that the West African Craton is palaeomagnetically unconstrained for almost 1.4 Ga (from ∼2.0 to 0.6 Ga), during which time its geographic position can only be determined using geological evidence for a West Africa – Amazonia connection. Unfortunately,

the geological record provides extremely limited constraints and it remains controversial whether the two cratons formed a coherent landmass throughout this 1.4 Ga or they separated and re-amalgamated to form part of Gondwana (Zhao et al., 2006; Li et al., 2008).

6.2.3 Neoproterozoic Sedimentation and Tectonic Events: Amalgamation of West Gondwana

The cratonic basement of West Africa is covered by large (1000-1500km in diameter) sedimentary basins (Fig. 6.1) where sedimentation started as early as 1100 Ma (Rooney et al., 2010). Following the start of sedimentation on passive margins, a period of continental extension is recognised all around the craton (eg, Cahen et al., 1984). Mid Neoproterozoic rifting is recorded by oceanic fragments in the Anti-Atlas to the north (Villeneuve and Cornée, 1994), tholeiitic cumulates in the Ougda complex to the east (Dostal et al., 1996), a nepheline syenite pluton in the Gurupi Belt, southern margin (Klein et al., 2005a) and rift related mafic volcanic rocks in the Bassaride Foldbelt (Villeneuve, 2008) (Fig. 6.1). None of these rifting events seem to have led to the development of full scale oceanic basins because none of the orogenic belts record consumption of significant amounts of oceanic crust (Hurley, 1973). It seems more likely that they were intra-cratonic rifts that opened briefly and closed on themselves (Rogers, 1996). The sequence of tectonic events in the individual margins will now be discussed in more detail.

Northern margin of the West African Craton

The Anti-Atlas mountains cover the northern margin of the craton (Fig. 6.1) in which evidence for a Neoproterozoic suture zone is exposed in a series of erosional ophiolitic inliers (Leblanc, 1976; Saquaque et al., 1989; Hefferan et al., 2000; Bousquet et al., 2008). Ophiolitic fragments are represented by slivers of mafic and ultramafic rocks, positioned in between Palaeoproterozoic basement rocks, early Neoproterozoic turbiditic sediments (derived from the craton, up to 4000m thick, Fekkak et al., 2000) and volcanic rocks belonging to the Neoproterozoic Saghro magmatic arc (Saquaque et al., 1989). According to Hefferan et al. (2000) the Saghro arc contains calc-alkaline plutons ranging in age from

∼780-580 Ma. Suturing of the West African Craton to the Saghro arc took place between 615 and 565 Ma, which was preceded by emplacement of the ophiolitic slivers at 685 Ma (Leblanc and Lancelot, 1980; Hefferan et al., 2000).

Ennih and Liégeois (2001), however, do not think the accretion of the Saghro arc caused such a major collision but that the Bou Azzar ophiolitic remnants plus the Saghro arc together were thrust upon the West African Craton by 685 Ma. These rocks was subsequently intruded at 585-560 Ma by high-K calc-alkaline batholiths followed by alkaline plutons (Aït Malek et al., 1998). These calc-alkaline plutons are not related to the island arc assemblage but record a phase of post-orogenic high-level magmatism equivalent to developments in the Tuareg Shield to the east of the craton (Liégeois et al., 1998). This model thus suggests a ∼100 m.y. (685 to 585 Ma) interval between arc-ophiolite emplacement and calc-alkaline magmatism. Collisional events with peri-Gondwanan terranes, which took place during this time interval (Nance et al., 2008), are not recorded in the Anti-Atlas, probably because the obducted Saghro arc was protected by the underlying cratonic lithosphere (Ennih and Liégeois, 2001). Post-orogenic sedimentation started shortly after the calc-alkaline volcanic rock emplacement (Ennih and Liégeois, 2001).

Further to the east, extending into Algeria, the Ougarta region (Fig. 6.1) shows a similar tectonic history to the Anti-Atlas. It comprises Neoproterozoic fine-grained clastic sedimentary rocks intercalated with, and overlain by, mafic lava flows (Dostal et al., 2002). Provenance of the sediments indicates they are derived directly from the cratonic basement and the chemistry of the lavas, which are depleted in Nb, Ta and Ti, indicates they formed in a backarc or rifted arc setting (Caby, 1996; Dostal et al., 2002). The sediments could be equivalent to the early Neoproterozoic sediments in the Anti-Atlas Belt and the volcanics probably corresponding to the emplacement of the Saghro inlier.

Eastern margin of the West African Craton

The eastern margin of the West African Craton is essentially a continuous fold belt which is sometimes referred to as the 'Trans-Saharan' fold belt or mobile zone (Trompette, 1994). In detail it can be subdivided into the Pharusides fold belt (Fig. 6.1) in the north record-

ing Neoproterozoic tectonic interaction between the craton and the Tuareg Shield (Caby, 2003), and the Dahomeyides Belt in the south (Fig. 6.1) marking the suture zone between the West African Craton and the Nigerian Shield (Attoh et al., 1997).

The Tuareg Shield has a complex Proterozoic tectonic and sedimentary history. It consists of at least 23 individual terranes which ultimately came to their current configuration at the end of the Pan-African events (∼550 Ma, Black et al., 1994; Caby, 2003). Tholeiitic cumulates, remnants of oceanic crust and a positive gravity anomaly all point to the existence of a Neoproterozoic basin at ∼800 Ma called the Pharusian ocean (Caby, 1994; Dostal et al., 1996). Eastward subduction of this ocean from 730 to 620 Ma formed the Tilemsi Island Arc complex which subsequently collided with the West African Craton at ∼620 – 580 Ma in a NE to SW oblique motion (Villeneuve and Cornée, 1994) resulting in some greenschist facies regional metamorphism (Caby, 2003). During this period syn-collisional granitoids were intruded diachronously throughout this part of the craton margin (Caby, 2003) but granitoid emplacement continued until 520 Ma in the central provinces of the Tuareg Shield (Azzouni-Sekkal et al., 2003; Acef et al., 2003). Cenozoic sedimentation eventually covered most of this Pharusian suture.

The Dahomeyides Belt shows a similar geodynamic history to the Pharusides fold belt. Mafic volcanic rocks record the opening of an early Neoproterozoic oceanic basin (Affaton et al., 1997, 1991), followed by collision between the passive margin of West Africa and several smaller terranes which are now part of the Nigerian Shield (Caby, 1989; Affaton et al., 1997). The Dahomeyide orogen is exposed in Ghana and Togo as a series of nappe complexes comprising passive margin sediments and suture related magmatic rocks. Geochronological data indicate peak metamorphic age of ca 610 Ma and final exhumation and cooling ages of 587 – 576 Ma (Attoh et al., 1997; Santos et al., 2008). East of the Tuareg and Nigerian Shields is the much larger Saharan Megacraton which extends to the Arabia-Nubia Shield to the east and occupies the north-central part of Africa (Abdelsalam et al., 2002).

The Dahomeyide orogenic belt is believed to have continued into South America during the Neoproterozoic although the continuation is largely buried beneath Phanerozoic basins in northeast Brazil (Lesquer et al., 1984).

Southern margin of the West African Craton

The southern margin of the craton lies in north-east Brazil where the Neoproterozoic Gurupi Belt (Fig. 6.2) marks the southern margin of the Palaeoproterozoic São Luís Block (Klein et al., 2005a). Within the Gurupi Belt, Palaeoproterozoic basement rocks are separated by strike-slip shear zones which seem to have been activated during the Neoproterozoic (Klein et al., 2005a). Apart from this tectonic activity two magmatic units are Neoproterozoic in age: a nepheline syenite pluton dated by U-Pb zircon analyses at 732±7 Ma (Klein et al., 2005a) records rifting while a peraluminous, muscovite-bearing granite (dated at 549±4 Ma) is interpreted to be a late- or post-tectonic intrusion (Klein and Moura, 2008). The Gurupi Belt records interaction between the São Luís Block to the north and the concealed Parnaíba Block to the south, the existence of which has been proposed on the basis of geophysical evidence (Brito Neves et al., 1984).

The Médio Coreaú Domain of the NW Borborema Province comprises sedimentary and volcano-sedimentary units that were deformed and metamorphosed in the Neoproterozoic (Fetter et al., 2000; Brito Neves et al., 2000). These sediments, which were deposited on a Palaeoproterozoic metamorphic basement, were intruded by numerous arc-related granites at 777±11 to 591±8 Ma (Fetter et al., 2003). Based on the timing of the events, as well as on internal structures of the belts and their (palaeo)geographical positions, the Médio Coreaú Domain has been correlated to the Gurupi Belt (Klein and Moura, 2008).

Western margin of the West African Craton

Three orogenic belts have been described along the western margin of the West African Craton recording a polyphase tectonic evolution: the late Neoproterozoic Rokelides Belt in the south, the more ancient Bassarides Belt in northern Guinea and southern Senegal and the Palaeozoic Mauritanides Belt in the north (Fig. 6.1; Dallmeyer and Lecorche, 1991; Villeneuve, 2008; Villeneuve et al., 2010). Sedimentation started in the late Mesoproterozoic and continued well into the Neoproterozoic until the emplacement of rift related magmatic rocks of 850 to 800 Ma (Villeneuve, 2008). Subsequent crustal thickening and compression during what is called the Pan-African I orogeny (ca. 650 Ma) resulted in the

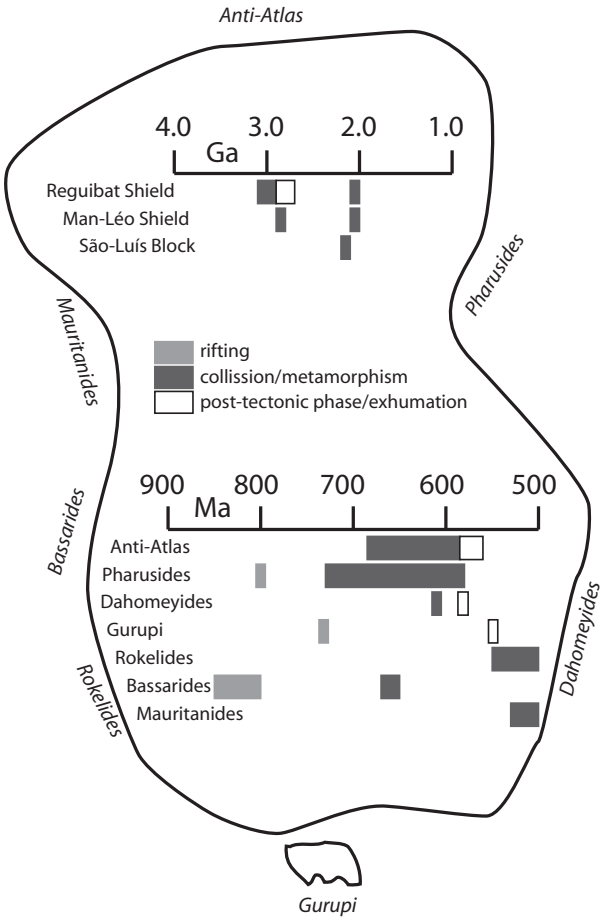

Figure 6.3. Time lines of Precambrian tectonothermal events on and around the West African Craton using ages described in the text. The relative locations of the Neoproterozoic belts are shown around an outline of the craton in west Africa and the São Luís Block in northern South America.

formation of the Bassarides Belt (Villeneuve and Dallmeyer, 1987; Villeneuve, 2008). This orogeny was the result of a collision between West Africa and a volcanic arc that was situated between the craton and the West Africa Neoproterozoic Ocean (Villeneuve et al., 2010). Closure of this ocean and collision with the Senegalese Block led to the Pan-African II orogeny (ca. 550 Ma) which shaped the Rokelides Belt but also affected the Bassarides and the southern part of the Mauritanides belts (Villeneuve, 2008). Remnants of an arc system are caught up in the Rokelides suture zone (Lytwyn et al., 2006) and the driving force might have been the approaching Amazonia Craton as this period coincides with the final stages of Gondwana amalgamation (Trompette, 1994). A series of minor compressional and extensional events followed afterwards and finally a late Palaeozoic collision

with Laurentia which resulted in extensive thrusting in the Mauritanides and a large part of the Bassarides belts (Villeneuve, 2008; Villeneuve et al., 2010).

6.2.4 Neoproterozoic basins

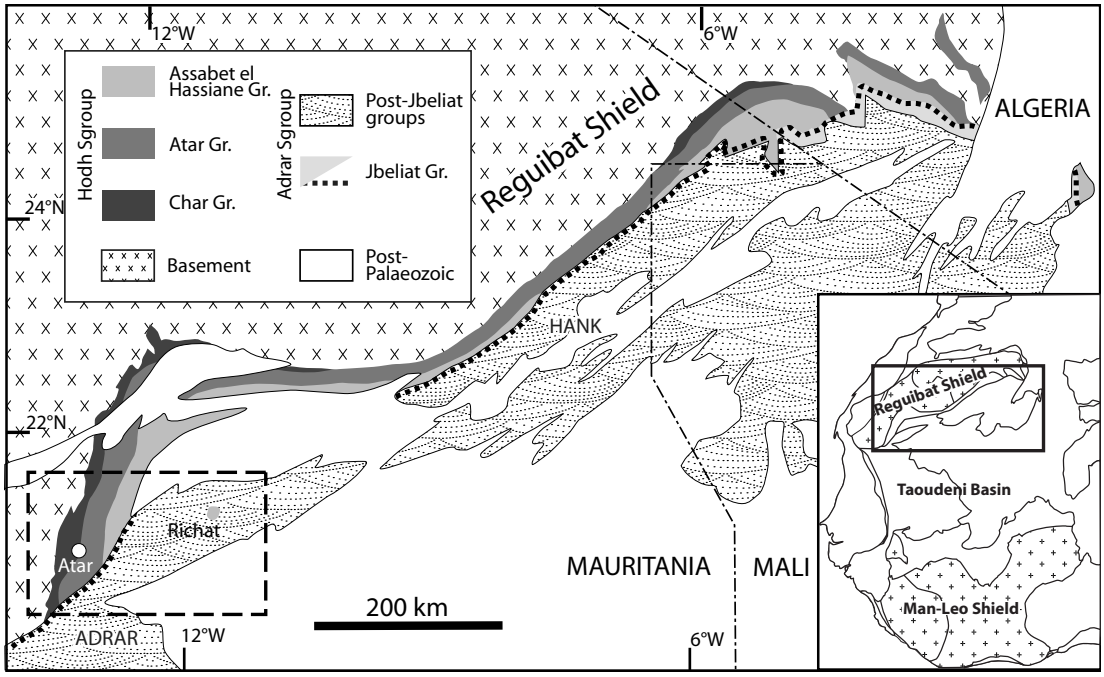

Figure 6.4. Simplified geological map of the northern part of the Taoudéni Basin (modified after Moussine-Pouchkine and Bertrand-Sarfati, 1997). It shows the Neoproterozoic sediments onlapping on the cratonic basement and covered by Phanerozoic sediments. The dashed box indicates the sampling area of this study and is an shown in Figure 6.6.

The cratonic basement is covered by several Neoproterozoic to Palaeozoic sedimentary basins of which the main three are the Taoudéni Basin in the centre, the Tindouf Basin to the north of the Reguibat Shield and the Volta Basin south-east of the Man-Léo Shield (Fig. 6.1). The Taoudéni Basin, on which this chapter is focused, is by far the largest, stretching from the Mauritanides in the west to the Pharusian suture zone in the east and from the Reguibat to the Man-Léo shield. It is on average 3000m thick and in the centre it is covered by Mesozoic and Cenozoic sediments. Sedimentation started at approximately 1.1 Ga but was interrupted locally at several stages during Pan-African events and during Variscan nappe emplacement in the Mauritanides belt.

Four supergroups have been identified in the Taoudéni Basin separated by major unconfor-

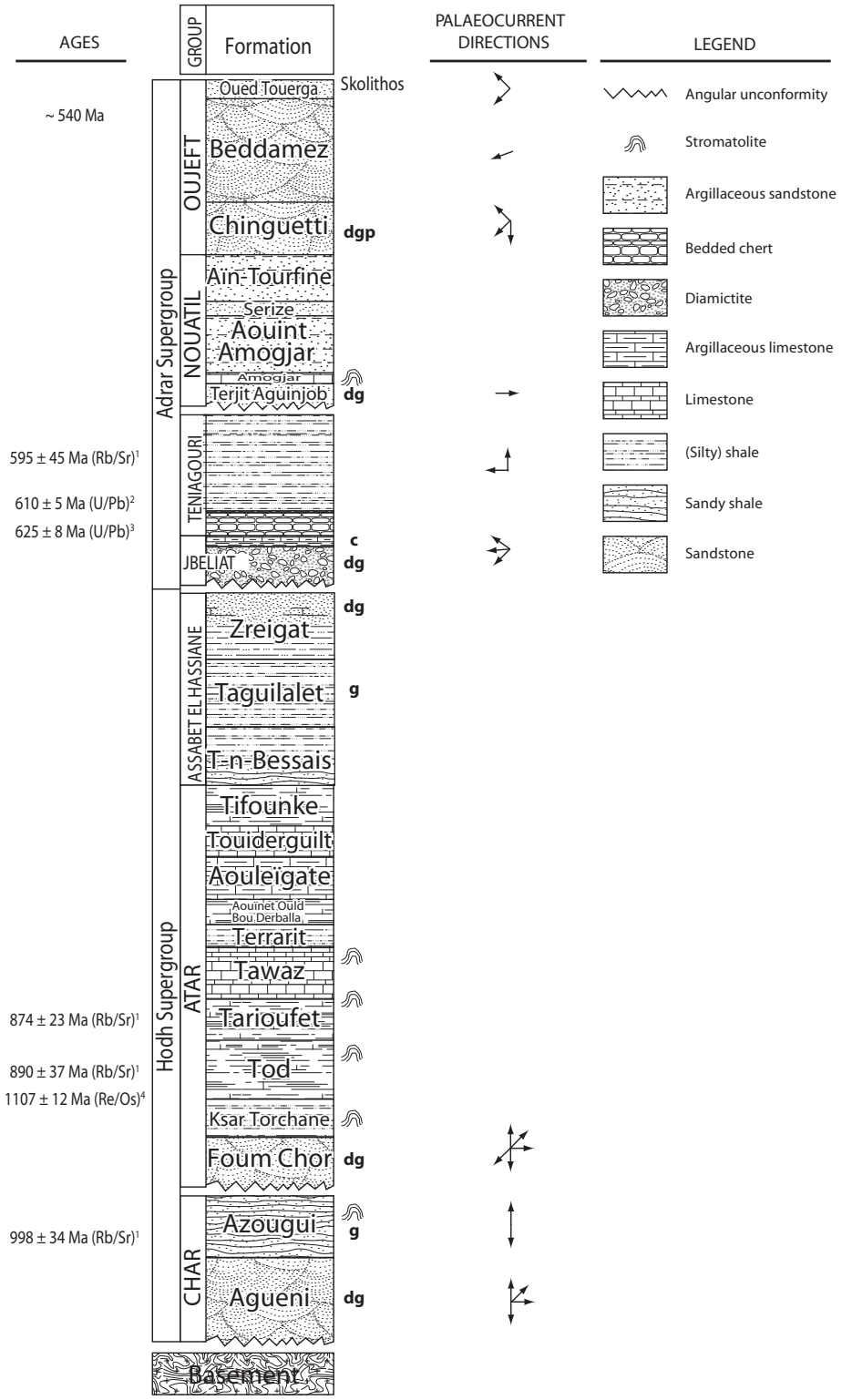

Figure 6.5. Stratigraphic column for the Hodh and Adrar Supergroups in the Adrar Sub-Basin . Stratigraphic levels where samples are collected for detrital zircon geochronology (**d**), provenance geochemistry (**g**), chemostratigraphy (**c**) and palaeomagnetism (**p**) are indicated. [1]Clauer (1976), [2]Lahondère et al. (2005), [3]Frischbutter et al. (2009), [4]Rooney et al. (2010). Palaeocurrent directions are from Lahondère et al. (2003) and Pitfield et al. (2004) and are based on foreset orientations.

mities (Trompette, 1973; Deynoux et al., 2006). The oldest two supergroups (Hodh and Adrar Supergroups, see Figure 6.5) span the Mesoproterozoic to Lower Palaeozoic and are well exposed in the Adrar Sub-Basin (Fig. 6.4) , just south of the Reguibat Shield, which is the type locality for the entire Taoudéni Basin (Trompette, 1973). The sedimentary rocks in the Adrar are relatively unaffected by the orogenies described above and form gently south-dipping unmetamorphosed sequences deposited on migmatised Eburnian basement. The overlying Dahr Supergroup and an unnamed supergroup are Ordovician-Silurian and Devonian-Carboniferous in age respectively. The youngest sediments are the Mesozoic to Cenozoic continental sediments largely covering the central and eastern part of the Taoudéni Basin.

6.2.5 The Adrar Sub-Basin

The type section for the Taoudéni Basin is in the Adrar Sub-Basin (Trompette, 1973) where the Hodh Supergroup is subdivided into the Char, Atar and Assabet el Hassiane groups (Fig. 6.5). These vary locally in thicknesses reflecting palaeorelief, reactivation of basement faults and regionally varying subsidence rates, but average thickness of the Hodh Supergroup is ca. 1300m (Deynoux et al., 2006). The Char Group consists of siliciclastic, shallow-marine units and is inferred to represent initial break-up phase during the Neoproterozoic, contemporaneous with the circum-craton rifting (Benan and Deynoux, 1998; Deynoux et al., 2006). The overlying Atar Group is a stromatolite-bearing sequence of carbonates and shales. Initially, an early Neoproterozoic age was assigned to the Hodh Supergroup based on stromatolite assemblages (Amard, 1986) and Rb-Sr dates of 890±37 and 874±23 Ma from clay minerals in the Atar Group (Clauer, 1976). However, new Re-Os data suggest a Mesoproterozoic age for these rocks (ca. 1100 Ma, Rooney et al., 2010) thereby redefining the start of sedimentation in the Taoudéni Basin with the Rb-Sr data interpreted as recording a diagenetic event. The Assabet el Hassiane Group overlies the Atar Group with an erosional disconformity and consists of fine-grained marine sediments which are well sorted and bedded (Trompette, 1973). The entire Hodh Supergroup was tilted and subjected to a long period of erosion, related to tectonic uplift during the main Pan-African events, prior to deposition of the Neoproterozoic to Palaeozoic Adrar Super-

group (Trompette, 1973; Deynoux, 1980).

The start of the Adrar Supergroup is marked by the Jbéliat Group which consists of diamictite deposits covered by a thin (ca. 5m) layer of dolomitised carbonate. It is overlain by bedded cherts and shales of the Téniagouri Group and this three-phase sequence of tillite, dolostone and cherts had long been called Triad and used as a marker horizon around the entire Taoudéni Basin (Zimmermann, 1960; Leprun and Trompette, 1969; Trompette, 1973; Deynoux et al., 1978; Deynoux, 1980). After initial discussions about the origin of these diamictites (Schermerhorn, 1974a; Deynoux and Trompette, 1976), reports of striated clasts and pavements and lacustrine varves with dropstones demonstrated the glacial influence during deposition of these rocks (Deynoux, 1980; Deynoux and Trompette, 1981; Deynoux, 1982, 1985; Pitfield et al., 2004). The Jbeliat Group was deposited by continental glaciers which are believed to have flowed from north of the Reguibat Shield (Deynoux, 1980) in southward direction, filling in palaeodepressions (Trompette, 1973; Álvaro et al., 2007). These deposits form one of the best-preserved purely continental records of a pre-Pleistocene ice sheet (Deynoux et al., 2006). A U-Pb age of 625±8Ma has been obtained from an ignimbrite ash deposit within the overlying Téniagouri Group (Fig. 6.5, Frischbutter et al., 2009). The upper part of the Adrar Supergroup consists of late Neoproterozoic and Palaeozoic, predominantly siliciclastic sedimentary rocks which are well exposed in the Adrar and form the prominent Atar cliffs (Pitfield et al., 2004).

6.3 Stratigraphy and Sampling

Samples for provenance geochemistry, geochronology (baddeleyite and detrital zircon dating), stable isotope chemostratigraphy and palaeomagnetism have been collected during a two-week fieldwork in January 2009. Samples were collected from most groups of the Hodh and Adrar supergroups (Table 6.1 and Figures 6.5 and 6.6) and the stratigraphy will be described in more detail. Detailed descriptions of analytical procedures can be found in Chapter 3. Stratigraphic nomenclature for the Adrar region is after Pitfield et al. (2004) which is largely following Trompette (1973). A selection of field photos can be found in Appendix A.2 starting on page 242.

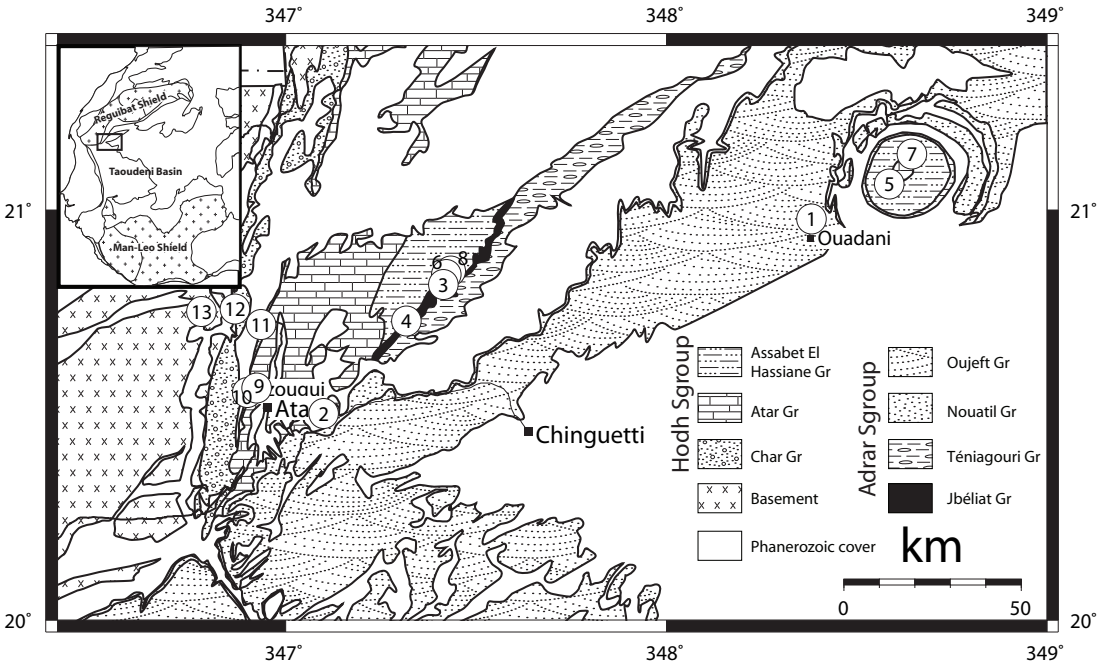

Figure 6.6. Simplified geological map of the sampling area. Numbers in the sampling localities correspond with the last column in Table 6.1.

6.3.1 Hodh Supergroup

Char Group

The Char Group comprises two formations of predominately siliciclastic sediments, the Agueni and overlying Azougui formations (Fig. 6.5). The Agueni Formation consists mainly of quartz arenites. Coarse-grained sandstone beds, occasionally conglomeratic, show cross-bedding and become more fine-grained upwards. Wave and current ripples at the top of the sandstone beds indicate palaeocurrents towards the ENE (Benan and Deynoux, 1998). The Agueni Formation forms a NNE-SSW oriented escarpment and its stratigraphic thickness is typically 150-200m. It overlies weathered Palaeoproterozoic basement rocks from the Reguibat Shield and starts with a conglomerate filling in topography (Trompette, 1973). The base of the overlying Azougui Formation is characterised by the occurrence of dolomitic sandstones and comprises mudstones, siltstones, sandstones and dolostones (Pitfield et al., 2004). It is sandstone dominated at our sampling locality (Fig. 6.6), but becomes mudstone dominated with dolostone occurrences further to the north

(Pitfield et al., 2004). The body of the formation is formed by massive red mudstones with thin beds of medium grained sandstone. Palaeocurrent directions, indicated by foreset orientations, are N-S-N (Benan and Deynoux, 1998). Dolostones occasionally contain stromatolitic laminae (Pitfield et al., 2004). The Azougui Formation starts on a gently eastward dipping slope above the first escarpment and forms the base of the next escarpment beneath the overlying sediments from the Atar group.

The depositional environment of the Char Group is interpreted by Benan and Deynoux (1998) as shoreline, the sandstones are tide-dominated and the mudstones which are found further to the north are shallow marine. The stromatolitic dolostones may represent supratidal deposits.

Seven samples have been taken from the base of the Agueni Formation for provenance geochemical analyses, spaced ca. 2m apart starting at the bottom, close to the underlying unconformity (no. 13 in Fig. 6.6). The contact with the basement was not exposed at this locality. The samples were taken from a very pure quartz arenite which showed some cross-bedding. Another 5 samples were taken from more fine-grained beds higher up in the section (no. 12 in Fig. 6.6). Observed sedimentary structures include ripple marks, cross bedding and mud cracks. Samples were taken for provenance geochemistry and one sample from the bottom quartz arenite for zircon separation.

Nine samples were taken from the the Azougui Formation at the bottom of the next escarpment, close to the village of Azougui (no. 11 in Fig. 6.6). The exposed rocks display an intercalation of siltstones and dolostones (Photo A.10) overlain by more coarse-grained cross-bedded sandstones grey to light pink in colour of the Foum Chor Formation of the Atar Group. Nine carbonaceous siltstone samples were taken from this unit for provenance geochemistry.

Atar Group

The Atar Group begins with the deposition of the Foum Chor siliciclastic sediments resting unconformably on top of the Char Group. According to Trompette (1994), this slight

angular unconformity represents a period of mountain glaciation, a suggestion that has never been confirmed and is lacking evidence for glacial influence. The base of the Foum Chor Formation is a coarse-grained, locally conglomeratic, cross-bedded sandstone, with beds becoming thinner and more fine-grained higher up in the section. Palaeocurrent directions change from N to NE at the base to SW in the middle of the formation (Benan and Deynoux, 1998). The top of the Foum Chor is a very coarse-grained sandstone with foresets indicating transport again to the east (Pitfield et al., 2004). These sandstone beds form a prominent west-facing scarp, the top of which is gently eastward dipping (Photo A.11a). The rest of the Atar Group consists of several formations comprising dolostones, stromatolitic limestones and shallow-marine lithofacies including shales, argillaceous siltstones and occasionally fine-grained sandstones (Trompette, 1994; Pitfield et al., 2004). The unconformity at the base of the overlying Adrar Supergroup locally erodes down to lower levels of the Atar Group.

The Foum Chor Formation is generally 100-135m thick and the maximum stratigraphic thickness of the entire Group is ∼700m (Pitfield et al., 2004). The age of the Foum Chor Formation is constrained by two minimum, probably diagenetic Rb-Sr ages of 890±37 and 874±23 Ma, obtained from clay minerals present in the overlying Tod Formation (Clauer, 1976). Recent Re-Os ages on organic rich sediments from drill cores indicate the Atar Group is Mesoproterozoic in age (1105±37, 1107±12 and 1109±22 Ma, Rooney et al., 2010).

Three samples were collected from cross-bedded, grey to light pink sandstones at the bottom of the Foum Chor formation, three more samples came from massive 1 – 1.5 m thick bedded quartz arenites at the top of the formation (no. 10 and 9 in Fig. 6.6). These beds are homogeneous, show large scale cross-bedding and are white to grey in colour. All six samples were used for provenance geochemistry analyses and zircons were separation from a sample from the bottom and one from the top of the formation.

Assabet el Hassiane Group

The Assabet el Hassiane Group starts with an erosional contact on top of the Atar Group and comprises marine siliciclastic sediments and carbonates. Most sediments are well-sorted, fine-grained, well-bedded siltstones, shales, fine-grained sandstones and dolomitised limestones. In the Hank region the group has been subdivided by Trompette (1973) into 6 formations, but only 3 formations are recognised in the Adrar (Pitfield et al., 2004): the T-n-Bessais, Taguilalet and the Zreigat formations (Fig. 6.5). Exposure is limited in places due to the highly erosive character of the base of the overlying Adrar Supergroup. The average stratigraphic thickness is 300-400m but varies locally, which has led some workers to suggest various tectonic events such as collisions related to the Pan-African Orogeny during deposition of the second half of the Atar Group and the Assabet el Hassiane Group (Bronner et al., 1980; Moussine-Pouchkine and Bertrand-Sarfati, 1997).

Samples for provenance geochemistry were collected from the Taguilalet and Zreigat formations in two localities. NW of the Atar Cliffs, medium- to fine-grained thinly bedded sandstones and shales were exposed just below the unconformity with the Jbeliat Group of the Adrar Supergroup (no. 8 and 6 in Fig. 6.6). In the Richat structure (Matton et al., 2005), east of Ouadane, partly recrystallised sandstones from both formations were sampled (no. 7 and 5 in Fig. 6.6).

6.3.2 Adrar Supergroup

Jbeliat Group

The Adrar Supergroup starts with glacial deposits of the Jbeliat Group resting unconformably on top of the Hodh Supergroup sediments or sometimes directly on the basement (Fig. 6.5; Trompette, 1973; Deynoux, 1980, 1982, 1985). The following summary of the lithology of the basal Jbeliat Group is largely based on detailed descriptions of Deynoux (1985).

The group consists of three sequences: two tillite-bearing units overlain by the third se-

supergroup	group	formation	samples	analysis	GPS coordinates	#
Adrar	Oujeft	Chinguetti	OUA 1-6	d,g,p	N 20.9289 W 011.5920	1
	Nouatil	Terjit Aguinjob	AMO 1-3	d,g	N 20.5045 W 012.9007	2
	Jbeliat	*dolostone*	JLT 1-19	c	N 20.8153 W 012.5889	3
			ABE 1-19	c	N 20.7305 W 012.6834	4
		diamictite	ABE 20,21	d,g	N 20.7305 W 012.6834	4
			LIAT 2,3,5,6	d,g	N 20.8186 W 012.5860	3
Hodh	Assabet	Zreigat	RICH 23-27	g	N 21.0632 W 011.4146	5
	El		ASS 7,8	d,g	N 20.8430 W 012.5779	6
	Hassiane	Taguilalet	RICH 4, 6-13	g	N 21.1367 W 011.3550	7
			ASS 1-6	g	N 20.8523 W 012.5672	8
	Atar	Foum Chor	FUO 1-3	d,g	N 20.5667 W 013.0775	9
			AZO 10-12	d,g	N 20.5562 W 013.1010	10
	Char	Azougui	AZO 1-9	g	N 20.7213 W 013.0657	11
		Agueni	AGU 8-12	g	N 20.7596 W 013.1338	12
			AGU 1-7	d,g	N 20.7536 W 013.2215	13
Ahmeyim Great Dyke			GTD 1-3	p	N 20.8145 W 014.4863	
			GTD 4-6	p	N 20.8039 W 014.4830	
			GTD-ZR	z	N 20.8045 W 014.4842	
			GTD 7,8	p,b	N 20.7163 W 014.5247	
			GTD 9,10	p	N 20.7155 W 014.5288	

Table 6.1. Description of sampling localities in the Adrar of Mauritania. g = provenance geochemistry, c = chemostratigraphy, d = detrital zircon geochronology, p = palaeomagnetism, z/b = zircon/baddeleyite geochronology. Numbers in the last column correspond to the numbers in Figure 6.6.

quence which contains sand-wedges and barite-bearing dolomite rocks. The basal tillite is only found in the Jbeliat area where the total thickness of the Jbeliat Group reaches 50 m. The second tillite can be found all along a ca. 125km long ridge (Fig. 6.4). Both sequences start with tillite on an erosional unconformity, underlain by striated pavements and succeeded by reworked glacial deposits such as conglomerates, cross-bedded sandstones and fine-grained sandstones with dropstones. The tillites can contain pebbles and boulders of variable sizes up to 0.8 m in diameter. Clasts make up ca. 10% of the total unit and are embedded in a micro-conglomeratic matrix. Microscopic observations of the matrix show detrital grains scattered in an argillaceous mixture. Grains are both rounded and angular and are of various composition, mostly quartz, feldspars and rock fragments but no carbonate grains. Well rounded quartz grains of millimetre scale are interpreted as aeolian (Trompette, 1973; Deynoux, 1985). The presence of both fresh and weathered feldspars indicates a mixed detritic origin. Well rounded quartz grains sometimes show embayments and splitting, which is explained as the result of syn-depositional glacial shearing.

Clasts lithologies are dominated by carbonates, dolostones, sandstones and basement

rocks, all reflecting bedrock lithologies of the Atar, Char and basement stratigraphic units. However, there is no clear relationship between the lithology of the clasts and that of the underlying strata, suggesting long glacial transport. Transport directions are indicated by pavement striations from N – NW in the Jbeliat area. Only a small (3 – 5%) portion of clasts are striated.

These two sequences are covered by the third sequence which begins with polygonal structures and sand wedges related to permafrost. These are followed by a thin but continuous dolomitised limestone of 3 – 5m thick, occasionally comprising sandy intercalations and are overlain by a persistent horizon of purple limestone. The dolostone is either well bedded (with well developed ripple mark structures) or is disrupted, brecciated and folded. Barite is found in the brecciated facies where it is crystallised in cracks and cavities. Purple limestones are overlying the dolostone with a sharp contact, are 30 – 50cm thick and mark the transition to bedded cherts and siltstones of the overlying Téniagouri Group.

The age of the Jbeliat Group is not well defined but is constrained by the Mesoproterozoic Re-Os ages for the Atar Group providing a maximum age for the entire Adrar Supergroup. Three zircon ages for volcanic tuffs of the Téniagouri Group provide a minimum age for the Jbeliat Group of 610±5 and 604±6 Ma from south Mauritania (Lahondère et al., 2005) and 625±8 Ma from north Mauritania (Frischbutter et al., 2009).

Samples have been collected from the Jbeliat Group at two localities along a ∼30m high ridge, close to the Jbeliat village (Fig. 6.6). The tillites were sampled at three different levels along a section at the LIAT locality for detrital zircon analysis (no 3 in Fig. 6.6, illustrated at Photo A.11b). The base consisted of medium to coarse-grained, pale green coloured massive sandstone (LIAT 2). The middle part contained clast rich, coarse-grained channel fill lenses (LIAT 5). Clasts were generally well rounded and had sizes up to 25cm (Photo A.12a). Towards the top, medium to fine-grained, cross-bedded red sandstones were found and sampled (LIAT 6, Photo A.12b). This section corresponds well with the section described by Deynoux (1985, cross-section A, Fig. 5). The massive green coloured sandstone at the bottom corresponds to Deynoux (1985)'s formation 'F IV' (glauconitic sandstones), the channel fill deposits with 'F V' (tillites and conglomeratic sandstones) and the red sandstones with 'F VI' ("Oued Jbeliad-Est" sandstones). This means that LIAT 2

is part of the first Jbeliat sequence while LIAT 5 and 6 are both part of sequence two. Resting on top of these two sequences are dolostones which are sampled and labelled JLT: starting with planar bedded, barite baring pink coloured dolostone unit of ∼3m thick (Photo A.13a), becoming grey and purple carbonates (Photo A.13b) and gradually more clastic material is introduced. On the surface wave ripples and dessication cracks can be observed. Cherts are found on the very top of the hill.

The ABE section (no. 4 in Fig. 6.6) is located to the south-west of the LIAT/JLT locality in the cliff section of the same ridge. At the base of this section, grey to purple/red shales contain thin intercalations of fine-grained sandstone. These are overlain by 2 – 3m of conglomerate (Photo A.14a), followed by fine-grained sandstone (Photo A.14b) which coarsens upwards before being truncated by a sharp contact beneath overlying dolomitic limestones. Clasts in the conglomerate are varying in size (up to 20cm) and lithology. They contain small pebbles of well rounded quartz, basement granite and schist but the majority is made up by (stromatolitic) carbonate clasts. These carbonate clasts are generally quite angular indicating they have undergone less transport than most of the other clasts. Four samples were collected: two from the conglomerate (ABE 20) and two from the overlying fine-grained sandstone (ABE 21). This sequence is interpreted as the second Jbeliat sequence (Formations 'F V' and 'F VI' of Deynoux, 1985) covered by the dolostones of the third sequence.

The dolostone starts with a pink, thinly bedded carbonate which shows ripple marks and cross-bedding (Photos A.15 and A.16) indicating E-W flow directions. The ripple marks become larger as the beds become thicker and the colour changes to grey higher up in the section. The dolostone sequence three has been sampled for chemostratigraphic analyses (ABE 1-19).

Téniagouri Group

The dolostone is overlain by bedded cherts and green shales of the Téniagouri Group. The lower unit of the group is 200-300m thick and consists of cherts, siliceous shales with occasional limestone beds and volcanic ash occurrences associated with post-glacial eustatic

transgression (Trompette, 1973; Bertrand-Sarfati et al., 1997; Flicoteaux and Trompette, 1998; Lahondère et al., 2003). The green shales gradually make way for the upper unit which comprises sandy tidal deposits and aeolian sandstones (Deynoux, 1980). Zircons extracted from tuff found within the Téniagouri Group in the Hank region yielded a U-Pb age of 625±8 Ma (Frischbutter et al., 2009). A Rb-Sr age of 595±45 Ma on shales from the Téniagouri Group is within error of this zircon age (Clauer, 1976). The Téniagouri Group is unconformably overlain by the transgressive Nouatil Group.

Nouatil Group

The Nouatil Group (200 – 300m thick) consists predominantly of siliciclastic formations which include siltstones, sandstones and conglomerates with variable grain sizes and occasionally calcareous cement (Trompette, 1973; Pitfield et al., 2004; Álvaro et al., 2007). The only exception is the Amogjar Formation: a stromatolite bearing well-bedded dolostone of 8 – 20m thick. The Nouatil Group rests unconformably upon underlying sediments or directly on basement rocks (Pitfield et al., 2004).

Three samples have been collected from the Terjit Aguinjob Formation at the base of the Nouatil Group (no. 2 in Fig. 6.6). They are derived from red-grey banded argillitic, coarse-grained siltstones ∼5m below the base of the Amogjar dolostone beds.

Oujeft Group

The Nouatil Group is conformably overlain by cross-bedded sandstones of the Oujeft Group (Trompette, 1973; Pitfield et al., 2004). The basal Chinguetti Formation, consists of thick, grey and pink coloured sandstone beds which form the top of the Atar Cliffs, a prominent escarpment in the Adrar region (Photo A.17a; Álvaro et al., 2007). The light grey to pink coloured beds show channel cross-bedding on the scale of tens of centimetres to several meters (Photo A.17b). Cross-bedded, feldspathic sandstones dominate the rest of the group. Geochronological constraints are obtained from the top of the Oued Touerga Formation with the occurrence of Scolithes traces, a Cambrian trace fossil usually associated

with high-energy environments (Desjardins et al., 2010). Brachiopod species indicating a late Cambrian to early Ordovician age are reported towards the top of the Oujeft Group (Legrand, 1969).

Six samples were collected from coarse/medium-grained arenitic sandstones near the village of Ouadane (no. 1 in Fig. 6.6). Palaeomagnetic samples were obtained from five of these samples which were oriented in the field and cored at the University of Edinburgh resulting in five sites and a total of 31 palaeomagnetic samples. One sample was collected for detrital zircon analysis. Provenance geochemistry analyses were performed on five samples.

6.3.3 Ahmeyim Great Dyke

The 1.5 km wide and > 100 km long Ahmeyim Great Dyke is exposed in Western Sahara and Mauritania and is cross-cutting Archaean basement rocks of the Reguibat Shield (Fig. 6.7). This gabbroic dyke is sampled at two localities where a total of 10 sites were collected for palaeomagnetism as well as two samples for radiometric dating. At the northern locality, a small, mafic dyke was found cross-cutting the Great Dyke. This smaller dyke contains olivine phenocrysts of up to 2cm diameter (Photo A.18b) and may belong to the NE trending 1.9 Ga mafic dyke swarm (described in Section 6.2.1). Close to the eastern margin of the Great Dyke light coloured xenolithic blocks were incorporated in the gabbro (Photo A.19a) and a sample was taken for zircon separation (GTD-ZR). At the northern locality palaeomagnetic sites GTD 1-3 were collected on the western side and GTD 4-6 on the eastern side of the Great Dyke. At the southern locality sites GTD 7,8 were collected of the eastern side and GTD 9,10 on the western side of the dyke. A sample for baddeleyite separation was taken from relatively coarse-grained gabbroic material at site GTD 8.

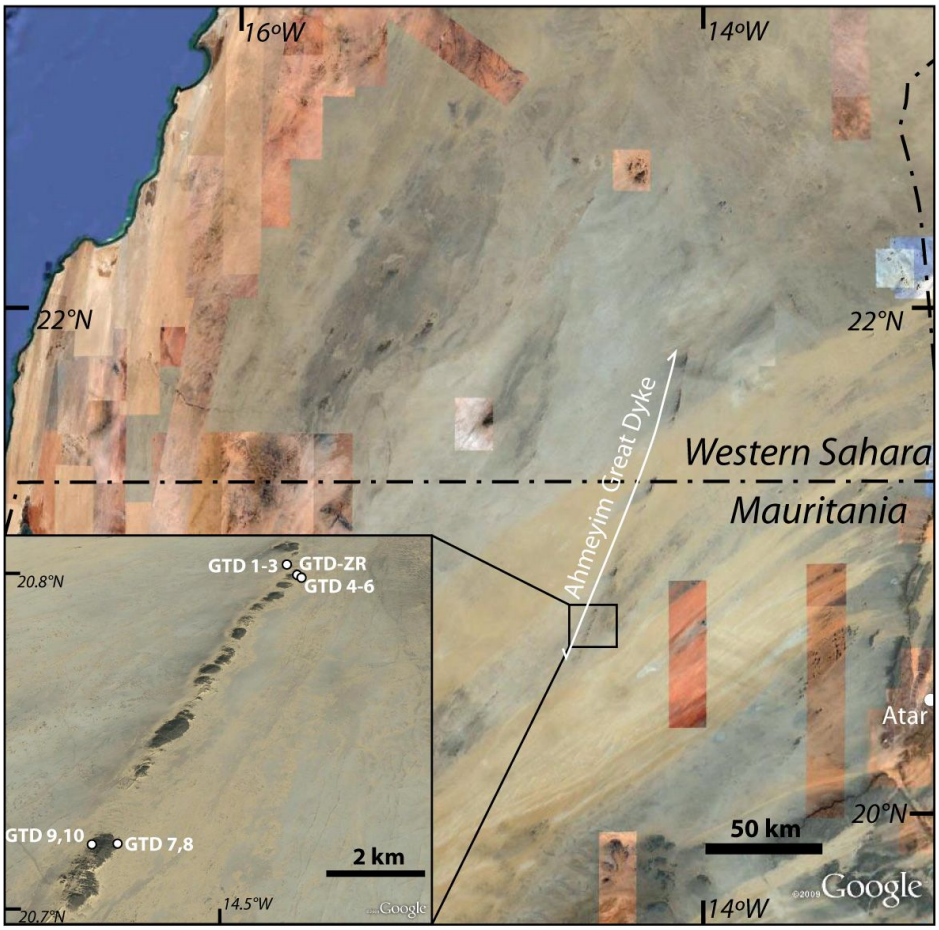

Figure 6.7. Google satellite image of the Ahmeyim Great Dyke.

6.4 Results

6.4.1 Detrital Zircon Dating

A minimum of 60 zircon grains were selected for analyses from 8 stratigraphic levels and the concordia diagrams of all successful analyses are shown in Figure 6.8. For the probability density plots in Figure 6.9 only those analyses that were within 10% of concordance are displayed resulting in a total number of concordant grains per unit between 25 (for sample AMO) and 108 (for sample FOU). The formations are characterised by the presence and absence of age peaks in the probability density plots which will now be described in detail. A number CL images are selected to represent each stratigraphic unit and are presented in

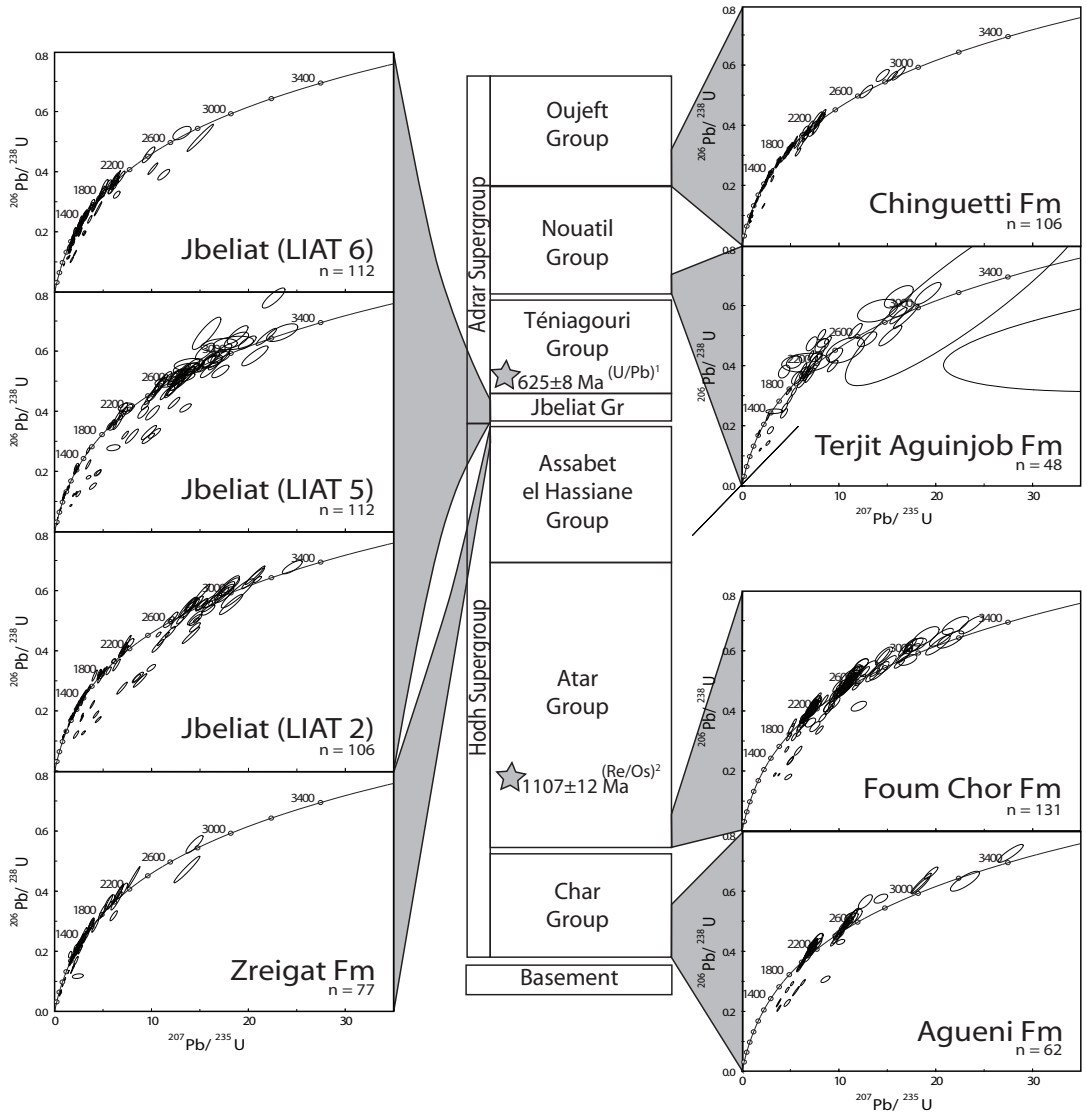

Figure 6.8. A simplified stratigraphic column with zircon concordia diagrams for 8 stratigraphic levels. n = total number of successful analyses. Grey stars are the most reliable age constraints for the stratigraphy, [1]Frischbutter et al. (2009), [2]Rooney et al. (2010).

Appendix S2.

Age groupings and trends

The two oldest samples (from the Char and Atar groups) show a remarkable similarity in their detrital zircon age spectra with two dominant Palaeoproterozoic peaks at ∼2474-70 and 2096-87 Ma and a minor contribution from Archaean grains (Fig. 6.9). Detrital zircon grains extracted from the cross-bedded sandstones of the Foum Chor Formation (sample FOU) show a minor peak at 2892 Ma which correlates with two grains from the Agueni Formation (sample AGU). The youngest grain for the Char and the Atar groups are 2052±20 and 1804±33 Ma respectively

All but one grain from the top of the Assabet el Hassiane Group (sample ASS, Zreigat Formation) are Proterozoic in age with a dominance of Mesoproterozoic ages. The largest group ranges from 1550 – 952±38 Ma (= youngest grain in sample) but has a clear peak around 1252 Ma. The profile shows 12 Palaeoproterozoic grains with two peaks at 1805 and 1980 Ma and one Archaean grain of 2725±41 Ma.

The profile of the first Jbeliat Group sample (LIAT 2) is significantly different from that of the underlying Assabet el Hassiane Group showing a much larger spread of ages. Ages range from 3257±33 to 667±9 Ma and fall in four main groups: Archaean grains show peaks at 3079, 2915, 2714 and 2585 Ma, two broad Palaeoproterozoic peaks at 2109 and 1853 Ma, a wide range of Mesoproterozoic ages with the largest peak at 1250 Ma and a narrow Neoproterozoic peak 689 Ma. A large gap of ∼400 Ma exists between Archaean and Palaeoproterozoic grains (2576 – 2148 Ma) and another gap of ∼200 Ma (966 – 768 Ma) separates the Neoproterozoic grains. The next sample above, obtained from the Jbeliat channel fill deposit (LIAT 5) shows a similar range in ages (3223±67 – 671±30 Ma) but grains are more clustered around a few prominent groupings. Archaean and early Palaeoproterozoic grains group around 2898, 2687 and 2470 Ma. This last peak is especially remarkable since it is completely absent in LIAT 2 and the 2585 peak of LIAT 2 is not present here. A few grains group around 2034 and the two youngest peaks are at 1197 and 695 Ma. This 1197 peak however is much smaller (only 4 grains) than the

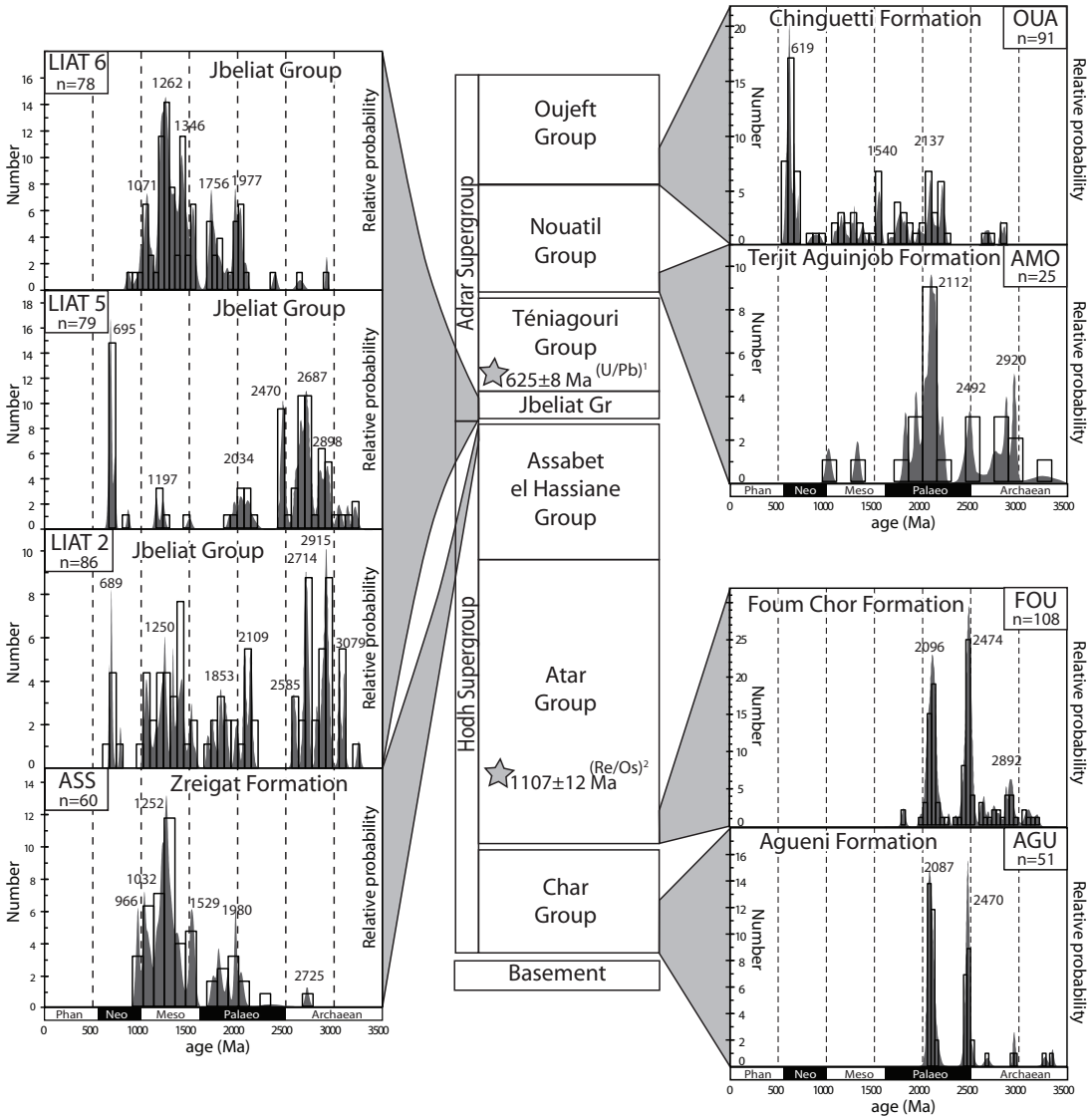

Figure 6.9. A simplified stratigraphic column with zircon probability density plots for 8 stratigraphic levels. For the timescale at the bottom: Palaeo, Palaeoproterozoic; Meso, Mesoproterozoic; Neo, Neoproterozoic; Phan, Phanerozoic. n = number of grains with a concordance between 90 and 110%. Grey stars are the most reliable age constraints for the stratigraphy, [1]Frischbutter et al. (2009), [2]Rooney et al. (2010).

Mesoproterozoic populations in the two samples below. LIAT 5 is marked by the absence rather than the presence of Mesoproterozoic grains. The stratigraphically highest Jbeliat sample (LIAT 6), obtained from just below the dolostone, shows more similarity with the Assabet el Hassiane Group sample (ASS): two broad Proterozoic groupings with peaks at 1977, 1756, 1346, 1262 and 1071 Ma. The absence of the 690 Ma peak observe in samples LIAT 2 and 5 is also significant. The consequences of these large changes in provenance are discussed in Section 6.5.

Many detrital zircons from the overlying Nouatil Group (sample AMO) were discordant (Fig. 6.8 but the concordant data show a return to the patterns observed in the lower part of the section. Especially two peaks at 2492 and 2112 Ma correlate well with the prominent peaks of the Atar and Char Group samples. Interestingly, in contrast to rocks older (Jbeliat) and younger (Oujeft), there are no grains younger than 1.0 Ga and only two grains younger than 1.8 Ga. It must be said however that the total number of concordant analyses is fairly low and it is possible that younger populations have been missed because of this.

Finally, the sample from the Oujeft Group (OUA, Chinguetti Formation) shows a shift to younger populations with an exceptionally dominant peak at 619 Ma. Minor peaks occur at 2137 and 1540, Archaean grains are almost absent in contrast to all older units. The youngest grain is 559±24 Ma and gives a maximum depositional age for the Chinguetti Formation (Oujeft Group) which is in good agreement with faunal evidence for an early Cambrian age.

Source regions

Archaean and Palaeoproterozoic rocks form significant parts of the exposed West African craton (Fig. 6.1) and represent likely sources for the majority of the detrital zircons present in the samples that are older than 2000 Ma (Fig. 6.9). Many samples include age peaks around 2900, 2700, 2470 and 2050 Ma all of which are strongly correlated with basement ages from the West African Reguibat Shield (eg, Auvray et al., 1992; Potrel et al., 1996, 1998; Deynoux et al., 2006; Schofield et al., 2006; Key et al., 2008). The western Ar-

chaean domain underwent granulite-facies metamorphism leading to the development of new gneissic fabrics with emplacement of anatectic granites, for example the 2891±1.5 Ma Bir Igueni Granite (Potrel et al., 1996, 1998; Key et al., 2008). Post-tectonic granitic magmatism is dated at 2726±7 Ma (Potrel et al., 1998). This basement has been exposed for a period of time considering that many Neoproterozoic sedimentary units directly overly cratonic basement (Pitfield et al., 2004).

A detrital age population of 2470 Ma is common throughout most samples. Zircon ages around 2450 Ma are generally rare (Dalziel, 1997; Condie et al., 2009a) as this period is often seen as one of magmatic quiescence and are often absent in detrital studies (eg, Johnson and Oliver, 2004; Condie et al., 2009b). Despite this, examples of early Palaeoproterozoic rock formation and magmatic activity do exist in the Mauritanides thrust belt as shown by U-Pb hydrothermal monazite ages in the northern Mauritanides (Meyer et al., 2006; Kolb et al., 2006). There are numerous mafic amphibolites which yield ^{40}Ar-^{39}Ar plateau ages on amphibole around 2420 Ma (Dallmeyer and Lecorche, 1990) from crystalline klippen from the northern Mauritanides. The exact timing and tectonics of this section of crust joining the West African Craton is not clear although this crustal segment had accreted before deposition of the Char Group at 1100 Ma (Rooney et al., 2010). This area, now located under, and caught up within, the Mauritanides must have been a major erosional source of sediments into the Taoudéni Basin. Ages around 2050 Ma represent magmatic activity associated with the Eburnian Orogeny which is widespread in the West African Craton and recorded in the Reguibat Shield (Schofield et al., 2006).

The West African Craton did not undergo any further major tectonothermal events between Eburnian stabilisation at ∼2000 Ma and the Pan-African Orogeny ∼660 Ma, and no rocks from the craton are known from the period ∼1700-1000 Ma (Ennih and Liegeois, 2008). Nevertheless zircons of this age range are well represented in our samples with groupings around 1550, 1250 and 1050 Ma. Palaeogeographic reconstructions of the peri-Gondwanan Avalonian and Cadomian terranes are often based on the relative abundance of Mesoproterozoic detrital zircon grains in Neoproterozoic and Cambrian deposits (e.g. Nance and Murphy, 1994). The absence of these grains is generally seen as a strong indication for a peri-West African genesis. The presence of many 1500 – 1000 Ma zircons in

our field area in the northern Taoudéni Basin has obviously large consequences for these models which will be discussed in Section 6.5.

	West Africa		External
population (Ma)	Reguibat	Mauritanides	
690	–	✓	–
1050	–	–	✓
1250	–	–	✓
1550	–	–	✓
2000	✓	–	–
2100	✓	–	–
2470	–	✓	–
2700	✓	–	–
2900	✓	–	–

Table 6.2. Age populations that occur prominently in more than one sample and their potential sources. The location of the Reguibat Shield and the Mauritanides Belt are indicated in Figure 6.1, the external sources are discussed in Section 6.5.

Zircons in the age range 700 – 550 Ma occur in the Jbeliat and in the Chinguetti formations and were possibly derived from Pan-African orogens which underlie vast areas east of the Trans-Saharan suture zone and the Mauritanides belt to the west of the Taoudéni Basin. Apart from reworked older basement, these Pan-African orogens contains juvenile calc-alkaline magmatic arcs of various ages (eg, Deynoux et al., 2006; Penaye et al., 2006; Tchameni et al., 2006; Küster et al., 2008). One possible source for the youngest zircons in the detrital populations is the Bou Naga granitic and rhyolitic ring complex, northern Mauritanides, dated at 676±8 and 687±5 Ma (Blanc et al., 1992).

6.4.2 Provenance Geochemistry

The following diagrams are aimed at identifying trends and/or strong deviations from average crustal and shale compositions. The complete geochemical composition of all samples is given in Appendix S4.2.

The level of element mobility and chemical weathering is investigated to test the suitability of these rocks for provenance characterisation. Major elements are used to calculate the chemical index of alteration (CIA) which is an index of oxide mobility (Fig. 6.10). The

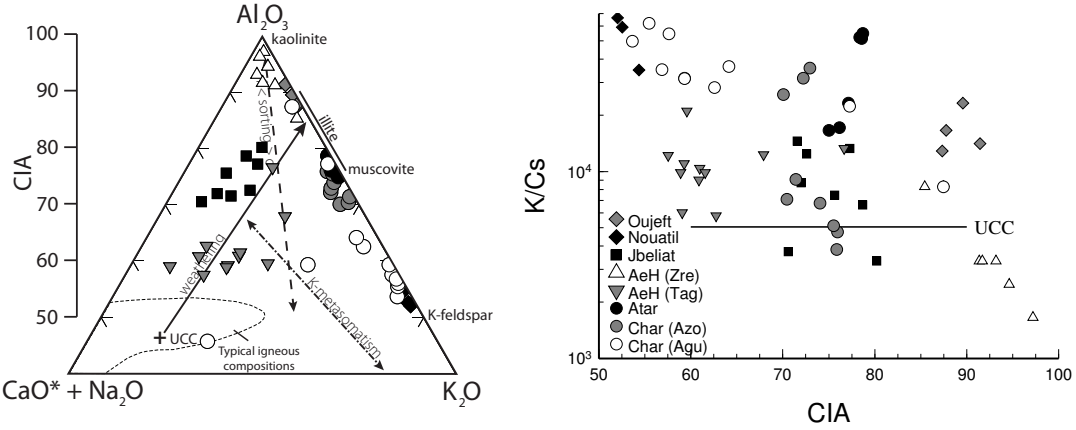

(a) A-CN-K diagram showing major oxides in molecular ratios. Note that only Al_2O_3 >40 is shown. Arrows are redrawn from Bahlburg and Dobrzinski (2011).

(b) CIA vs. K/Cs after McLennan et al. (1990). The upper continental crust has a K/Cs ratio of about 5050 (McLennan, 2001).

Figure 6.10. Major element geochemistry plots to indicate the level of chemical weathering and element mobility. The legend to the symbols in both diagrams is shown in **(b)**. Individual Group (Formation) names are in stratigraphic order, see Figure 6.5 for full details. Abbreviations: Agu, Agueni Formation; Azo, Azougui Formation; AeH, Assabet el Hassiane; Tag, Taguilalet Formation; Zre, Zreigat Formation.

Char and Atar groups plot very high on the weathering trend and show various degrees of K-enrichment which is a common diagenetic effect in sediments (Condie and Wronkiewicz, 1990). Medium CIA levels (∼60) are indicated for the Taguilalet Formation of the Assabet el Hassiane Group while high chemical weathering is shown in the Zreigat Formation (>85, Fig. 6.10a). The Jbeliat Group plots along the crustal weathering trend and has average CIA values, comparable to that of the post Archaean average shale (PAAS, CIA = 70). The Nouatil Group shows a surprisingly low CIA of around 53, probably reflecting a high K-feldspar content. The sandstones from the Oujeft Group plot high up the weathering trend which is not surprising considering the weathered appearance of the coarse-grained sandstones. A slight trend can be observed in Figure 6.10b from low CIA and high K/Cs ratio for Char and Nouatil Group samples to high CIA and low K/Cs for the Zreigat Formation of the Assabet el Hassiane Group. This means that both the Oujeft Group and the Zreigat Formation samples are not very reliable provenance indicators.

Minor and trace element ratios are used in Figure 6.11 to identify compositional trends. The figure shows a very rhyolitic signature for the majority of formations and no clear trend can be observed. The only outliers are a few samples from the Char Group which

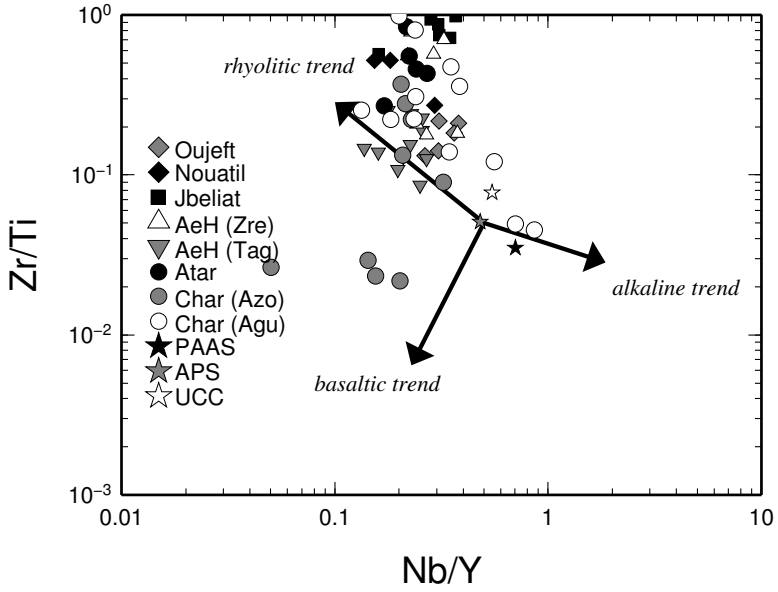

Figure 6.11. Composition trends for sedimentary rocks after Winchester and Floyd (1977). Legend is explained in Figure 6.10 and: PAAS, post Archaean average shale after Taylor and McLennan (1985); APS, average Proterozoic shale after Condie (1993); UCC, average upper continental crust after McLennan (2001).

plot on the alkaline and basaltic side of the average upper continental crust composition. Four samples from the Azougui Formation (Char – Azo) are worth noting for their low SiO_2 concentration (around 12%) and depletion in Hf and Zr (Fig. 6.11, Appendix S4.2). These samples are not very suitable provenance indicators and interpretation should be done with care.

Rare earth elements (REE) are useful provenance indicators because their insolubility means they can withstand weathering and diagenesis relatively well. The REE are averaged for each group in Figure 6.12 and most show a very PAAS-like pattern: light REE (LREE) enrichment, a pronounced Eu anomaly and a relatively flat heavy REE (HREE) pattern. Most units are relatively rich in SiO_2 (i.e. well above the PAAS value of 63%) which causes overall depletion of REE with respect to PAAS. The Agueni Formation (Char – Agu) is most depleted in HREE compared to all other formations (LA/Yb of 21.7 compared to 9.5 for PAAS). The Taguilalet Formation (AeH – Tag) and the Nouatil Group are noted for their LREE depletion especially La.

The plot in Figure 6.13 is used to detect the presence of (ultra)mafic source components.

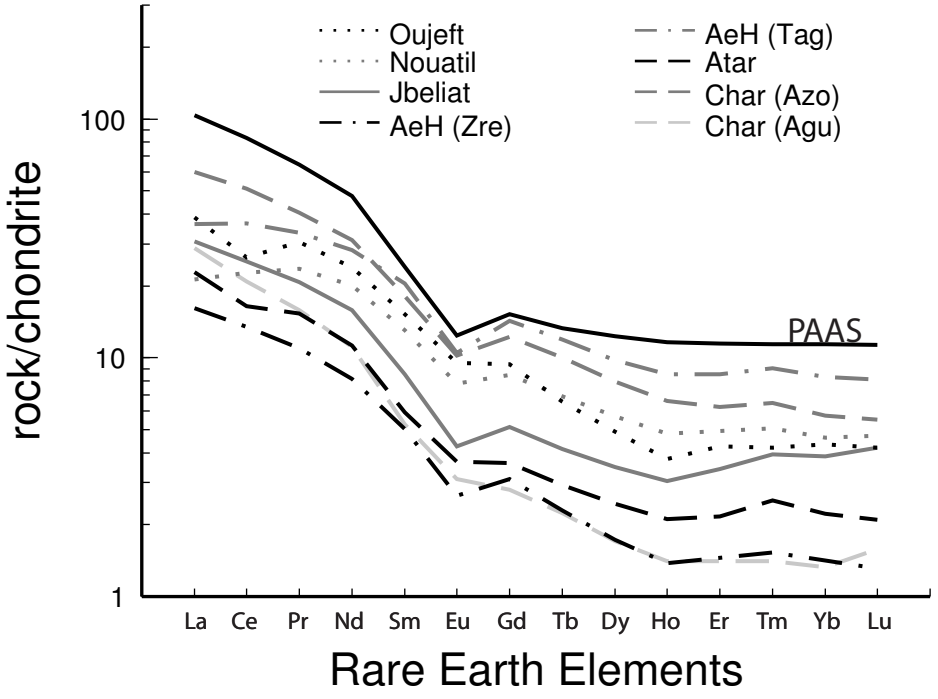

Figure 6.12. REE patterns, chondrite normalised (Taylor and McLennan, 1985), showing averages per rock unit. The black solid line is the composition of PAAS (McLennan, 1989).

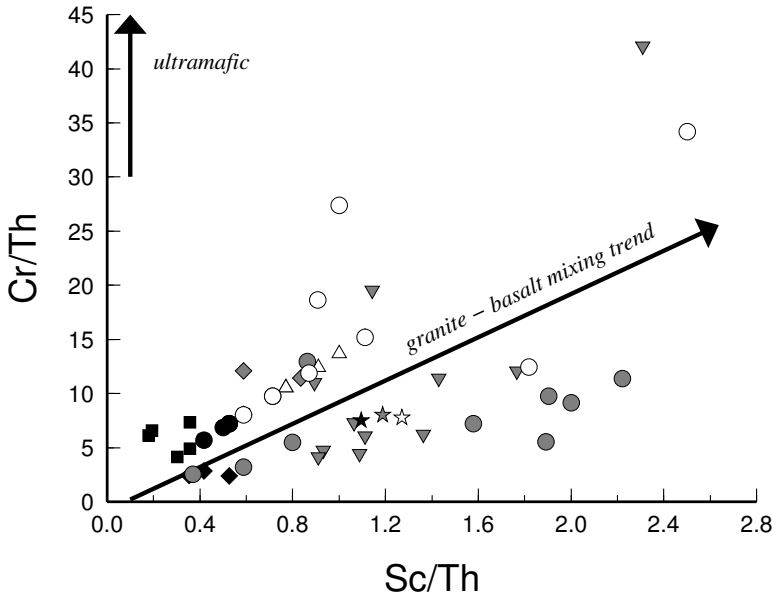

Figure 6.13. Compositional trend diagram to identify the presence of (ultra)mafic source components. Legend is explained in Figure 6.10.

Ultramafic rocks are extremely enriched in Cr, slightly enriched in Sc but are generally depleted in Th. The trend line in the figure is based on the average composition of granite and basalt who's ratios make them plot at 0.1,0.2 and 50,500 respectively, while ultramafic komatiite has a Cr/Th ratio of $>1*10^4$ (Condie and Wronkiewicz, 1990). Two samples from the Zreigat Formation (AeH – Zre) are very enriched in Cr and plot outside the figure with Cr/Th ratios of 86 and 73. This points to a slightly mafic, probably local, source because samples from nearby outcrops do not show this Cr enrichment. All other samples plot close to a granite-basalt mixing trend, mostly around or below UCC and PAAS composition, pointing to the absence of (ultra)mafic material.

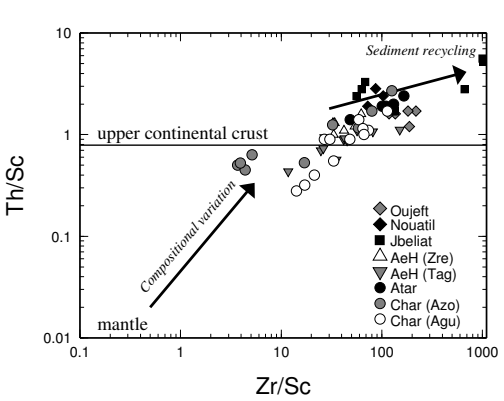

(a) Zr/Sc vs. Th/Sc after McLennan et al. (1990).

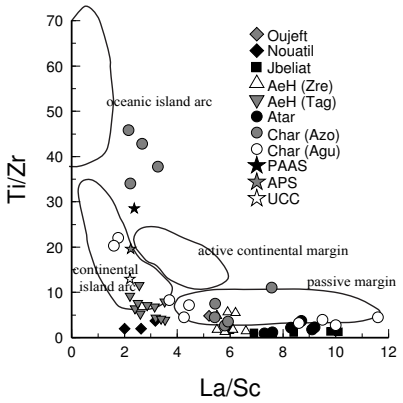

(b) La/Sc vs. Ti/Zr after Bhatia and Crook (1986).

Figure 6.14. Compositional trends and the influence of recycling. Legend is explained in Figure 6.10.

On a plot of Zr/Sc versus Th/Sc (Fig. 6.14a) both variations in composition between mantle and upper crust, and sediment recycling through zircon enrichment can be identified. High levels of enrichment/recycling are shown for the Atar, the Nouatil and the Oujeft groups. Some samples of the Char Group indicate influence from more fractionated sources and so do some of the Taguilalet Formation samples, indicating a mixture of diverse sources. Three samples of the Jbeliat Group are extremely enriched in Zr. Zr depletion makes four Char (Azo) samples plot far away from all others but these four samples were already classified as outliers in Figure 6.11. Their position in both Figure 6.14a and 6.14b is not taken to be representative for the Char Group. Figure 6.14b is aimed at identifying upper crust influence which is reflected in a high La concentration (as well as all other LREE). A passive margin setting is indicated for the majority of samples from the Char,

Atar, the Zreigat Formation (upper Assabet el Hassiane), Jbeliat and Oujeft groups. Clearly different from these are samples from the Taguilalet Formation and the Nouatil Group. They are relatively high in Sc and low in La pointing to the presence of less fractionated sources. They plot closest to the continental arc field.

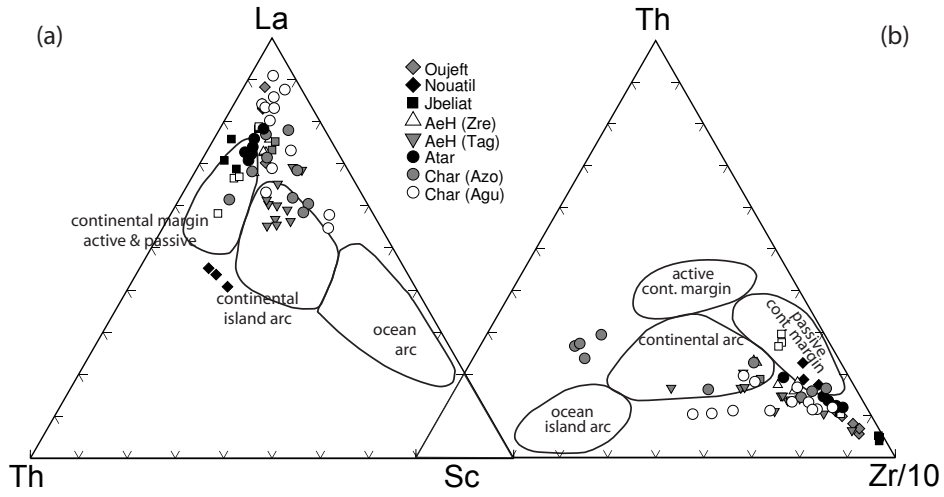

Figure 6.15. Discrimination diagrams to determine the tectonic setting of the depo centre. All diagrams and fields are after Bhatia and Crook (1986). Legend is explained in Figure 6.10.

A continental passive margin is also demonstrated by the ternary plots in Figure 6.15. Again the Taguilalet Formation plots in a continental arc field. The Char Group shows a mixture of sources even when ignoring the four outliers in Figure 6.15b. The Nouatil Group samples are depleted in La (Fig. 6.15a) but plot in a passive margin field in Figure 6.15b.

No clear stratigraphic trend can be extracted from these diagrams and it seems that the geochemical characterisation is dominated by lithological variations. Many of the analysed samples are sandstones with high silica content and the diagrams indicate a passive margin setting for these units. Samples from the Char Group and Taguilalet Formation show a mixture of sources (Fig. 6.13 and 6.14). Both the Taguilalet Formation and the Nouatil Group are notably depleted in LREE, especially La. Analysis of the Jbeliat Group indicates the diamictite is dominated by consistent, (highly) recycled material but has seen little chemical alteration which is expected for sub-glacial deposits.

6.4.3 Stable Isotopes

Stable carbon isotope ratios in carbonate sedimentary rocks are considered a reliable proxy for the isotopic composition of ancient seawater. Carbon isotopes are relatively insensitive to diagenesis e.g. when compared to oxygen isotopes owing to the relatively low carbonate concentrations in diagenetic fluids (Banner and Hanson, 1990, see Chapter 4). Variations in the stable isotopes ^{12}C and ^{13}C are expressed as $\delta^{13}C$ while oxygen isotopes ^{16}O and ^{18}O are expressed as $\delta^{18}O$. Both isotope ratios are plot in Figure 6.16 for rocks from the Adrar region. A considerable proportion of the samples plots in the lithification trend which could mean that these oxygen isotope values are primary. However, in such a case oxygen and carbon isotope ratios are expected to vary in a covariant way and a lack of correlation for the majority of data suggests they are not acquired simultaneously and that the $\delta^{18}O$ signal has a diagenetic origin. Profiles of $\delta^{13}C$ are commonly used for chemostratigraphic correlations of Neoproterozoic sedimentary sequences, especially because a lack of radiometric ages for Precambrian rocks impedes establishing more reliable correlation schemes (Halverson et al., 2005).

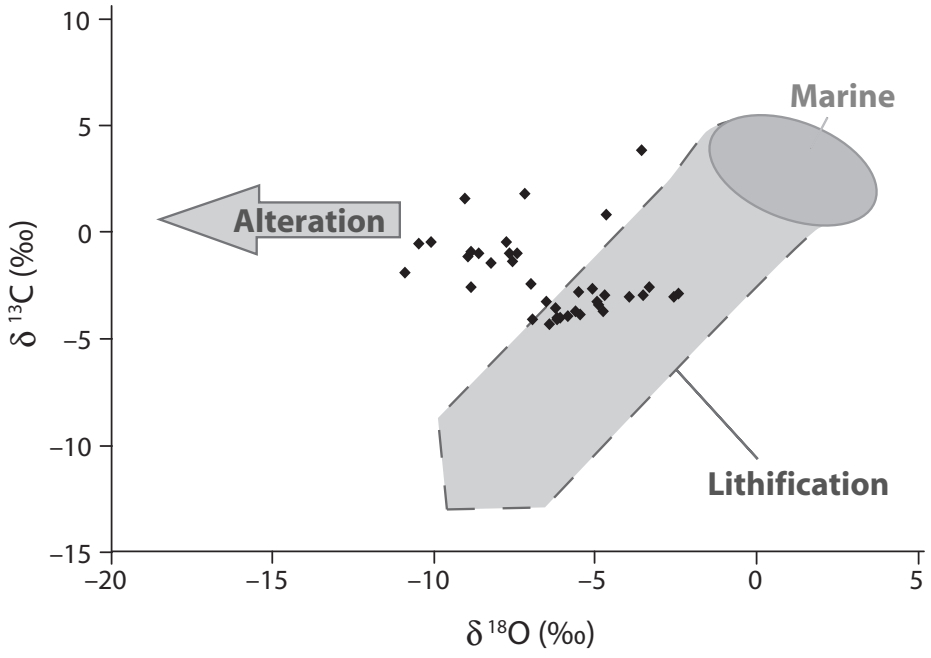

Figure 6.16. Stable isotopes of carbon versus oxygen for two sampling localities in the Adrar region (Knauth and Kennedy, 2009, after). Isotope data are listed in Appendix S3.2.

In the Adrar Sub-Basin $\delta^{13}C$ values are obtained from the carbonates on top of the Jbe-

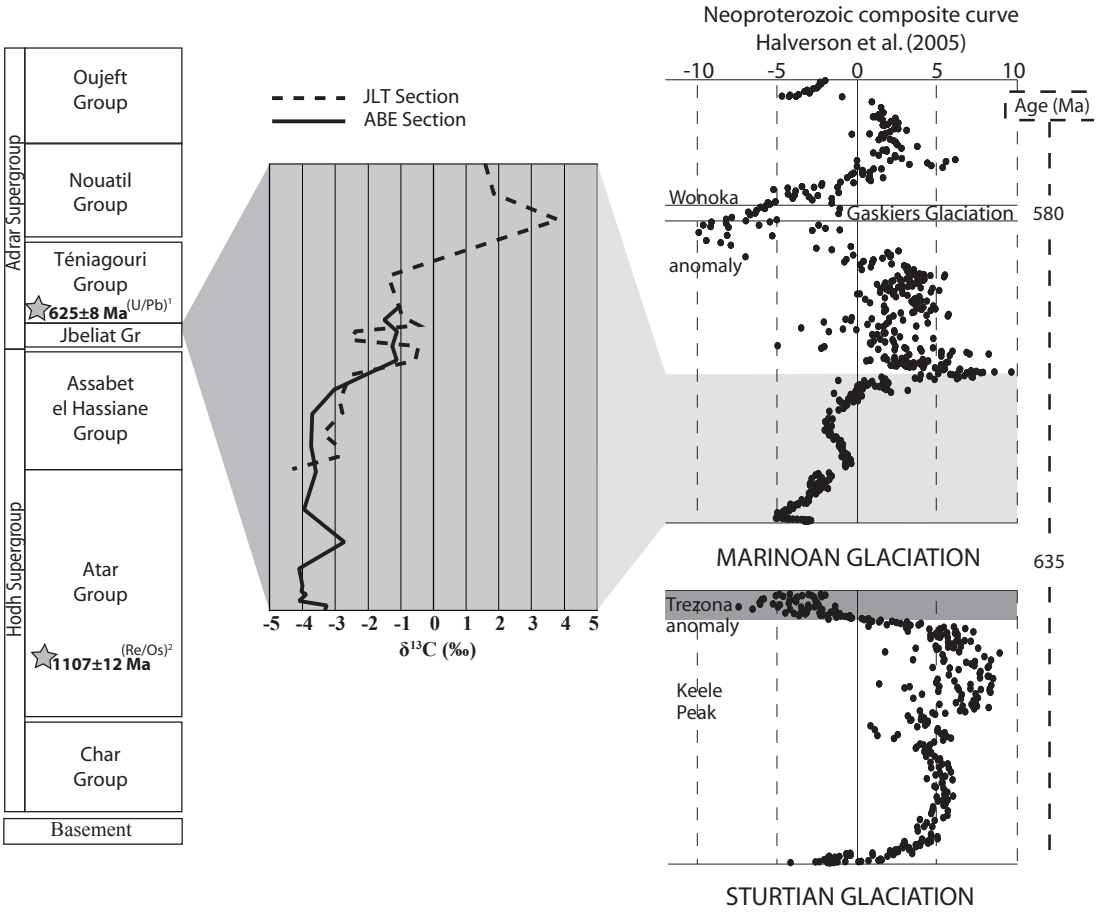

Figure 6.17. δ^{13}C(‰) variation diagram for the dolostone above the Jbeliat diamictite. Isotope data are listed in Appendix S3.2. Grey stars are ages: [1]Frischbutter et al. (2009), [2]Rooney et al. (2010).

liat Group tillites in two locations: the JLT and the ABE localities (nos. 3 and 4 in Fig. 6.6). Stratigraphic variation of δ^{13}C is displayed in Figure 6.17. The two sequences are correlated based on the δ^{13}C isotope profiles and recording starts with the first carbonate appearance in both sections. Since field observations identified continuous sedimentation in both localities it is suggested that carbonate deposition in this area was slightly diachronous. The combined curve is the longest continuous profile obtained from the Adrar region, previous chemostratigraphic studies of the Jbeliat sequence lacked either a clear negative onset (Álvaro et al., 2007) or a full recovery to positive values (Shields et al., 2007b). These 'incomplete' profiles are either illustrating the diachronous character of the carbonates or indicate significant nonconformities within this part of the stratigraphy.

Underlying carbonate units from the Atar Group exhibit different δ^{13}C values (Shields et al., 2007b) that lie entirely outside the range from the cap dolostones. There is a return to more positive values in the groups overlying the Jbeliat Group (which have very limited carbonate components). A thin, mostly silicified stromatolitic dolostone bed (Amogjar Formation) within the lower part of the Nouatil Group yielded $\delta^{13}C = 0.3‰$ (Shields et al., 2007b).

The start of the profile shows constant negative values, balancing around -3.8‰, before gradually recovering to positive values. This negative to positive trend is consistent with the upper part of the globally extensive Marinoan cap carbonate sequences and allows us to correlate the Jbeliat Group with glacial deposits from other cratons worldwide occurring at the end of the Cryogenic Era (Halverson et al., 2005). Even though the rise in δ^{13}C seems to happen slowly and smoothly, it is fairly rapid when compared to other post-Marinoan carbonate sections like the Maieberg cap-carbonate sequence in Namibia where negative values are recorded for at least 400m of carbonate stratigraphy (Hoffman and Schrag, 2002). These rocks however are recoding marine passive margin deposits whereas the Jbeliat records continental glacial deposits. It is likely that sedimentation was not continuous during deposition of the overlying limestone/chert/shale units. The correlation of this isotope stratigraphy with world-wide sequences along with the zircon data helps to put these Mauritanian glacial rocks into a global context and date them more precisely. This will be discussed in Section 6.5 below.

6.4.4 Age of the Ahmeyim Great Dyke

Zircon dating

A felsic xenolith from the eastern margin of the Great Dyke was sampled (GTD-ZR) to investigate the presence of inherited zircon grains and growth rims recording dyke emplacement. The rock yielded many crystal fragments varying in size from 10 to 100 μm but most were <50 μm (Fig. 6.18). Cathodoluminescence (CL) imaging revealed complex zoning and identified magmatic grains, magmatic grains with (metamorphic) overgrowths, grains where part of the original zoning was destroyed and replaced with complex meta-

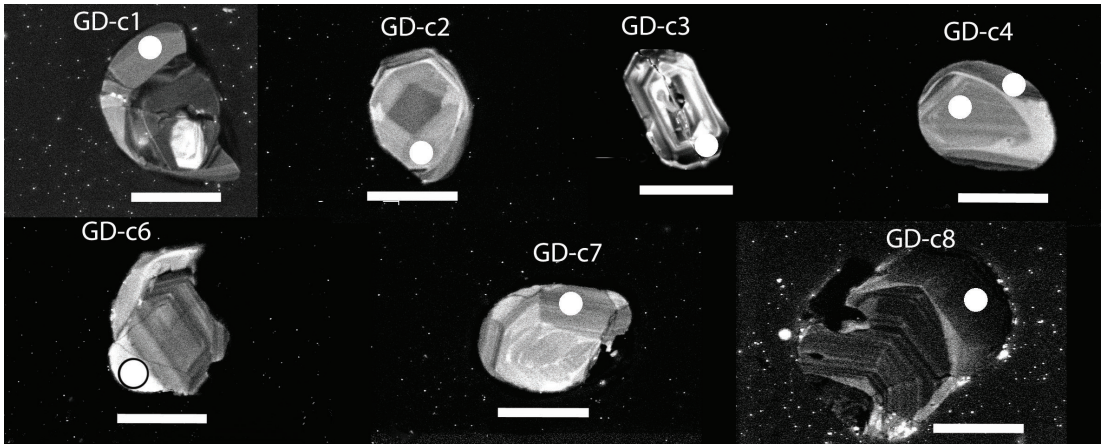

Figure 6.18. CL images of zircons extracted from sample GTD-ZR. Each white bar is 50μm long and corresponds with the nearest grain. Spot locations are indicated by the white dots.

morphic growths, completely metamorphic grains. Complex zoning is to be expected for a xenolith which is incorporated in such a large volcanic body. In the field the edges of the blocks show partial mixing with the gabbroic host rock (Photo A.19a).

Table 6.3. Detailed results of all zircon analyses from the Ahmeyim Great Dyke. All errors are 2σ.

Analysis	U(ppm)	$^{206}Pb/^{238}U$	$^{207}Pb/^{235}U$	$^{207}Pb/^{206}Pb$	
		Ratios			$\int$**206%**
GD-c1	357	0.39351± 0.00823	6.5224 ± 0.26941	0.12021± 0.00428	0.49
GD-c2	223	0.13965± 0.00279	1.23751± 0.05987	0.06473± 0.00285	1.02
GD-c3	1155	0.03174± 0.00074	0.23197± 0.01281	0.05301± 0.00266	0.03
GD-c4-1	116	0.16419± 0.00407	1.68327± 0.08199	0.07435± 0.00312	
GD-c4-2	106	0.16434± 0.00374	1.61761± 0.07444	0.07139± 0.00286	
GD-c6	665	0.39138± 0.00957	6.80413± 0.28091	0.12609± 0.00419	0.14
GD-c7	113	0.32238± 0.01069	4.97318± 0.28181	0.11188± 0.00514	1.58
GD-c8	864	0.20890± 0.00393	2.36772± 0.09688	0.08220± 0.00299	0.33
		Ages (Ma)			**conc.%**
GD-c1		2139 ± 38	2049 ± 36	1960 ± 64	109
GD-c2		837 ± 16	818 ± 27	766 ± 93	109
GD-c3		201 ± 5	212 ± 11	329 ± 114	61
GD-c4-1		980 ± 23	1002 ± 31	1051 ± 85	93
GD-c4-2		981 ± 21	977 ± 29	969 ± 82	101
GD-c6		2129 ± 44	2086 ± 37	2044 ± 89	104
GD-c7		1801 ± 52	1815 ± 48	1830 ± 83	98
GD-c8		1223 ± 21	1233 ± 29	1250 ± 71	98

Only eight analyses were performed because very few zonations were large enough to be confident that laser ablation would be targeting a single zone. The analyses were performed using a 25 μm spot size, U concentrations were all >100 ppm and the results are shown in Table 6.3. Common lead concentrations were low for most analyses ($\int$206

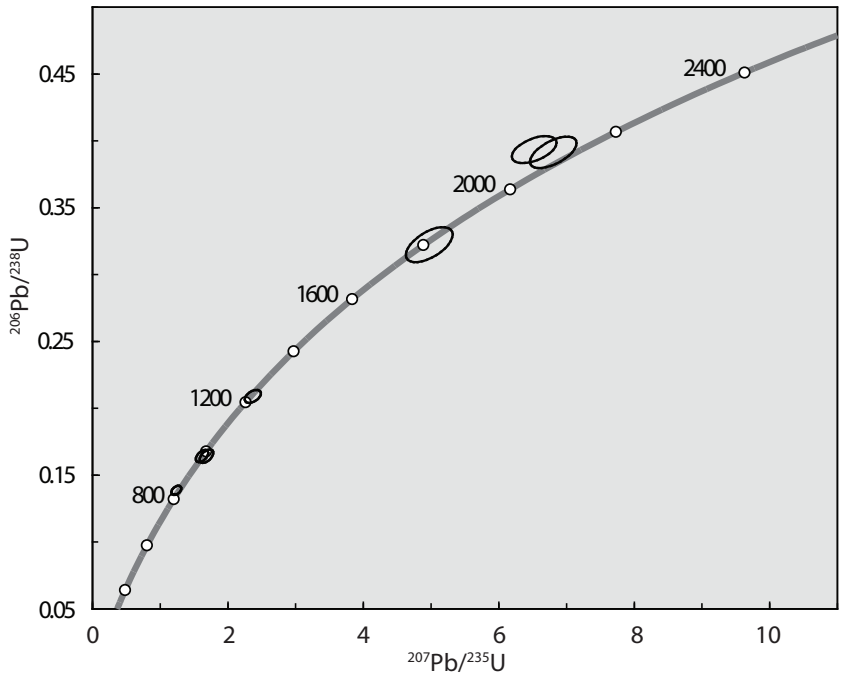

Figure 6.19. Concordia diagram for zircons from the Great Dyke. Ellipses are 2σ.

<0.5%) except two for which a correction was applied. One analysis (GD-c3) resulted in highly discordant ages (discordance of 61%). This particular grain is relatively small, heavily zoned and has a high U content (1155 ppm) which probably caused the grain damage seen in Figure 6.18. The spot crosses several zones and this result is not considered reliable. The seven other analyses are plot on a concordia diagram in Figure 6.19. The results show three Palaeoproterozoic ages: two around 2100 and one around 1800 Ma. One grain plots around 1250 Ma, two around 1000 Ma and one ∼800 Ma grain. These ages do not correspond very well with U-Pb zircon ages obtained by Pitfield et al. (2004) which were 550, 600, 750, 2000 and 2500 Ma. All errors are <6%.

Baddeleyite dating

From sample GTD 8 about 150 baddeleyites were separated. Three fractions have been run (Fig. 6.20), and the reproducibility in ^{207}Pb-^{206}Pb ages is remarkable (all three analysis within ca. 1 Ma). But unfortunately none is concordant and two fractions overlap completely. Unforced regression yields a lower intercept of approximately 200 Ma, which

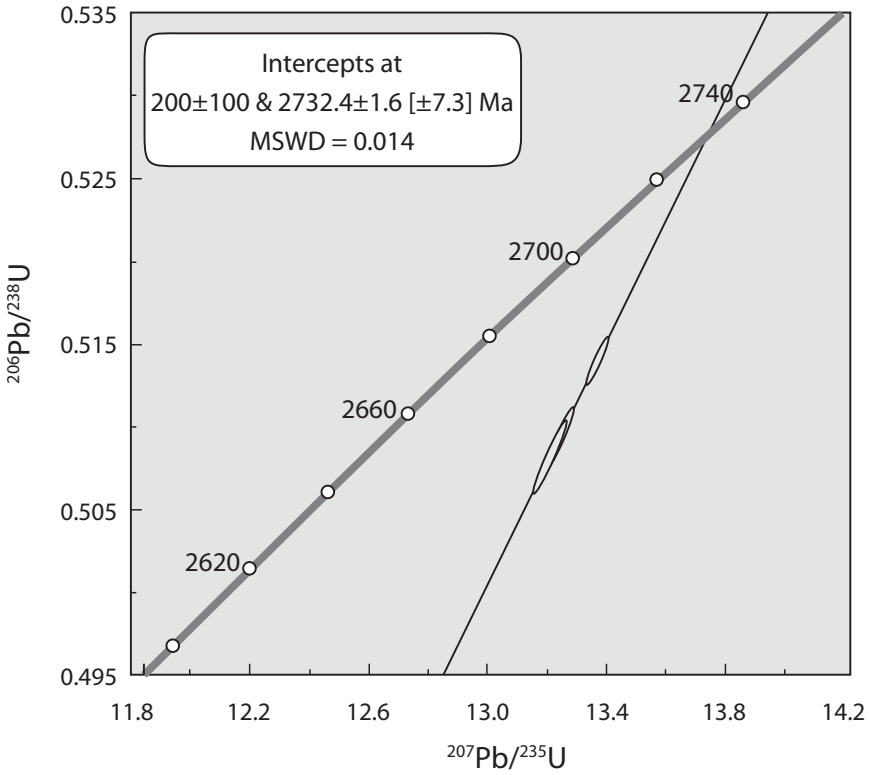

Figure 6.20. U-Pb Concordia diagram for sample GTD 8 from the Great Dyke of Mauritania. Uncertainty estimate in square brackets includes uncertainties in U-Pb decay constants.

could be due to a slight Pb loss, possibly related to the opening of the Atlantic Ocean. The upper intercept is 2732±2 Ma. Since this age is based on baddeleyite rather than zircon inheritance is not a factor and this age is considered to be primary.

The interpretation of the different ages from both the zircon and baddeleyite crystals and the implications of the geochronological results are discussed in Section 6.5.

Emplacement age

Baddeleyite is a common accessory mineral in silica-poor magmatic rocks such as carbonatites, kimberlites and gabbros. Baddeleyite only rarely occurs as xenocrysts (Schärer et al., 1997) and is highly resistant to metamorphism and hydrothermal alteration (Heaman and LeCheminant, 1993; Lumpkin, 1999). During metamorphism baddeleyite often develops a rim of metamorphic zircon which can sometimes facilitate dating both the age of crys-

tallization (baddeleyite) and the age of metamorphism (zircon rim, Wingate et al., 1998). For zircon, crystallization during metamorphism is common and has been recorded for a wide range of temperatures and pressures (e.g. Bea and Montero, 1999; Hoskin and Black, 2000). Fluid-present recrystallization can occur even at low (<200°C) temperatures as recorded both by experimental and natural studies (Geisler et al., 2002, 2003).

Baddeleyite does not commonly occur in felsic (silica-rich) rocks which argues against inheritance of the extracted crystals from the country rocks (which are dominated by migmatic gneisses and tonalitic plutons). For these reasons the baddeleyite age of 2732±2 Ma for the Ahmeyim Great Dyke is interpreted to be the primary age of crystallization. The wide age range obtained from zircon crystals extracted from the xenolith probably reflects post-emplacement thermal events. Only the ∼2100 Ma and possibly the ∼1800 Ma grains can be linked to a well known orogenic event which is recorded in the Reguibat Shield, the Eburnian orogeny at ca. 2 Ga. But as demonstrated by Geisler et al. (2003) recrystallization of zircon can be achieved by dissolution and re-precipitation during hydrothermal alteration at such low metamorphic conditions that it does not require major tectonothermal events to explain the youngest zircons found in the Great Dyke.

6.4.5 Palaeomagnetic Results

Ahmeyim Great Dyke

Palaeomagnetic samples were collected at 10 sites (36 samples) and specimens were demagnetised by stepwise heating up to 600°C. Intensities of the natural remanent magnetisation (NRM) were typically 2 – 4A/m and all samples show very consistent behaviour: a single component is directed towards the origin in orthogonal projection of the results and the intensity decreases slowly during heating up to 580°C and rapidly after heating up to 600°C (Fig. 6.21). The experiments resulted in very well defined palaeomagnetic directions for the individual samples but a high degree of within site scatter which is clearly visible in an equal area projection of the results (Fig. 6.21c). Stereographic projections of the distribution of sample magnetisation directions of each palaeomagnetic site are shown in Appendix S5. An overall site mean direction could not be calculated from these results.

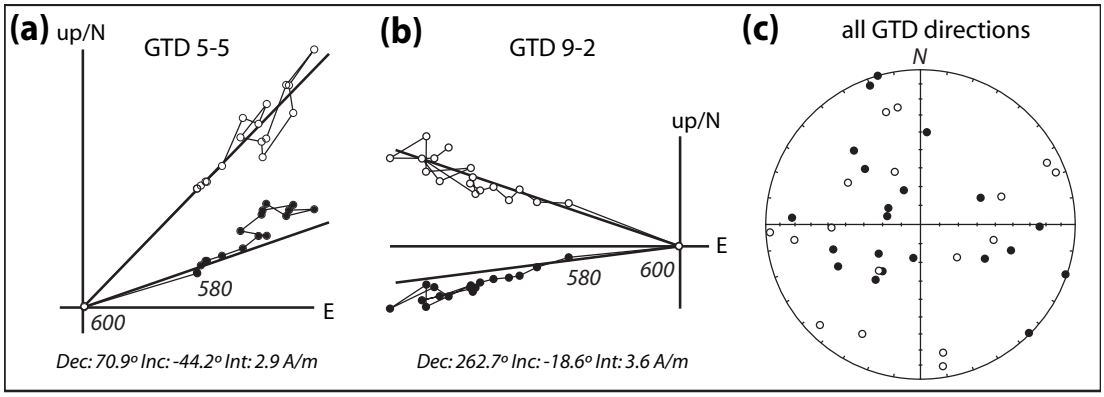

Figure 6.21. Typical demagnetisation behaviour for samples from the Ahmeyim Great Dyke. (**a**) and (**b**): two representative samples showing rapid demagnetisation between 580 and 600°C. (**c**) equal area projection of all sample directions from the 10 GTD sites.

Two samples were selected for rock magnetic experiments: one from the northern locality (GTD 5) and one from the southern locality (GTD 9). The experiments were carried out to identify the magnetic carrier in these rocks. Isothermal remanent magnetisation (IRM) acquisition curves were analysed (Fig. 6.22) using modelling software developed by Kruiver et al. (2001). Both samples show saturation of the IRM after applying a field of ca. 200 mT. One coercivity component is used to fit the IRM curves in Figure 6.22a-d and this component is characterised by fields at which half of the SIRM is reached ($B_{1/2}$) of 37 – 55 mT. High temperature susceptibility curves were acquired and are shown in Figure 6.22e and f. The heating curve in both samples is flat and shows a sharp drop in susceptibility around 580°C. The cooling curve follows the heating curve down to 580° after which the susceptibility continues to increase slowly down to 400°C. The sharp drop/increase in susceptibility at 580°C is taken as an approximation to the Curie temperature of the main magnetic phase in the rock samples.

The rock magnetic experiments point to the presence of a single magnetic carrier with a Curie temperature of ca. 580°C and a $B_{1/2}$ of 37 – 55 mT. These are typical values for magnetite and the results correspond well with the behaviour during demagnetisation of the NRM which showed unblocking temperatures between 580° and 600°C (Fig. 6.21).

Even though sampling at the very top of the outcrops was avoided, it seems likely that the NRM of the samples is completely destroyed. The relatively high intensities (up to 4 A/m)

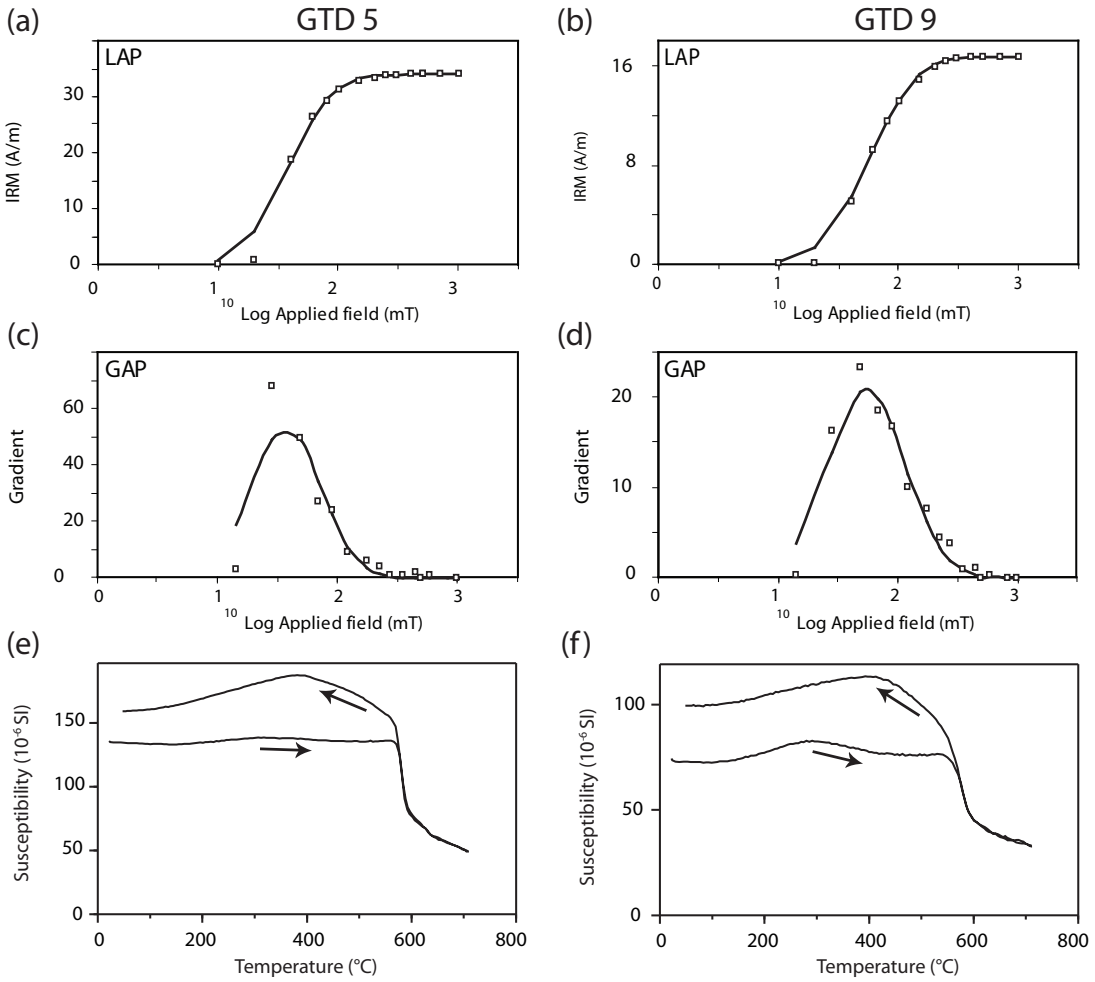

Figure 6.22. Rock magnetic experiments for two sample of the Ahmeyim Great Dyke. Results of the IRM experiments: linear acquisition plots (LAPs) in (**a**) and (**b**), gradient acquisition plots (GAPs) in (**c**) and (**d**). Results of the high temperature susceptibility measurements are shown in (**e**) and (**f**).

found in the majority of samples suggests they are struck by lightning. The huge range of zircon age data indicates the occurrence of possibly several (hydro)thermal events which potentially have had a strong influence on the magnetisation of the rocks.

Oujeft Group sandstones

Five oriented hand samples from the Chinguetti Formation (Oujeft Group) were cored and palaeomagnetically analysed. After removal of a poorly defined low unblocking temperature overprint below heating to 200°C, samples of site OUA 1 yielded a well defined

site	component	n	T(°C)	Tilt dip/dipdir	stratigraphic D(°)	stratigraphic I(°)	tilt corrected D(°)	tilt corrected I(°)	κ	α95(°)
OUA 1		5	200–550	03/044	173.2	26.3	172.0	28.2	2.5	61.8
OUA 2	1	6	20–100	03/044	001.8	13.7	002.2	11.5	49.4	9.6
	2	6	100–200	03/044	155.3	10.2	154.8	11.3	561.9	2.8
	3	6	200–640	03/044	292.3	34.5	294.3	35.6	4.0	38.1
OUA 3	1	6	20-300	03/044	002.7	31.8	003.9	29.5	639.5	2.7
	2	6	300–620	03/044	300.6	-3.8	300.4	-3.1	2.9	47.7
OUA 4		6	20–640	03/044	216.4	-62.1	217.1	-59.1	255.1	4.5
OUA 5		8	20–640	03/044	228.2	21.5	228.3	24.5	127.1	4.9

Table 6.4. Summary of all palaeomagnetic directions for the Oujeft Group. Different components are numbered, n gives the number of analysed samples for each site, T is the temperature range of each component, κ is Fisher's precision parameter (Fisher, 1953), α95 is the 95% cone of confidence.

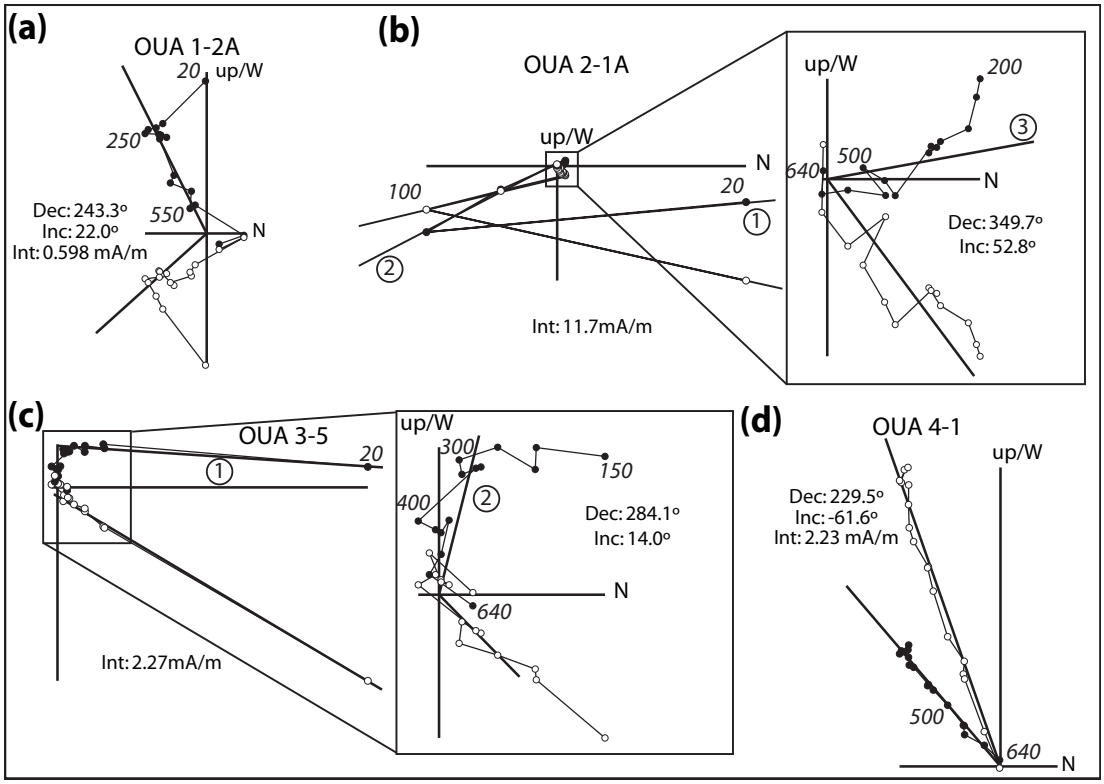

Figure 6.23. Typical demagnetisation behaviour for samples from the Chinguetti Formation (Oujeft Group). Individual components are labeled in b and c. Behaviour of samples from site OUA 5 is identical to that shown in d.

magnetisation, directed towards the origin in orthogonal projections (Fig. 6.23a), with unblocking temperature 200 – 550°C. Site OUA 2 yielded three stable components: one between 20 and 100°C, a second component between 100 and 200°C and a third component between 200 and ca. 640°C (Fig. 6.23b). The third component is directed towards

the origin in orthogonal projections. Site OUA 3 displayed two stable components: between 20 and 300°C and between 300 and ca. 620°C (directed towards the origin, Fig. 6.23c). Sites OUA 4 and 5 both displayed a single stable magnetic component, directed towards the origin in orthogonal projections, and demagnetised below the detection limit of the magnetometer after heating to 640°C. Stereographic projections of the distribution of sample magnetisation directions of each palaeomagnetic site are shown in Appendix S5.

Both component 1 of OUA 2 (20 – 100°C) and component 1 of OUA 3 (20 – 300°C) plot very close to the present day field direction at the locality (inclination = 37.4°) and are therefore interpreted as recently acquired magnetisations. Also the medium temperature component of OUA 2 (100 – 200°C) is interpreted to be a younger overprint although the meaning of its southward direction is not clear. Of the five high temperature components only those of site OUA 4 and OUA 5 are well defined with $\alpha 95 < 16°$, but the inclinations of both site mean directions are separated by ∼84°. All site mean directions differ so much that no overall site mean could be calculated and any palaeogeographic interpretations based on these results would bear no significance.

6.5 Discussion and Conclusions

6.5.1 Geochronology and Correlation of Diamictites

The glaciogenic 'triad' sequence has long been used as a chronostratigraphic marker horizon across the Taoudéni Basin (Zimmermann, 1960) and the Volta Basin (Leprun and Trompette, 1969). Its synchronicity has been challenged by the discovery of two fossils of the species *Aldanella attleborensis* in a calcareous dolomite of the Walidiala Valley, SW Taoudéni Basin (Culver et al., 1988). These are early Cambrian in age which has been the reason for several publications to postulate a Cambrian age for the entire glaciation (Culver and Hunt, 1991; Bertrand-Sarfati et al., 1995). Subsequent sampling however has not led to more finds of these fossils (Porter et al., 2004) and the original sample is suspected to be derived from a loose block (Porter et al., 2004; Shields et al., 2007a). Recent reports of U-Pb zircon analyses, obtained from volcanic intercalation in Téniagouri Group equivalents

in the Hodh and Hank regions (Lahondère et al., 2005; Frischbutter et al., 2009), rule out a Cambrian and even a Gaskiers age (∼580 Ma) for the tillites in the Taoudéni Basin. A U-Pb zircon age of 625±8 Ma was obtained from the base of the Azlaf Group which is the Téniagouri Group equivalent in the Hank region, NE Taoudéni Basin (Frischbutter et al., 2009). In this study, the youngest detrital zircon from the Jbeliat Group is found near base of the sequence and is 667±9 Ma. This narrows the depositional age and thus the timing of glaciation down to a period between 667 and 625 Ma.

Zircons extracted from the Téniagouri Group in the southern Taoudéni Basin yielded ages of 609.7±5.5 and 604±6 Ma (Lahondère et al., 2005) which are significantly younger than the 625±8 Ma in the north. It is not known where exactly in the stratigraphy these samples were derived from so it is possible that the Téniagouri Group, ranging in stratigraphic thickness from 300 – 400m in the Adrar and Hank regions to 750m in the Hodh region, represents ∼15 Ma of sedimentation history. Alternatively these results could mean the sequences are diachronous.

Based on δ^{13}C isotope profiles of overlying dolomite formations the tillites have been correlated with glaciogenic rocks in the SW Taoudéni Basin (Shields et al., 2007a), the NW Taoudéni Basin (Shields et al., 2007b) and the Volta Basin (Porter et al., 2004). Our results confirm and extend the previously obtained chemostratigraphic record for the Adrar region. The relatively quick return to positive values compared to other post Marinoan sections is interpreted to indicate very condensed deposition of the post-glacial sequences. If a global correlation is permitted, the carbonates (dolostone and purple limestone) represent a maximum of 10 Ma, between the end of the glaciation (635 Ma, Hoffmann et al., 2004) and the start of the overlying Téniagouri Group (625 Ma, Frischbutter et al., 2009). These limestones were also interpreted to be a highly condensed unit by Shields et al. (2007b) who showed that this unit is strongly varying in thickness (between 50cm to 6m in the Atar Cliff area alone, Álvaro et al., 2007; Shields et al., 2007b).

6.5.2 Sedimentological Implications of Changes in Provenance around the Jbeliat Group

The detrital zircon profiles from the Assabet el Hassiane Group below and the three levels from within the glaciogenic Jbeliat Group show some remarkable changes (Fig. 6.9). The Assabet el Hassiane Group is marked by the dominance of Mesoproterozoic grains centred on 1250 Ma. This population is less prominent in the stratigraphically higher LIAT 2 sample of the Jbeliat Group and is almost absent in the next sample above (LIAT 5). The LIAT 2 and 5 units, which are correlated to two different stages of the terrigenous glaciation (Deynoux, 1985), contain grains from the mid-Neoproterozoic (ca. 700 Ma) to Archaean. This change in provenance may be linked to a change in drainage systems and it is suggested that the first glaciers brought the older and younger material into the basin. Indeed, if glaciers moved southward from the Archaean and Palaeoproterozoic Reguibat Shield (Fig. 6.4, Deynoux, 1980), the oldest populations could have been derived from recycled sediments of the Hodh Supergroup, directly from the basement rocks or a combination of both. The topmost sample from the Jbeliat Group (LIAT 6) shows a return to ages found in the Assabet el Hassiane Group and contains hardly any Archaean grains. The absence of older populations suggest material is derived from the east, south or west but not from the north.

The three samples from the Jbeliat Group (which has a stratigraphic thickness of ca. 20m) yield rather different zircon population profiles. These changes are very relevant to the interpretation of palaeoenvironment and, in this case, ice sheet dynamics. These results show that zircon populations in one sedimentary unit (i.e. a Group) can not be evaluated using one sample alone. A single sample is only representative of the stratigraphic level it was derived from.

6.5.3 Consequences of the Mesoproterozoic Zircons for Palaeozoic Palaeogeography

The detrital zircon data presented here highlight the presence of exotic terranes outbound of the West African Craton at least around ∼635 Ma (i.e. the time of deposition for the Jbeliat Group). This information is important in understanding the palaeogeography of

the West African Craton and constraining the timing of accretion for its surrounding arc terranes.

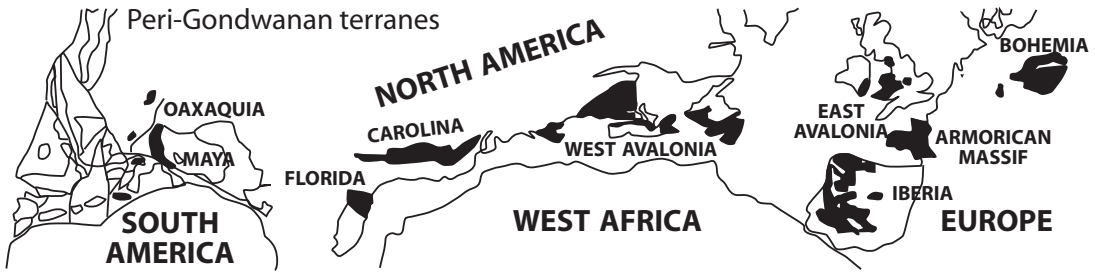

Figure 6.24. Location of peri-Gondwanan terranes before opening of the Atlantic Ocean (after Nance et al., 2008).

Early Palaeozoic accretion at the periphery of the northern margin of Gondwana resulted in the Cadomian deformational event. The presence of Cadomian age basement rocks in various blocks of the Variscan and Appalachian orogens clearly indicates their tectonic affinities to Gondwana in Palaeozoic times (Nance and Murphy, 1994). The precise position of these blocks, now found along the western margin of North America and in south and central Europe (Fig. 6.24), is uncertain due to a long Palaeozoic and Mesozoic history of orogenesis and break-up. A combination of Nd and U-Pb detrital zircon isotopic data are used to support palaeogeographic reconstructions: Detrital zircon populations within Palaeozoic sediments for these terranes and the presence or lack of Mesoproterozoic grains is taken in the literature as indicating either a South American or West African origin of the terranes respectively (Tait et al., 2000; Friedl et al., 2000; Nance et al., 2008; Bahlburg et al., 2010). However, clearly the results presented here indicate the relative proportions of Mesoproterozoic grains can not be used as markers for proximity to these Gondwana constituents.

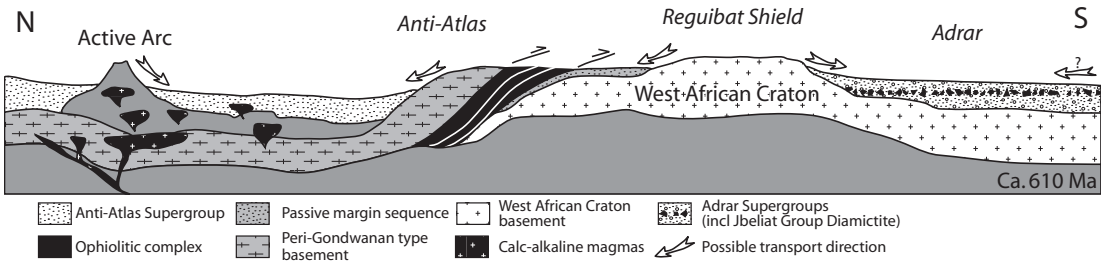

Figure 6.25. Geological sketch showing the possible transport directions for zircons found in the Anti-Atlas Supergroup sedimentary rocks to the north and in the Adrar sequences to the south of the Reguibat Shield. Modified after Abati et al. (2010).

The presence of large Mesoproterozoic populations in late Neoproterozoic rocks from the Adrar Sub-Basin raises questions concerning provenance and the reconstructions as it provides a Mesoproterozoic source through reworking. However, a recent detrital zircon study of the late Neoproterozoic (<610 Ma) Saghro Group in the Anti-Atlas mountain belt in Morocco demonstrated the total absence of Mesoproterozoic grains (Abati et al., 2010). The sediments in this basin, situated on the northern margin of the West African Craton, are characterised by detrital zircon ages matching a Neoproterozoic volcanic arc formed to the north and Archaean and Palaeoproterozoic basement ages on the Reguibat Shield. The fact that the Reguibat Shield provided detritus but that no Mesoproterozoic grains made it into the Saghro Group suggest the Reguibat Shield acted as a major barrier for sediment transport (Fig. 6.25). The lack of arc signatures in the provenance geochemistry results of this study can be seen as additional evidence for this barrier which prohibited arc-derived material to enter the Taoudéni Basin.

The two cratons where Mesoproterozoic magmatic rocks are known and which were nearest to West Africa during the time of sedimentation of the Jbeliat Group are Amazonia and Baltica (Fig. 1.1). The Amazon Craton in northern South America contains several Mesoproterozoic provinces e.g. the 1.86 – 1.52 Ga Rio Negro Province, the 1.76 – 1.47 Ga Rondonia Province and the 1.33 – 0.99 Ga Sunsas Province (Fig. 6.26, Santos et al., 2000). On Baltica numerous U-Pb zircon ages are recording Mesoproterozoic magmatic events in the Eastern Segment (southern Sweden) and Telemarkia Terrane (southern Norway) of the Sveconorwegian Orogen (Fig. 6.26, Bingen et al., 2005; Bingen and Solli, 2009, and references therein). These cratons may have acted as sources for our field area which implies large (>1000s km) transport distances. In most Neoproterozoic reconstructions the Mesoproterozoic portions of these cratons are directed away from West Africa to face the western margin of Laurentia (see Rodinia models in Chapter 2). The model that brings these landmasses closest together is that of Li et al. (2008) where along margin transport could have brought zircons from both potential source areas to the Taoudéni Basin (Fig. 6.26). In the reconstruction as proposed by Evans (2009) Baltica is excluded as a potential source (it being on the other side of Laurentia). Amazonia is suggested to be connected to West Africa although the Mesoproterozoic provinces are directed away from West Africa facing an open ocean. Future research might shed more light on whether the zircons from

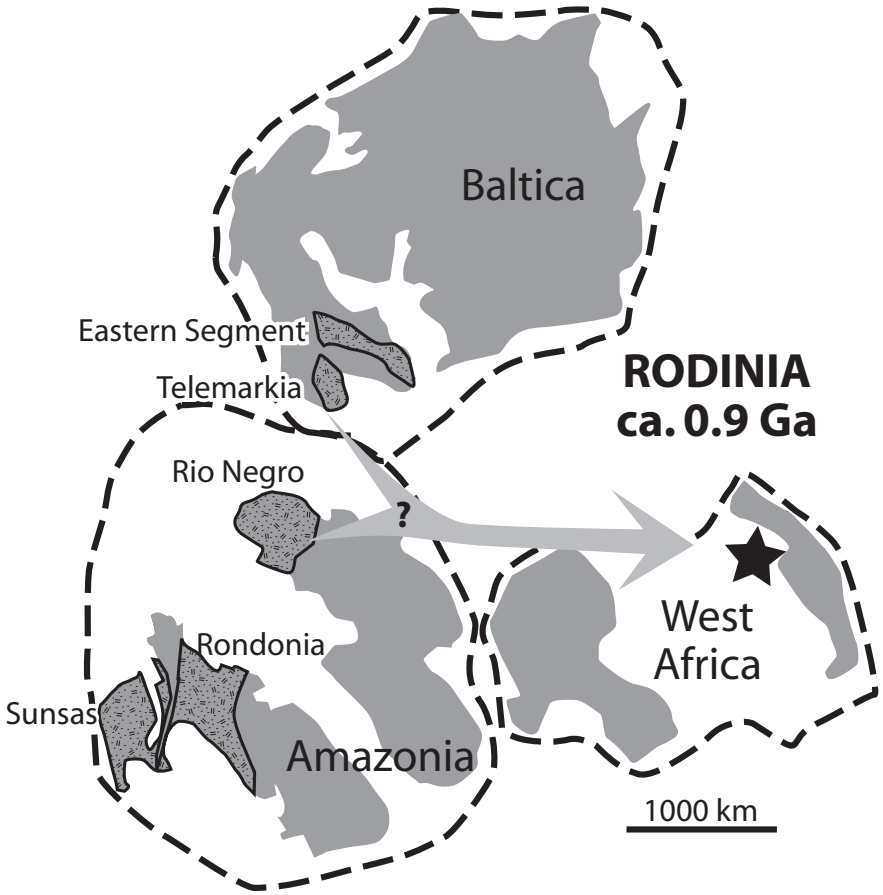

Figure 6.26. Rodinia configuration (after Li et al., 2008) showing Precambrian basement (grey), field area (star) and potential Mesoproterozoic sources (crosses pattern).

West Africa were sourced on Baltica and this could provide important implications for these Rodinia reconstructions.

Rodinia assembled around 1.0 Ga and started breaking up during the Neoproterozoic. Rifting between Baltica and Laurentia is recorded by the Egersund dyke swarm in southern Norway, dated at 616±3 Ma (U-Pb Baddeleyite, Bingen et al., 1998), by the 608±1 Ma Sarek Dyke Swarm in northern Sweden (TIMS U-Pb zircon ages, Svenningsen, 2001) and by the 580 – 560 Ma Seiland Igneous Province in northern Norway (TIMS U-Pb zircon ages, Roberts et al., 2010). The 590 – 560 Ma Volhyn basalts (whole rock ^{40}Ar-^{39}Ar ages, Elming et al., 2007) in the Ukraine might record breakaway of Baltica from Amazonia. Predrift configurations, e.g. the configuration as proposed by Li et al. (2008), would thus have lasted until ca. 610 Ma and transport of Mesoproterozoic detritus across Rodinia could

have taken place until that time.

6.5.4 Implications of Newly Dated Ahmeyim Great Dyke

Regional significance

Two terranes have been recognised in the Archaean Province of the Reguibat Shield and they are separated by a major ductile shear zone, the Tâçarât-Inemmaûdene Shear Zone (TISZ, Key et al., 2008). The terranes show a different Mesoarchaean geological history: the Choum-Rag el Abiod Terrane to the east of the TISZ consists of migmatic orthogneisses which record crustal growth between 3.50 and 3.45 Ga (Auvray et al., 1992; Potrel et al., 1996). These rocks have been affected by granulite facies metamorphism around 3.20 – 2.99 Ga (as dated by whole rock Sm-Nd and SHRIMP zircon ages) which generated a new gneissic fabric (Potrel et al., 1998). The Tasiast-Tijirit Terrane on the other side of the TISZ comprises migmatic gneisses and greenstone belts which are both dated at ca. 2.97 Ga (Key et al., 2008). The migmatic gneisses underlie the greenstone lithologies and all of them are affected by post-greenstone intrusion of biotite-tonalites and granodiorites dated at 2.93 Ga (Chardon, 1997; Key et al., 2008).

The timing of transpressive shearing in the TISZ is constrained between 2984±111 Ma for a deformed granite within the shear zone and a 2726±7 Ma granite which cross-cuts TISZ structures in the Chom-Rag el Abiod Terrane (Potrel et al., 1998; Key et al., 2008). Both terranes record bimodal, post-tectonic magmatism. In the Choum-Rag el Abiod Terrane U-Pb zircon ages for felsic volcanic rocks of 2715±11 and 2726±7 Ma have been obtained by Auvray et al. (1992) and Potrel et al. (1998) respectively. A granulitic gabbro from within this terrane has been dated at 2.74 Ga (Auvray et al., 1992). Previous records of post-tectonic magmatism in the Tasiast-Tijirit Terrane were limited to undated, coarse-grained to pegmatitic muscovite-granite intrusions which cross-cut all other lithologies (Key et al., 2008). The Ahmeyim Great Dyke, now dated at 2732±2 Ma, confirms the bimodal character of this magmatic phase in the Tasiast-Tijirit Terrane which was already recognised previously in the Choum-Rag el Abiod Terrane. The dyke cross-cuts but follows the boundaries of the Ahmeyim Greenstone Belt to the east and to the west the Gleibat

el Fhoud tonalitic pluton dated at 2912±35 Ma by single zircon evaporation (Key et al., 2008). The dyke is unaffected by the ductile deformation and thus confirms the minimum age of ca. 2730 Ma for the TISZ event. The NNE-SSW trend of the dyke is sub-parallel to the TISZ.

Global significance

Several large igneous events have reported ages that are close to the 2732±2 Ma Baddeleyite age for the Great Dyke. The Central Slave Basement Complex of the Slave Province (Canada) is intruded by several mafic dyke swarms of which the oldest is dated by U-Pb zircon at 2734±2 Ma (Bleeker et al., 1999). Also in Canada, the Superior Province contains the Mulcahy Lake layered gabbro intrusion which is dated at 2733±1 Ma (Morrison et al., 1985). Zircons from two gabbro-diabase dykes on the Kola Peninsula of the Baltic Shield (Russia) yielded ages of 2738±6 and 2739±11 Ma (Yegorov and Bayanova, 1999). Lastly, newly dated dykes which intrude the Uauá Subdomain of the Serrinha Block of the São Francisco Craton (Brazil) yield ages similar to those of the Great Dyke: bimodal dyke intrusion has been reported in this part of the Palaeoproterozoic Itabuna-Salvador-Curaça orogen (Oliveira et al., 2010) and ages for tholeiitic and noritic dykes are 2624±7 and 2726±3 Ma respectively (*Ernst et al., www.supercontinent.org project, unpublished and probably confidential data*). These coeval magmatic ages may be used in palaeogeographic reconstructions and suggest proximity of the Reguibat Shield to the São Francisco Craton and possibly to the Slave Province and the Baltic Shield during the Mesoarchaean. Unfortunately the palaeomagnetic data obtained from the Great Dyke did not yield a stable primary magnetic direction and cannot be used as evidence for these constructions.

Chapter 7

Summary

7.1 Introduction

The west coast of Africa is largely defined by the West African Craton to the north and the Congo Craton in central Africa. Both cratons consist of Archaean and Palaeoproterozoic blocks which stabilised during Mesoproterozoic orogenies and both cratons exhibit vast Neoproterozoic sedimentary basins. West Africa and Congo have coexisted in their current relative positions roughly since formation of supercontinent Gondwana which consolidated around the Precambrian – Cambrian boundary (ca. 550 Ma). Both cratons contain diamictite bearing Neoproterozoic sedimentary sequences and these sequences have in the past been correlated based on lithostratigraphy (see for example Deynoux et al., 1978, 1985). These studies stressed the existence of many lithostratigraphic similarities, however, a lack of geochronological data prohibited robust correlations. Despite the fact that many more recent studies of the rocks on both cratons have been published, correlations are still largely based on lithostratigraphic and chemostratigraphic data and detailed radiometric constraints remain sparse.

Neoproterozoic rock records from many continents provide evidence for apparent extreme climatic changes with the stratigraphic juxtaposition of glaciogenic and warm water carbonate rocks. Where palaeomagnetic data are available, low latitude of deposition for

these glacial sequences are indicated. As described in Chapter 1, some of the models proposed to explain the phenomena of low latitude glaciation require extreme scenarios such as the Snowball Earth Hypothesis which envisages global glaciations, or the High Obliquity Model which suggests large changes in the Earth's rotational axis. Of vital importance to all of these models is detailed knowledge of palaeogeography and chronological correlation of the deposits worldwide. The aim of this thesis is to provide a framework for correlating glaciogenic diamictites found along the western margin of the Congo Craton and in the north-central Taoudéni Basin on the West African Craton, to determine the palaeogeographic setting and to evaluate the depositional palaeolatitude. The techniques employed include U-Pb dating (of zircon and baddeleyite), sedimentary geochemistry and palaeomagnetic analyses (details in Chapter 3).

Many controversies surround palaeogeographic models for both the Congo and West Africa cratons, especially during the early Neoproterozoic before amalgamation of Gondwana (see Chapter 2). It remains unclear whether or not the Congo Craton was part of supercontinent Rodinia and West Africa is palaeomagnetically unconstrained from the Palaeoproterozoic until the late Neoproterozoic. An important aim of this thesis is to resolve long lasting uncertainties concerning the palaeogeographic positions of the Congo Craton and the West African Craton in the Neoproterozoic. The thesis provides a detailed examination of tillite bearing Neoproterozoic sedimentary sequences from these two cratons. The results of these analyses, as presented in Chapters 4 – 6, are summarised below.

7.2 Clues for Neoproterozoic Palaeogeography of the Congo and West African Cratons

The West Congolian Group sedimentary sequence records the Neoproterozoic evolution of the western margin of the Congo Craton. Lithostratigraphy and whole rock geochemistry presented in Chapter 4 show the development of a passive margin with highly recycled clastic sediments which were intruded by 694±4 Ma tholeiitic magmatic rocks and are overlain by a transgressive series of successively sandstones, siltstones and carbonate deposits. The clastic sediments of the Mpioka Subgroup near the top of the West Congolian

Group have previously been interpreted as molasse deposits for the Araçuaí orogen belt to the west. Detrital zircon geochronology from this subgroup, however, indicates provenance from the north (the Ntem Complex in Congo Republic and Cameroon) and from the south (the Kaoko and Damara belts in Angola and Namibia) but not from the Araçuaí Orogen (see Chapter 4). Their detrital zircon profile shows that detritus from this orogenic belt did not enter the West Congo Belt during the Neoproterozoic and suggests that the Araçuaí orogenic belt formed outbound of the Congo Craton until final consolidation of Gondwana.

In West Africa, Neoproterozoic sedimentary sequences of the Taoudéni Basin just south of the cratonic Reguibat Shield were analysed for their geochemistry, detrital zircons content and palaeomagnetic characteristics (Chapter 6). The results indicate the presence of predominantly highly recycled sediments and the upper part of the sequence is characterised by a prominent Mesoproterozoic detrital zircon population. Rocks of this age are previously unidentified within west and northern Africa which raises at least two important questions. Firstly, what are the source rocks of the Mesoproterozoic grains? Two cratons where Mesoproterozoic magmatic rocks are known and which might have been relatively near to West Africa during the Neoproterozoic are Amazonia and Baltica. These cratons may have acted as sources for our field area but this implies large (>1000s km) transport distances. Our results favour the reconstruction of Li et al. (2008) which brings Amazonia and Baltica closest together. The reconstruction by Evans (2009) is the least favourite since it puts Laurentia between Baltica and West Africa. More research is needed to establish clear relationships between detrital zircons and their potential source areas, e.g. zircons could be characterised by analysing inclusions, trace element composition and isotope signatures. Secondly, these Mesoproterozoic populations require a re-evaluation of palaeogeographic reconstructions of peri-Gondwanan terranes. Reconstructions are often based on the relative abundance of Mesoproterozoic detrital zircon grains in Neoproterozoic and Cambrian deposits. The absence or presence of these age populations are used as markers of proximity to West Africa or Amazonia respectively. The presence of large Mesoproterozoic populations in late Neoproterozoic rocks from West Africa raises questions concerning provenance and these reconstructions as it provides a Mesoproterozoic source through reworking.

7.3 Correlating Diamictites

A U-Pb baddeleyite age of 694±4 Ma has been obtained from syn-glacial volcanic rocks found within the Lower Diamictite Formation in the West Congo Belt (Chapter 4). This diamictite, the older of two glacial units in the West Congolian Group, has previously been correlated with the Kaigas and Chuos diamictites in Namibia, with the Grand Conglomerate in the Katanga Belt (Zambia) and with the Lower Tillite Formation of the Lindi Supergroup in the Central African Republic (Frimmel et al., 2006; Poidevin, 2007; Tait et al., 2011). The age of the Kaigas Formation is well constrained by a U-Pb SHRIMP age of 751.9±5.5 Ma for overlying volcanic rocks (Borg and Armstrong, 2002) and the Grand Conglomerate has been dated at 735±5 Ma (Key et al., 2001). Both these diamictites can thus not be coeval with the Lower Diamictite Formation. This shows that on the Congo Craton alone at least three pulses of glaciation occurred between ca. 755 and 690 Ma. Similar ages to those identified here are obtained from the Windermere Supergroup in central Idaho where the glacial Edwardsburg Formation is dated at 685±7 and 684±4 Ma (Lund et al., 2003).

Direct ages for the Upper Diamictite Formation in the West Congo Belt are absent. Based on lithostratigraphy it has been correlated with the Namibian Ghaub Formation which is found along the southern border of the Congo Craton and is dated at 635.5±1.2 Ma (Hoffmann et al., 2004). This correlation is based on 1): the sudden occurrence of the diamictite in a transgressive sequence of carbonate deposits 2): the diamictite is capped by a striking layer of pink, laminated dolostone (cap carbonate). A newly obtained chemostratigraphic profile of stable carbon isotopes for the West Congolian Group supports this correlation. After correlation with the global Neoproterozoic carbon isotope record (Halverson et al., 2005) the Upper Diamictite seems to be coeval with the Marinoan glacial event. An age of ca. 635 Ma is consistent with the geochronological results from this study (Chapter 4) where a maximum age of 707±23 Ma is determined by the youngest detrital zircon grain in a rock sample from the Upper Diamictite Formation.

In West Africa the terrigenous glaciogenic Jbeliat Group in the northern Taoudéni Basin has previously been correlated with glaciogenic rocks in the SW Taoudéni Basin (Shields et al., 2007a), the NW Taoudéni Basin (Shields et al., 2007b) and the Volta Basin (Porter

et al., 2004). New δ^{13}C isotope results from dolomite formations overlying the Jbeliat Group are used to construct a chemostratigraphic profile for the Adrar region (Chapter 6). Comparison of cross-craton carbon isotope profiles makes a correlation of glaciogenic rocks more reliable. Based on these chemostratigraphic results the Jbeliat diamictite is correlated globally with the 635 Ma Marinoan glacial event. A recent age for the overlying Téniagouri Group (625 Ma, Frischbutter et al., 2009) and the shape of the carbon isotope profile both suggest very condensed deposition of post-glacial sequences.

7.4 Palaeomagnetic Results: Cambrian Remagnetisation

Stable palaeomagnetic results for the Congo Craton were obtained from siltstones and carbonate rocks below and above the Upper Diamictite Formation (ca. 635 Ma) of the West Congolian Group in the West Congo Belt (see Chapter 5). Both the palaeomagnetic directions and bedding attitudes of the rocks below and above the diamictite are indistinguishable from each other. Combining the directions resulted in an overall mean of D = 324°, I = 61°before and D = 342°, I = 66° after tectonic correction (α_{95} = 3°, N = 18). Proximity of the corresponding *in situ* palaeomagnetic pole (31°N, 344°E) to the Cambrian APWP of Gondwana, in conjunction with a lack of reliable fieldtests, strongly suggests a remagnetisation of the rocks. From the rock magnetic experiments it is concluded that the remnance is mainly carried by titanomagnetite which may be authigenically formed by thermal alteration of siderite during the Araçuaí-West Congo Orogen. From the position of our *in situ* pole between the 530 and 520 Ma Gondwana reference poles this remagnetisation has been assigned an approximate age of 525 Ma. Palaeomagnetic resetting may be the result of post-orogenic buoyancy driven fluid flow which has been shown to have remagnetised carbonates on the São Francisco Craton around the same time (D'Agrella-Filho et al., 2000; Trindade et al., 2004). Sphalerite and galena mineralisations which cross-cut Palaeozoic red beds in the West Congo Belt are potentially linked to this phase of fluid-flow and form targets for dating this event by applying Rb-Sr and Re-Os geochronology.

7.5 Concluding Remarks

The Snowball Earth Hypothesis has been the most popular and perhaps the most fiercely criticised theory to explain low latitude glaciations. An important implication which follows from worldwide glaciation is that deposits need to be globally synchronous. This requires detailed geochronological data which are still lacking for many of the Neoproterozoic glaciogenic deposits. This study presents new results for glacial rocks on the Congo and West Africa cratons with important consequences for global synchronicity.

The Lower Diamictite Formation in the Congo Craton, now precisely dated at 694±4 Ma, allows comparison to other well dated Cryogenian glacial deposits. Over the past decade an increasing number of radiometric age constraints reveal a complex pattern in temporal distribution of mid Cryogenian glaciogenic deposits. Our new age might have one correlative in North America (Idaho) but none on the Congo Craton where two precisely dated glaciations are both significantly older. This strongly implies that a globally synchronous Sturtian glacial event did not exist. The Sturtian rather represents a period between ca. 755 and 660 Ma during which several local glaciations occurred, none of which were global.

The late Cryogenian Marinoan glacial event has been directly dated in two localities and both dates are remarkably similar: 635.5±1.2 Ma for a tuffaceous bed within the Ghaub Formation of southern Namibia (Hoffmann et al., 2004) and 635.2±0.6 Ma for an ash bed directly overlying the Nantuo Diamictite in South China (Condon et al., 2005). Litho- and chemostratigraphic analyses presented in this thesis all favour a correlation of the Lower Diamictite Formation in the West Congo Belt and the Jbeliat Group in the Taoudéni Basin with the Marinoan providing further evidence for the global character of this event. The Snowball Earth Hypothesis could explain the synchronous deposition of these glaciogenic deposits.

The 525 Ma palaeomagnetic pole presented here gives a palaeolatitude for the West Congo Belt (5°S, 14°E) of 43±9°. The youngest reliable Precambrian pole is the 748 Ma Mbozi pole which implies a palaeolatitude of 23±4°. In combination with the geological record it seems extremely unlikely that the Congo Craton moved out of the subtropics during the

second half of the Neoproterozoic. The Upper Diamictite is likely deposited at low latitude which is in agreement with the Snowball Earth Hypothesis.

Bibliography

Abati, J., A. M. Aghzer, A. Gerdes, and N. Ennih, 2010: Detrital zircon ages of Neoproterozoic sequences of the Moroccan Anti-Atlas belt. *Precambrian Research*, **181 (1-4)**, 115–128.

Abbot, D. S. and R. T. Pierrehumbert, 2010: Mudball: Surface dust and Snowball Earth deglaciation. *J. Geophys. Res.*, **115 (D3)**, D03 104.

Abdelsalam, M. G., J.-P. Liégeois, and R. J. Stern, 2002: The Saharan Metacraton. *Journal of African Earth Sciences*, **34 (3-4)**, 119–136.

Acef, K., J. P. Liégeois, A. Ouabadi, and L. Latouche, 2003: The Anfeg post-collisional Pan-African high-K calc-alkaline batholith (Central Hoggar, Algeria), result of the LATEA microcontinent metacratonization. *Journal of African Earth Sciences*, **37 (3-4)**, 295–311.

Affaton, P., L. Aguirre, and R.-P. Ménot, 1997: Thermal and geodynamic setting of the Buem volcanic rocks near Tiélé, Northwest Bénin, West Africa. *Precambrian Research*, **82 (3-4)**, 191–209.

Affaton, P., M. Rahaman, R. Trompette, and J. Sougy, 1991: The Dahomeyide Orogen: tectonothermal evolution and relationships with the Volta basin. *The West African Orogens and Circum-Atlantic Correlatives*, R. D. Dallmeyer and J. P. Lecorche, Eds., Springer, Berlin, 107–122.

Agassiz, L., 1866: Traces of Glaciers under the Tropics. *Unpublished paper read before the National Assembly of Sciences, Washington, DC, August 12th*.

Agnor, C. B., R. M. Canup, and H. F. Levison, 1999: On the Character and Consequences of Large Impacts in the Late Stage of Terrestrial Planet Formation. *Icarus*, **142 (1)**, 219–237.

Aït Malek, H., D. Gasquet, J.-M. Bertrand, and J. Leterrier, 1998: Géochronologie U-Pb sur zircon de granitoïdes éburnéens et panafricains dans les boutonnières protérozoïques d'Igherm, du Kerdous et du Bas Drâa (Anti-Atlas occidental, Maroc). *Comptes Rendus de l'Académie des Sciences - Series IIA - Earth and Planetary Science*, **327 (12)**, 819–826.

Alkmim, F., S. Marshak, A. Pedrosa-Soares, G. Peres, S. Cruz, and A. Whittington, 2006: Kinematic evolution of the Araçuaí-West Congo orogen in Brazil and Africa: Nutcracker tectonics during the Neoproterozoic assembly of Gondwana. *Precambrian Research*, **149**, 43–64.

Alkmim, F. F., S. Marshak, and M. A. Fonseca, 2001: Assembling West Gondwana in the Neoproterozoic: Clues from the São Francisco craton region, Brazil. *Geology*, **29 (4)**, 319–322.

Alvarenga, C. d., C. A. V. Moura, P. d. Sousa Gorayeb, and F. d. Assis Matos de Abreu, 2000: Paraguay and Araguaia Belts. *Tectonic Evolution of South America*, U. G. Cordani, E. Milani, A. Thomaz Filho, and D. Campos, Eds., GSA, 31st Internatnioal Geological Congress, Rio de Janeiro, 183–193.

Alvarez, P. and J.-C. Maurin, 1991: Evolution sédimentaire et tectonique du bassin protérozoïque supérieur de Comba (Congo) : Stratigraphie séquentielle du Supergroupe Ouest-Congolien et modèle d'amortissement sur décrochements dans le contexte de la tectogénèse panafricaine. *Precambrian Research*, **50 (1-2)**, 137–171.

Alvarez, P., J.-C. Maurin, and J.-P. Vicat, 1995: La formation de l'inkisi (Supergroupe ouest-congolien) en Afrique centrale (Congo et Bas-Zaïre): un delta d'âge Paléozoïque comblant un bassin en extension. *Journal of African Earth Sciences*, **20 (2)**, 119–131.

Álvaro, J. J., M. Macouin, B. Bauluz, S. Clausen, and M. Ader, 2007: The Ediacaran sedimentary architecture and carbonate productivity in the Atar cliffs, Adrar, Mauritania: Palaeoenvironments, chemostratigraphy and diagenesis. *Precambrian Research*, **153 (3-4)**, 236–261.

Amard, B., 1986: Microfossiles (Acritarches) du Proterozoique superieur dans les shales de la formation d'Atar (Mauritanie). *Precambrian Research*, **31 (1)**, 69–95.

Appel, P., V. Schenk, and A. Schumann, 2005: P-T path and metamorphic ages of pelitic schists at Murchison Falls, NW Uganda: Evidence for a Pan-African tectonometamorphic event in the Congo Craton. *Eur J Mineral*, **17 (5)**, 655–664.

Arthaud, M. H., R. Caby, R. A. Fuck, E. L. Dantas, and C. V. Parente, 2008: Geology of the northern Borborema Province, NE Brazil and its correlation with Nigeria, NW Africa. *Geological Society, London, Special Publications*, **294 (1)**, 49–67.

Attoh, K., R. D. Dallmeyer, and P. Affaton, 1997: Chronology of nappe assembly in the Pan-African Dahomeyide orogen, West Africa: evidence from 40Ar/39Ar mineral ages. *Precambrian Research*, **82 (1-2)**, 153–171.

Attoh, K., D. Hawkins, S. Bowring, and B. Allen, 1991: U-Pb zircon ages of gneisses from the Pan-African Dahomeyide orogen, West Africa. *EOS Transactions of the American Geophysical Union*, **72**, 299.

Auvray, B., J. J. Peucat, A. Potrel, J. P. Burg, C. Caruba, R. Dars, and K. Lo, 1992: New radiometric data on the Archean of the Reguibat Rise (Amsaga, Mauritania). *Comptes Rendus De L Academie Des Sciences Serie II*, **315 (1)**, 63–70.

Azzouni-Sekkal, A., J.-P. Liégeois, F. Bechiri-Benmerzoug, S. Belaidi-Zinet, and B. Bonin, 2003: The "Taourirt" magmatic province, a marker of the closing stage of the Pan-African orogeny in the Tuareg Shield: review of available data and Sr-Nd isotope evidence. *Journal of African Earth Sciences*, **37 (3-4)**, 331–350.

Babinski, M., W. R. Van Schmus, and F. Chemale, 1999: Pb-Pb dating and Pb isotope geochemistry of Neoproterozoic carbonate rocks from the São Francisco basin, Brazil: implications for the mobility of Pb isotopes during tectonism and metamorphism. *Chemical Geology*, **160 (3)**, 175–199.

Bahlburg, H., V. Carlotto, and J. Cárdenas, 2006: Evidence of Early to Middle Ordovician arc volcanism in the Cordillera Oriental and Altiplano of southern Peru, Ollantaytambo Formation and Umachiri beds. *Journal of South American Earth Sciences*, **22 (1-2)**, 52–65.

Bahlburg, H. and N. Dobrzinski, 2011: A review of the Chemical Index of Alteration (CIA) and its application to the study of Neoproterozoic glacial deposits and climate transitions. *The Geological Record of Neoproterozoic Glaciations*, E. Arnaud, G. Halverson, and G. Shields-Zhou, Eds., Geological Society, London, Memoir, London, Vol. in press.

Bahlburg, H., J. D. Vervoort, and S. A. DuFrane, 2010: Plate tectonic significance of Middle Cambrian and Ordovician siliciclastic rocks of the Bavarian Facies, Armorican Terrane Assemblage, Germany – U-Pb and Hf isotope evidence from detrital zircons. *Gondwana Research*, **17 (2-3)**, 223–235.

Banner, J. L. and G. N. Hanson, 1990: Calculation of simultaneous isotopic and trace element variations during water-rock interaction with applications to carbonate diagenesis. *Geochimica et Cosmochimica Acta*, **54 (11)**, 3123–3137.

Basei, M. A. S., H. E. Frimmel, A. P. Nutman, and F. Preciozzi, 2008: West Gondwana amalgamation based on detrital zircon ages from Neoproterozoic Ribeira and Dom Feliciano belts of South America and comparison with coeval sequences from SW Africa. *Geological Society, London, Special Publications*, **294 (1)**, 239–256.

Basei, M. A. S., O. Siga, H. Masquelin, O. Harara, J. Reis Neto, and F. Preciozzi, 2000: The Som Feliciano Belt of Brazil and Uruguay and its foreland domain. *Tectonic evolution of South America*, U. Cordani, E. Milani, A. Thomaz Filho, and D. Campos, Eds., GSA, 31st International Geological Congress, Rio de Janiero, 311–334.

Bea, F. and P. Montero, 1999: Behavior of accessory phases and redistribution of Zr, REE, Y, Th, and U during metamorphism and partial melting of metapelites in the lower crust: an example from the Kinzigite Formation of Ivrea-Verbano, NW Italy. *Geochimica et Cosmochimica Acta*, **63 (7-8)**, 1133–1153.

Benan, C. A. A. and M. Deynoux, 1998: Facies analysis and sequence stratigraphy of neoproterozoic Platform deposits in Adrar of Mauritania, Taoudeni basin, West Africa. *Geologische Rundschau*, **87 (3)**, 283–302.

Benn, D. I. and D. J. A. Evans, 1996: The interpretation and classification of subglacially-deformed materials. *Quaternary Science Reviews*, **15 (1)**, 23–52.

Bertolino, S. R. A., U. Zimmermann, and F. J. Sattler, 2007: Mineralogy and geochemistry of bottom sediments from water reservoirs in the vicinity of Córdoba, Argentina: Environmental and health constraints. *Applied Clay Science*, **36 (1-3)**, 206–220.

Bertrand-Sarfati, J., R. Flicoteaux, A. Moussine-Pouchkine, and A. A. Ait Kaci, 1997: Lower Cambrian apatitic stromatolites and phospharenites related to the glacio-eustatic cratonic rebound (Sahara, Algeria). *Journal of Sedimentary Research*, **67 (5)**, 957–974.

Bertrand-Sarfati, J., A. Moussine-Pouchkine, B. Amard, and A. AÃ¯t Kaci Ahmed, 1995: First Ediacaran fauna found in western Africa and evidence for an Early Cambrian glaciation. *Geology*, **23 (2)**, 133–136.

Bessoles, B., 1977: Géologie de l'Afrique. Le craton Ouest Africain. Tech. rep.

Bhatia, M. R. and K. A. W. Crook, 1986: Trace-Element Characteristics of Graywackes and Tectonic Setting Discrimination of Sedimentary Basins. *Contributions to Mineralogy and Petrology*, **92 (2)**, 181–193.

Bidgood, D. E. and W. B. Harland, 1961: Palaeomagnetism in some East Greenland sedimentary rocks. *Nature*, **189**, 633–634.

Biggin, A. J., G. Strik, and C. G. Langereis, 2009: The intensity of the geomagnetic field in the late-Archaean: new measurements and an analysis of the updated IAGA palaeointensity database. *Earth Planets and Space*, **61 (1)**, 9–22.

Billa, M., J.-L. Feybesse, G. Bronner, C. Lerouge, J.-P. Milési, S. Traoré, and S. Diaby, 1999: Les formations à quartzites rubanés ferrugineux des Monts Nimba et du Simandou: des unités empilées tectoniquement, sur un soubassement plutonique Archéen (craton de Kénéma-Man), lors de l'orogène Éburnéen. *Comptes Rendus de l'Académie des Sciences - Series IIA - Earth and Planetary Science*, **329 (4)**, 287–294.

Binda, P. L. and J. G. Van Eden, 1972: Sedimentological evidence on the origin of the Precambrian Great Conglomerate (Kundelungu Tillite), Zambia. *Palaeogeography, Palaeoclimatology, Palaeoecology*, **12 (3)**, 151–168.

Bingen, B., D. Demaiffe, and O. Breemen, 1998: The 616 Ma Old Egersund Basaltic Dike Swarm, SW Norway, and Late Neoproterozoic Opening of the Iapetus Ocean. *The Journal of Geology*, **106 (5)**, 565–574.

Bingen, B. and A. Solli, 2009: Geochronology of magmatism in the Caledonian and Sveconorwegian belts of Baltica: synopsis for detrital zircon provenance studies. *Norwegian Journal of Geology*, **89 (4)**, 267–290.

Bingen, B., et al., 2005: Timing of continental building in the Sveconorwegian orogen, SW Scandinavia. *Norwegian Journal of Geology*, **85**, 87–116.

Bispo-Santos, F., et al., 2008: Columbia revisited: Paleomagnetic results from the 1790 Ma colider volcanics (SW Amazonian Craton, Brazil). *Precambrian Research*, **164 (1-2)**, 40–

49.

Black, R., L. Latouche, J. Liégeois, R. Caby, and J. M. Bertrand, 1994: Pan-African displaced terranes in the Tuareg shield (central Sahara). *Geology*, **22 (7)**, 641–644.

Blanc, A., J. Bernard-Griffiths, R. Caby, C. Caruba, R. Caruba, R. Dars, S. Fourcade, and J. J. Peucat, 1992: U-Pb dating and isotopic signature of the alkaline ring complexes of Bou Naga (Mauritania): its bearing on late proterozoic plate tectonics around the West African craton. *Journal of African Earth Sciences*, **14 (3)**, 301–311.

Bleeker, W., J. Ketchum, and W. Davis, 1999: The Central Slave Basement Complex, Part II: age and tectonic significance of high-strain zones along the basement-cover contact. *Canadian Journal of Earth Sciences*, **36 (7)**, 1111–1130.

Boher, M., W. Abouchami, A. Michard, F. Albarede, and N. T. Arndt, 1992: Crustal Growth in West Africa at 2.1 Ga. *J. Geophys. Res.*, **97 (B1)**, 345–369.

Bond, G. C., P. A. Nickeson, and M. A. Kominz, 1984: Breakup of a supercontinent between 625 Ma and 555 Ma: new evidence and implications for continental histories. *Earth and Planetary Science Letters*, **70 (2)**, 325–345.

Borg, G. and R. Armstrong, 2002: Isotopic SHRIMP age dating of zircons from igneous basement and rhyolitic cover rocks at Skorpion, Souther Namibia. *11th Symposium of IAGOD and GEOCONGRESS*, Windhoek, 4.

Boudzoumou, F. and R. Trompette, 1988: La chaîne panafricaine ouest-congolienne au Congo (Afrique Equatoriale): un socle polycylique charrié sur un domaine subautochtone formé par l'aulacogène du Mayombe et le bassin de l'Ouest-Congo. *Bull. Soc. Géol. Fr.*, **6**, 889–896.

Boulton, G. S., 1972: Modern Arctic glaciers as depositional models for former ice sheets. *Journal of the Geological Society*, **128 (4)**, 361–393.

Bousquet, R., R. El Mamoun, O. Saddiqi, B. Goffe, A. Moller, and A. Madi, 2008: Melanges and ophiolites during the Pan-African orogeny: the case of the Bou-Azzer ophiolite suite (Morocco). *Geological Society, London, Special Publications*, **297 (1)**, 233–247.

Bowring, S., P. Myrow, E. Landing, J. Ramezani, and J. Grotzinger, 2003: Geochronological constraints on terminal Proterozoic events and the rise of metazoans. *Geophys. Res. Abstr. (EGS, Nice)*, **5 (13219)**.

Bowring, S. A., J. P. Grotzinger, D. J. Condon, J. Ramezani, M. J. Newall, and P. A. Allen, 2007: Geochronologic constraints on the chronostratigraphic framework of the Neoproterozoic Huqf Supergroup, Sultanate of Oman. *Am J Sci*, **307 (10)**, 1097–1145.

Brasier, M., G. McCarron, R. Tucker, J. Leather, P. Allen, and G. Shields, 2000: New U-Pb zircon dates for the Neoproterozoic Ghubrah glaciation and for the top of the Huqf Supergroup, Oman. *Geology*, **28 (2)**, 175–178.

Briden, J. C., 1968: Paleomagnetism of the Ntonya Ring Structure, Malawi. *Journal of Geophyisical Research*, **73**.

Briden, J. C., E. McClelland, and D. C. Rex, 1993: Proving the Age of a Paleomagnetic Pole - the Case of the Ntonya Ring Structure, Malawi. *Journal of Geophysical Research-Solid Earth*, **98 (B2)**, 1743–1749.

Brito Neves, B., M. Campos Neto, and R. A. Fuck, 1999: From Rodinia to Western Gondwana: an approach to the Brasiliano-Pan African cycle and orogenic collage. *Episodes*, **22**, 155–166.

Brito Neves, B., E. Santos, and W. R. Van Schmus, 2000: Tectonic history of the Borborema Province. *Tectonic Evolution of South America*, U. Cordani, E. Milani, A. Thomaz Filho, and D. Campos, Eds., GSA, 31st International Geological Congress, Rio de Janeiro, 151–182.

Brito Neves, B. B., R. A. Fuck, U. G. Cordani, and A. Thomaz Filho, 1984: Influence of basement structures on the evolution of the major sedimentary basins of Brazil: A case

of tectonic heritage. *Journal of Geodynamics*, **1 (3-5)**, 495–510.

Brito Neves, B. B. d. and U. G. Cordani, 1991: Tectonic evolution of South America during the Late Proterozoic. *Precambrian Research*, **53 (1-2)**, 23–40.

Brito Neves, B. d., W. van Schmus, E. Dos Santos, M. Campos Neto, and M. Kozuch, 1995: O evento Cariris Velhos na Província Borborema: integração de dados, implicações e perspectivas. *Revista Brasileira de Geociências*, **25 (4)**, 279–296.

Brock, A., 1967: Palaeomagnetic Result from the Hook Intrusives of Zambia. *Nature*, **216 (5113)**, 359–360.

Bronner, G., J. Roussel, R. Trompette, and N. Clauer, 1980: Genesis and geodynamic evolution of the Taoudeni Cratonic Basin (Upper Precambrian and Paleozoic), Western Africa. *Dynamics of Plate Interior Geodynamics Series*, American Geophysical Union, Vol. 1, 81–90.

Brookfield, M. E., 1993: Neoproterozoic Laurentia-Australia fit. *Geology*, **21 (8)**, 683–686.

Buchan, K., R. Ernst, M. Hamilton, S. Mertanan, L. Pesonen, and S.-A. Elming, 2001: Rodinia: the evidence from integrated palaeomagnetism and U-Pb geochronology. *Precambrian Research*, **110**, 9–32.

Buchan, K. L., S. Mertanen, R. G. Park, L. J. Pesonen, S. Å. Elming, N. Abrahamsen, and G. Bylund, 2000: Comparing the drift of Laurentia and Baltica in the Proterozoic: the importance of key palaeomagnetic poles. *Tectonophysics*, **319 (3)**, 167–198.

Budyko, M., 1969: The effect of solar radiation variations on the climate of the Earth. *Tellus*, **21**, 611–619.

Bullard, E., J. Everett, and A. Smith, 1965: The fit of the continents around the Atlantic: Symposium on Continental Drift. *Philosophical Transactions of the Royal Society of London*, **258**, 41–51.

Burrett, C. and R. Berry, 2000: Proterozoic Australia-Western United States (AUSWUS) fit between Laurentia and Australia. *Geology*, **28 (2)**, 103–106.

Caby, R., 1989: Precambrian terranes of Benin Nigeria and Northeast Brazil and the Late Proterozoic South Atlantic. *Terranes in the Circum-Atlantic Paleozoic Orogens*, R. D. Dallmeyer, Ed., Geological Society of America, Special Papers, Vol. 230, 145–158.

Caby, R., 1994: Precambrian coesite from northern Mali: first record and implications for plate tectonics in the trans-Saharan segment of the Pan-African belt. *European Journal of Mineralogy*, **6**, 145–158.

Caby, R., 1996: Rapport de la mission de terrain dans le Grand Sud-Ouest Algérien (7-22 novembre 1996). Tech. rep.

Caby, R., 2003: Terrane assembly and geodynamic evolution of central-western Hoggar: a synthesis. *Journal of African Earth Sciences*, **37 (3-4)**, 133–159.

Caby, R., C. Delor, and O. Agoh, 2000: Lithologie, structure et métamorphisme des formations birimiennes dans la région d'Odienné (Côte d'Ivoire): rôle majeur du diapirisme des plutons et des décrochements en bordure du craton de ManLithology, structure and metamorphism of the Birimian formations in the Odienné area [Ivory Coast]: the major role played by plutonic diapirism and strike-slip faulting at the border of the Man Craton. *Journal of African Earth Sciences*, **30 (2)**, 351–374.

Caen-Vachette, M., Y. Vialette, J.-P. Bassot, and P. Vidal, 1988: Apport de la géochronologie isotopique à la connaissance de la géologie gabonaise. *Chronique de la Recherche Minière*, **491**, 35–54.

Cahen, L., 1978: La stratigraphie et la tectonique du Supergroupe Ouest-Congolien dans les zones médiane et externe de l'orogène Ouest-Congolien (Pan-Africain) au Bas-zaire et dans les régions voisines. *Annals of the Royal Museum for Central Africa, Tervuren, in-8°, Sci. Géol.*, **83**, 150.

Cahen, L., 1982: Geochronological correlation of the late precambrian sequences on and around the stable zones of equatorial Africa. *Precambrian Research*, **18**, 73–86.

Cahen, L. and J. Lepersonne, 1981a: Proterozoic diamictites of Lower Zaïre. *In: Hambrey, M.J., and Harland, W.B., editors, Earth's Pre-Pleistocene Glacial Record: Cambridge, Cambridge University Press*, 153–157.

Cahen, L. and J. Lepersonne, 1981b: Upper Proterozoic diamictites of Shaba (formerly Katanga) and neighbouring regions of Zambia. *in: Hambrey, M.J., and Harland, W.B., editors, Earth's Pre-Pleistocene Glacial Record: Cambridge, Cambridge University Press*, 162–166.

Cahen, L., N. Snelling, J. Delhal, J. Vail, M. Bonhomme, and D. Ledent, 1984: *The Geochronology and Evolution of Africa*. Clarendon Press, Oxford.

Calver, C. R., L. P. Black, J. L. Everard, and D. B. Seymour, 2004: U-Pb zircon age constraints on late Neoproterozoic glaciation in Tasmania. *Geology*, **32 (10)**, 893–896.

Calver, C. R. and M. R. Walter, 2000: The late Neoproterozoic Grassy Group of King Island, Tasmania: correlation and palaeogeographic significance. *Precambrian Research*, **100 (1-3)**, 299–312.

Carvalho, H., J. P. Crasto, Z. C. G. Silva, and Y. Vialette, 1987: The Kibaran cycle in Angola - a discussion. *Geological Journal*, **22 (S2)**, 85–102.

Carvalho, H. d., C. Tassinari, P. M. Alves, F. Guimarães, and M. C. Simões, 2000: Geochronological review of the Precambrian in western Angola: links with Brazil. *Journal of African Earth Sciences*, **31 (2)**, 383–402.

Chardon, D., 1997: Les déformations continentales archéennes. Exemples naturels et modèlisation thermomécanique. Tech. rep., Rennes.

Clauer, N., 1976: Chimie isotopique du strontium des milieux sédimentaires. Application à la géochronologie de la couverture du craton ouest-africain. *Mem. Sci. Geol.*, **45**, 1–256.

Clauer, N. and A. Kröner, 1979: Strontium and argon isotopic homogenization of pelitic sediments during low-grade regional metamorphism: The pan-African upper Damara sequence of Northern Namibia (South West Africa). *Earth and Planetary Science Letters*, **43 (1)**, 117–131.

Coleman, A., 1926: *Ice Ages: Recent and Ancient*. Macmillan, London.

Coleman, A., 1932: Glaciations and continental drift. *Geographical Journal*, **LXXIX**, 252–255.

Coleman, A., 1939: Ice ages in the geological column. *Geological Society of America Bulletin*, **50**, 449–452.

Condie, K. C., 1993: Chemical composition and evolution of the upper continental crust: Contrasting results from surface samples and shales. *Chemical Geology*, **104 (1-4)**, 1–37.

Condie, K. C., 2002a: Breakup of a Paleoproterozoic Supercontinent. *Gondwana Research*, **5 (1)**, 41–43.

Condie, K. C., 2002b: The supercontinent cycle: are there two patterns of cyclicity? *Journal of African Earth Sciences*, **35 (2)**, 179–183.

Condie, K. C., E. Belousova, W. L. Griffin, and K. N. Sircombe, 2009a: Granitoid events in space and time: Constraints from igneous and detrital zircon age spectra. *Gondwana Research*, **15 (3-4)**, 228–242.

Condie, K. C., C. O'Neill, and R. C. Aster, 2009b: Evidence and implications for a widespread magmatic shutdown for 250 My on Earth. *Earth and Planetary Science Letters*, **282 (1-4)**, 294–298.

Condie, K. C. and D. J. Wronkiewicz, 1990: The Cr/Th ratio in Precambrian pelites from the Kaapvaal Craton as an index of craton evolution. *Earth and Planetary Science Letters*, **97 (3-4)**, 256–267.

Condon, D., M. Zhu, S. Bowring, W. Wang, A. Yang, and Y. Jin, 2005: U-Pb Ages from the Neoproterozoic Doushantuo Formation, China. *Science*, **308**, 95–98.

Cordani, U. G., M. S. D'Agrella-Filho, B. B. Brito-Neves, and R. I. F. Trindade, 2003: Tearing up Rodinia: the Neoproterozoic palaeogeography of South American cratonic fragments. *Terra Nova*, **15 (5)**, 350–359.

Cordani, U. G., K. Sato, W. Teixeira, C. C. G. Tassinari, and M. A. S. Basei, 2000: Crustal evolution of the South American platform. *Tectonic Evolution of South America*, U. G. Cordani, E. Milani, A. Thomaz Filho, and D. Campos, Eds., GSA, 31st International Geological Congress, Rio de Janeiro, 19–40.

Cordani, U. G. and W. Teixeira, 2007: Proterozoic accretionary belts in the Amazonian Craton. *Geological Society of America Memoirs*, **200**, 297–320.

Corsetti, F. and N. Lorentz, 2006: On Neoproterozoic Cap Carbonates as Chronostratigraphic Markers. *Neoproterozoic Geobiology and Paleobiology*, S. Xiao and A. Kaufman, Eds., Springer, 273–294.

Corsetti, F. A. and A. J. Kaufman, 2003: Stratigraphic investigations of carbon isotope anomalies and Neoproterozoic ice ages in Death Valley, California. *Geological Society of America Bulletin*, **115 (8)**, 916–932.

Crawford, A. R. and B. Daily, 1971: Probable Non-synchroneity of Late Precambrian Glaciations. *Nature*, **230 (5289)**, 111–112.

Culver, S. and D. Hunt, 1991: Lithostratigraphy of the Precambrian-Cambrian boundary sequence in the southwestern Taoudeni Basin, West Africa. *Journal of African Earth Sciences*, **13 (3/4)**, 407–413.

Culver, S. J., J. Pojeta, and J. E. Repetski, 1988: First record of Early Cambrian shelly microfossils from west Africa. *Geology*, **16 (7)**, 596–599.

da Silva, L. C., A. C. Pedrosa-Soares, T. L. R., and R. Armstrong, 2008: Tonian rift-related, A-type continental plutonism in the Araçuaí Orogen, eastern Brazil: New evidence for the breakup stage of the São Francisco-Congo Paleocontinent. *Gondwana Research*, **13 (4)**, 527–537.

Dada, S. S., 2008: Proterozoic evolution of the Nigeria-Boborema province. *Geological Society, London, Special Publications*, **294 (1)**, 121–136.

D'Agrella-Filho, M. S., M. Babinski, R. I. F. Trindade, W. R. Van Schmus, and M. Ernesto, 2000: Simultaneous remagnetization and U-Pb isotope resetting in Neoproterozoic carbonates of the São Francisco craton, Brazil. *Precambrian Research*, **99 (3-4)**, 179–196.

D'Agrella-Filho, M. S., I. I. G. Pacca, R. I. F. Trindade, W. Teixeira, M. I. B. Raposo, and T. C. Onstott, 2004: Paleomagnetism and 40Ar/39Ar ages of mafic dikes from Salvador (Brazil): new constraints on the São Francisco craton APW path between 1080 and 1010 Ma. *Precambrian Research*, **132 (1-2)**, 55–77.

D'Agrella-Filho, M. S., E. Tohver, J. a. O. S. Santos, S.-Å. Elming, R. I. F. Trindade, I. I. G. Pacca, and M. C. Geraldes, 2008: Direct dating of paleomagnetic results from Precambrian sediments in the Amazon craton: Evidence for Grenvillian emplacement of exotic crust in SE Appalachians of North America. *Earth and Planetary Science Letters*, **267 (1-2)**, 188–199.

Dallmeyer, R. D. and J. P. Lecorche, 1990: 40 Ar/ 39 Ar polyorogenic mineral age record within the southern Mauritanide Orogen (M'Bout-Bakel region), West Africa. *Am J Sci*, **290 (10)**, 1136–1168.

Dallmeyer, R. D. and J. P. Lecorche, 1991: *The West African Orogens and Circum-Atlantic Correlatives*. Springer, Berlin.

Daly, M. C., S. R. Lawrence, K. Diemu-Tshiband, and B. Matouana, 1992: Tectonic evolution of the Cuvette Centrale, Zaire. *Journal of the Geological Society*, **149 (4)**, 539–546.

Dalziel, I., 1997: Neoproterozoic-Paleozoic geography and tectonics: Review, hypothesis,

environmental speculation. *GSA Bulletin*, **109 (1)**, 16–42.

Dalziel, I. W., 1991: Pacific margins of Laurentia and East Antarctica-Australia as a conjugate rift pair: Evidence and implications for an Eocambrian supercontinent. *Geology*, **19 (6)**, 598–601.

Danderfer, A., B. De Waele, A. J. Pedreira, and H. A. Nalini, 2009: New geochronological constraints on the geological evolution of Espinhaço basin within the São Francisco Craton–Brazil. *Precambrian Research*, **170 (1-2)**, 116–128.

De Paepe, P., J. Hertogen, and L. Tack, 1975: Mise en évidence de laves en coussins dans les faciès volcaniques basiques du massif de Kimbungu (Bas-Zaïre) et implications pour le magmatisme ouest-congolien. *Annales Société Géologique Belgique*, **98**, 251–270.

De Waele, B., S. Johnson, and S. Pisarevsky, 2008: Palaeoproterozoic to Neoproterozoic growth and evolution of the eastern Congo Craton: Its role in the Rodinia puzzle. *Precambrian Research*, **160 (1-2)**, 127–141.

de Wit, M. J., J. Stankiewicz, and C. Reeves, 2008: Restoring Pan-African-Brasiliano connections: more Gondwana control, less Trans-Atlantic corruption. *Geological Society, London, Special Publications*, **294 (1)**, 399–412.

Deblond, A., L. E. Punzalan, A. Boven, and L. Tack, 2001: The Malagarazi supergroup of southeast Burundi and its correlative Bukoba supergroup of northwest Tanzania: Neo- and Mesoproterozoic chronostratigraphic constraints from Ar-Ar ages on mafic intrusive rocks. *Journal of African Earth Sciences*, **32 (3)**, 435–449.

Dekkers, M. J., 1989: Magnetic properties of natural pyrrhotite. II. High- and low-temperature behaviour of Jrs and TRM as function of grain size. *Physics of the Earth and Planetary Interiors*, **57 (3-4)**, 266–283.

Delhal, J. and D. Ledent, 1976: Age et évolution comparée des gneiss migmatitiques prézadiniens des régions de Boma et de Mpozo-Tombagadio (Bas-Zaïre). *Annales Société Géologique Belgique*, **99**, 165–187.

Delhaye, F. and Sluys, 1923-4 and 1928-9: Observations ayant servi a l'elaboration de l' "Esquisse géologique du Congo occidental". Etude du systeme Schisto-Calcaire. *Annales Société Géologique Belgique*, **1er - 3er memoire**, 50–91 et 69–114.

Delpomdor, F., 2007: Lithostratigraphie et sédimentologie de la chaîne Ouest Congolienne du Néoprotérozoïque supérieur (Formation de la Diamictite supérieure et Sous-Groupe du Schisto-Calcaire) Bas-Congo, République Démocratique du Congo. Ph.D. thesis, Université libre de Bruxelles.

Delpomdor, F., A. R. Préat, and L. Tack, 2009: Microstructures within glaciogenic Neoproterozoic Diamictites around the Congo River Basin (CRB) in Democratic Republic of Congo - a comparative micromorphological study. *Rodinia: Supercontinents, Superplumes and Scotland*, Geological Society of London Fermor Meeting 2009, Edinburgh, Scotland.

Delpomdor, F., L. Tack, and A. R. Preat, 2008: Microstructures in the Neoproterozoic tillites around the Congo River Basin (CRB, Democratic Republic of the Congo (DRC) - Comparison with the Karoo tillites from the Dekese borehole in the CRB. *22nd Colloquium African Geology (CAG22)*, Hammamet, Tunisia, Vol. Abstracts volume 108.

Des Marais, D. J. and J. G. Moore, 1984: Carbon and its isotopes in mid-oceanic basaltic glasses. *Earth and Planetary Science Letters*, **69 (1)**, 43–57.

Desjardins, P. R., M. Mángano, L. A. Buatois, and B. R. Pratt, 2010: Skolithos pipe rock and associated ichnofabrics from the southern Rocky Mountains, Canada: colonization trends and environmental controls in an early Cambrian sand-sheet complex. *Lethaia*, **in press**.

Deynoux, M., 1980: Les formations glaciaires du Précambrien terminal et de la fin de l'Ordovicien en Afrique de l'ouest. Deux exemples de glaciation d'inlandis sur une plateforme stable. Tech. rep., Marseille.

Deynoux, M., 1982: Periglacial polygonal structures and sand wedges in the late precambrian glacial formations of the taoudeni basin in Adrar of Mauretania (West Africa). *Palaeogeography, Palaeoclimatology, Palaeoecology*, **39 (1-2)**, 55–70.

Deynoux, M., 1985: Terrestrial or waterlain glacial diamictites? Three case studies from the late Precambrian and late Ordovician glacial drifts in West Africa. *Palaeogeography, Palaeoclimatology, Palaeoecology*, **51 (1-4)**, 97–141.

Deynoux, M., P. Affaton, R. Trompette, and M. Villeneuve, 2006: Pan-African tectonic evolution and glacial events registered in Neoproterozoic to Cambrian cratonic and foreland basins of West Africa. *Journal of African Earth Sciences*, **46 (5)**, 397–426.

Deynoux, M., J. Sougy, and R. Trompette, 1985: Lower Palaeozoic rocks of West Africa and the Western part of Central Africa. *Lower Palaeozoic of North-western and West-central Africa*, C. Holland, Ed., Wiley, Chichester, 337–495.

Deynoux, M. and R. Trompette, 1976: Late Precambrian mixtites: glacial and/or nonglacial? Dealing especially with the mixtites of West Africa. *American Journal of Science*, **276 (10)**, 1302–1315.

Deynoux, M. and R. Trompette, 1981: Late Precambrian tillites of the Taoudeni Basin. *Earth's Pre-Pleistocene Glacial Record*, W. Harland and M. Hambrey, Eds., Cambridge University Press, 123–131.

Deynoux, M., R. Trompette, N. Clauer, and J. Sougy, 1978: Upper Precambrian and Lowermost Palaeozoic correlations of West Africa and in the Western Part of Central Africa. Probable diachronism of the Late Precambrian tillite. *Geologische Rundschau*, **67 (2)**, 615–630.

Dillon, W. and J. Sougy, 1974: Geology of west Afica and Canary and Cape Verde Islands. *The Ocean Basins and Margins*, A. E. M. Nairn and F. Stehl, Eds., Plenum, New York, Vol. 2, The North Atlantic, 315–390.

Djama, L., 1988: Le massif granitique de Mfoubou et le socle métamorphique de Guéna (chaîne du Mayombe-Congo). Pétrologie-Géochimie-Géochronologie. Ph.D. thesis, Université Nancy, 175 pp.

Donnadieu, Y., F. Fluteau, G. Ramstein, C. Ritz, and J. Besse, 2003: Is there a conflict between the Neoproterozoic glacial deposits and the snowball Earth interpretation: an improved understanding with numerical modeling. *Earth Planet. Sci. Lett.*, **208**, 101–112.

Dostal, J., R. Caby, C. Dupuy, C. Mevel, and J. Owen, 1996: Inception and demise of a Neoproterozoic ocean basin: evidence from the Ougda complex, western Hoggar (Algeria). *Geologische Rundschau*, **85 (4)**, 619–631.

Dostal, J., R. Caby, J. D. Keppie, and M. Maza, 2002: Neoproterozoic magmatism in Southwestern Algeria (Sebkha el Melah inlier): a northerly extension of the Trans-Saharan orogen. *Journal of African Earth Sciences*, **35 (2)**, 213–225.

Doumbia, S., A. Pouclet, A. Kouamelan, J. J. Peucat, M. Vidal, and C. Delor, 1998: Petrogenesis of juvenile-type Birimian (Paleoproterozoic) granitoids in Central Côte-d'Ivoire, West Africa: geochemistry and geochronology. *Precambrian Research*, **87 (1-2)**, 33–63.

Dunlop, D. and Ö. Özdemir, 1997: *Rock Magnetism: Fundamentals and Frontiers*. Cambridge University Press.

Dunphy, J. M. and J. N. Ludden, 1998: Petrological and geochemical characteristics of a Paleoproterozoic magmatic arc (Narsajuaq terrane, Ungava Orogen, Canada) and comparisons to Superior Province granitoids. *Precambrian Research*, **91 (1-2)**, 109–142.

Dussin, I. and T. Dussin, 1995: Suerprupo Espinhaço: Modelo de evolução geodinãmica. *Geonomos*, **3**, 19–26.

Dutoit, A., 1921: Land connections between the other continents and South Africa in the past. *South African Journal of Geology*, **18**, 120–140.

Dürr, S. B. and D. P. Dingeldey, 1996: The Kaoko belt (Namibia): Part of a late Neoproterozoic continental-scale strike-slip system. *Geology*, **24 (6)**, 503–506.

Eagles, G., 2007: New angles on South Atlantic opening. *Geophysical Journal International*, **168 (1)**, 353–361.

Edwards, M., 1984: Sedimentology of the Upper Proterozoic glacial record, Vestertana Group, Finnmark, North Norway. *Norges Geologiske Undersøkelse Bulletin*, **394**, 1–76.

Ellwood, B. B., W. Balsam, B. Burkart, G. J. Long, and M. L. Buhl, 1986: Anomalous Magnetic Properties in Rocks Containing the Mineral Siderite: Paleomagnetic Implications. *J. Geophys. Res.*, **91 (B12)**, 12 779–12 790.

Elming, S., S. Kravchenko, P. Layer, O. Rusakov, A. Glevasskaya, N. Mikhailova, and V. Bachtadse, 2007: Palaeomagnetism and 40Ar/39Ar age determinations of the Ediacaran traps from the southwestern margin of the East European Craton, Ukraine: relevance to the Rodinia break-up. *Journal of the Geological Society*, **164 (5)**, 969–982.

Elming, S.-A., M. S. D'Agrella-Filho, L. M. Page, E. Tohver, R. I. Trindade, I. I. Pacca, M. C. Geraldes, and W. Teixeira, 2009: A palaeomagnetic and $^{40}Ar/^{39}Ar$ study of late precambrian sills in the SW part of the Amazonian craton: Amazonia in the Rodinia reconstruction. *Geophysical Journal International*, **178 (1)**, 106–122.

Embleton, B. and G. Williams, 1986: Low palaeolatitude of deposition for late Precambrian periglacial varvites in South Australia: Implications for paleoclimatology. *Earth Planet. Sci. Lett.*, **79**, 419–430.

Ennih, N. and J.-P. Liégeois, 2001: The Moroccan Anti-Atlas: the West African craton passive margin with limited Pan-African activity. Implications for the northern limit of the craton. *Precambrian Research*, **112 (3-4)**, 289–302.

Ennih, N. and J.-P. Liegeois, 2008: The boundaries of the West African craton, with special reference to the basement of the Moroccan metacratonic Anti-Atlas belt. *Geological Society, London, Special Publications*, **297 (1)**, 1–17.

Evans, D., 2000: Stratigraphic, geochronological and paleomagnetic constraints upon the Neoproterozoic climatic paradox. *American Journal of Science*, **3000**, 347–433.

Evans, D., 2003: A fundamental Precambrian-Phanerozoic shift in earth's glacial style? *Tectonophysics*, **375**, 353–385.

Evans, D., 2006: Proterozoic low orbital obliquity and axial-dipolar geomagnetic field from evaporite palaeolatitudes. *Nature*, **444**, 51–55.

Evans, D. A. D., 2009: The palaeomagnetically viable, long-lived and all-inclusive Rodinia supercontinent reconstruction. *Geological Society, London, Special Publications*, **327 (1)**, 371–404.

Evans, D. A. D., Z. X. Li, J. L. Kirschvink, and M. T. D. Wingate, 2000: A high-quality mid-Neoproterozoic paleomagnetic pole from South China, with implications for ice ages and the breakup configuration of Rodinia. *Precambrian Research*, **100 (1-3)**, 313–334.

Eyles, C. H. and N. Eyles, 1983: Sedimentation in a large lake: A reinterpretation of the late Pleistocene stratigraphy at Scarborough Bluffs, Ontario, Canada. *Geology*, **11 (3)**, 146–152.

Eyles, N., 1993: Earth's glacial record and its tectonic setting. *Earth-Science Reviews*, **35 (1-2)**, 1–248.

Eyles, N. and N. Januszczak, 2004: 'Zipper-rift': a tectonic model for Neoproterozoic glaciations during the breakup of Rodinia after 750 Ma. *Earth-Science Reviews*, **65**, 1–73.

Fanning, C. and P. Link, 2004: U-Pb SHRIMP ages of Neoproterozoic (Sturtian) glaciogenic Pocatello Formation, southeastern Idaho. *Geology*, **32**, 881–884.

Fanning, C. and P. Link, 2008: Age constraints for the Sturtian Glaciation; data from the Adelaide Geosyncline, South Australia and Pocatello Formation, Idaho, USA. *Neopro-*

terozoic extreme climates and the origin of early metazoan life, Selwyn Symposium of the GSA Victoria Division, S. Gallagher and M. Wallace, Eds., Geological Society of Australia Extended Abstracts, Vol. 91, 57–62.

Fedo, C. M., H. W. Nesbitt, and G. M. Young, 1995: Unraveling the Effects of Potassium Metasomatism in Sedimentary-Rocks and Paleosols, with Implications for Paleoweathering Conditions and Provenance. *Geology*, **23 (10)**, 921–924.

Fekkak, A., M. Boualoul, L. Badra, M. Amenzou, A. Saquaque, and I. E. El-Amrani, 2000: Origine et contexte geotectonique des depots detritiques du groupe neoproterozoïque inferieur de Kelaat Mgouna (Anti-Atlas Oriental, Maroc)Origin and geotectonic setting of lower neoproterozoic kelaat Mgouna detrital material [eastern Anti-Atlas, Morocco]. *Journal of African Earth Sciences*, **30 (2)**, 295–311.

Fetter, A. H., T. J. Saraiva dos Santos, W. R. Van Schmus, P. C. Hackspacher, B. Bley de Brito Neves, M. H. Arthaud, J. A. Nogueira Neto, and E. Wernick, 2003: Evidence for Neoproterozoic Continental Arc Magmatism in the Santa Quitéria Batholith of Ceará State, NW Borborema Province, NE Brazil: Implications for the Assembly of West Gondwana. *Gondwana Research*, **6 (2)**, 265–273.

Fetter, A. H., W. R. Van Schmus, T. Santos, J. A. Nogueira Neto, and M. H. Arthaud, 2000: U-Pb and Sm-Nd geochonological constraints on the crustal evolution and basement architecture of Ceará State, NW Borborema province, NE Brazil: implications for the existence of the Paleoproterozoic supercontinent 'Atlantica'. *Revista Brasileira de Geociências*, **30**, 102–106.

Feybesse, J.-L. and J.-P. Milési, 1994: The Archaean/Proterozoic contact zone in West Africa: a mountain belt of décollement thrusting and folding on a continental margin related to 2.1 Ga convergence of Archaean cratons? *Precambrian Research*, **69 (1-4)**, 199–227.

Fisher, R., 1953: Dispersion on a sphere. *Proceedings of the Royal Society of London*, **A217**, 295–305.

Flicoteaux, R. and R. Trompette, 1998: Cratonic and foreland Early Cambrian phosphorites of West Africa: palaeoceanographical and climatical contexts. *Palaeogeography, Palaeoclimatology, Palaeoecology*, **139 (3-4)**, 107–120.

Flint, R., 1957: *Glacial Geology and the Pleistocene Epoch*. Wiley, New York.

Floyd, P. A. and J. A. Winchester, 1978: Identification and discrimination of altered and metamorphosed volcanic rocks using immobile elements. *Chemical Geology*, **21 (3-4)**, 291–306.

Font, E., A. Nedelec, R. I. F. Trindade, M. Macouin, and A. Charriere, 2006: Chemostratigraphy of the Neoproterozoic Mirassol d'Oeste cap dolostones (Mato Grosso, Brazil): An alternative model for Marinoan cap dolostone formation. *Earth and Planetary Science Letters*, **250 (1-2)**, 89–103.

Fralick, P., 2003: Geochemistry of clastic sedimentary rocks: ratio techniques. *Geochemistry of Sediments and Sedimentary Rocks: Evolutionary Considerations to Mineral-Deposit-Forming Environments*, D. R. Lentz, Ed., Geological Association of Canada, GEOText, 4th ed., 85–104.

Franssen, L. and L. André, 1988: The Zadinian Group (late Proterozoic, Zaire) and its bearing on the origin of the West-Congo orogenic belt. *Precambrian Research*, **38 (3)**, 215–234.

Friedl, G., F. Finger, N. J. McNaughton, and I. R. Fletcher, 2000: Deducing the ancestry of terranes: SHRIMP evidence for South America-derived Gondwana fragments in central Europe. *Geology*, **28 (11)**, 1035–1038.

Frimmel, H., L. Tack, M. Basei, A. Nutman, and A. Boven, 2006: Provenance and chemostratigraphy of the Neoproterozoic West Congolian Group in the Democratic Republic of Congo. *Journal of African Earth Sciences*, **46**, 221–239.

Frimmel, H. E., 2009: Trace element distribution in Neoproterozoic carbonates as palaeoenvironmental indicator. *Chemical Geology*, **258 (3-4)**, 338–353.

Frimmel, H. E., 2010: On the reliability of stable carbon isotopes for Neoproterozoic chemostratigraphic correlation. *Precambrian Research*, **In Press, Corrected Proof**.

Frimmel, H. E. and W. Frank, 1998: Neoproterozoic tectono-thermal evolution of the Gariep Belt and its basement, Namibia and South Africa. *Precambrian Research*, **90 (1-2)**, 1–28.

Frischbutter, A., Y. Callec, O. Reynolds, and O. Serrano, 2009: New evidence for Marinoan and Hirnantian glaciation events and the significance for hydrocarbon potential in the Northern Taoudeni Basin, Mauritania. *Glaciogenic Reservoirs and Hydrocarbon Systems*, The Geological Society of London, London.

Garven, G., 1995: Continental-Scale Groundwater Flow and Geologic Processes. *Annual Review of Earth and Planetary Sciences*, **23 (1)**, 89–117.

Geikie, J., 1894: *The Great Ice Age*. 3rd ed. Spottiswoode and Co., London.

Geisler, T., R. T. Pidgeon, W. van Bronswijk, and R. Kurtz, 2002: Transport of uranium, thorium, and lead in metamict zircon under low-temperature hydrothermal conditions. *Chemical Geology*, **191 (1-3)**, 141–154.

Geisler, T., A. A. Rashwan, M. K. W. Rahn, U. Poller, H. Zwingmann, R. T. Pidgeon, H. Schleicher, and F. Tomaschek, 2003: Low-temperature hydrothermal alteration of natural metamict zircons from the Eastern Desert, Egypt. *Mineral Mag*, **67 (3)**, 485–508.

Geissman, J. W., M. Jackson, S. S. Harlan, and R. Van Der Voo, 1991: Paleomagnetism of Latest Cambrian-Early Ordovician and Latest Cretaceous-Early Tertiary Rocks of the Florida Mountains, Southwest New Mexico. *J. Geophys. Res.*, **96 (B4)**, 6053–6071.

Germs, G. J. B., 1995: The Neoproterozoic of southwestern Africa, with emphasis on platform stratigraphy and paleontology. *Precambrian Research*, **73 (1-4)**, 137–151.

Gevers, T., 1931: An ancient tillite in South West Africa. *Trans. Geol. Soc. S. Afr.*, **34**, 1–17.

Gifkins, C., W. Herrmann, and R. Large, 2005: *Altered Volcanic Rocks; A guide to description and interpretation*. CODES, Univeristy of Tasmania, Hobart, Australia.

Gillett, S. L. and D. R. Van Alstine, 1982: Remagnetization and tectonic rotation of Upper Precambrian and Lower Paleozoic strata from the desrt range, southern Nevada. *J. Geophys. Res.*, **87 (B13)**, 10 929–10 953.

Goodwin, A., 1996: *Principles of Precambrian geology*. Academic Press, London.

Goscombe, B., R. Armstrong, and J. M. Barton, 2000: Geology of the Chewore Inliers, Zimbabwe: constraining the Mesoproterozoic to Palæozoic evolution of the Zambezi Belt. *Journal of African Earth Sciences*, **30 (3)**, 589–627.

Goscombe, B., D. Gray, R. Armstrong, D. A. Foster, and J. Vogl, 2005: Event geochronology of the Pan-African Kaoko Belt, Namibia. *Precambrian Research*, **140 (3-4)**, 103.e1–103.e41.

Goscombe, B., M. Hand, and D. Gray, 2003a: Structure of the Kaoko Belt, Namibia: progressive evolution of a classic transpressional orogen. *Journal of Structural Geology*, **25 (7)**, 1049–1081.

Goscombe, B., M. Hand, D. Gray, and J. Mawby, 2003b: The Metamorphic Architecture of a Transpressional Orogen: the Kaoko Belt, Namibia. *Journal of Petrology*, **44 (4)**, 679–711.

Gower, C. F., 1996: The evolution of the Grenville Province in eastern Labrador, Canada. *Geological Society, London, Special Publications*, **112 (1)**, 197–218.

Gradstein, F., J. Ogg, and A. Smith, 2004: *A Geologic Time Scale*. Cambridge University Press, Cambridge.

Gray, D., D. Foster, B. Goscombe, C. Passchier, and R. Trouw, 2006: 40Ar/39Ar ther-

mochronology of the Pan-African Damara Orogen, Nambibia, with implications for tectonothermal and geodynamic evolution. *Precambrian Research*, **150**, 49–72.

Gray, D. R., D. A. Foster, J. G. Meert, B. D. Goscombe, R. Armstrong, R. A. J. Trouw, and C. W. Passchier, 2008: A Damara orogen perspective on the assembly of southwestern Gondwana. *Geological Society, London, Special Publications*, **294 (1)**, 257–278.

Gresse, P. G. and G. J. B. Germs, 1993: The Nama foreland basin: sedimentation, major unconformity bounded sequences and multisided active margin advance. *Precambrian Research*, **63 (3-4)**, 247–252, 259–272.

Grommé, C. S., T. L. Wright, and D. L. Peck, 1969: Magnetic Properties and Oxidation of Iron-Titanium Oxide Minerals in Alae and Makaopuhi Lava Lakes, Hawaii. *J. Geophys. Res.*, **74 (22)**, 5277–5293.

Guimarães, I. P., A. F. Da Silva Filho, C. N. Almeida, W. R. Van Schmus, J. a. M. M. Araújo, S. C. Melo, and E. B. Melo, 2004: Brasiliano (Pan-African) granitic magmatism in the Pajeú-Paraíba belt, Northeast Brazil: an isotopic and geochronological approach. *Precambrian Research*, **135 (1-2)**, 23–53.

Halliday, A., C. Graham, M. Aftalion, and P. Dymoke, 1998: Short Paper: The depositional age of the Dalradian Supergroup: U-Pb and Sm-Nd isotopic studies of the Tayvallich Volcanics, Scotland. *Journal of the Geological Society*, **146**, 3–6.

Halverson, G., P. Hoffman, D. Schrag, A. Maloof, and A. Rice, 2005: Toward a Neoproterozoic composite carbon-isotope record. *GSA Bulletin*, **117 (9/10)**, 1181–1207.

Halverson, G. P., B. P. Wade, M. T. Hurtgen, and K. M. Barovich, 2010: Neoproterozoic chemostratigraphy. *Precambrian Research*, **182 (4)**, 337–350.

Hambrey, M. J. and W. Harland, (Eds.) , 1981: *Earth's Pre-Pleistocene Glacial Record*. Cambridge University Press, Cambridge.

Hanson, R. E., 2003: Proterozoic geochronology and tectonic evolution of southern Africa. *Geological Society, London, Special Publications*, **206 (1)**, 427–463.

Hanson, R. E., M. S. Wardlaw, T. J. Wilson, and G. Mwale, 1993: U—Pb zircon ages from the Hook granite massif and Mwembeshi dislocation: constraints on Pan-African deformation, plutonism, and transcurrent shearing in Central Zambia. *Precambrian Research*, **63 (3-4)**, 189–209.

Harland, W., 1964: Critical evidence for a great Infracambrian glaciation. *Geologische Rundschau*, **54**, 45–61.

Harland, W. and J. Rudwick, 1964: The Great Infra-Cambrian Ice Age. *Scientific American*, **120 (August)**, 28–36.

Harland, W. B. and D. E. T. Bidgood, 1959: Palaeomagnetism in some Norwegian Sparagmites and the Late pre-Cambrian ice age. *Nature*, **184**, 1860–1862.

Hartmann, L. A., 2002: The Mesoproterozoic Supercontinent Atlantica in the Brazilian Shield - Review of Geological and U-Pb Zircon and Sm-Nd Isotopic Evidence. *Gondwana Research*, **5 (1)**, 157–163.

Heaman, L. M. and A. N. LeCheminant, 1993: Paragenesis and U-Pb systematics of baddeleyite (ZrO2). *Chemical Geology*, **110 (1-3)**, 95–126.

Hefferan, K. P., H. Admou, J. A. Karson, and A. Saquaque, 2000: Anti-Atlas (Morocco) role in Neoproterozoic Western Gondwana reconstruction. *Precambrian Research*, **103 (1-2)**, 89–96.

Heilbron, M. and N. Machado, 2003: Timing of terrane accretion in the Neoproterozoic-Eopaleozoic Ribeira orogen (se Brazil). *Precambrian Research*, **125 (1-2)**, 87–112.

Hein, K. A. A., V. Morel, O. Kagoné, F. Kiemde, and K. Mayes, 2004: Birimian lithological succession and structural evolution in the Goren segment of the Boromo-Goren Greenstone Belt, Burkina Faso. *Journal of African Earth Sciences*, **39 (1-2)**, 1–23.

Hirdes, W. and D. W. Davis, 2002: U-Pb zircon and rutile metamorphic ages of Dahomeyan garnet-hornblende gneiss in southeastern Ghana, West Africa. *Journal of African Earth Sciences*, **35 (3)**, 445–449.

Hirt, A. M. and A. U. Gehring, 1991: Thermal Alteration of the Magnetic Mineralogy in Ferruginous Rocks. *J. Geophys. Res.*, **96 (B6)**, 9947–9953.

Hoffman, P., 1991: Did the Breakout of Laurentia Turn Gondwanaland Inside-Out? *Science*, **252**, 1409–1412.

Hoffman, P., 1999: The break-up of Rondinia, birth of Gondwana, true polar wander and the snowball Earth. *Journal of African Earth Sciences*, **28 (1)**, 17–33.

Hoffman, P., D. Hawkins, C. Isachsen, and S. Bowring, 1996: Precise U-Pb zirocn ages for early Damaran magmatism in the Summas Mountains and Welwitschia inlier, northern Damara belt, Namibia. *Geological Survey of Namibia Communications*, **11**, 47–52.

Hoffman, P., A. Kaufman, G. Halverson, and D. Schrag, 1998: A Neoproterozoic Snowball Earth. *Science*, **281**, 1342–1346.

Hoffman, P. and D. Schrag, 2002: The snowball Earth hypothesis: testing the limits of global change. *Terra Nova*, **14**, 129–155.

Hoffman, P. F., 1989: Speculations on Laurentia's first gigayear (2.0 to 1.0 Ga). *Geology*, **17 (2)**, 135–138.

Hoffman, P. F., C. R. Calver, and G. P. Halverson, 2009: Cottons Breccia of King Island, Tasmania: Glacial or non-glacial, Cryogenian or Ediacaran? *Precambrian Research*, **172 (3-4)**, 311–322.

Hoffman, P. F. and Z.-X. Li, 2009: A palaeogeographic context for Neoproterozoic glaciation. *Palaeogeography, Palaeoclimatology, Palaeoecology*, **277 (3-4)**, 158–172.

Hoffmann, K.-H., D. Condon, S. Bowring, and J. Crowley, 2004: U-Pb ziron date from the Neoproterozoic Ghaub Formation, Namibia: Constraints on Marinoan glaciation. *Geology*, **32 (9)**, 817–820.

Hoskin, P. and L. Black, 2000: Metamorphic zircon formation by solid-state recrystallization of protolith igneous zircon. *Journal of Metamorphic Geology*, **18 (4)**, 423–439.

Huang, B., B. Xu, C. Zhang, Y. Li, and R. Zhu, 2005: Paleomagnetism of the Baiysi volcanic rocks (ca. 740 Ma) of Tarim, Northwest China: A continental fragment of Neoproterozoic Western Australia? *Precambrian Research*, **142**, 83–92.

Hurley, P. M., 1973: On the origin of the 450±200 m.y. orogenic belts. *Implications of Continental Drift to the Earth Sciences*, D. Tarling and S. Runcorn, Eds., Academic Press, London, Vol. 2, 1083–1089.

Hurley, P. M., et al., 1967: Test of Continental Drift by Comparison of Radiometric Ages: A pre-drift reconstruction shows matching geologic age provinces in West Africa and Northern Brazil. *Science*, **157 (3788)**, 495–500.

Hurowitz, J. and S. McLennan, 2005: Geochemistry of Cambro-Ordovician Sedimentary Rocks of the Northeastern United States: Changes in Sediment Sources at the Onset of Taconian Orogenesis. *The Journal of Geology*, **113 (5)**, 571–587.

Hyde, W., T. Crowley, S. Baum, and R. Peltier, 2000: Neoproterozoic 'snowball Earth' simulations with a coupled climate/ice-sheet model. *Nature*, **405**, 425–429.

Irvine, T. N. and W. R. A. Baragar, 1971: Guide to Chemical Classification of Common Volcanic Rocks. *Canadian Journal of Earth Sciences*, **8 (5)**, 523–&.

Iyer, S. S., J. Hoefs, and H. R. Krouse, 1992: Sulfur and lead isotope geochemistry of galenas from the Bambui Group, Minas Gerais, Brazil; implications for ore genesis. *Economic Geology*, **87 (2)**, 437–443.

Jackson, S. E., N. J. Pearson, W. L. Griffin, and E. A. Belousova, 2004: The application of laser ablation-inductively coupled plasma-mass spectrometry to in situ U-Pb zircon

geochronology. *Chemical Geology*, **211 (1-2)**, 47–69.

Jenkins, G. S., 2004: High Obliquity as an alternative hypothesis to early and late Proterozoic extreme climate conditions. *Extreme Proterozoic Geology, Geochemistry and Climate*, **146**, 183–192.

John, T., V. Schenk, K. Haase, E. Scherer, and F. Tembo, 2003: Evidence for a Neoproterozoic ocean in south-central Africa from mid-oceanic-ridge-type geochemical signatures and pressure-temperature estimates of Zambian eclogites. *Geology*, **31 (3)**, 243–246.

John, T., V. Schenk, K. Mezger, and F. Tembo, 2004: Timing and PT Evolution of Whiteschist Metamorphism in the Lufilian Arc-Zambezi Belt Orogen (Zambia): Implications for the Assembly of Gondwana. *The Journal of Geology*, **112 (1)**, 71–90.

Johnson, S., B. De Waele, D. Evans, W. Banda, F. Tembo, J. Milton, and K. Tani, 2007a: Geochronology of the Zambezi Supracrustal Sequence, Southern Zambia: A Record of Neoproterozoic Divergent Processes along the Southern Margin of the Congo Craton. *The Journal of Geology*, **115 (3)**, 355–374.

Johnson, S. P., B. De Waele, and K. A. Liyungu, 2006: U-Pb sensitive high-resolution ion microprobe (SHRIMP) zircon geochronology of granitoid rocks in eastern Zambia: Terrane subdivision of the Mesoproterozoic Southern Irumide Belt. *Tectonics*, **25 (6)**, TC6004.

Johnson, S. P., B. de Waele, F. Tembo, C. Katongo, K. Tani, Q. Chang, T. Iizuka, and D. Dunkley, 2007b: Geochemistry, Geochronology and Isotopic Evolution of the Chewore-Rufunsa Terrane, Southern Irumide Belt: a Mesoproterozoic Continental Margin Arc. *Journal of Petrology*, **48 (7)**, 1411–1441.

Johnson, S. P. and G. J. H. Oliver, 2000: Mesoproterozoic oceanic subduction, island-arc formation and the initiation of back-arc spreading in the Kibaran Belt of central, southern Africa: evidence from the Ophiolite Terrane, Chewore Inliers, northern Zimbabwe. *Precambrian Research*, **103 (3-4)**, 125–146.

Johnson, S. P. and G. J. H. Oliver, 2004: Tectonothermal history of the Kaourera Arc, northern Zimbabwe: implications for the tectonic evolution of the Irumide and Zambezi Belts of south central Africa. *Precambrian Research*, **130 (1-4)**, 71–97.

Johnson, S. P., T. Rivers, and B. De Waele, 2005: A review of the Mesoproterozoic to early Palaeozoic magmatic and tectonothermal history of south-central Africa: implications for Rodinia and Gondwana. *Journal of the Geological Society*, **162 (3)**, 433–450.

Jones, D. L., P. L. McFadden, A. Kröner, and M. O. McWilliams, 1992: Palaeomagnetic results from the late Precambrian Chela Group of southwest Angola. *Precambrian Research*, **59 (1-2)**, 1–13.

Kampunzu, A., D. Kapenda, and B. Manteka, 1991: Basic magmatism and geotectonic evolution of the Pan African belt in central Africa: evidence from the Katangan and West Congolian segments. *Tectonophysics*, **190**, 363–371.

Kampunzu, A. B., 2001: Assembly and Break-up of Rodinia – No Link With Gondwana Assembly. *Gondwana Research*, **4 (4)**, 647–650.

Karlstrom, K., S. S. Harlan, M. L. Williams, J. McLelland, J. W. Geissman, and K.-I. Åhäll, 1999: Refining Rodinia: Geological Evidence for the Australia-Western U.S. connection in the Proterozoic. *GSA Today*, **9 (10)**, 1–7.

Karlstrom, K. E., K.-I. Åhäll, S. S. Harlan, M. L. Williams, J. McLelland, and J. W. Geissman, 2001: Long-lived (1.8-1.0 Ga) convergent orogen in southern Laurentia, its extensions to Australia and Baltica, and implications for refining Rodinia. *Precambrian Research*, **111 (1-4)**, 5–30.

Kaufman, A., A. Knoll, and G. Narbonne, 1997: Isotopes, ice ages, and terminal Proterozoic earth history. *Proceedings of the National Academy of Sciences of the United States of America*, **94**, 6600–6605.

Kaufman, A. J., J. M. Hayes, A. H. Knoll, and G. J. B. Germs, 1991: Isotopic composi-

tions of carbonates and organic carbon from upper Proterozoic successions in Namibia: stratigraphic variation and the effects of diagenesis and metamorphism. *Precambrian Research*, **49 (3-4)**, 301–327.

Kendall, B., R. A. Creaser, C. R. Calver, T. D. Raub, and D. A. D. Evans, 2009: Correlation of Sturtian diamictite successions in southern Australia and northwestern Tasmania by Re-Os black shale geochronology and the ambiguity of "Sturtian"-type diamictite-cap carbonate pairs as chronostratigraphic marker horizons. *Precambrian Research*, **172 (3-4)**, 301–310.

Kennedy, M., 1996: Stratigraphy, sedimentology, and isotopic geochemistry of Australian Neoproterozoic postglacial dolostone: deglaciation, C13 excursions, and carbonate precipitation. *Journal of Sedimentary Research*, **66**, 1050–1064.

Kennedy, M., N. Christie-Blick, and L. Sohl, 2001: Are Proterozoic cap carbonates and isotopic excursions a record of gas hydrate destabilization following Earth's coldest intervals? *Geology*, **29 (5)**, 443–446.

Kennedy, M., B. Runnegar, A. Prave, K.-H. Hoffmann, and M. Arthur, 1998: Two or four Neoproterozoic glaciations? *Geology*, **26 (12)**, 1059–1063.

Key, R., A. Liyungu, F. Njamue, V. Somwe, J. Banda, P. Mosley, and R. Armstrong, 2001: The western arm of the Lufilian Arc in NW Zambia and its potential for copper mineralization. *Journal of African Earth Sciences*, **33**, 503–528.

Key, R. M., et al., 2008: Two Mesoarchaean terranes in the Reguibat shield of NW Mauritania. *Geological Society, London, Special Publications*, **297 (1)**, 33–52.

Kilner, B., C. Mac Niocaill, and M. Brasier, 2005: Low-latitude glaciation in the Neoproterozoic of Oman. *Geology*, **33 (413-416)**.

Kirschvink, J. L., 1978: Precambrian-Cambrian boundary problem - magnetostratigraphy of Amadeus Basin, central Australia. *Geological Magazine*, **115 (2)**, 139–150.

Kirschvink, J. L., 1980: The least-squares line and plane and the analysis of palaeomagnetic data. *Geophysical Journal of the Royal Astrological Society*, **62**, 699–718.

Kirschvink, J. L., 1992: *Late Proterozoic Low-Latitude Global Glaciation: the Snowball Earth*. The Proterozoic Biosphere: A Multidisciplinary Study, Cambridge University Press.

Kirschvink, J. L., R. L. Ripperdan, and D. A. Evans, 1997: Evidence for a Large-Scale Reorganization of Early Cambrian Continental Masses by Inertial Interchange True Polar Wander. *Science*, **277 (5325)**, 541–545.

Klein, E. L. and C. A. V. Moura, 2008: Sao Luis Craton and Gurupi Belt (Brazil): possible links with the West African Craton and surrounding Pan-African belts. *Geological Society, London, Special Publications*, **294 (1)**, 137–151.

Klein, E. L., C. A. V. Moura, R. S. Krymsky, and W. L. Griffin, 2005a: The Gurupi Belt, northern Brazil: Lithostratigraphy, geochronology, and geodynamic evolution. *Precambrian Research*, **141 (3-4)**, 83–105.

Klein, E. L., C. A. V. Moura, and B. L. S. Pinheiro, 2005b: Paleoproterozoic Crustal Evolution of the São Luís Craton, Brazil: Evidence from Zircon Geochronology and Sm-Nd Isotopes. *Gondwana Research*, **8 (2)**, 177–186.

Klerkx, J., J. Liégeois, J. Lavreau, and W. Claessen, 1987: Crustal evolution of northern Kibaran belt in eastern and central Africa. *Proterozoic Lithosphereic Evolution*, A. Kröner, Ed., American Geophysical Union, Geodynamics Series, Vol. 17, 217–233.

Knauth, L. P. and M. J. Kennedy, 2009: The late Precambrian greening of the Earth. *Nature*, **460 (7256)**, 728–732.

Knoll, A., 1991: End of the Proterozoic Eon. *Scientific American*, **265 (October)**, 64–73.

Knoll, A., J. Hayes, A. Kaufman, K. Swett, and I. Lambert, 1986: Secular variation in carbon isotope ratios from Upper Proterozoic successions of Svalbard and East Greenland.

Nature, **321**, 832–838.

Knoll, A. H. and S. B. Carroll, 1999: Early Animal Evolution: Emerging Views from Comparative Biology and Geology. *Science*, **284 (5423)**, 2129–2137.

Kokonyangi, J., R. Armstrong, A. B. Kampunzu, M. Yoshida, and T. Okudaira, 2004: U-Pb zircon geochronology and petrology of granitoids from Mitwaba (Katanga, Congo): implications for the evolution of the Mesoproterozoic Kibaran belt. *Precambrian Research*, **132 (1-2)**, 79–106.

Kokonyangi, J. W., A. B. Kampunzu, R. Armstrong, M. Yoshida, T. Okudaira, M. Arima, and D. A. Ngulube, 2006: The Mesoproterozoic Kibaride belt (Katanga, SE D.R. Congo). *Journal of African Earth Sciences*, **46 (1-2)**, 1–35.

Kolb, J., G. Sakellaris, and F. Meyer, 2006: Controls on hydrothermal Fe oxide-Cu-Au-Co mineralization at the Guelb Moghrein deposit, Akjoujt area, Mauritania. *Mineralium Deposita*, **41 (1)**, 68–81.

Kooijman, E., D. Upadhyay, K. Mezger, M. Raith, and J. Berndt, in preparation: Response of the U-Pb system and trace elements in zircon to UHT contact metamorphism: a case study from the contact aureole of the Kadavur anorthosite complex, southeastern India. *Mineralogy and Petrology*.

Kröner, A., 2001: Du Toit Memorial Lecture 1999: The Mozambique belt of East Africa and Madagascar: significance of zircon and Nd model ages for Rodinia and Gondwana supercontinent formation and dispersal. *South African Journal of Geology*, **104 (2)**, 151–166.

Kröner, A. and U. Cordani, 2003: African, Southern Indian and South American cratons were not part of the Rodinia supercontinent: evidence from field relationships and geochronology. *Tectonophysics*, **375**, 325–352.

Kröner, A. and H. Correia, 1973: Further evidence for glaciogenic origin of Late Precambrian mixtites in Angola. *Nature-Physical Science*, **246 (155)**, 115–117.

Kröner, S., A. Kröner, C. W. Passchier, U. Poller, M. T. D. Wingate, K. H. Hofmann, J. Konopásek, and J. M. Barton, 2004: U-Pb and Pb-Pb zircon ages for metamorphic rocks in the Kaoko Belt of Northwestern Namibia: A Palaeo- to Mesoproterozoic basement reworked during the Pan-African orogeny. *South African Journal of Geology*, **107 (3)**, 455–476.

Kruiver, P. P., M. J. Dekkers, and D. Heslop, 2001: Quantification of magnetic coercivity components by the analysis of acquisition curves of isothermal remanent magnetisation. *Earth and Planetary Science Letters*, **189 (3-4)**, 269–276.

Küster, D., J.-P. Liégeois, D. Matukov, S. Sergeev, and F. Lucassen, 2008: Zircon geochronology and Sr, Nd, Pb isotope geochemistry of granitoids from Bayuda Desert and Sabaloka (Sudan): Evidence for a Bayudian event (920-900 Ma) preceding the Pan-African orogenic cycle (860-590 Ma) at the eastern boundary of the Saharan Metacraton. *Precambrian Research*, **164 (1-2)**, 16–39.

Lacassie, J. P., F. Herve, and B. Roser, 2006: Sedimentary provenance study of the post-Early Permian to pre-Early Cretaceous metasedimentary Duque de York Complex, Chile. *Revista Geologica De Chile*, **33 (2)**, 199–219.

Lahondère, D., D. Thieblemont, J. C. Goujou, J. Roger, A. Moussine-Pouchkine, J. Le Metour, A. Cocherie, and C. Guerrot, 2003: Notice explicative des cartes géologiques et gîtologiques à 1/200 000 et 1/500 000 du Nord de la Mauritanie. Tech. rep., Nouakchot, Mauritanie.

Lahondère, D., et al., 2005: Notice explicative des cartes géologiques à 1/200 000 et 1/500 000 de l'extrème sud de la Mauritanie. Tech. rep., BRGM/RC-54273-FR, Nouakchott, Mauritania.

Large, R. R., J. B. Gemmell, H. Paulick, and D. L. Huston, 2001: The Alteration Box Plot: A Simple Approach to Understanding the Relationship between Alteration Mineralogy and

Lithogeochemistry Associated with Volcanic-Hosted Massive Sulfide Deposits. *Economic Geology*, **96 (5)**, 957–971.

Laux, J. H., M. M. Pimentel, E. L. Dantas, R. Armstrong, and S. L. Junges, 2005: Two neoproterozoic crustal accretion events in the Brasília belt, central Brazil. *Journal of South American Earth Sciences*, **18 (2)**, 183–198.

Lawver, L. and C. Scotese, 1987: A revised reconstruction of gondwanaland. *Gondwana six: Structure, Tectonics and Geophysics*, G. McKenzie, Ed., AGU, Washington, DC, AGU Geophysics Monographs Series, Vol. 40, 14–24.

Le Guerroué, E., P. A. Allen, and A. Cozzi, 2006: Chemostratigraphic and sedimentological framework of the largest negative carbon isotopic excursion in Earth history: The Neoproterozoic Shuram Formation (Nafun Group, Oman). *Precambrian Research*, **146 (1-2)**, 68–92.

Le Hir, G., G. Ramstein, Y. Donnadieu, and Y. Goddéris, 2008: Scenario for the evolution of atmospheric pCO2 during a snowball Earth. *Geology*, **36 (1)**, 47–50.

Leblanc, M., 1976: Proterozoic oceanic crust at Bou Azzer. *Nature*, **261**, 34–35.

Leblanc, M. and J. R. Lancelot, 1980: Geodynamic interpretation of Pan-African region (Late Precambrian) in Anti-Atlas (Morocco) from geological and geochronological data. *Canadian Journal of Earth Sciences*, **17 (1)**, 142–155.

Ledru, P., V. Johan, J. P. Milési, and M. Tegyey, 1994: Markers of the last stages of the Palaeoproterozoic collision: evidence for a 2 Ga continent involving circum-South Atlantic provinces. *Precambrian Research*, **69 (1-4)**, 169–191.

Legrand, P., 1969: Description de Westonia chudeaui nov. sp., Brachiopode inarticulé de l'Adrar mauritanien (Sahara occidental). *Bull. Soc. géol. Fr.*, **11**, 251–256.

Lemoine, S., P. Tempier, J. P. Bassot, M. Caen-Vachette, Y. Vialette, S. Touré, and U. Wenmenga, 1990: The Burkinian orogenic cycle, precursor of the Eburnian orogeny in West Africa. *Geological Journal*, **25 (2)**, 171–188.

Lemon, N. and V. Gostin, 1990: Glacigenic sediments of the late Proterozoic Elatina Formation and equivalents. *The evolution of a late Precambrian-early Palaeozoic rift complex: The Adelaide Geosyncline*, J. Jago and P. Moore, Eds., Geological Society of Australia Special Publication, Vol. 16, 149–163.

Lentz, D. R., 1998: Petrogenetic evolution of felsic volcanic sequences associated with Phanerozoic volcanic-hosted massive sulphide systems: the role of extensional geodynamics. *Ore Geology Reviews*, **12 (5)**, 289–327.

Lepersonne, J., 1951: Données nouvelles sur la stratigraphie des terrains anciens du Bas-Congo. *Bull. Soc. Géol. Belg.*, **60**, 169–189.

Lepersonne, J., 1973: Feuille Ngungu au 1/200,000 et notice explicative. Tech. rep., Département des Mines, Direction de la Géologie, République du Zaïre.

Lepersonne, J., 1974: Carte géologique du Zaïre au 1/2,000,000 et notice explicative. Tech. rep., Département des Mines, Direction de la Géologie, République du Zaïre.

Leprun, J. C. and R. Trompette, 1969: Volta subdivison of Gobnangou Massif (Upper Volta Republic) into 2 discordant series separated by a tillite of probable Eocambrian age. *Comptes Rendus Hebdomadaires Des Seances De L Academie Des Sciences Serie D*, **269 (22)**, 2187–&.

Lesquer, A., J. F. Beltrao, and F. A. M. De Abreu, 1984: Proterozoic links between Northeastern Brazil and West Africa: A plate tectonic model based on gravity data. *Tectonophysics*, **110 (1-2)**, 9–13, 15, 17–26.

Levrard, B. and J. Laskar, 2003: Climate friction and the Earth's obliquity. *Geophys. J. Int.*, **154**, 970–990.

Li, Y., Y. Li, R. Sharps, M. McWilliams, and Z. Gao, 1991: Sinian paleomagnetic results

from the Tarim block, western China. *Precambrian Research*, **49 (1-2)**, 61–71.

Li, Z., 2000: New palaeomagnetic results from the 'cap dolomite' of the Neoproterozoic Walsh Tillite, northwestern Australia. *Precambrian Research*, **100**, 359–370.

Li, Z., et al., 2008: Assembly, configuration, and break-up history of Rodinia: A synthesis. *Precambrian Research*, **160 (1-2)**, 179–210.

Liégeois, J.-P., J. Navez, J. Hertogen, and R. Black, 1998: Contrasting origin of post-collisional high-K calc-alkaline and shoshonitic versus alkaline and peralkaline granitoids. The use of sliding normalization. *Lithos*, **45 (1-4)**, 1–28.

Lottermoser, B. and P. Ashley, 2000: Geochemistry, petrology and origin of Neoproterozoic ironstones in the eastern part of the Adelaide Geosyncline, South Australia. *Precambrian Research*, **101**, 49–67.

Lottes, A. L. and D. B. Rowley, 1990: Reconstruction of the Laurasian and Gondwanan segments of Permian Pangaea. *Geological Society, London, Memoirs*, **12 (1)**, 383–395.

Lowrie, W., 1990: Identification of ferromagnetic minerals in a rock by coercivity and unblocking temperature properties. *Geophys. Res. Lett.*, **17**.

Ludwig, K. R., 1998: On the Treatment of Concordant Uranium-Lead Ages. *Geochimica et Cosmochimica Acta*, **62 (4)**, 665–676.

Ludwig, K. R., 1999: Using Isoplot/Ex, Version 2.01: a geochronlogical toolkit for Microsoft Excel. *Berkeley Geochronology Center Special Publication*, **1a**, 47.

Ludwig, K. R., 2003: A Geochronological Toolkit for Microsoft Excel. *Berkeley Geochronology Center Special Publication*, **4**, 75.

Lumpkin, G. R., 1999: Physical and chemical characteristics of baddeleyite (monoclinic zirconia) in natural environments: an overview and case study. *Journal of Nuclear Materials*, **274 (1-2)**, 206–217.

Lund, K., J. Aleinikoff, K. Evans, and C. Fanning, 2003: SHRIMP U-Pb geochronology of Neoproterozoic Windermere Supergroup, central Idaho: implications for rifting of western Laurentia and synchroneity of Sturtian glacial deposits. *Geol. Soc. Amer. Bull.*, **115**, 349–372.

Lytwyn, J., K. Burke, and S. Culver, 2006: The nature and location of the suture zone in the Rokelide orogen, Sierra Leone: Geochemical evidence. *Journal of African Earth Sciences*, **46 (5)**, 439–454.

Macambira, M., 1983: Geologia e ocorrências minerais da braquianticlinal do Lontra (GO). Ph.D. thesis, Universidade Federal do Pará.

Machado, N. and G. Gauthier, 1996: Determination of 207Pb/206Pb ages on zircon and monazite by laser-ablation ICPMS and application to a study of sedimentary provenance and metamorphism in southeastern Brazil. *Geochimica et Cosmochimica Acta*, **60 (24)**, 5063–5073.

Macouin, M., J. Besse, M. Ader, S. Gilder, Z. Yang, Z. Sun, and P. Agrinier, 2004: Combined paleomagnetic and isotopic data from Doushantuo carbonates, South China: implications for the "snowball Earth" hypothesis. *Earth Planet. Sci. Lett.*, **224**, 387–398.

Mahan, K. H., B. P. Wernicke, and M. J. Jercinovic, 2010: Th-U-total Pb geochronology of authigenic monazite in the Adelaide rift complex, South Australia, and implications for the age of the type Sturtian and Marinoan glacial deposits. *Earth and Planetary Science Letters*, **289 (1-2)**, 76–86.

Maloof, A. C., G. P. Halverson, J. Kirschvink, D. P. Schrag, B. P. Weiss, and P. F. Hoffman, 2006: Combined paleomagnetic, isotopic, and stratigraphic evidence for true polar wander from the Neoproterozoic Akademikerbreen Group, Svalbard, Norway. *GSA Bulletin*, **118 (9/10)**, 1099–1124.

Mantovani, M. S. M. and B. B. de Brito Neves, 2005: The Paranapanema Lithospheric

Block: Its Importance for Proterozoic (Rodinia, Gondwana) Supercontinent Theories. *Gondwana Research*, **8 (3)**, 303–315.

Martin, H., 1965: Beobachtungen zum problem der jung-Präkambrischen glazialen ablagerungen in Südwestafrika. *Geologische Rundschau*, **54 (1)**, 115–127.

Martins-Neto, M. A., 2000: Tectonics and sedimentation in a paleo/mesoproterozoic rift-sag basin (Espinhaço basin, southeastern Brazil). *Precambrian Research*, **103 (3-4)**, 147–173.

Matton, G., M. Jébrak, and J. K. Lee, 2005: Resolving the Richat enigma: Doming and hydrothermal karstification above an alkaline complex. *Geology*, **33 (8)**, 665–668.

Maurin, J.-C., 1993: La chaîne Panafricaine Ouest-Congolienne: corrélation avec le domaine Est-Brésilien et hypothèse géodynamique. *Bull. Soc. géol. Fr.*, **764**, 51–60.

Maurin, J.-C., J. Mpemba-Boni, C. Pin, and J. P. Vicat, 1990: La granodiorite de Les Saras un témoin de magmatisme éburnéen (2 Ga) au sein de la chaîne panafricaine du Mayombe (Congo). *Comptes Rendus Académie Sciences, Paris*, **310**, 571–575.

Maurin, J.-C., et al., 1991: La chaîne protérozoïque ouest-congolienne et son avant-pays au Congon nouvelles données géochronologiques et struturales, implications en Afrique centrale. *Comptes Rendus Académie Sciences, Paris*, **312**, 1327–1334.

Mayer, A., A. W. Hofmann, S. Sinigoi, and E. Morais, 2004: Mesoproterozoic Sm-Nd and U-Pb ages for the Kunene Anorthosite Complex of SW Angola. *Precambrian Research*, **133 (3-4)**, 187–206.

Mbede, E., A. Kampunzu, and R. Armstrong, 2004: Neoproterozoic inheritance during Cainozoic rifting in the Western and Southwestern branches of the East African Rift system: Evidence from carbonatite and alkaline intrusions.

McCabe, C. and R. Elmore, 1989: The occurrence and origin of Late Paleozoic remagnetization in the sedimentary rocks of North America. *Rev. Geophys.*, **27 (4)**, 471–494.

McCausland, P. J. A., R. Van der Voo, and C. M. Hall, 2007: Circum-Iapetus paleogeography of the Precambrian-Cambrian transition with a new paleomagnetic constraint from Laurentia. *Precambrian Research*, **156 (3-4)**, 125–152.

McElhinny, M. W., C. M. Powell, and S. A. Pisarevsky, 2003: Paleozoic terranes of eastern Australia and the drift history of Gondwana. *Tectonophysics*, **362 (1-4)**, 41–65.

McFadden, P., 1990: A new fold-test for palaeomagnetic studies. *Geophys. J. Int.*, **103**, 163–169.

McFadden, P. and M. McElhinny, 1988: The combined analysis of regamnetisation circles and direct observations in paleomagnetism. *Earth Planet. Sci. Lett.*, **87**, 161–172.

McFadden, P. and M. McElhinny, 1990: Classification of the Reversal Test in Paleomagnetism. *Geophys. J. Int.*, **103 (3)**, 725–729.

McLennan, S., B. Bock, S. Hemming, J. Hurowitz, S. Lev, and D. McDaniel, 2003: The roles of provenance and sedimentary processes in the geochemistry of sedimentary rocks. *Geochemistry of sediments and sedimentary rocks: Evolutionary Considerations to Mineral-Deposit-Forming Environments*, D. R. Lentz, Ed., Geological Association of Canada, GEOText, 4th ed., 7–38.

McLennan, S., S. Hemming, D. McDaniel, and G. Hanson, 1993: Geochemical approaches to sedimentation, provenance, and tectonics. *Geological Society of America Special Paper*, **284**, 21–40.

McLennan, S., S. Taylor, M. McCulloch, and J. Maynard, 1990: Geochemical and Nd-Sr isotopic composition of deep-sea turbidites: Crustal evolution and plate tectonic associtations. *Geochimica et Cosmochimica Acta*, **54**, 2015–2050.

McLennan, S. M., 1989: Rare earth elements in sedimentary rocks: influence of provenance and sedimentary processes. *Geochemistry and mineralogy of rare earth elements*, B. Lipin and G. McKay, Eds., Mineralogical Society of America, Washington, D.C., Re-

views in Mineralogy, Vol. 21, 169–200.

McLennan, S. M., 2001: Relationships between the trace element composition of sedimentary rocks and upper continental crust. *Geochem. Geophys. Geosyst.*, **2**.

McNamara, A. K., C. Mac Niocaill, B. A. Van der Pluijm, and R. Van der Voo, 1997: Paleomagnetic results from the Avalon Terrane (Marystown Group) and implications for Late Neoproterozoic paleogeography. *EOS Transactions of the American Geophysical Union*, **78 (17)**, 117.

McWilliams, M. and A. Kröner, 1981: Paleomagnetism and Tectonic Evolution of the Pan-African Damara Belt, Southern Africa. *Journal of Geophyisical Research*, **86 (B6)**, 5147–5162.

Meert, J. and B. Lieberman, 2008: The Neoproterozoic assembly of Gondwana and its relationship to the Ediacaran-Cambrian radiation. *Gondwana Research*, **14**, 5–21.

Meert, J. and R. Van der Voo, 1996: Paleomagnetic and 40Ar/39Ar study of the Sinyai Dolerite, Kenya: Implications for Gondwana assembly. *Journal of Geology*, **104**, 131–142.

Meert, J. and R. van der Voo, 1997: The assembly of Gondwana 800-550 Ma. *J. Geodynamics*, **23 (3/4)**, 223–235.

Meert, J., R. Van der Voo, and S. Ayub, 1995: Paleomagnetic investigation of the Neoproterozic Gagwe lavas and Mbozi complex, Tanzania and the assembly of Gondwana. *Precambrian Research*, **74**, 225–244.

Meert, J. G., 1999: A paleomagnetic analysis of Cambrian true polar wander. *Earth and Planetary Science Letters*, **168 (1-2)**, 131–144.

Meert, J. G., 2002: Paleomagnetic Evidence for a Paleo-Mesoproterozoic Supercontinent Columbia. *Gondwana Research*, **5 (1)**, 207–215.

Menzies, J., 2000: Micromorphological analyses of microfabrics and microstructures indicative of deformation processes in glacial sediments. *Geological Society, London, Special Publications*, **176 (1)**, 245–257.

Menzies, J., J. J. M. van der Meer, and J. Rose, 2006: Till–as a glacial "tectomict", its internal architecture, and the development of a "typing" method for till differentiation. *Geomorphology*, **75 (1-2)**, 172–200.

Meyer, F. M., J. Kolb, G. A. Sakellaris, and A. Gerdes, 2006: New ages from the Mauritanides Belt: recognition of Archean IOCG mineralization at Guelb Moghrein, Mauritania. *Terra Nova*, **18 (5)**, 345–352.

Milani, E. and A. Thomaz Filho, 2000: Sedimentary basins of South America. *Tectonic Evolution of South America*, U. Cordani, E. Milani, A. Thomaz Filho, and D. Campos, Eds., GSA, 31st Internatnioal Geological Congress, Rio de Janeiro, 389–452.

Milesi, J. P., et al., 2006: An overview of the geology and major ore deposits of Central Africa: Explanatory note for the 1:4,000,000 map "Geology and major ore deposits of Central Africa". *Journal of African Earth Sciences*, **44 (4-5)**, 571–595.

Miller, R. G., 1983: The Pan-African Damara Orogen of Namibia. *The Damara Orogen, Special Publication of the Geological Society of South Africa*, R. G. Miller, Ed., Vol. 11, 431–515.

Montes-Lauar, C., et al., 1997: Panafrican Rb-Sr isochron ages of magmatic rocks from northern Cameroon. Preliminary results. *Sourth-American Symposium on Isotope Geology*, Campos do Jordão, São Paulo, Brazil, 204–205 (extended abstracts).

Moores, E. M., 1991: Southwest U.S.-East Antarctic (SWEAT) connection: A hypothesis. *Geology*, **19 (5)**, 425–428.

Morel, P., 1981: Paleomagnetism of a Pan-African diorite: A Late Precambrian pole for Western Africa. *Geophysical Journal of the Royal Astrological Society*, **65 (2)**, 493–503.

Morrison, D. A., D. W. Davis, J. L. Wooden, D. D. Bogard, D. E. Maczuga, W. C. Phinney, and L. D. Ashwal, 1985: Age of the Mulcahy Lake intrusion, northwest Ontario, and implications for the evolution of greenstone-granite terrains. *Earth and Planetary Science Letters*, **73 (2-4)**, 306–316.

Moura, C. A. V., B. L. S. Pinheiro, A. C. R. Nogueira, P. S. S. Gorayeb, and M. A. Galarza, 2008: Sedimentary provenance and palaeoenvironment of the Baixo Araguaia Supergroup: constraints on the palaeogeographical evolution of the Araguaia Belt and assembly of West Gondwana. *Geological Society, London, Special Publications*, **294 (1)**, 173–196.

Moussine-Pouchkine, A. and J. Bertrand-Sarfati, 1997: Tectonosedimentary subdivisions in the Neoproterozoic to Early Cambrian cover of the Taoudenni Basin (Algeria-Mauritania-Mali). *Journal of African Earth Sciences*, **24 (4)**, 425–443.

Nance, R. D. and J. B. Murphy, 1994: Contrasting basement isotopic signatures and the palinspastic restoration of peripheral orogens: Example from the Neoproterozoic Avalonian-Cadomian belt. *Geology*, **22 (7)**, 617–620.

Nance, R. D., et al., 2008: Neoproterozoic-early Palaeozoic tectonostratigraphy and palaeogeography of the peri-Gondwanan terranes: Amazonian v. West African connections. *Geological Society, London, Special Publications*, **297 (1)**, 345–383.

Nemchin, A. A. and P. A. Cawood, 2005: Discordance of the U-Pb system in detrital zircons: Implication for provenance studies of sedimentary rocks. *Sedimentary Geology*, **182 (1-4)**, 143–162.

Néron de Surgy, O. and J. Laskar, 1997: On the long term evolution of the spin of the Earth. *Astronomy and Astrophysics*, **318**, 975–989.

Nesbitt, H. W., G. Markovics, and R. C. Price, 1980: Chemical processes affecting alkalis and alkaline earths during continental weathering. *Geochimica et Cosmochimica Acta*, **44 (11)**, 1659–1666.

Nesbitt, H. W. and G. M. Young, 1982: Early Proterozoic Climates and Plate Motions Inferred from Major Element Chemistry of Lutites. *Nature*, **299 (5885)**, 715–717.

Nesbitt, H. W. and G. M. Young, 1984: Prediction of some weathering trends of plutonic and volcanic rocks based on thermodynamic and kinetic considerations. *Geochimica et Cosmochimica Acta*, **48 (7)**, 1523–1534.

Nesbitt, H. W., G. M. Young, S. M. McLennan, and R. R. Keays, 1996: Effects of chemical weathering and sorting on the petrogenesis of siliciclastic sediments, with implications for provenance studies. *Journal of Geology*, **104 (5)**, 525–542.

Neves, S. P., O. Bruguier, D. Bosch, J. M. R. da Silva, and G. Mariano, 2008: U-Pb ages of plutonic and metaplutonic rocks in southern Borborema Province (NE Brazil): Timing of Brasiliano deformation and magmatism. *Journal of South American Earth Sciences*, **25 (3)**, 285–297.

Neves, S. P., O. Bruguier, A. Vauchez, D. Bosch, J. M. R. d. Silva, and G. Mariano, 2006: Timing of crust formation, deposition of supracrustal sequences, and Transamazonian and Brasiliano metamorphism in the East Pernambuco belt (Borborema Province, NE Brazil): Implications for western Gondwana assembly. *Precambrian Research*, **149 (3-4)**, 197–216.

Noce, C. M., N. Machado, and A. C. Pedrosa-Soares, 2000: Chronology of Late Proterozoic-Cambrian granitic magmatism in the Araçuaí belt, Eastern Brazil, based on single zircon evaporation dating. *Revista Brasileira de Geociências*, **30**, 25–29.

Nogueira, A., C. Riccomini, A. Sial, C. Moura, and T. Fairchild, 2003: Soft-sediment deformation at the base of the Neoproterozoic Puga cap carbonate (southwestern Amazon craton, Brazil): Confirmation of rapid icehouse to greenhouse transition in snowball Earth. *Geology*, **31 (7)**, 613–616.

Nomade, S., Y. Chen, A. Pouclet, G. Féraud, H. Théveniaut, B. Y. Daouda, M. Vidal, and

C. Rigolet, 2003: The Guiana and the West African Shield Palaeoproterozoic grouping: new palaeomagnetic data for French Guiana and the Ivory Coast. *Geophysical Journal International*, **154 (3)**, 677–694.

North, G. R., R. F. Cahalan, and J. Coakley, James A., 1981: Energy Balance Climate Models. *Rev. Geophys.*, **19 (1)**, 91–121.

Nystuen, J. P., A. Andresen, R. A. Kumpulainen, and A. Siedlecka, 2008: Neoproterozoic basin evolution in Fennoscandia, East Greenland and Svalbard. *Episodes*, **31 (1)**, 35–43.

Nürnberg, D. and R. D. Müller, 1991: The tectonic evolution of the South Atlantic from Late Jurassic to present. *Tectonophysics*, **191 (1-2)**, 27–53.

Oliveira, E. P., N. J. McNaughton, and R. Armstrong, 2010: Mesoarchaean to Palaeoproterozoic growth of the northern segment of the Itabuna-Salvador-Curaca orogen, Sao Francisco craton, Brazil. *Geological Society, London, Special Publications*, **338 (1)**, 263–286.

Oliver, G. J. H., S. P. Johnson, I. S. Williams, and D. A. Herd, 1998: Relict 1.4 Ga oceanic crust in the Zambezi Valley, northern Zimbabwe: Evidence for Mesoproterozoic supercontinental fragmentation. *Geology*, **26 (6)**, 571–573.

Oliver, J., 1986: Fluids expelled tectonically from orogenic belts: Their role in hydrocarbon migration and other geologic phenomena. *Geology*, **14 (2)**, 99–102.

Onstott, T. C. and R. B. Hargraves, 1981: Proterozoic transcurrent tectonics: palaeomagnetic evidence from Venezuela and Africa. *Nature*, **289 (5794)**, 131–136.

Oyhantcabal, P., S. Siegesmund, K. Wemmer, S. Presnyakov, and P. Layer, 2009: Geochronological constraints on the evolution of the southern Dom Feliciano Belt (Uruguay). *Journal of the Geological Society*, **166 (6)**, 1075–1084.

Paes, V., 1999: Geologia e geoquímica da região de Alvarenga, Minas Gerais: Implicaões geotectonicas e metalogeneticas. Ph.D. thesis, Universidade Federal de Minas Gerais, 149 pp.

Pais, M. A., J. L. Le Mouël, K. Lambeck, and J. P. Poirier, 1999: Late Precambrian paradoxical glaciation and obliquity of the Earth - a discussion of dynamical constraints. *Earth and Planetary Science Letters*, **174 (1-2)**, 155–171.

Paixao, M. A. P., A. A. Nilson, and E. L. Dantas, 2008: The Neoproterozoic Quatipuru ophiolite and the Araguaia fold belt, central-northern Brazil, compared with correlatives in NW Africa. *Geological Society, London, Special Publications*, **294 (1)**, 297–318.

Park, J., 1997: Paleomagnetic evidence for low-latitude glaciation during deposition of the Neoproterozoic Rapitan Group, Mackinzie Mountains, N.W.T., Canada. *Canadian Journal of Earth Sciences*, **34**, 34–49.

Passchier, C. W., R. A. J. Trouw, A. Ribeiro, and F. V. P. Paciullo, 2002: Tectonic evolution of the southern Kaoko belt, Namibia. *Journal of African Earth Sciences*, **35 (1)**, 61–75.

Pearce, J., 1983: Role of the sub-continental lithosphere in magma genesis at active continental margins. *Continental basalts and mantle xenoliths*, C. J. Hawkesworth and M. J. Norry, Eds., Shiva, Nantwich, 230–249.

Pearce, J. A. and G. H. Gale, 1977: Identification of ore-deposition environment from trace-element geochemistry of associated igneous host rocks. *Geological Society, London, Special Publications*, **7 (1)**, 14–24.

Pearce, J. A. and M. J. Norry, 1979: Petrogenetic Implications of Ti, Zr, Y, and Nb Variations in Volcanic-Rocks. *Contributions to Mineralogy and Petrology*, **69 (1)**, 33–47.

Pedrosa-Soares, A., U. Cordani, and A. Nutman, 2000: Constraining the age of Neoproterozoic glaciation in eastern Brazil: First U-Pb (SHRIMP) data of detrital zircons. *Revista Brasileira de Geociências*, **30 (1)**, 58–61.

Pedrosa-Soares, A., C. Noce, C. Wiedemann, and C. Pinto, 2001: The Araçuaí-West-Congo

Orogen in Brazil: an overview of a confined orogen formed during Gondwanaland assembly. *Precambrian Research*, **110**, 307–323.

Pedrosa-Soares, A. C., F. F. Alkmim, L. Tack, C. M. Noce, M. Babinski, L. C. Silva, and M. A. Martins-Neto, 2008: Similarities and differences between the Brazilian and African counterparts of the Neoproterozoic Aracuai-West Congo orogen. *Geological Society, London, Special Publications*, **294 (1)**, 153–172.

Pedrosa-Soares, A. C., P. Vidal, O. H. Leonardos, and B. B. de Brito Neves, 1998: Neoproterozoic oceanic remnants in eastern Brazil: Further evidence and refutation of an exclusively ensialic evolution for the Araçuaí-West Congo orogen. *Geology*, 519–522.

Pedrosa-Soares, A. C. and C. Wiedemann, 2000: Evolution of the Araçuaí belt and its connection to the Ribeira Belt, Eastern Brazil. *Tectonic Evolution of South America*, U. Cordani, E. Milani, A. Thomaz Filho, and D. Campos, Eds., GSA, 31st International Geological Congress, Rio de Janeiro, 265–285.

Penaye, J., A. Kröner, S. F. Toteu, W. R. Van Schmus, and J.-C. Doumnang, 2006: Evolution of the Mayo Kebbi region as revealed by zircon dating: An early (ca. 740 Ma) Pan-African magmatic arc in southwestern Chad. *Journal of African Earth Sciences*, **44 (4-5)**, 530–542.

Perrin, M., D. Elston, and A. Moussine-Pouchkine, 1988: Paleomagnetism of Proterozoic and Cambrian strata, Adrar de Mauritanie, cratonic West Africa. *Journal of Geophyisical Research*, **93 (B3)**, 2159–2178.

Perrin, M. and M. Prévot, 1988: Uncertainties about the Proterozoic and Paleozoic polar wander path of the West African craton and Gondwana: evidence for successive remagnetization events. *EPSL*, **88**, 337–347.

Pesonen, L. J., et al., 2003: Palaeomagnetic configuration of continents during the Proterozoic. *Tectonophysics*, **375 (1-4)**, 289–324.

Phillips, E., J. Merritt, C. Auton, and N. Golledge, 2007: Microstructures in subglacial and proglacial sediments: understanding faults, folds and fabrics, and the influence of water on the style of deformation. *Quaternary Science Reviews*, **26 (11-12)**, 1499–1528.

Pierrehumbert, R., 2005: Climate dynamics of a hard snowball Earth. *Journal of Geophyisical Research*, **110**, D01 111.

Pierrehumbert, R. T., 2004: High levels of atmospheric carbon dioxide necessary for the termination of global glaciation. *Nature*, **429**, 646–649.

Pimentel, M. M., R. A. Fuck, H. Jost, C. Ferreira-Filho, and S. de Araújo, 2000: The basement of the Brasília fold belt and the Goiás magmatic arc. *Tectonic Evolution of South America*, U. G. Cordani, E. Milani, A. Thomaz Filho, and D. Campos, Eds., GSA, 31st International Geological Congress, Rio de Janeiro, 195–229.

Pin, C. and J. L. Poidevin, 1987: U-Pb zircon evidence for a pan-african granulite facies metamorphism in the central african republic. a new interpretation of the high-grade series of the northern border of the congo craton. *Precambrian Research*, **36 (3-4)**, 303–312.

Piper, J. D. A., 1972: Paleomagnetic Study of Bukoban System, Tanzania. *Geophysical Journal of the Royal Astronomical Society*, **28 (2)**, 111–&.

Piper, J. D. A., 1975: Palaeomagnetic correlations of Precambrian formations of east-central Africa and their tectonic implications. *Tectonophysics*, **26 (1-2)**, 135–161.

Piper, J. D. A., 1976: Palaeomagnetic evidence for a Proterozoic super-continent. *Phil. Trans. R. Soc Lond. A*, **280**, 469–490.

Piper, J. D. A., 1982: The Precambrian palaeomagnetic record: the case for the Proterozoic Supercontinent. *Earth and Planetary Science Letters*, **59 (1)**, 61–89.

Piper, J. D. A., 1987: *Palaeomagnetism and the continental crust*. Open Univeristy Press, Milton Keynes.

Piper, J. D. A., 2000: The Neoproterozoic Supercontinent: Rodinia or Palaeopangaea? *Earth and Planetary Science Letters*, **176 (1)**, 131–146.

Pisarevsky, S. A., J. B. Murphy, P. A. Cawood, and A. S. Collins, 2008: Late Neoproterozoic and Early Cambrian palaeogeography: models and problems. *Geological Society, London, Special Publications*, **294 (1)**, 9–31.

Pisarevsky, S. A., M. T. D. Wingate, C. M. Powell, S. Johnson, and D. A. D. Evans, 2003: Models of Rodinia assembly and fragmentation. *Geological Society, London, Special Publications*, **206 (1)**, 35–55.

Pitfield, P. E. J., R. M. Key, C. Waters, M. Hawkins, D. Schofield, S. C. Loughlin, and R. Barnes, 2004: Notice explicative des cartes géologiques et gîtologiques au 1/200 000 et 1/500 000 du Sud de la Mauritanie. Tech. rep., Nouakchott, Mauritania.

Piuzana, D., M. M. Pimentel, R. A. Fuck, and R. Armstrong, 2003: Neoproterozoic granulite facies metamorphism and coeval granitic magmatism in the Brasilia Belt, Central Brazil: regional implications of new SHRIMP U-Pb and Sm-Nd data. *Precambrian Research*, **125 (3-4)**, 245–273.

Plank, T. and C. H. Langmuir, 1998: The chemical composition of subducting sediments and its consequences for the crust and mantle. *Chem. Geol.*, **145**, 325–394.

Pohl, W., 1994: Metallogeny of the northeastern Kibara belt, Central Africa–Recent perspectives. *Ore Geology Reviews*, **9 (2)**, 105–130.

Poidevin, J.-L., 2007: Stratigraphie isotopique du strontium et datation des formations carbonatées et glaciogéniques néoprotérozoique du Nord et de l'Ouest du craton du Congo. *Comptes Rendus Geoscience*, **339**, 259–273.

Pollard, D. and J. Kasting, 2005: Snowball Earth: A thin-ice solution with flowing sea glaciers. *Journal of Geophyisical Research*, **110**, C07 010.

Pollard, D. and J. F. Kasting, 2004: Climate-ice sheet simulations of Neoproterozoic glaciation before and after collapse to Snowball Earth. *Extreme Proterozoic Geology, Geochemistry and Climate*, G. Jenkins, M. A. S. McMenamin, C. P. McKay, and L. Sohl, Eds., Amer Geophysical Union, Washington, Geophysical Monograph Series, Vol. 146, 91–105.

Ponte-Neto, C., 2001: Contribuição ao estudo da Formação do Gondwana Ocidental: Novos dados paleomagnéticos. Ph.D. thesis, IAG-USP, 106 pp.

Porada, H., 1989: Pan-African rifting and orogenesis in southern to equatorial Africa and eastern Brazil. *Precambrian Research*, **44 (2)**, 103–136.

Porada, H. and V. Berhorst, 2000: Towards a new understanding of the Neoproterozoic-early palæozoic Lufilian and northern Zambezi belts in Zambia and the Democratic Republic of Congo. *Journal of African Earth Sciences*, **30 (3)**, 727–771.

Porter, S., A. Knoll, and P. Affaton, 2004: Chemostratigraphy of Neoproterozoic cap carbonates from the Volta Basin, West Africa. *Precambrian Research*, **130**, 99–112.

Potrel, A., J. J. Peucat, and C. M. Fanning, 1998: Archean crustal evolution of the West African Craton: example of the Amsaga Area (Reguibat Rise). U—Pb and Sm—Nd evidence for crustal growth and recycling. *Precambrian Research*, **90 (3-4)**, 107–117.

Potrel, A., J. J. Peucat, C. M. Fanning, B. Auvray, J. P. Burg, and C. Caruba, 1996: 3.5 Ga old terranes in the West African Craton, Mauritania. *Journal of the Geological Society*, **153 (4)**, 507–510.

Prave, A. R., 1996: Tale of three cratons: Tectonostratigraphic anatomy of the Damara orogen in northwestern Namibia and the assembly of Gondwana. *Geology*, **24 (12)**, 1115–1118.

Preiss, W. V., 2000: The Adelaide Geosyncline of South Australia and its significance in Neoproterozoic continental reconstruction. *Precambrian Research*, **100 (1-3)**, 21–63.

Preiss, W. V. and B. G. Forbes, 1981: Stratigraphy, correlation and sedimentary history of

Adelaidean (late Proterozoic) basins in Australia. *Precambrian Research*, **15 (3-4)**, 255–304.

Prokoph, A., G. A. Shields, and J. Veizer, 2008: Compilation and time-series analysis of a marine carbonate [delta]18O, [delta]13C, 87Sr/86Sr and [delta]34S database through Earth history. *Earth-Science Reviews*, **87 (3-4)**, 113–133.

Prokoph, A. and J. Veizer, 1999: Trends, cycles and nonstationarities in isotope signals of phanerozoic seawater. *Chemical Geology*, **161**, 225–240.

Renne, P. R., T. C. Onstott, M. S. D'Agrella-Filho, I. G. Pacca, and W. Teixeira, 1990: 40Ar/39Ar dating of 1.0-1.1 Ga magnetizations from the São Francisco and Kalahari cratons: tectonic implications for Pan-African and Brasiliano mobile belts. *Earth and Planetary Science Letters*, **101 (2-4)**, 349–366.

Rice, A. H. N. and C.-C. Hofmann, 2000: Evidence for a glacial origin of Neoproterozoic III striations at Oaibaccannjar'ga, Finnmark, northern Norway. *Geological Magazine*, **137 (04)**, 355–366.

Rino, S., Y. Kon, W. Sato, S. Maruyama, M. Santosh, and D. Zhao, 2008: The Grenvillian and Pan-African orogens: World's largest orogenies through geologic time, and their implications on the origin of superplume. *Gondwana Research*, **14 (1-2)**, 51–72.

Roberts, R., F. Corfu, T. Torsvik, C. Hetherington, and L. Ashwal, 2010: Age of alkaline rocks in the Seiland Igneous Province, Northern Norway. *Journal of the Geological Society*, **167 (1)**, 71–81.

Rocci, G., G. Bronner, and M. Deschamps, 1991: Crystalline basement of the West African Craton. *The West African Orogens and Circum-Atlantic Correlatives*, R. D. Dallmeyer and J. Lécorché, Eds., Springer, Berlin, 31–61.

Rochette, P., G. Fillion, J. L. Mattei, and M. J. Dekkers, 1990: Magnetic transition at 30-34-Kelvin in pyrrhotite - insight into a widespread occurrence of this mineral in rocks. *Earth and Planetary Science Letters*, **98 (3-4)**, 319–328.

Rogers, J. J. W., 1996: A History of Continents in the past Three Billion Years. *The Journal of Geology*, **104 (1)**, 91–107.

Rogers, J. J. W. and M. Santosh, 2002: Configuration of Columbia, a Mesoproterozoic Supercontinent. *Gondwana Research*, **5 (1)**, 5–22.

Rogers, J. J. W. and M. Santosh, 2003: Supercontinents in Earth History. *Gondwana Research*, **6 (3)**, 357–368.

Rogers, J. J. W., R. Unrug, and M. Sultan, 1995: Tectonic assembly of Gondwana. *Journal of Geodynamics*, **19 (1)**, 1–34.

Rollinson, H., 1993: *Using geochemical data: evaluation, presentation, interpretation*. Geochemstry series, Longman Scientific & Technical, Harlow, Essex.

Rollinson, H. R., 1983: The geochemistry of mafic and ultramafic rocks from the Archaean Greenstone Belts of Sierra-Leone. *Mineralogical Magazine*, **47**, 267–280.

Rooney, A. D., D. Selby, J.-P. Houzay, and P. R. Renne, 2010: Re-Os geochronology of a Mesoproterozoic sedimentary succession, Taoudeni basin, Mauritania: Implications for basin-wide correlations and Re-Os organic-rich sediments systematics. *Earth and Planetary Science Letters*, **289 (3-4)**, 486–496.

Sandwell, D. and W. Smith, 1995: Map of marine gravity anomaly from satellite altimtery. [scale 1:31,000,000]. Scripps Institute of Oceanography.

Santos, J. a. O. S., L. A. Hartmann, H. E. Gaudette, D. I. Groves, N. J. McNaughton, and I. R. Fletcher, 2000: A New Understanding of the Provinces of the Amazon Craton Based on Integration of Field Mapping and U-Pb and Sm-Nd Geochronology. *Gondwana Research*, **3 (4)**, 453–488.

Santos, T. J. S. d., A. H. Fetter, and J. A. N. Neto, 2008: Comparisons between the north-

western Borborema Province, NE Brazil, and the southwestern Pharusian Dahomey Belt, SW Central Africa. *Geological Society, London, Special Publications*, **294 (1)**, 101–120.

Saquaque, A., H. Admou, J. Karson, K. Hefferan, and I. Reuber, 1989: Precambrian accretionary tectonics in the Bou Azzer-El Graara region, Anti-Atlas, Morocco. *Geology*, **17 (12)**, 1107–1110.

Sayles, R., 1919: *Seasonal deposition of aqueo-glacial sediments*, Vol. Coll. XLVII. Mem. Mus. Comp. Zool. Harv.

Schermerhorn, L., 1974a: Late Precambrian mixtites: glacial and/or nonglacial? *American Journal of Science*, **274**, 673–824.

Schermerhorn, L., 1981: Late Precambrian tilloids of northwest Angoloa. *In: Hambrey, M.J., and Harland, W.B., editors, Earth's Pre-Pleistocene Glacial Record: Cambridge, Cambridge University Press*, 158–161.

Schermerhorn, L. J. G., 1974b: No evidence for glacial origin of late Precambrian tilloids in Angola. *Nature*, **252**, 114–115.

Schlager, W., 1991: Depositional bias and environmental change–important factors in sequence stratigraphy. *Sedimentary Geology*, **70 (2-4)**, 109–130.

Schmidt, P. and G. Williams, 1995: The Neoproterozoic climatic paradox: Equatorial palaeolatitude for Marinoan glaciation near sea level in South Australia. *Earth Planet. Sci. Lett.*, **134**, 107–124.

Schmidt, P., G. Williams, and B. Embleton, 1991: Low palaeolatitude of Late Proterozoic glaciation: early timing of remanence in haematite of the Elatina Formation, South Australia. *Earth Planet. Sci. Lett.*, **105**, 355–367.

Schofield, D., M. Horstwood, P. Pitfield, Q. Crowley, A. Wilkinson, and H. Sidaty, 2006: Timing and kinematics of Eburnean tectonics in the central Reguibat Shield, Mauritania. *Journal of the Geological Society*, **163 (3)**, 549–560.

Schärer, U., F. Corfu, and D. Demaiffe, 1997: U—Pb and Lu—Hf isotopes in baddeleyite and zircon megacrysts from the Mbuji-Mayi kimberlite: constraints on the subcontinental mantle. *Chemical Geology*, **143 (1-2)**, 1–16.

Seth, B., A. Kröner, K. Mezger, A. A. Nemchin, R. T. Pidgeon, and M. Okrusch, 1998: Archaean to Neoproterozoic magmatic events in the Kaoko belt of NW Namibia and their geodynamic significance. *Precambrian Research*, **92 (4)**, 341–363.

Shields, G., 2005: Neoproterozoic cap carbonates: a critical appraisal of existing models and the plumeworld hypothesis. *Terra Nova*, **17**, 299–310.

Shields, G., M. Deynoux, S. Culver, M. Brasier, P. Affaton, and D. Vandamme, 2007a: Neoproterozoic glaciomarine and cap dolostone facies of the southwestern Taoudéni Basin (Walidiala Valley, Senegal/Guinea, NW Africa). *Comptes Rendus Geoscience*, **339**, 186–199.

Shields, G. A., M. Deynoux, H. Strauss, H. Paquet, and D. Nahon, 2007b: Barite-bearing cap dolostones of the Taoudéni Basin, northwest Africa: Sedimentary and isotopic evidence for methane seepage after a Neoproterozoic glaciation. *Precambrian Research*, **153 (3-4)**, 209–235.

Shipunov, S., A. Muraviev, and M. Bazhenov, 1998: A new conglomerate test in palaeomagnetism. *Geophys. J. Int.*, **133**, 721–725.

Smith, A. G., 1997: Estimates of the Earth's spin (geographic) axis relative to Gondwana from glacial sediments and paleomagnetism. *Earth-Science Reviews*, **42 (3)**, 161–179.

Söderlund, U. and L. Johansson, 2002: A simple way to extract baddeleyite (ZrO2). *Geochem. Geophys. Geosyst.*, **3**.

Sohl, L., N. Christie-Blick, and D. Kent, 1999: Paleomagnetic polarity reversals in Marinoan (ca. 600 Ma) glacial deposits of Australia: Implications for the duration of low-latitude

glaciation in Neoproterozoic time. *GSA Bulletin*, **111 (8)**, 1120–1139.

Söllner, F. and R. A. J. Trouw, 1997: The Andrelândia depositional cycle (Minas Gerais/Brazil), a post-transamazonic sequence south of the São Francisco Craton: Evidence from U-Pb dating on zircons of a metasediment. *Journal of South American Earth Sciences*, **10 (1)**, 21–28.

Soulaimani, A. and M. Burkhard, 2008: The Anti-Atlas chain (Morocco): the southern margin of the Variscan belt along the edge of the West African craton. *Geological Society, London, Special Publications*, **297 (1)**, 433–452.

Stacey, J. S. and J. D. Kramers, 1975: Approximation of terrestrial lead isotope evolution by a two-stage model. *Earth and Planetary Science Letters*, **26 (2)**, 207–221.

Stanistreet, I. G. and E. G. Charlesworth, 2001: Damaran basement-cored fold nappes incorporating pre-collisional basins, Kaoko Belt, Namibia, and controls on Mesozoic supercontinental break-up. *South African Journal of Geology*, **104 (1)**, 1–12.

Stern, R. J., 2008: Neoproterozoic crustal growth: The solid Earth system during a critical episode of Earth history. *Gondwana Research*, **14 (1-2)**, 33–50.

Sun, S.-s. and W. F. McDonough, 1989: Chemical and isotopic systematics of oceanic basalts: implications for mantle composition and processes. *Geological Society, London, Special Publications*, **42 (1)**, 313–345.

Svenningsen, O. M., 2001: Onset of seafloor spreading in the Iapetus Ocean at 608 Ma: precise age of the Sarek Dyke Swarm, northern Swedish Caledonides. *Precambrian Research*, **110 (1-4)**, 241–254.

Svoboda, J., 2004: *Magnetic Techniques for the Treatment of Materials*. Kluwer Academic Publishers, Dordrecht, The Netherlands.

Swanson-Hysell, N. L., A. C. Maloof, B. P. Weiss, and D. A. D. Evans, 2009: No asymmetry in geomagnetic reversals recorded by 1.1-billion-year-old Keweenawan basalts. *Nature Geosci*, **2 (10)**, 713–717.

Sylvester, P. J. and K. Attoh, 1992: Lithostratigraphy and Composition of 2.1 Ga Greenstone Belts of the West African Craton and Their Bearing on Crustal Evolution and the Archean-Proterozoic Boundary. *The Journal of Geology*, **100 (4)**, 377–393.

Sylvester, P. J. and M. Ghaderi, 1997: Trace element analysis of scheelite by excimer laser ablation-inductively coupled plasma-mass spectrometry (ELA-ICP-MS) using a synthetic silicate glass standard. *Chemical Geology*, **141 (1-2)**, 49–65.

Tack, L., 1975: Bijdrage tot de studie van de geologie, de petrografie en de petrologie van het Mahumbiaan van Neder-Zaïre. Ph.D. thesis, Rijksuniversiteit Gent (Belgium), 200 + annexes pp.

Tack, L., M. Wingate, J.-P. Liégeois, M. Fernandez-Alonso, and A. Deblond, 2001: Early Neoproterozoic magmatism (1000-910 Ma) of the Zadinian and Mayumbian Groups (Bas-Congo): onset of Rodinia rifting at the western edge of the Congo craton. *Precambrian Research*, **110**, 277–306.

Tack, L., M. T. D. Wingate, B. De Waele, J. Meert, E. Belousova, B. Griffin, A. Tahon, and M. Fernandez-Alonso, 2010: The 1375 Ma "Kibaran event" in Central Africa: Prominent emplacement of bimodal magmatism under extensional regime. *Precambrian Research*, **180 (1-2)**, 63–84.

Tait, J., M. Schatz, V. Bachtadse, and H. Soffel, 2000: Palaeomagnetism and Palaeozoic palaeogeography of Gondwana and European terranes. *Geological Society, London, Special Publications*, **179 (1)**, 21–34.

Tait, J. A., F. Delpomdor, A. R. Préat, G. Straathof, V. Kanda Nkula, and L. Tack, 2011: Neoproterozoic Sequences of the West Congo and Lindi/Ubangi Supergroups in the Congo Craton, central Africa. *The Geological Record of Neoproterozoic Glaciations*, E. Arnaud, G. Halverson, and G. Shields-Zhou, Eds., Geological Society, London, Memoir, London,

Vol. in press.

Tauxe, L. and K. P. Kodama, 2009: Paleosecular variation models for ancient times: Clues from Keweenawan lava flows. *Physics of the Earth and Planetary Interiors*, **177 (1-2)**, 31–45.

Taylor, S. and S. McLennan, 1985: *The Continental Crust: its Composition and Evolution*. Blackwell Scientific Publications, Oxford.

Tchameni, R., K. Mezger, N. E. Nsifa, and A. Pouclet, 2000: Neoarchæan crustal evolution in the Congo Craton: evidence from K rich granitoids of the Ntem Complex, southern Cameroon. *Journal of African Earth Sciences*, **30 (1)**, 133–147.

Tchameni, R., A. Pouclet, J. Penaye, A. A. Ganwa, and S. F. Toteu, 2006: Petrography and geochemistry of the Ngaoundéré Pan-African granitoids in Central North Cameroon: Implications for their sources and geological setting. *Journal of African Earth Sciences*, **44 (4-5)**, 511–529.

Tera, F. and G. J. Wasserburg, 1972: U-Th-Pb systematics in three Apollo 14 basalts and the problem of initial Pb in lunar rocks. *Earth and Planetary Science Letters*, **14 (3)**, 281–304.

Théveniaut, H., C. Delor, J. M. Lafon, P. Monié, P. Rossi, and D. Lahondère, 2006: Paleoproterozoic (2155-1970 Ma) evolution of the Guiana Shield (Transamazonian event) in the light of new paleomagnetic data from French Guiana. *Precambrian Research*, **150 (3-4)**, 221–256.

Thiéblemont, D., J. C. Goujou, E. Egal, A. Cocherie, C. Delor, J. M. Lafon, and C. M. Fanning, 2004: Archean evolution of the Leo Rise and its Eburnean reworking. *Journal of African Earth Sciences*, **39 (3-5)**, 97–104.

Tohver, E., M. D'Agrella-Filho, and R. Trindade, 2006: Paleomagnetic record of Africa and South America for the 1200-500 Ma interval, and evaluation of Rodinia and Gondwana assemblies. *Precambrian Research*, **147**, 193–222.

Tohver, E., B. A. van der Pluijm, R. Van der Voo, G. Rizzotto, and J. E. Scandolara, 2002: Paleogeography of the Amazon craton at 1.2 Ga: early Grenvillian collision with the Llano segment of Laurentia. *Earth and Planetary Science Letters*, **199 (1-2)**, 185–200.

Torquato, J., A. Ferreira da Silva, U. G. Cordani, and K. Kawashita, 1979: Evolução Geológica do Cinturão Móvel do Quipungo no Ocidente de Angola. *An. Acad. Brasil Cienc.*, **51**, 133–143.

Torsvik, T. H., K. C. Lohmann, and B. A. Sturt, 1995: Vendian glaciations and their relation to the dispersal of Rodinia: Paleomagnetic constraints. *Geology*, **23 (8)**, 727–730.

Torsvik, T. H. and E. F. Renström, 2001: Cambrian palaeomagnetic data from Baltica: implications for true polar wander and Cambrian palaeogeography. *Journal of the Geological Society*, **158 (2)**, 321–329.

Toteu, S. F., amp, a.c.u.t.e..i.x, J. Penaye, and Y. P. Djomani, 2004: Geodynamic evolution of the Pan-African belt in central Africa with special reference to Cameroon. *Canadian Journal of Earth Sciences*, **41**, 73–85.

Toteu, S. F., R. Y. Fouateu, J. Penaye, J. Tchakounte, A. C. S. Mouangue, W. R. Van Schmus, E. Deloule, and H. Stendal, 2006: U-Pb dating of plutonic rocks involved in the nappe tectonic in southern Cameroon: consequence for the Pan-African orogenic evolution of the central African fold belt. *Journal of African Earth Sciences*, **44 (4-5)**, 479–493.

Toteu, S. F., W. R. Van Schmus, J. Penaye, and J. B. Nyobé, 1994: U—Pb and Sm—N edvidence for Eburnian and Pan-African high-grade metamorphism in cratonic rocks of southern Cameroon. *Precambrian Research*, **67 (3-4)**, 321–347.

Trindade, R., M. D'Agrella-Filho, M. Babinski, E. Font, and B. Brito Neves, 2004: Paleomagnetism and geochronology of the Bebedouro cap carbonate: evidence for continental-scale Cambrian remagnetization in the São Francisco, Brazil. *Precambrian Research*, **128**, 83–103.

Trompette, R., 1973: Le Précambrien supérieur et le Paléozoique inférieur de l'Adrar de

Mauritanie (bordure occidentale de Bassin de Taoudeni, Afrique de l'oust). Un exemple de sédimentation de craton. Etude sédimentologique. Tech. rep., Marseille.

Trompette, R., 1994: *Geology of Western Gondwana (2000 - 500 Ma)*. A.A.Balkema.

Trompette, R., 1997: Neoproterozoic (600 Ma) aggregation of Western Gondwana: a tentative scenario. *Precambrian Research*, **82 (1-2)**, 101–112.

Trompette, R. and F. Boudzoumou, 1988: Palaeogeographic significance of stromatolitic buildups on late proterozoic platforms: The example of the West Congo basin. *Palaeogeography, Palaeoclimatology, Palaeoecology*, **66 (1-2)**, 101–112.

Trouw, R., M. Heilbron, A. Ribeiro, F. Paciullo, C. M. Valeriano, J. C. H. Almeida, M. Tupinambá, and R. Andreis, 2000: The central segment of the Ribeira belt. *Tectonic Evolution of South America*, U. Cordani, E. Milani, A. Thomaz Filho, and D. Campos, Eds., GSA, 31st International Geological Congress, Rio de Janeiro, 287–310.

Unrug, R., 1992: The supercontinent cycle and gondwanaland assembly: Component cratons and the timing of suturing events. *Journal of Geodynamics*, **16 (4)**, 215–240.

Urban, H., B. Stribrny, and H. J. Lippolt, 1992: Iron and manganese deposits of the Urucum District, Mato Grosso do Sul, Brazil. *Economic Geology*, **87 (5)**, 1375–1392.

Usui, T., K. Kobayashi, and E. Nakamura, 2002: U-Pb isotope systematics of micro-zircon inclusions - Implications for the age and origin of eclogite xenolith from the Colorado Plateau. *Proceedings of the Japan Academy Series B-Physical and Biological Sciences*, **78 (3)**, 51–56.

Utzmann, A., T. Hansteen, and H.-U. Schmincke, 2002: Trace element mobility during sub-seafloor alteration of basaltic glass from Ocean Drilling Program site 953 (off Gran Canaria). *International Journal of Earth Sciences*, **91 (4)**, 661–679.

Valeriano, C. M., N. Machado, A. Simonetti, C. S. Valladares, H. J. Seer, and L. S. A. Simões, 2004: U-Pb geochronology of the southern Brasília belt (SE-Brazil): sedimentary provenance, Neoproterozoic orogeny and assembly of West Gondwana. *Precambrian Research*, **130 (1-4)**, 27–55.

Valeriano, C. M., M. M. Pimentel, M. Heilbron, J. C. H. Almeida, and R. A. J. Trouw, 2008: Tectonic evolution of the Brasilia Belt, Central Brazil, and early assembly of Gondwana. *Geological Society, London, Special Publications*, **294 (1)**, 197–210.

Valeriano, C. M., L. S. A. Simões, W. Teixeira, and M. Heilbron, 2000: Southern Brasília belt (SE Brazil): tectonic discontinuities, K-Ar data and evolution during the Neoproterozoic Brasíliano orogeny. *Revista Brasileira de Geociências*, **30**, 195–199.

Valladares, C., N. Machado, M. Heilbron, and G. Gauthier, 2004: Ages of Detrital Zircon from Siliciclastic Successions South of the São Francisco Craton, Brazil: Implications for the Evolution of Proterozoic Basins. *Gondwana Research*, **7 (4)**, 913–921.

van der Meer, J. J. M., 1993: Microscopic evidence of subglacial deformation. *Quaternary Science Reviews*, **12 (7)**, 553–587.

van der Meer, J. J. M., 1997: Particle and aggregate mobility in till: Microscopic evidence of subglacial processes. *Quaternary Science Reviews*, **16 (8)**, 827–831.

van der Meer, J. J. M., J. Menzies, and J. Rose, 2003: Subglacial till: the deforming glacier bed. *Quaternary Science Reviews*, **22 (15-17)**, 1659–1685.

Van der Voo, R., 1990: The reliability of paleomagnetic data. *Tectonophysics*, **184**, 1–9.

Van der Voo, R. and J. G. Meert, 1991: Late Proterozoic paleomagnetism and tectonic models: a critical appraisal. *Precambrian Research*, **53 (1-2)**, 149–163.

van Loon, A. J., 2008: Could 'Snowball Earth' have left thick glaciomarine deposits? *Gondwana Research*, **14 (1-2)**, 73–81.

van Schmus, W. R., E. P. Oliveira, A. F. da Silva Filho, S. F. Toteu, J. Penaye, and I. P. Guimaraes, 2008: Proterozoic links between the Borborema Province, NE Brazil, and

the Central African Fold Belt. *Geological Society, London, Special Publications*, **294 (1)**, 69–99.

van Staden, A., T. Naidoo, U. Zimmermann, and G. J. B. Germs, 2006: Provenance analysis of selected clastic rocks in Neoproterozoic to lower Paleozoic successions of southern Africa from the Gariep Belt and the Kango Inlier. *South African Journal of Geology*, **109 (1-2)**, 215–232.

Veizer, J., et al., 1999: 87Sr/86Sr, d13C and d18O evolution of Phanerozoic seawater. *Chemical Geology*, **161**, 59–88.

Vellutini, P. and J.-P. Vicat, 1983: Sur l'origine des formations conglomératiques de base du géosynclinal ouest-congolien (Gabon, Congo, Zaïre, Angola). *Precambrian Research*, **23 (1)**, 87–101.

Vermeesch, P., 2004: How many grains are needed for a provenance study? *Earth and Planetary Science Letters*, **224 (3-4)**, 441–451.

Vicat, J. P. and A. Pouclet, 2000: Palaeo- and Neoproterozoic granitoids and rhyolites from the West Congolian Belt (Gabon, Congo, Cabinda, north Angola): chemical composition and geotectonic implications. *Journal of African Earth Sciences*, **31 (3-4)**, 597–617.

Vidal, M. and G. Alric, 1994: The palaeoproterozoic (Birimian) of Haute-Comoé in the West African craton, Ivory Coast: a transtensional back-arc basin. *Precambrian Research*, **65 (1-4)**, 207–229.

Villeneuve, M., 2008: Review of the orogenic belts on the western side of the West African craton: the Bassarides, Rokelides and Mauritanides. *Geological Society, London, Special Publications*, **297 (1)**, 169–201.

Villeneuve, M. and J. J. Cornée, 1994: Structure, evolution and palaeogeography of the West African craton and bordering belts during the Neoproterozoic. *Precambrian Research*, **69 (1-4)**, 307–326.

Villeneuve, M. and R. D. Dallmeyer, 1987: Geodynamic evolution of the mauritanide, bassaride, and rokelide orogens (West Africa). *Precambrian Research*, **37 (1)**, 19–28.

Villeneuve, M., A. El Archi, and J. Nzamba, 2010: Les chaînes de la marge occidentale du Craton Ouest-Africain, modèles géodynamiques. *Comptes Rendus Geosciences*, **342 (1)**, 1–10.

Ward, W., 1974: Climatic Variations on Mars 1. Astronomical Theory of Insolation. *Journal of Geophyisical Research*, **79 (24)**, 3375–3386.

Wegener, A., 1912: The origin of continents. *Geologische Rundschau*, **3**, 276–292.

Wegener, A., 1967: *The Origin of Continents and Oceans*. Methuen, London.

Weil, A. B., R. Van der Voo, C. Mac Niocaill, and J. G. Meert, 1998: The Proterozoic supercontinent Rodinia: paleomagnetically derived reconstructions for 1100 to 800 Ma. *Earth and Planetary Science Letters*, **154 (1-4)**, 13–24.

Wiedenbeck, M., et al., 1995a: 3 Natural Zircon Standards for U-Th-Pb, Lu-Hf, Trace-Element and Ree Analyses. *Geostandards Newsletter*, **19 (1)**, 1–23.

Wiedenbeck, M., et al., 1995b: Three natural zircon standards for U-Th-Pb, Lu-Hf, trace element and REE analyses. *Geostandards and Geoanalytical Research*, **19 (1)**, 1–23.

Wiedenbeck, M., et al., 2004: Further Characterisation of the 91500 Zircon Crystal. *Geostandards and Geoanalytical Research*, **28 (1)**, 9–39.

Williams, D., J. Kasting, and L. Frakes, 1998: Low-latitude glaciation and rapid changes in the Earth's obliquity explained by obliquity-oblateness feedback. *Nature*, **396**, 453–455.

Williams, G., 1993: History of the Earth's obliquity. *Earth-Science Reviews*, **34**, 1–45.

Williams, G., 2000: Geological Constraints on the Precambrian History of Earth's Rotation and the Moon's Orbit. *Reviews of Geophysics*, **38 (1)**, 37–59.

Williams, G. E., 2008: Proterozoic (pre-Ediacaran) glaciation and the high obliquity, low-latitude ice, strong seasonality (HOLIST) hypothesis: Principles and tests. *Earth-Science Reviews*, **87 (3-4)**, 61–93.

Willis, B., 1944: Continental drift: Ein märchen. *American Journal of Science*, **242**, 509–513.

Winchester, J. A. and P. A. Floyd, 1977: Geochemical discrimination of different magma series and their differentiation products using immobile elements. *Chemical Geology*, **20**, 325–343.

Windley, B., 1995: *The Evolving Continents*. Wiley, Chichester.

Wingate, M. T. D., I. H. Campbell, W. Compston, and G. M. Gibson, 1998: Ion microprobe U-Pb ages for Neoproterozoic basaltic magmatism in south-central Australia and implications for the breakup of Rodinia. *Precambrian Research*, **87 (3-4)**, 135–159.

Wingate, M. T. D., S. A. Pisarevsky, and D. A. D. Evans, 2002: Rodinia connections between Australia and Laurentia: no SWEAT, no AUSWUS? *Terra Nova*, **14 (2)**, 121–128.

Wu, F., R. Van der Voo, and R. J. E. Johnson, 1986: Eocambrian paleomagnetism of the Boston Basin - evidence for displaced terane. *Geophysical Research Letters*, **13 (13)**, 1450–1453.

Yegorov, D. and T. Bayanova, 1999: Start of Dike Intrusion and Banded Iron Formation Genesis on the Kola Peninsula (Baltic Shield): Proterozoic or Archaean? *Journal of Conference Abstracts (Cambridge Publications), Abstract Volume of European Union of Geosciences meeting*, **4 (1 (EUG10))**, 134.

Young, G. M., 1976: Iron-formation and glaciogenic rocks of the Rapitan Group, northwest territories, Canada. *Precambrian Research*, **3**, 137–158.

Zhang, S., G. Jiang, and Y. Han, 2008: The age of the Nantuo Formation and Nantuo glaciation in South China. *Terra Nova*, **20 (4)**, 289–294.

Zhao, G., P. A. Cawood, S. A. Wilde, and M. Sun, 2002a: Review of global 2.1-1.8 Ga orogens: implications for a pre-Rodinia supercontinent. *Earth-Science Reviews*, **59 (1-4)**, 125–162.

Zhao, G., P. A. Cawood, S. A. Wilde, and M. Sun, 2002b: Review of global 2.1-1.8 Ga orogens: implications for a pre-Rodinia supercontinent. *Earth-Science Reviews*, **59 (1-4)**, 125–162.

Zhao, G., M. Sun, S. A. Wilde, and S. Li, 2004: A Paleo-Mesoproterozoic supercontinent: assembly, growth and breakup. *Earth-Science Reviews*, **67 (1-2)**, 91–123.

Zhao, G., M. Sun, S. A. Wilde, S. Li, and J. Zhang, 2006: Some key issues in reconstructions of Proterozoic supercontinents. *Journal of Asian Earth Sciences*, **28 (1)**, 3–19.

Zijderveld, J., 1967: A.C. demagnetization of rocks: analysis of results. *In: D.W. Collinson, K.M. Creer, S.K. Runcorn (Eds.), Methods in Paleomagnetism, Elsevier, NewYork*, pp. 245–286.

Zimmermann, M., 1960: Nouvelle subdivision des séries antégothlandiennes de l'Afrique occidentale (Mauritanie, Soudan, Sénégal). *21th Sess. Intern. Geol. Congr.*, Copenhagen, Vol. part VIII, 26–36.

Acknowledgements

It all happened very quickly four years ago (thanks to Cor Langereis for pointing out the opportunity) when I decided to start a PhD in Edinburgh. Not once did I regret making that decision and there are a lot of people who I would like to thank for making it such a wonderful time.

In the first place it has been my supervisor Jenny Tait with her continuing support which meant that I have very much enjoyed every stage of this project. I have always felt privileged with the opportunities that I have been given to travel to many exciting places around the world, to be part of the team here in Edinburgh and to collaborate with a wide variety of inspiring people who I have met at conferences, at other universities and in the field. I would like to thank her also for letting me do my own work at my own pace and for her time she spent correcting my written work.

I would like to thank Udo Zimmermann for introducing me to the field of provenance studies and for helping me understand a lot more of the periodic table of elements. His positive attitude continues to be very inspiring.

Many thanks go to everyone who helped in organising the field expeditions: staff of the Royal Museum for Central Africa in Tervuren, especially Luc Tack and Max Fernandez-Alonso, are thanked for helping to organise fieldwork in the Congo. Roger Key from the British Geological Survey provided invaluable support for our fieldwork in Mauritania. Assistance in the field by Valentin Kanda Nkula, Emmanuel Cibambula, Khalidou B. Lô, N'Diaye Ousmane (who sadly passed away in autumn 2010), Med El Moctar O. Dahmada but also by Hugh Rice, Mark Edwards and the family Pettersen is greatly acknowledged. Fieldwork would not have been possible, and certainly much less enjoyable, without them!

I would like to thank everyone who facilitated and assisted me in various laboratories: John Craven, Nicola Cayzer and Nic Odling for the facilities I used here in Edinburgh,

Tony Fallick and Julie Dougans from SUERC, Cor Langereis and Mark Dekkers from Fort Hoofddijk in Utrecht, Pat Kelly and Marion Marshall for all the zircon work they did for me in Australia, Eizo Nakamura, Yoshiko Nakano, Tatsuki Tsujimori, Katsura Kobayashi and Chie Sakaguchi from ISEI (Japan), Jasper Berndt from Münster, Richard Ernst and Ulf Söderlund for their enthusiasm and for the great results from the baddeleyite dating.

All my colleagues of the Marie Curie Excellence Team are thanked for their help and advise, especially Sergei Pisarevsky, Graeme Nicoll, Chris Rowan, Anna Reynolds and Clare Peters. Graeme and Chris: it was great doing fieldwork together! Allan Pike and Jim Smith are thanked for their their never-ending willingness to help and their great sense of humour in the lab.

Thanks to staff at the School of GeoSciences, especially Sally, Helena, Rachel, Lisa, Rosanna, Justin, Andy and Simon, who have helped me over the years. Also thanks to the postgraduate students (I'm not even going to start a list...) who made it such a great place to work.

The feedback of Richard Glen of the Geological Survey of New South Wales (Australia) has greatly improved my written work. My examiners Anthony Morris and Simon Harley are thanked for their constructive feedback and encouragements to put my work into publications. Jelle Assink and Folkert de Boer are thanked for helping me build my bibliography.

Finally I would like to thank my family and friends, especially my parents for their continuing support and frequent visits during the past four years. And Vera: thanks for making my life here in Edinburgh complete. Ik ben heel blij dat we dit avontuur samen zijn aangegaan!

This thesis was written using LaTeX. Figures are created using Generic Mapping Tools and/or Adobe Illustrator.

This PhD was fully funded by the European Union through the Marie Curie FP6 Action Excellence Grant 42409.

Appendix A

Photos

A.1 DRC

Figure A.1. Ripple marks in a layer of quartz arenite of the Sansikwa Subgroup at the DZI locality.

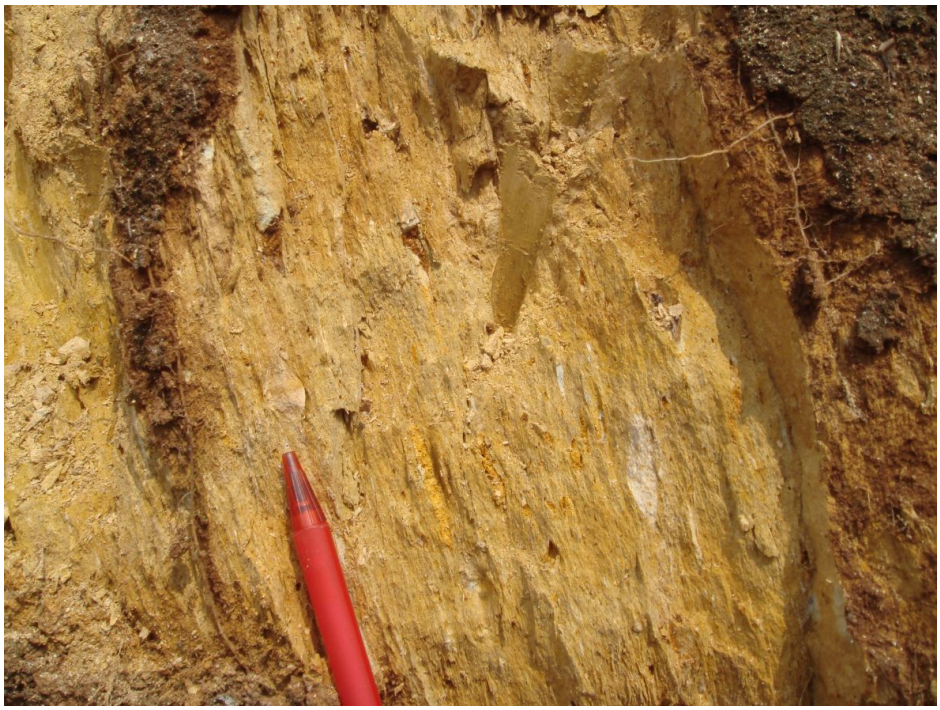

(a) The Lower Diamictite Subgroup at the BANGU locality illustrating the unconsolidated nature of the material. An elongated clast (white) can be seen on the right hand side.

(b) A polished section through a hand sample of the volcanic breccia from the KAS locality. The large clasts mainly consist of weather plagioclase, the goundmass consists of chloritised volcanic glass.

Figure A.2. Field photos Bas-Congo (DRC).

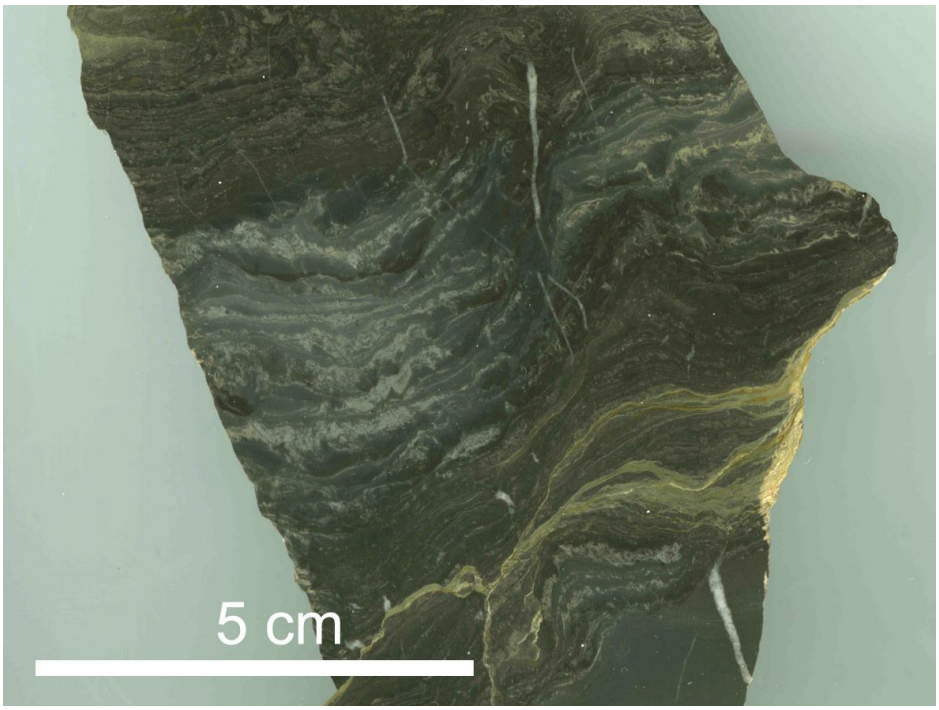

(a) Microbial laminites in the carbonates of the Haut-Shiloango Subgroup from the SAF locality, 2-3 m below the contact with the Upper Diamictite.

(b) Brecciated carbonates of the Haut-Shiloango Subgroup immediately below the Upper Diamictite Formation, SAF locality.

Figure A.3. Field photos Bas-Congo (DRC).

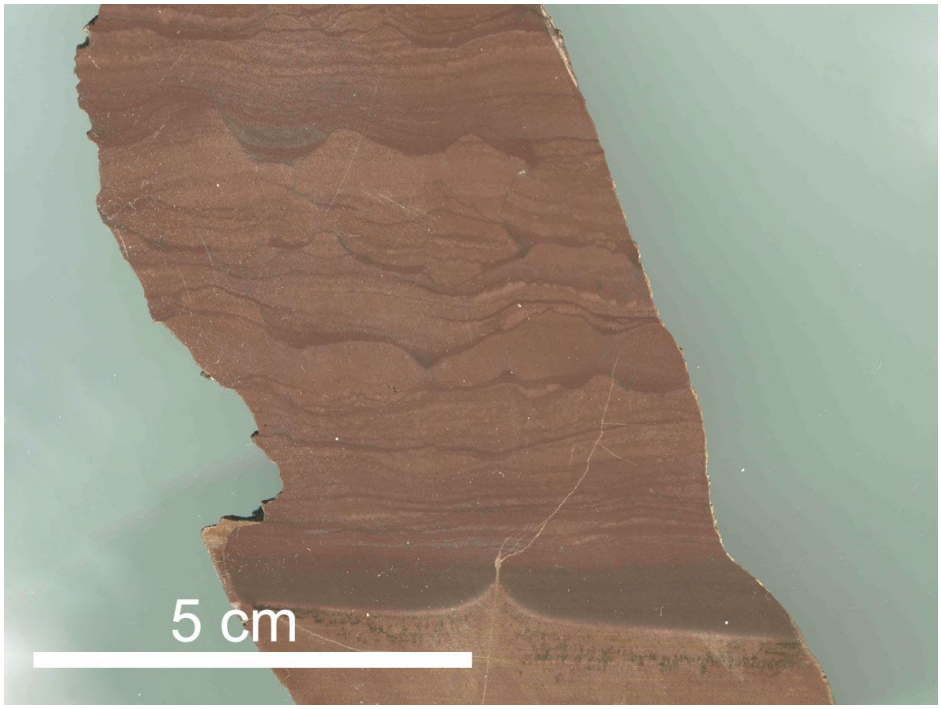

(a) Polished section of dolomitised carbonate of the Schisto-Calcaire Subgroup at the KWI locality. Sedimentary structures which indicate a high-energy depositional environment can be seen, in particular: flame structures and load casts due to dewatering of water saturated layers and flaser bedding which are wave ripples filled in by finer grained sediment.

(b) Cross bedding in dolomitised carbonate of the Schisto-Calcaire Subgroup at the SNEL locality.

Figure A.4. Field photos Bas-Congo (DRC).

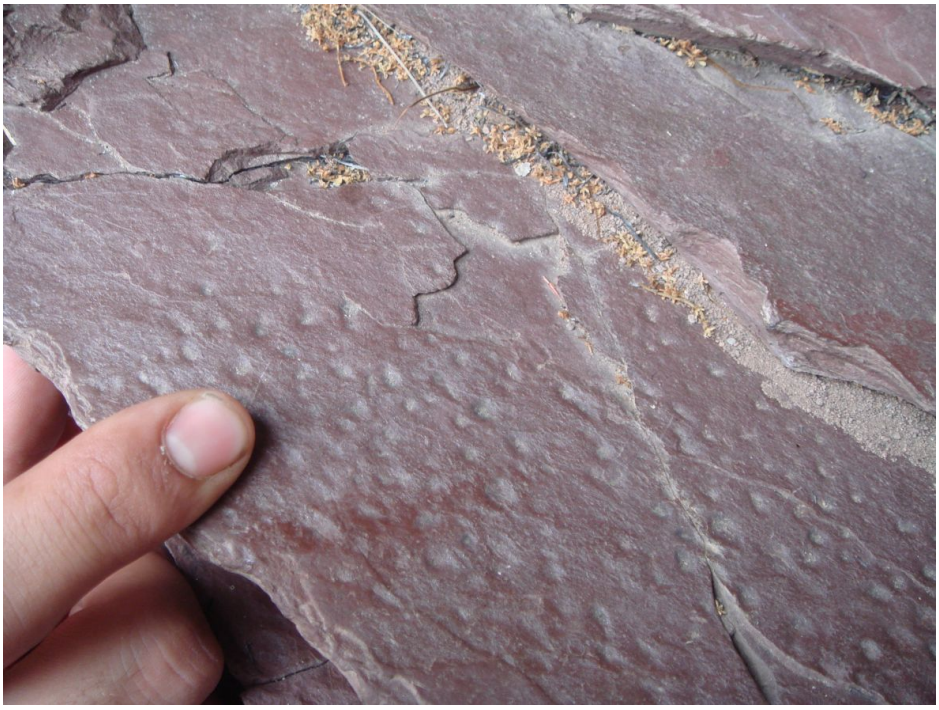

(a) Raindrops preserved in red shales of the Mpioka Subgroup at the VAP locality.

(b) Ripple marks in '3D' view in sandstone of the Mpioka Subgroup at the VAP locality (fallen leaf for scale).

Figure A.5. Field photos Bas-Congo (DRC).

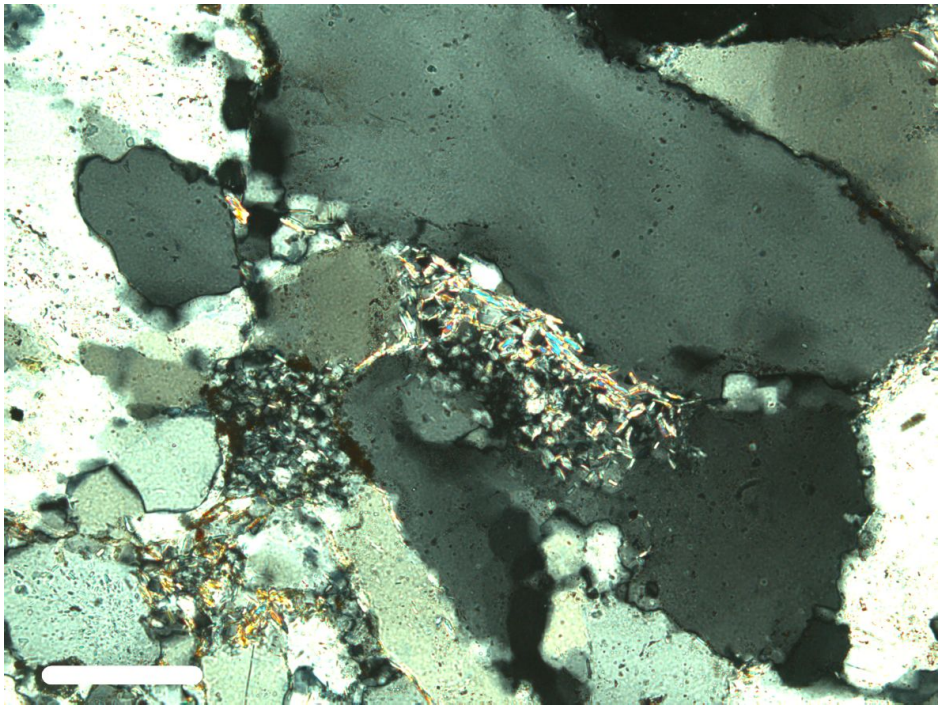

(a) Photomicrograph of a quartz arenite of the Sansikwa Group at the DZI locality showing twinning in large quartz grains and pore-space filling by small quartz grains and micas.

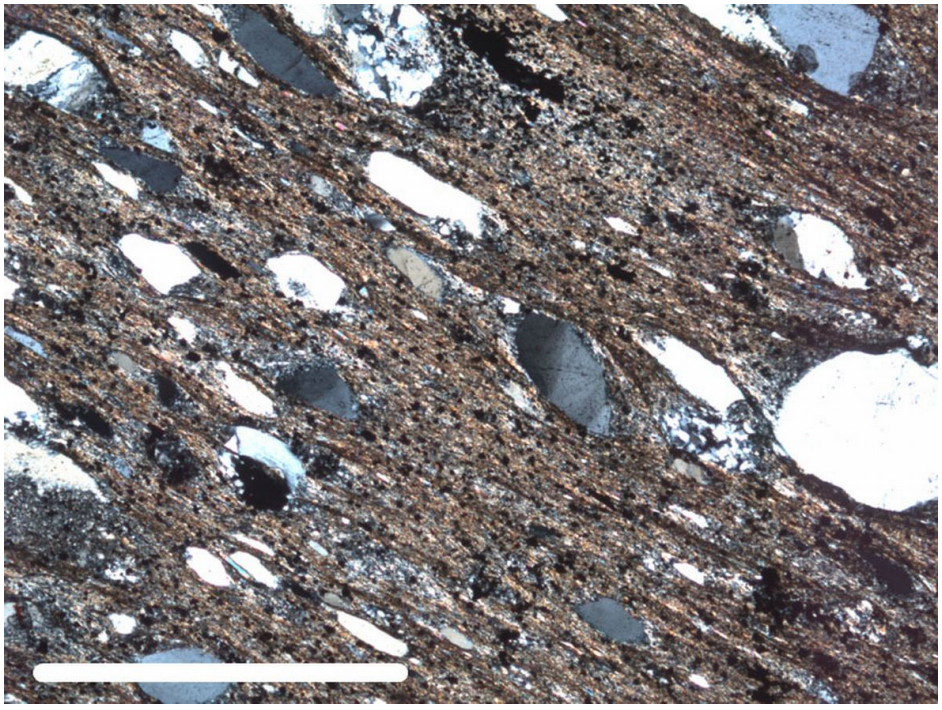

(b) Photomicrograph of a strongly deformed sample of the Lower Diamictite Formation from the BANGU locality. Larger grains are predominantly quartz, the fabric consists of fine-grained quartz and clay minerals.

Figure A.6. Photomicrographs Bas-Congo (DRC), the white bars are 1mm..

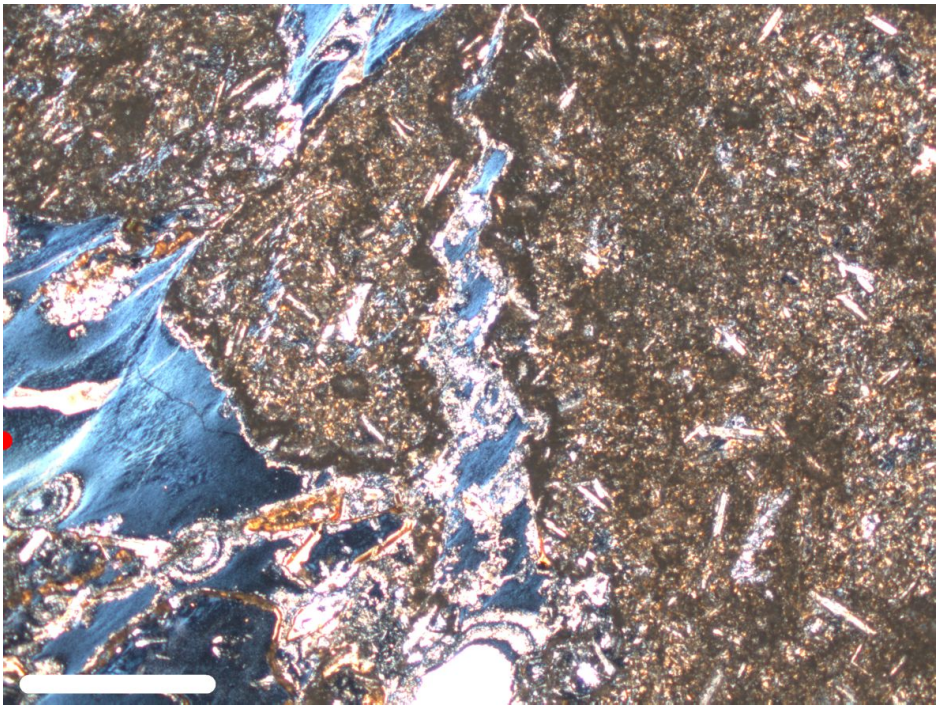

(a) Photomicrograph of a volcanic breccia from within the Lower Diamictite Formation at the KAS locality. The brown parts are altered plagioclase clasts and matrix glass (blue, chloritised) filling in cracks in the clasts.

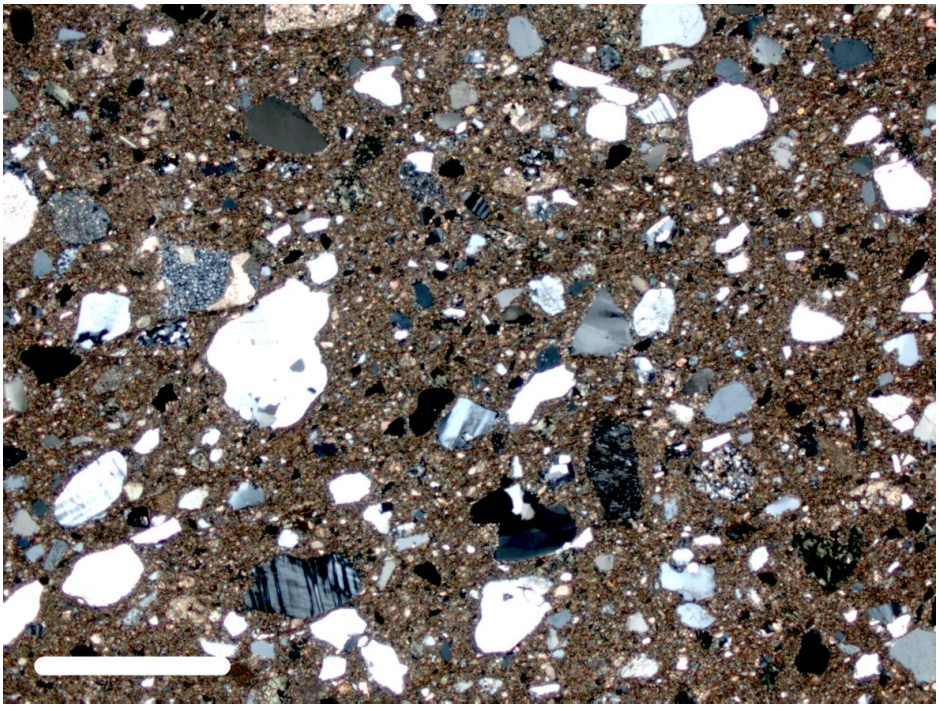

(b) Photomicrograph of a sample from the Upper Diamictite Formation at the KUM locality. Grains are predominantly quartz but also include lithic fragments and altered clay minerals and carbonate fragments. The matrix consists of fine grained quartz and clay minerals.

Figure A.7. Photomicrographs Bas-Congo (DRC), the white bars are 1mm.

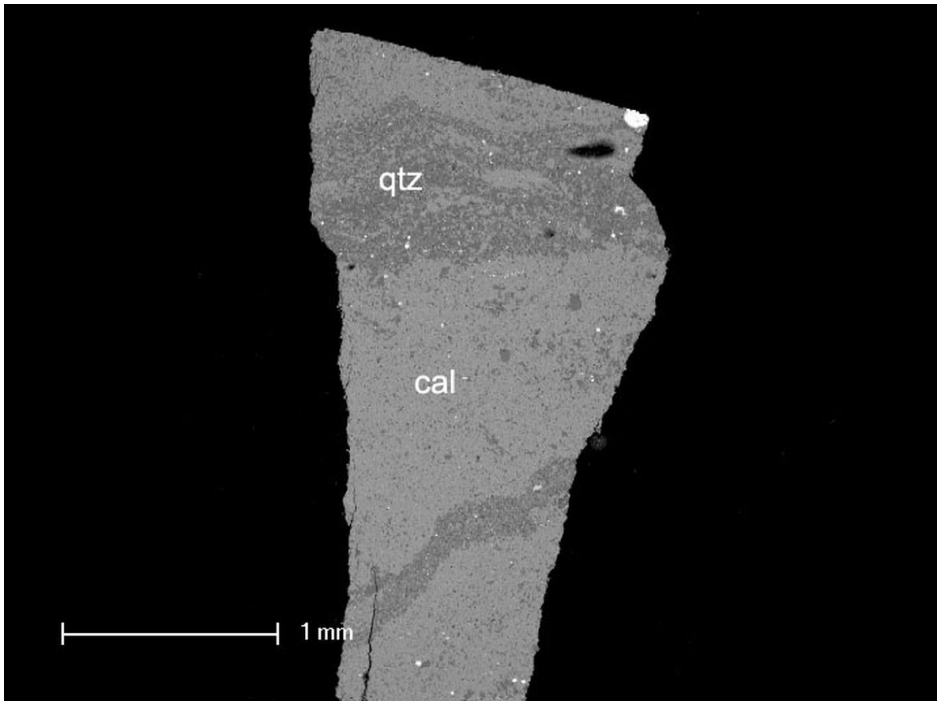

(a) SEM backscatter image of carbonate from the Haut-Shiloango Subgroup sampled at the SAF locality. $CaCO_3$ is light grey coloured while the dark grey colour shows SiO_2.

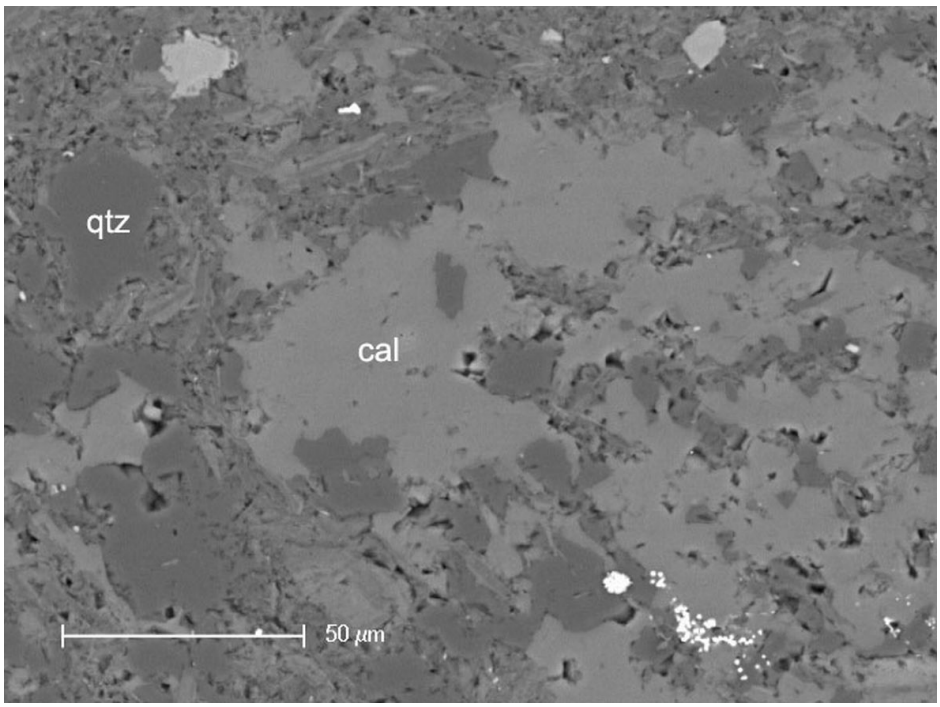

(b) Zoomed section of Figure A.8a showing the mixture of quartz and carbonate with a few sulphate crystals (bright spots).

Figure A.8. Photomicrographs Bas-Congo (DRC), obtained using a scanning electron microscope (SEM).

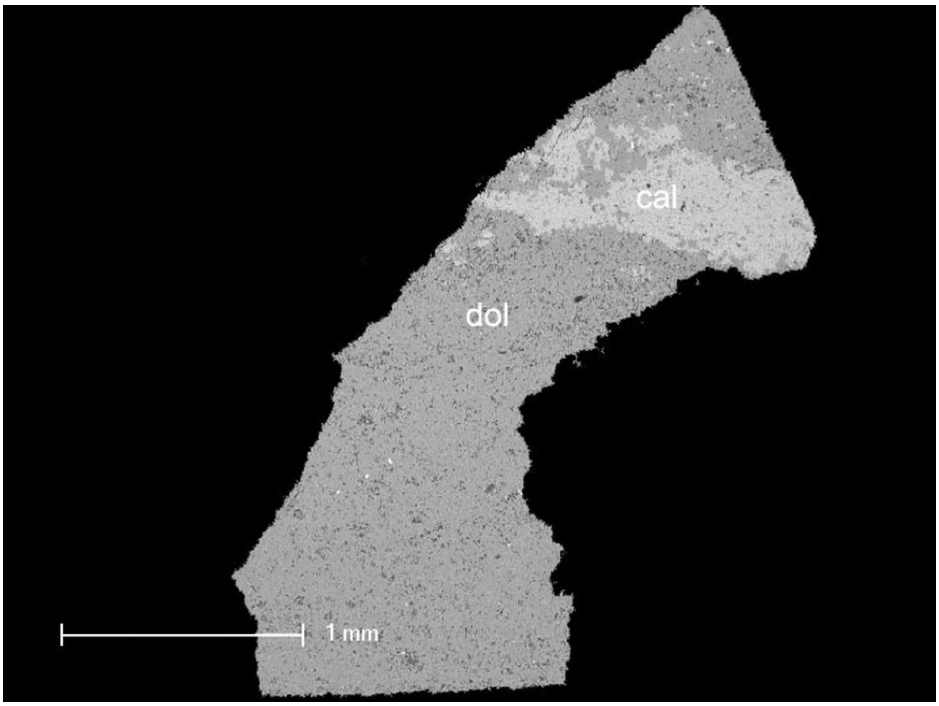

(a) SEM backscatter image of carbonate from the Schisto-Calcaire Subgroup sampled at the SAF locality. The dark and the light grey colours indicate dolomite and calcite respectively.

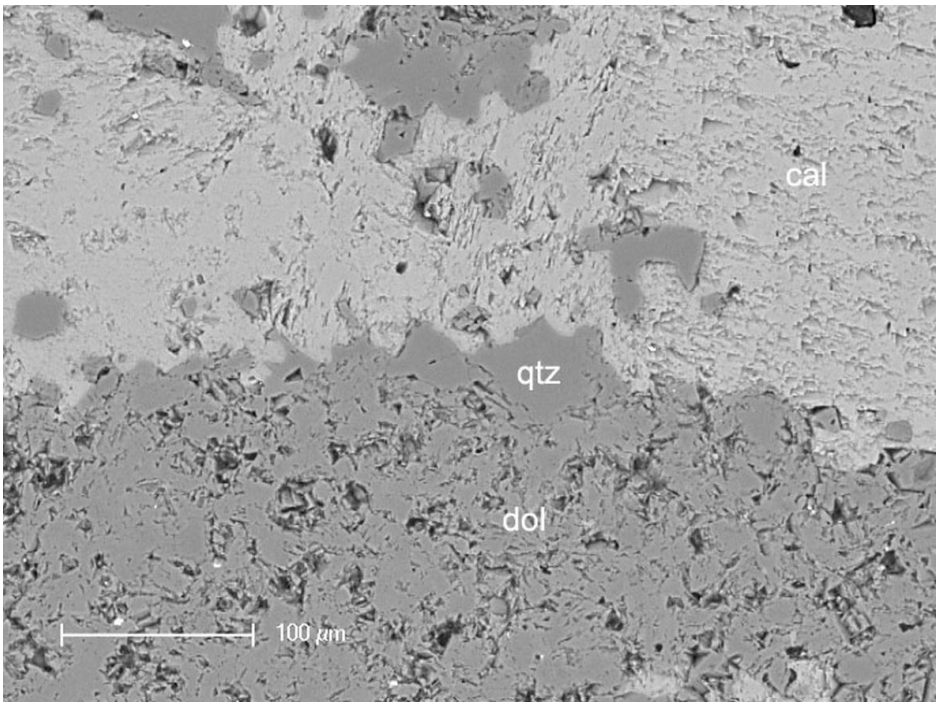

(b) Zoomed section of Figure A.9a showing the relationship between carbonate, dolomite and quartz.

Figure A.9. Photomicrographs Bas-Congo (DRC).

A.2 Mauritania

Figure A.10. Silts (brown and purple colours) and dolostones (pink colour) of the Azougui Formation at the AZO locality.

(a) Cliffs of the Foum Chor Formation, taken from the AZO locality looking approx. north.

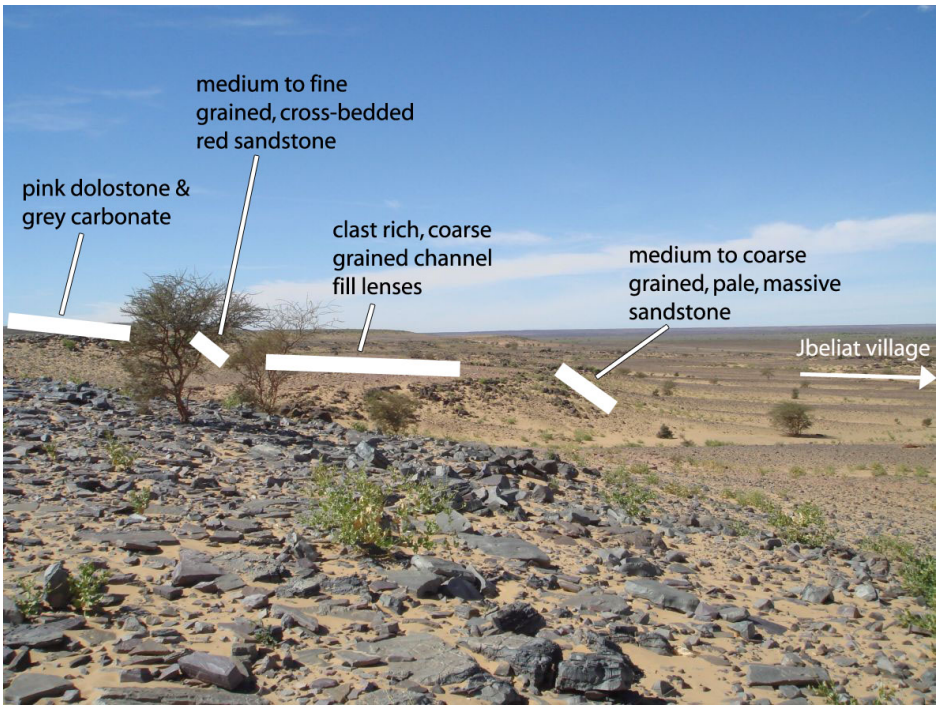

(b) Jbeliat section near village (LIAT) looking approx. east. The section shows the position of three tillite samples described in Chapter 6 and of the dolostones on top of the tillites.

Figure A.11. Field photos Adrar (Mauritania).

(a) Diamictite channel fill, Jbeliat Formation (LIAT 5).

(b) Cross-bedded sandstone, Jbeliat Formation (LIAT 6).

Figure A.12. Field photos Adrar (Mauritania).

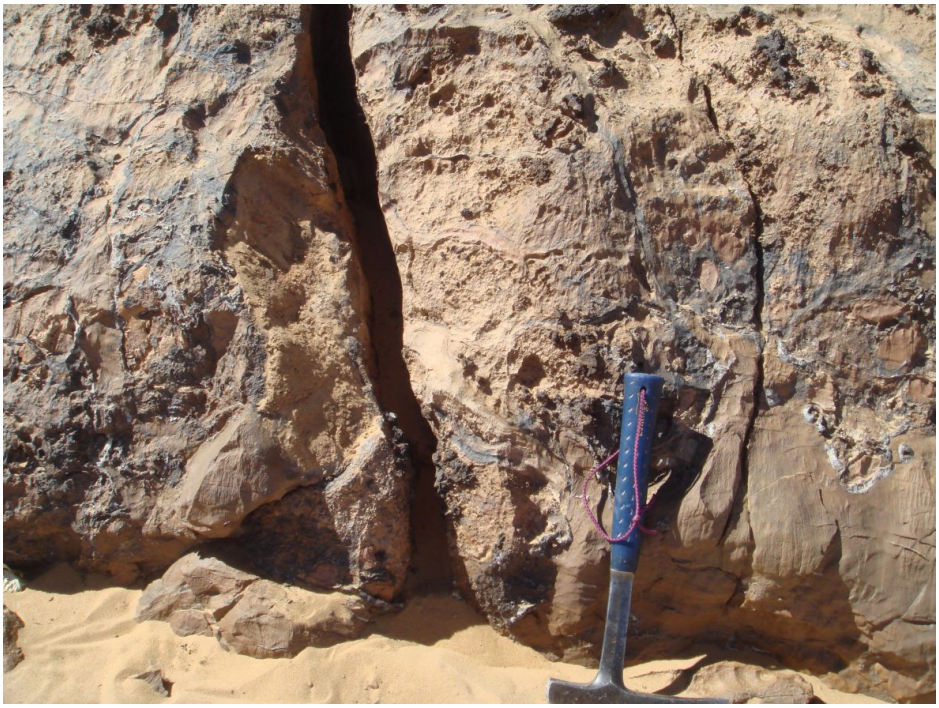

(a) Barite veins in pink dolostone, Jbeliat Formation (JLT).

(b) Purple limestone, Jbeliat Formation (JLT).

Figure A.13. Field photos Adrar (Mauritania).

(a) Carbonate clasts in conglomerate, Jbeliat Formation (ABE 20).

(b) Fine grained, pebbly sandstone, Jbeliat Formation (ABE 21).

Figure A.14. Field photos Adrar (Mauritania).

(a) Well bedded dolostone, Jbeliat Formation (ABE locality).

(b) Folding in disturbed dolostone beds, Jbeliat Formation (ABE locality).

Figure A.15. Field photos Adrar (Mauritania).

(a) Wave ripples in bedded dolostone, Jbeliat Formation (ABE locality).

(b) Contact with pebbly sandstone (underneath hammer) and dolostone, Jbeliat Formation (ABE locality).

Figure A.16. Field photos Adrar (Mauritania).

(a) Atar Cliffs with the Chinguetti Formation sandstones at the top.

(b) Cross-bedded sandstones of the Chinguetti Formation at the OUA locality.

Figure A.17. Field photos Adrar (Mauritania).

(a) Ahmeyim Great Dyke, view from the northern locality looking south.

(b) Ahmeyim Great Dyke, Olivine phenocrysts in cross-cutting dyke at northern locality.

Figure A.18. Field photos Adrar (Mauritania).

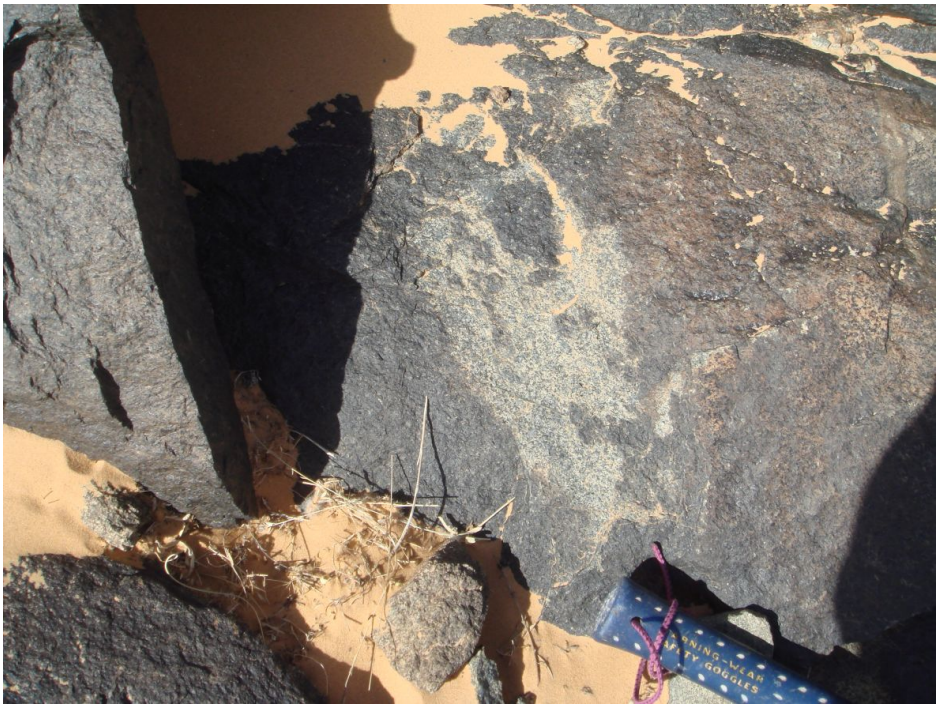

(a) Ahmeyim Great Dyke, felsic xenolith.

(b) Ahmeyim Great Dyke, palaeomagnetic sampling.

Figure A.19. Field photos Adrar (Mauritania).